

**Working towards a New Sustainable
Rechargeable Battery; Zinc, Conducting
Polymer and Deep Eutectic Solvent
System**

by

**Claire Fullarton MChem
Department of Chemistry
University of Leicester**

**A doctoral thesis
submitted for the degree of**

**Doctor of Philosophy
at the University of Leicester
2014**

**Working towards a New Sustainable Rechargeable Battery; Zinc, Conducting
Polymer and Deep Eutectic Solvent System**

Claire Fullarton

Electronically conducting polymers based on functionalised thiophenes and pyrroles have continued to stimulate academic interest as well as starting to be employed in practical applications and uses.

This thesis describes studies of the electronic properties of mixed thiophene-pyrrole polymers (based on custom synthesised mixed monomer precursors) and polymers electrodeposited from commercially available monomers, pyrrole and 3,4-ethylenedioxythiophene, in respect to energy storage applications including batteries and ion selective membranes. In such applications the movement of ion and solvent through the polymer film during oxidation and reduction cycles is critical to application and function, *e.g.* charging rate, metal ion permeability or adhesion stability.

Recently the unexpected behaviour of polypyrrole in choline chloride based ionic liquids has been described. These liquids are especially attractive because of their unique solubility profiles, high stability, low volatility and low toxicity. This thesis describes the electrochemical characterisation, DC capacitance behaviour and ion/solvent transport properties of conducting polymers using a range of electrochemical methodologies in combination with acoustic impedance electrochemical quartz crystal microbalance techniques (EQCM) and

X-Ray Photo-electron Spectroscopy (XPS). The behaviour of several mixed thiophene-pyrrole films, polypyrrole and poly 3,4-ethylenedioxythiophene in different electrolyte media; deep eutectic solvents (DESs), conventional organic solvents and aqueous media are contrasted in this thesis.

PEDOT and one of the mixed thiophene-pyrrole polymers (poly 2-(thiophene-2-yl)-1H pyrrole) gave the highest DC capacitances of the polymers investigated, with high values observed in both choline chloride based (Type III) and zinc based (Type IV) DESs. The ion dynamics of the polymers p-doping in the DESs, observed to fit gravimetric data recorded, was able to show a marked difference in the ion transfers between DES types and a conventional organic solvent, acetonitrile. Both polymers in acetonitrile and the zinc based DES (ZnCl_2 / EG) satisfied the electro-neutrality condition through dominance of anion transfers. Whereas, polymers in the choline chloride based DES (Ethaline) satisfied the electro-neutrality condition through dominance of choline cation transfers (in the opposite direction to anion transfers).

This research involved work towards the development of a new class of rechargeable batteries based on a Zinc-Polymer system incorporating a novel, inexpensive, environmentally sustainable solvent. This work is necessitated by the problems associated with petrol and diesel powered vehicles and the limitations of batteries available for electric vehicles.

Acknowledgements

PolyZion was an FP7 framework programme European-led consortium combining world-class research organisations in ionic liquids, conducting polymers, zinc deposition, pulse charging and batteries. Several SME (small / medium enterprise) partners with expertise in technology development and specialised materials, combined with large industrial partners holding industrial experience of battery manufacture and state-of-the-art testing facilities were part of the project.

I would like to acknowledge the University of Leicester and the FP7 framework programme European-led consortium for funding this research.

I would like to thank all my colleagues at the University of Leicester for their support, encouragement and resources that have helped me complete this research. I would like to express my gratitude to my supervisor Prof. Karl Ryder and other academics in the Physical Chemistry research group, Prof. Andrew Abbott, Prof. Robert Hillman, Dr Robert Harris, Dr Andrew Ballantyne, Dr Emma Smith and Dr Gero Frisch for their assistance and guidance. I owe the biggest thanks to my family and friends for being so supportive.

I would like to dedicate this work to the loving memory of my Auntie, Janet Easton. She has been a huge inspiration in my life. She always looked forward and strived to find solutions to every problem.

	Page
Abstract	i
Acknowledgements	iii
Contents	iv
Abbreviations	x
Chapter 1	
Introduction	
1.1 Advantages of Electric Vehicles	2
1.2 Types of Batteries	3
1.2.1 Lead Acid (Pb-Acid)	5
1.2.2 Nickel Metal Hydride (NiMH)	6
1.2.3 Lithium Ion (Li-Ion)	7
1.2.4 Current State of the Art for Commercial Zinc Batteries	9
1.3 Zinc-Polymer (Zn-Polymer) Battery Concept	
1.3.1 PolyZion Battery	10
1.3.2 Current Research into Zn-Polymer Batteries	13
1.4 Battery Electrolytes	15
1.5 Ionic Liquids (ILs) and Deep Eutectic Solvents (DESS)	15
1.6 Zinc Anode	17
1.7 Conducting Polymer Cathode	18
1.8 References	25

Chapter 2

Experimental Methodology

2.1	Electrochemical Quartz Crystal Microbalance (EQCM)	29
2.2	X-Ray Photo-electron Spectroscopy (XPS)	34
2.3	References	37

Chapter 3

Experimental and Data Analysis Procedures

3.1	Materials	
3.1.1	Monomer Solution Preparation	41
3.1.2	Deep Eutectic Solvent (DES) Formulations	42
3.1.2.1	Type II	43
3.1.2.2	Type III	43
3.1.2.3	Type IV	43
3.2	Polymer DC Capacitance Studies	
3.2.1	Experimental	
3.2.1.1	General Experimental	44
3.2.1.2	Bracketed Electrolyte	
	DC Capacitance Experiments	46
3.2.1.3	Long Term Cycling	
	DC Capacitance Experiments	47

3.2.2	Data Analysis	47
3.2.2.1	Mass, Thickness and Polymerisation Efficiency Determination	47
3.2.2.2	DC Capacitance from Chronoamperometric Studies	49
3.2.2.3	DC Capacitance from Cyclic Voltammetric Studies	50
3.3	Electrochemical Quartz Crystal Microbalance (EQCM) Polymer Studies	
3.3.1	Experimental	51
3.3.2	Data Fitting	54
3.3.3	Data Analysis	60
3.4	X-Ray Photo-electron Spectroscopy (XPS)	
3.4.1	Experimental	60
3.4.2	Spectrometer Settings	62
3.5	Determination of the Electrochemically Active Area of an Electrode by Chronoamperometry	63
3.6	References	65

Chapter 4

Polymer DC Capacitance Studies

4.1	Introduction	
4.1.1	Determination of DC Capacitance	68
4.1.2	Current Research on DC Capacitances of Conducting Polymers	71

4.2	Objectives	73
4.3	Results and Discussion	73
4.3.1	Potentiodynamic Polymer Deposition	76
4.3.2	Mass, Thickness, Polymerisation Efficiency Determination and DC Capacitance by Chronoamperometry	78
4.3.3	DC Capacitance by Cyclic Voltammetric Studies	81
4.3.3.1	Mass Specific Capacitances of PEDOT Films	82
4.3.3.2	Mass Specific Capacitances of PPy Films	89
4.3.3.3	Mass Specific Capacitances of PTP (LiClO₄ / MeCN) Films	90
4.3.3.4	Mass Specific Capacitance of PEDOT-hexylPy Films	99
4.4	Conclusions	100
4.5	References	103

Chapter 5

Comparison of the Charging Behaviour of PEDOT in DESs

5.1	Introduction	
5.1.1	Objectives	105
5.1.2	Experimental	110
5.2	Results and Discussion - Redox Driven Exchange Processes of Potentiodynamically Deposited PEDOT	112
5.2.1	Behaviour in 0.1 M LiClO₄ / MeCN	113
5.2.2	Behaviour in ZnCl₂ / EG (Type IV) DES	118
5.2.3	Behaviour in Ethaline (Type III) DES	137
5.2.4	Behaviour in Ethaline containing 0.3 M ZnCl₂	141

5.3	Conclusions	143
5.4	References	146

Chapter 6

Comparison of the Charging Behaviour of PTP in DESs

6.1	Introduction	149
	6.1.1 Objectives	149
	6.1.2 Literature Review on Monomer TP	151
	6.1.3 Experimental	161
6.2	Redox Driven Exchange Processes of PTP	
	6.2.1 Behaviour in LiClO₄ / MeCN	166
	6.2.2 Behaviour in ZnCl₂ / EG (Type IV) DES	170
	6.2.3 Behaviour in Ethaline (Type III) DES	174
	6.2.4 Behaviour in Ethaline containing 0.3 M ZnCl₂	180
6.3	Conclusions	182
6.4	References	185

Chapter 7

XPS of Conducting Polymer Films

7.1	Introduction	
	7.1.1 Objectives	187
	7.1.2 Experimental	190

7.2	Elemental Composition of PEDOT Films	
7.2.1	Pristine PEDOT Film	192
7.2.2	PEDOT Redox Behaviour in LiClO ₄ / MeCN	196
7.2.3	PEDOT Redox Behaviour in Ethaline (Type III) DES	198
7.2.4	PEDOT Redox Behaviour in ZnCl ₂ / EG (Type IV) DES	200
7.3	Elemental Composition of PTP Films	
7.3.1	Pristine PTP Film	201
7.3.2	PTP Redox Behaviour in LiClO ₄ / MeCN	205
7.3.3	PTP Redox Behaviour in Ethaline (Type III) DES	205
7.3.4	PTP Film XPS Sulphur : Nitrogen Ratios	206
7.4	Summary of XPS Data	
7.4.1	PEDOT Films	209
7.4.2	PTP Films	211
7.5	Conclusions	213
7.6	References	215

Chapter 8

Conclusions and Further Work

8.1	Conclusions	217
8.2	Further Work	218

Abbreviations

ChCl	Choline Chloride
CV	Cyclic Voltammogram
DC	Direct Current
DES	Deep Eutectic Solvent
EDAX	Energy Dispersive Analysis by X-Rays
EG	Ethylene Glycol
EQCM	Electrochemical Quartz Crystal Microbalance
ESCA	Electron Spectroscopy for Chemical Analysis
EV	Electric Vehicle
FAB	Fast Atom Bombardment
FTIR	Fourier Transform Infrared Spectroscopy
FWHH	Full Width at Half Height
HBD	Hydrogen Bond Donor
HEV	Hybrid Electric Vehicle
HSA	Hemi-Spherical Analyser
IL	Ionic Liquid
MSC	Mass Specific Capacitance
PG	Propylene Glycol
QAS	Quaternary Ammonium Salt
RT	Room Temperature
SCE	Standard Calomel Electrode
SEM	Scanning Electron Microscopy
TSM	Thickness Shear Mode
XPS	X-Ray Photo-electron Spectroscopy

Chapter 1

Introduction

1.1 Advantages of Electric Vehicles

1.2 Types of Batteries

1.2.1 Lead Acid (Pb-Acid)

1.2.2 Nickel Metal Hydride (NiMH)

1.2.3 Lithium Ion (Li-Ion)

1.2.4 Current State of the Art for Commercial Zinc Batteries

1.3 Zinc-Polymer (Zn-Polymer) Battery Concept

1.3.1 PolyZion Battery

1.3.2 Current Research into Zn-Polymer Batteries

1.4 Battery Electrolytes

1.5 Ionic Liquids (ILs) and Deep Eutectic Solvents (DESs)

1.6 Zinc Anode

1.7 Conducting Polymer Cathode

1.8 References

Chapter 1

Introduction

1.1 Advantages of Electric Vehicles

Currently, most vehicles on the roads are petrol or diesel powered, which have issues concerning high environmental impact, longevity of the fuel supply and cost of the fuel, with petrol prices ≈ 16 p per mile, being higher than the cost of the electricity used in electric vehicles ≈ 3 p per mile ^{[1][2]}. Exhaust fumes emitted from internal combustion engines contain high proportions of CO₂ and NO_x gases, which have a detrimental effect on the global atmosphere, in regards to ozone depletion and global warming. Protocols have been employed to lower CO₂ emissions *e.g.* Montreal and Kyoto protocol ^[3], however, more measures are required to lower emissions further in sectors other than just manufacturing industries. In 2005, 15% of global greenhouse gas emissions originated from the transport sector, 73% of which came from road transport ^[4]. This, along with rising fossil fuel prices yearly and the fear of the looming shortage of peak oil (predicted to run out in next 150 years) has created a high interest drive to develop new batteries for electric vehicles (EVs) and hybrid EVs.

Current battery technologies for HEVs and small EVs have technological limitations, high costs in regards to the components needed to produce the vehicle and / or environmental limitations. Despite this the global market for HEVs and EVs is growing rapidly and is expected to top \$2 billion by 2015.

This research project encompasses fundamental material and process advances in ionic liquids electrolytes, rechargeable zinc electrodes and conducting polymers.

1.2 Types of Batteries

A battery is a device which converts chemical energy through redox reactions to electrical energy. Batteries come in two types, either primary or secondary batteries. Primary batteries are built in a charged state and can only be used once. Secondary batteries, more commonly known as rechargeable batteries can be used multiple times. However, there will be a limit on how many times it can be charged and discharged.

Within the battery sector, the term anode refers to the negative electrode, where oxidation of the electrode material takes place during discharge, releasing electrons to the external circuitry. Therefore, the term cathode refers to the positive electrode where reduction of the electrode material takes place, accepting electrons from the external circuitry.

The total amount of energy the battery can hold (*i.e.* charge storage capability) is defined as the energy density (W h kg^{-1}). It is optimum to have a high energy density for a longer usage time. Power density (W kg^{-1}) indicates the amount of power a battery can deliver when required *i.e.* the delivery rate of charge. In vehicles or any other electronic applications, it is essential for the battery to supply enough power to drive multiple tasks with a constant operating voltage. Comparison of the performances of different energy storage devices can easily be visualised by plotting power density as a function of energy density. This is known as a Ragone plot ^[5], presented in **Fig. 1.1**.

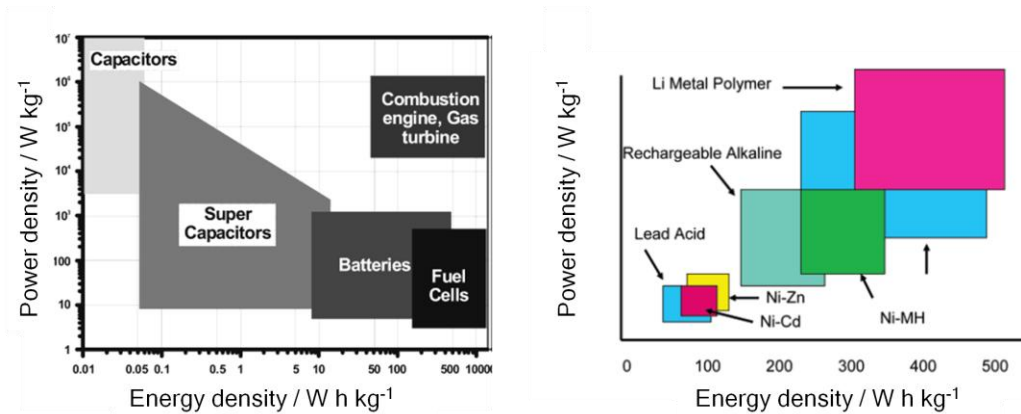


Fig. 1.1 - A Ragone plot of different energy storage devices (images from Winter and Brodd^[5]).

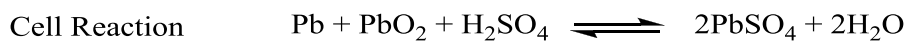
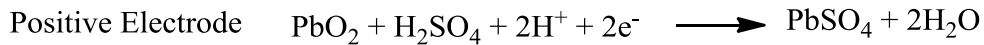
Commercially available EVs utilise either a Pb-Acid (*e.g.* 1998 Ford Ranger EV, milk floats and fork-lift trucks), NiMH (*e.g.* Toyota Prius) or a recent better technological development Li-Ion batteries (*e.g.* Post 2004 Toyota Prius and Tesla Roadster Model S)
[6] [7] [10].

The key incentives and aims of developing new batteries chemistries are to^{[5] [8] [9]}:

- Increase energy densities
- Increase power densities
- Extend the lifetime of the batteries (*i.e.* reduce maintenance)
- Extend temperature range (*i.e.* have the ability be to used in hot / cold climates)
- Improve the energy content compared to petrol / diesel powered vehicles
- Reduce component costs to be comparable to petrol / diesel powered vehicles
- Develop a good general purpose battery system

1.2.1 Lead Acid (Pb-Acid)

The Pb-Acid battery consists of a lead anode, a lead dioxide cathode and a sulphuric acid electrolyte. The lead species are converted to lead sulphate and water to release electrical energy.



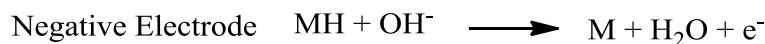
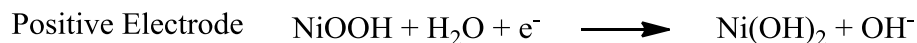
This system is one of the most commonly used, as the components are cheap and it performs reliably. They are generally used as starter batteries for internal combustion engine vehicles termed SLI batteries (starting-lighting-ignition batteries), traction units in pallet trucks (*e.g.* milk floats), as emergency back-up power units and in applications that generally require a high load current ^[10]. The open circuit potential of a Pb-Acid cell is 2.06 V with a theoretical energy density of 167 W h kg⁻¹. This is much higher than the energy density that can be realistically achievable because of inefficiencies related to the inert components of the battery; for 1 hour and 5 hour discharge times the energy density is 40 W h kg⁻¹ and 35 W h kg⁻¹ respectively. As well as the inert components reducing the achievable energy storage capabilities, irreversible energy losses may occur with other components of the device and there may also be limited utilisation of the active material due to poor ion mobility within the active material ^[5].

The power density achieved for a short period discharge is 250 W kg⁻¹ (corresponding to a current density of 300 mA cm⁻²) ^[10]. Pb-Acid batteries can be prone to gassing, H₂ and O₂ can be given off when fully charged or nearly fully charged, occurring when all

the lead sulphate has been converted back to Pb and PbO₂. This has the potential to cause a potentially hazardous build up of pressure inside the device. This safety issue has been averted through the development of the valve regulated sealed Pb-Acid battery (VRLA Battery), which releases the pressure if it becomes too high. Pb-Acid batteries can self discharge by sulphation (PbSO₄) when left for a long period (> 2 weeks) in a partially discharged state, as PbSO₄ is not conducting and can form large crystals when left over time, which is harder to convert back to Pb and PbO₂. A slow recharge of the battery can potentially rectify this problem if it arises ^[11]. The advantage of a Pb-Acid battery is that it has a low internal resistance (*i.e.* minimal drop in voltage when current is drawn from the battery) ^[11]. However, these batteries do have low energy densities ^[10].

1.2.2 Nickel Metal Hydride (NiMH)

The NiMH battery consists of a nickel oxyhydroxide cathode and a metal electrode with the ability to form a stable hydride (metal hydride anode), with an aqueous sodium or potassium hydroxide electrolyte.



The open circuit potential of a NiMH cell is 1.3 V with a theoretical energy density of 278 W h kg⁻¹; with *ca.* 65 W h kg⁻¹ realistically achievable. The power density is normally *ca.* 200 W kg⁻¹ ^[10]. NiMH batteries are easier to dispose of compared to Ni / Cd primary batteries and also more environmentally friendly. These are also much

safer than Ni / H₂ rechargeable (secondary) batteries due to the use of a metal hydride compared to hydrogen gas. These batteries have found large scale use in a variety of wireless consumer products. Self discharge and drops in capacity do have a high chance of occurring with NiMH batteries, which are major drawbacks of this technology ^[10]. Disadvantages of this technology also include poor charge retention and deterioration of battery performance if over charged ^[11].

1.2.3 Lithium Ion (Li-Ion)

Pb-Acid and NiMH battery technologies have reached their practical limits in terms of performance, thus are unable to keep up with demands for high power ($> 500 \text{ W kg}^{-1}$) and energy density ($>100 \text{ W h kg}^{-1}$), *i.e.* a large number of cells are required for a high output voltage.

Li-Ion batteries were developed in an aim to overcome performance issues associated with previous technologies, with Sony commercialising the first Li-Ion battery in 1991 ^[11]. However, Li-Ion batteries do have multiple drawbacks. They have a reduced lifetime in comparison to Pb-Acid and NiMH batteries, variable temperature dependent performance and components associated with high costs; chemicals and packaging ^[6]. The major concern is with the safety of the cell modules, which are constructed in sealed polymer bags. Upon impact, overexposure or malfunction due to contaminants, short circuiting of the battery can occur, which leads to extreme gas / heat formation and electrical sparking. This causes the polymer bag to expand and rupture to vent the gas inside, which can then potentially ignite, this is termed thermal runaway.

The Li-Ion battery consists of a lithiated carbon material for the anode, a metal oxide intercalated with lithium cathode, in an organic electrolyte containing a lithium-based salt. Recently solid polyethylene oxide (PEO) based electrolytes have been employed in Li-Ion batteries ^[12]. This is an improvement because of the enhanced safety of the solid electrolyte in comparison to liquid electrolytes.



The metal oxide used can vary the capacity of the battery and its temperature stability *e.g.* LiNiO₂ has a high capacity but can decompose at lower temperatures than LiMn₂O₄ and LiCoO₂ (LiMn₂O₄ and LiCoO₂ have a lower capacity than LiNiO₂) ^{[11][12]}.

Depending on the materials used, the open circuit potential can vary between 2.5 – 4 V with a theoretical energy density of 750 W h kg⁻¹ with *ca.* 80 – 90 W h kg⁻¹ practically achievable. The power density given for a short period discharge is *ca.* 100 W kg⁻¹. Li-Ion batteries are higher in terms of energy density than NiMH and Pb-Acid batteries, but have a lower power density. However, they have the advantage of using lighter weight materials than the other technologies, thereby improving the power to weight ratio of the EV or hybrid EV. They also have the advantage of a high operating voltage range.

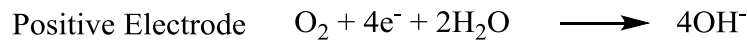
Li-Ion batteries are also used in commercial items such as mobile phones and laptops. The greater cost of components of Li-Ion batteries compared to NiMH and Pb-Acid

batteries brings about another drawback to this technology, along with the safety concerns highlighted above. Disadvantages of Li-Ion batteries include the use of a non aqueous electrolyte which can increase the internal resistance of the battery. Li-Ion batteries can also exhibit capacity fade, *i.e.* a drop in performance over time, this can result from a multitude of factors associated with electrolyte or active material deterioration.

1.2.4 Current State of the Art for Commercial Zinc Batteries

At present, there are a few zinc based batteries which are commercially available with the most reported types being Ag-Zn and Zn-Air batteries. A Ag-Zn battery consists of a AgO cathode and a Zn anode. This is an expensive battery technology due to the use of Ag, therefore limiting the use in commercial electrical vehicles and tends to only be restricted for use in specialist applications such as air and space travel, weapons technology and high value electronic products. This battery has a very high power density ($500 - 800 \text{ W kg}^{-1}$) and open circuit potential of 1.86 V and an energy density of ($80 - 100 \text{ W kg}^{-1}$).

Zn-Air batteries are recent technological innovations that have the ability to attain high energy densities and utilise low cost components. Initially they were produced as primary batteries and essentially refuelled by inserting a new zinc anode once the initial zinc electrode has been spent ^{[7] [13]}. The electrode reactions for a standard Zn-Air battery are described below.



Research is being conducted to improve Zn-Air batteries, due to problems associated with the metal electrode and the air catalyst. Zn-Air batteries are currently being developed as rechargeable batteries. Their chemistry means that this type of battery could essentially be described as a hybrid between a battery and a fuel cell. However, Zn-Air batteries do have problems associated with the parasitic reaction shown above which produces hydrogen which can then react with the zinc causing a reduction in the amount of active material present, effecting the lifetime of the Zn-Air battery ^[13]. Also, Li-Air batteries are being researched however these batteries are some way off from commercial production. Both these technologies will probably be the most likely competition for the Zn-Polymer rechargeable battery being developed in this research.

1.3 Zinc-Polymer (Zn-Polymer) Battery Concept

1.3.1 PolyZion Battery

The concept explored by this project is to create a class of novel Zn-Polymer batteries, which aim to address some of the issues associated with the previous technologies discussed above. These systems combine new low cost, air and moisture insensitive and environmentally benign solvents called Deep Eutectic Solvents (DESs) (analogous to

ionic liquids), deposition of nano-structured zinc deposits and the behaviour of conducting polymers within these media. The advantages associated with the use of a DES electrolyte within the battery are high current efficiency, low gassing and the elimination of zinc dendritic growth. The Zn-Polymer battery system is shown below in **Fig. 1.2** along with the electrode reactions and overall cell reaction.

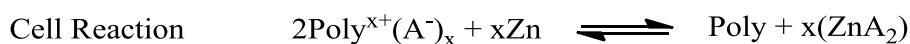
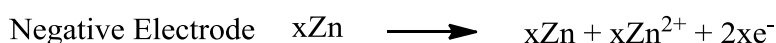
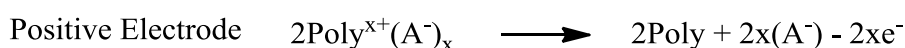
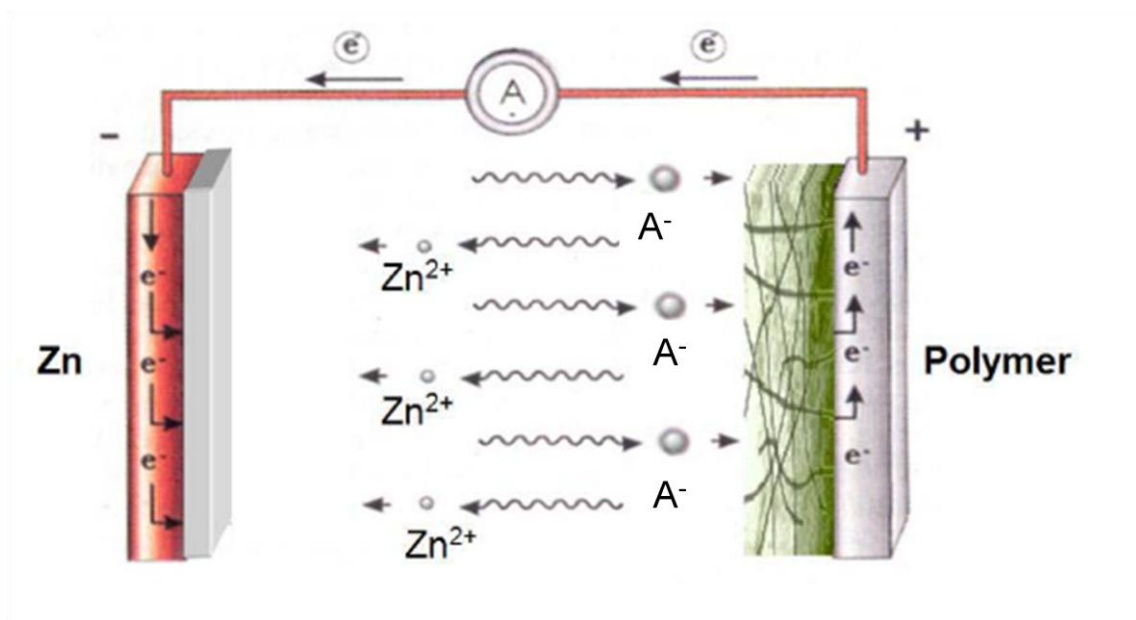


Fig. 1.2 - Schematic of the charging of the Zn-Polymer battery, electrode reactions and the overall cell reaction. A^- represents the anion of the DES.

The developments in zinc rechargeable batteries were initially beset with two major difficulties, namely dendritic growth and hydrogen gas evolution. Dendrites (branch like metal deposits) build up during charge-discharge cycling and inevitably lead to short circuits unless abated. Hydrogen evolution on the other hand, takes place during recharge and as a result of self-discharge. The use of DESs should help to overcome

these two problems. The DES electrolyte will strive to eliminate hydrogen gas evolution due to the absence of water and a greater electrochemical potential stability range (wider cathodic window) As well as optimising the DES for nano-structured zinc deposition, a key objective is to investigate the behaviour of conducting polymers in the DESs. The incorporation of a conducting polymer will aim to increase the overall power output by negating the need for a membrane separator for the two halves of the cell. In addition the light weight polymeric material will also strive to improve power / energy density *i.e.* power to weight ratio.

One benefit of not using a membrane separator is that Ohmic drop across the cell is minimised; this is especially important for high current applications such as electric vehicles and load-levelling. Other benefits arise from the simplification of the cell design; omitting the cell membrane both reduces construction costs and means there is one fewer component that has the potential to fail. Due to the very different chemistries of the two electrode systems, the behaviour of the zinc and polymer electrodes are considered separately. The behaviour of the polymer electrode will be the focus of this thesis, in terms of investigating the coupled charge / mass transport of the polymer, to be able to understand the influence of the DES on the overall cell performance of the proposed system. In this project the aim will be to address the behaviour of conducting polymers in high ionic strength and solvent free electrolytes; the ingress and egress of counter ions (and potentially co-ions) into and out of the polymer matrix during redox switching; how the structure of the polymer matrix affects counter-ion mobility; rate of charge / discharge of the polymer; and double layer effects. Recent research suggests that the electrochemical performance of conducting polymers in ionic liquids is superior

in terms of cycleability and fast reversible redox behaviour compared to aqueous and organic electrolytes ^[17].

The performance targets for the Zn-Polymer battery are to achieve a power density in the region of 1 kW kg⁻¹, an energy density of 100 W h kg⁻¹, a life cycle greater than 100 cycles, a large open circuit potential (\approx 1.9 V) and a cell cost of less than £ 400 per kW h. **Table 1.1** summarises the PolyZion cell targets along with comparative battery specifications for existing technologies. This shows the development of a Zn / Polymer / DES battery aims to improve energy density in comparison to previous technologies as well as reducing production costs due to its very simple design. The prices in **Table 1.1** do not include circuitry and casing costs (prices shown are between 30 – 50% of actual cost); however construction and integration costs are common to all technologies.

Table 1.1 - PolyZion cell targets and comparative battery specifications for existing technologies.

Cell Metric	Battery		
	NiMH	Li-ion	PolyZion
Specific Cell Energy Density / W h kg ⁻¹	50 - 100	100 - 200	250 <i>feasible</i>
Specific Cell Power Density / W kg ⁻¹	150 - 500	1000 - 2000	1000
Open Cell Potential per cell / V	1.2	3.2 - 3.7	1.9
Cycle life	500 - 1500	> 1500	> 1000
Price (€ / kW h)	500 - 1000	500 - 1000	< 500

The background and the innovative technology for each cell component are described in the sections below.

1.3.2 Current Research into Zn-Polymer Batteries

A number of groups are investigating the Zn-Polymer battery concept. A zinc poly(aniline-co-m-aminophenol) battery has been produced by Zhang *et al.* ^[14]

incorporating a zinc anode (on a Pt foil) with a poly(aniline-co-m-aminophenol) film on two sides of a Pt foil and employing an ammonium chloride aqueous electrolyte containing 2 M ZnCl_2 at pH 4.7. The battery was charged and discharged between 0.75 V and 1.45 V, with a capacity and energy density of $137.5 \text{ A h kg}^{-1}$ and 152 W h kg^{-1} respectively, for a discharge process with a 1 mA current, a 1.11 V discharge voltage and a Coulombic efficiency of 91.6%. An issue of increased charge transfer resistance occurred due to the high concentration of zinc chloride, which caused a formation of a layer of ZnCl_2 on the polymer cathode ^[14].

A zinc-polyaniline rechargeable battery has recently been reported by Li *et al.* ^[15] consisting of a Zn foil anode, a polyaniline cathode (polymerised from dilute sulphuric acid containing 1.2 M 1-ethyl-3-methylimidazolium-ethyl sulphate (EMIES)) with a ZnCl_2 containing ammonium chloride solution at pH 6. For a discharge current of 0.5 mA cm^{-2} , a 1.2 V discharge voltage gave capacity and energy densities of $141.2 \text{ A h kg}^{-1}$ and $169.4 \text{ W h kg}^{-1}$ respectively and a Coulombic efficiency of 89.4%. The higher pH in this case, gave corrosion protection to the zinc, which reduced any potential self discharge, loss of capacity of the battery and zinc dendrite formation ^[15].

Zhijiang and Chengwei ^[16] have tested the feasibility of a zinc polyindole battery comprising of a zinc foil anode, a polyindole based cathode (composite with a poly(tetrafluoroethylene) binder and carbon black) and an aqueous ZnCl_2 electrolyte at pH 6. This achieved $80 - 60 \text{ A h kg}^{-1}$ capacity density at discharge current densities $200 - 1000 \text{ A m}^{-2}$.

1.4 Battery Electrolytes

The other component critical for a battery, as well as electrode composition is the electrolyte; this provides separation between electrodes and a source of dopants during redox reactions.

The voltage range over which the electrolyte is neither oxidised or reduced, is classified as the potential window of a system. Conventional electrolytes (aqueous or organic solvents) suffer from narrow potential windows (*i.e.* high potentials can cause decomposition of the solvent and hydrogen evolution) and a high volatility, which affects operational voltage, battery lifetime and has issues regarding environmental safety. Conventional electrolytes are partially responsible for limitations of polymers in battery applications, such as poor environmental stability and short lifetimes ^[17]. Utilising an ionic liquid (IL) or DES electrolyte should help to tackle the issues associated with the previous technologies above.

1.5 Ionic Liquids (ILs) and Deep Eutectic Solvents (DESS)

A basic definition of an IL is a molten salt, which has an m.p. generally taken as $< 100^{\circ}\text{C}$, but with the m.p. of the individual components being significantly higher.

ILs aim to facilitate a high energy density for the battery through a wide electrochemical potential window. ILs exhibit a low volatility, due to the low vapour pressure of the components *cf.* organic solvents.

Abbott *et al.* ^[18] have developed a range of solvents termed Deep Eutectic Solvents (DESS), which are based on similar principles to ionic liquids. They consist of a cation

(salt) and complex anion, which interact by H-bonds (from a hydrogen bond donor) or metal halide bonds through the anion of the salt compared to conventional ILs which interact through electrostatic forces ^[18]. These liquids have many advantages over conventional ionic liquids, such as imidazolium salts and chloro-metallate melts, in that they are much cheaper and tolerant to a wide variety of operating conditions including tolerance to moderate amounts of water (*ca.* 5%) ^[19]. Initially three eutectic types were produced and classified simply using the general formula $[R_1R_2R_3RN^+] X^- \cdot Y^-$

Type I Eutectic $Y = MCl_x$, $M = Zn, Sn, Fe, Al, Ga$

Type II Eutectic $Y = MCl_x \cdot yH_2O$ or $M(NO_3)_x \cdot yH_2O$ $M = Cr, Co, Cu, Ni, Fe, Zn$

Type III Eutectic $Y = R_5Z$, $Z = CONH_2, COOH, OH$

Type II eutectics consist of a quaternary ammonium salt $[R_1R_2R_3RN^+] X^-$ and a hydrated metal salt $Y = MCl_x \cdot yH_2O$ or $M(NO_3)_x \cdot yH_2O$. The quaternary ammonium salt used is choline chloride, (2-hydroxyethyl)trimethylammonium chloride (ChCl) which performs better than other quaternary ammonium salts, due to being asymmetric and containing a polar functional group (these both aid in lowering the freezing point and eutectic point of the eutectic).

Type III eutectics consist of ChCl and a hydrogen bond donor either ethylene glycol (Ethaline), propylene glycol (Propaline) or urea (Reline).

The newest additions to the DESs series are Type IV eutectics ^[20] consisting of a metal halide and a hydrogen bond donor. These were thought to be a hybrid between Type I and Type III eutectics described above, however DESs only formed from a small range

of metal salts and hydrogen bond donor combinations ^[20]. This suggested that metal complex formation occurred through the bonding of oxygen or nitrogen from the donor to the metal centre, not solely through hydrogen bonding. Type IV eutectics differ from Type III eutectics, in that they have a lower viscosity, which allows ease of handling and improves ion mobility in the liquid, arising from a lesser degree of hydrogen bonding *cf.* Type III eutectics. Type II and IV eutectics contain a high concentration of Zn species in solution, required for the deposition / dissolution of Zn, potentially giving them an advantage over Type III eutectics. All the DES types are air and moisture stable, beneficial for ease and low cost of the large scale production of electrolyte required for an electrochemical device compared to conventional ionic liquids which require an inert atmosphere (N₂ or Ar⁺).

1.6 Zinc Anode

Zinc is an excellent material for battery applications; it is abundant, inexpensive, non-toxic and lightweight relative to most metals. As mentioned above the adoption of zinc electrodes into rechargeable batteries has initially been beset by zinc dendritic growth during deposition and hydrogen evolution, caused by charging and discharging of the cell. Zinc has been used as a battery electrode, largely in primary batteries as charge-discharge issues are not a problem, as the cells are only used once.

The charging of the cell involves the deposition of metallic zinc at the electrode which is at a potential which places it in competition with hydrogen evolution if an aqueous electrolyte is used in the battery. In fact if the electrolyte is sufficiently acidic, self-discharge of the battery will occur, whereby zinc reacts with the aqueous electrolyte also forming hydrogen. This is not only a safety concern (exploding cells) but also

lowers cell efficiency and shelf-life. The DES electrolyte should eliminate problems associated with self-discharge of rechargeable Zn cells because of the very low proton activity of many DES type ionic liquids, even when their components are protic (*e.g.* choline chloride and ethylene glycol) *i.e.* the liquids have Brønsted acidity^[18].

A second issue, of no less importance, is that the zinc deposits often take the form of dendrites, with the consequence of both poor adhesion of the zinc deposit and the possibility of short circuits (from long needle-shaped crystallites). For these reasons previous rechargeable Zn battery technologies are well known to have either a poor life-cycle, or involve complex electrode structures, additives, shielding layers or zinc slurries in an attempt to avoid dendritic growth^{[21][22][27]}. Numerous researchers are investigating solutions to combat these problems in zinc batteries^{[15][23]}. As discussed earlier, there are now alternative technologies such as Zn-Air^{[13][24]}. But the Zn / Polymer / DES battery is simple and potentially inexpensive.

1.7 Conducting Polymer Cathode

Conducting polymers have continued to stimulate academic interest in terms, of polymer dynamics and exploitation of physical properties for practical applications; including electrochromic displays *e.g.* ‘smart windows’, chemical / bio sensors, actuators *e.g.* valves and artificial limbs^[25], corrosion protection and energy storage / conversion^[26].

Conducting (π conjugated) polymers are ideal materials for battery electrodes due to being lightweight (advantageous in vehicle applications, where low weight is essential for performance to improve the power: weight ratio) and also have a good potential

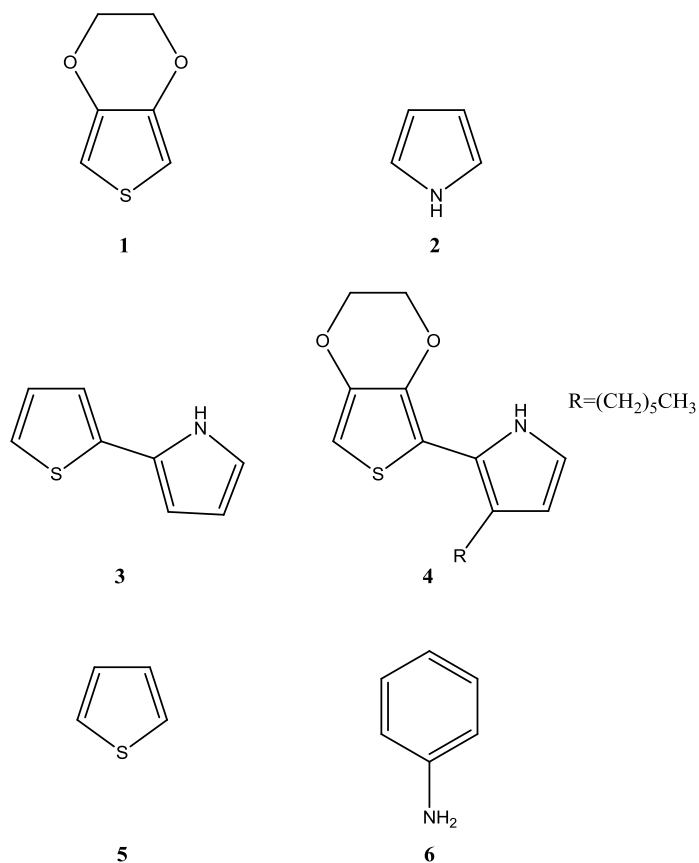
range over which they are conducting. This is better for the battery to achieve a higher output voltage (*i.e.* a low anodic oxidation potential for monomer and high redox potential of polymer will be optimum).

During charging / discharging of a polymer cathode, the polymer mass on the electrode would remain essentially constant, as no deposition or dissolution occurs. This has an added benefit over metal electrodes where metal deposition and dissolution occur during battery usage. Therefore, no morphological features are formed from polymer films that could potentially cause short circuiting with the other electrode, *cf.* dendrites during metal deposition (this is an issue with zinc deposited from aqueous systems ^[27]). This negates the use of a separator membrane in a battery cell which contains at least one polymer electrode ^[26]. Also the preparation of a polymer film costs less in comparison to metal electrodes. However, there is the potential for the polymer to swell during charging / discharging due to the ingress and egress of counter-ions and solvent; this can be accounted for in the cell design. Polymer swelling would be a problem that could lead to short circuiting of the battery and / or possibly detachment from the electrode.

Polymerisation of a heterocyclic monomer proceeds via cation radical formation by oxidation, either chemically (using an oxidising agent *e.g.* lead dioxide PbO₂ or ferric chloride FeCl₃ ^[28]) or electrochemically (by applying a positive potential) ^[28]. Examples of heterocycles that can be polymerised to produce conducting polymers are shown below in **Scheme 1.1**, aniline **6** a cyclic compound can also be polymerised by oxidation. Of the compounds shown, the behaviour of polymers from EDOT **1**, pyrrole **2** and the novel monomers PTP **3** and EDOT-hexylPy **4** were investigated in

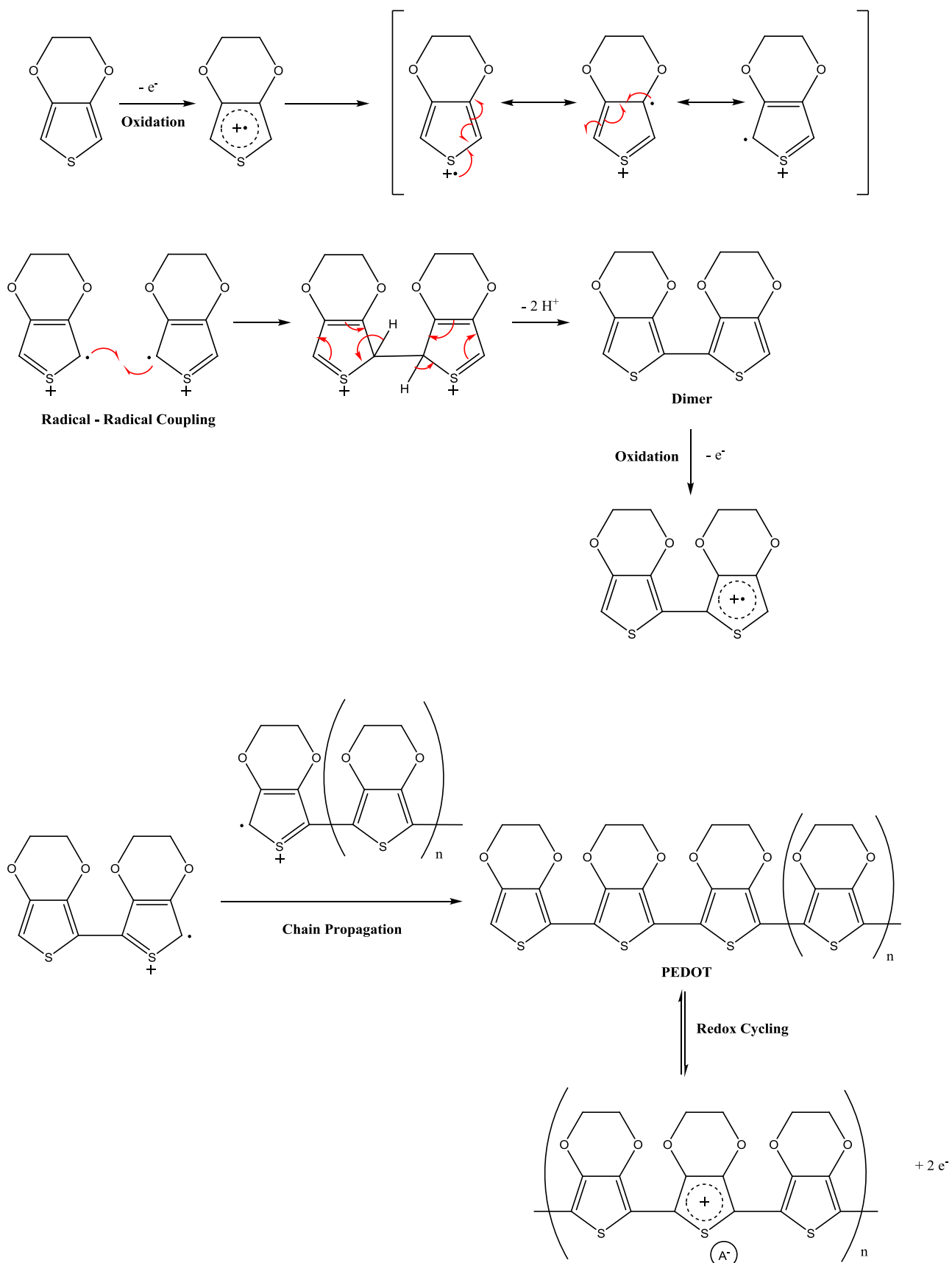
this thesis. Thiophene **5** and aniline **6** were omitted from this study due to time constraints and also to focus efforts on only a few polymer systems (polymers from heterocyclic monomers **1 – 4**).

PEDOT has received a great deal of attention for use in electronic devices and has recently been utilised as a material for binders in Li-Ion batteries because of its high conductivity (500 S cm^{-1}) and charge capacity $\approx 30 \text{ mA h g}^{-1}$ after 500 cycles ^[29]. The redox and conductive properties rely on the transfer of ions between the polymer film and the electrolyte ^[30]. Investigation of mobile species transfer by using electrochemical quartz crystal microbalance (EQCM) experiments are the focus of this research and attempts to go beyond the state of the art to quantify this behaviour of polymer films in high ionic media.



Scheme 1.1 - A selection of monomers which can be polymerised to produce conducting polymers, 3,4-ethylenedioxythiophene **1**, pyrrole **2**, 2-(thiophene-2-yl)-1H pyrrole **3**, 2-(2,3-dihydrothieno[3,4-b][1,4]dioxin-5-yl)-1H-pyrrole **4**, thiophene **5** and aniline **6**.

The mechanism of polymerisation is shown in **Scheme 1.2** using EDOT as an example. Two cation radicals couple and dehydrogenation proceeds to form a dimer followed by chain propagation (**Scheme 1.2**). The same mechanism occurs for other heterocyclic monomers.



Scheme 1.2 - Polymerisation of EDOT beginning with formation of a dimer by radical coupling, leading to polymer chain propagation and PEDOT redox cycling, A^- = anion to maintain charge neutrality.

π conjugated chains are not solely responsible for conductivity in the film, the ions in solution are necessary too. The oxidised polymer can be termed p-doped (positively doped) and for neutrality, charge compensating species (dopants) are incorporated into the film or expelled during growth. This can be summarised in a two step reaction; oxidation of monomer to a neutral film and partial charge formation to form a conductive polymer (cationic form) ^[28] (**Scheme 1.2**). To acquire an appreciable conductivity, partial charge extraction from the chain occurs as a consequence of dopants in the polymerisation electrolyte. Conduction of charge throughout the film depends on intra-chain mobility (resonance charge transport along chain) and inter-chain mobility (involving the hopping or tunnelling of charge between chains). As the energy for intra-chain transport is much lower than inter-chain, the intra-chain transport (resonance) occurs first and when the radical cation (formed by removal of $1 e^-$ over a series of 3 monomer units) reaches the end of a chain or a defect in the chain, inter-chain (charge hopping) proceeds to a neighbouring chain ^[28].

Conducting polymerisation electrochemically produces a direct coating onto a conducting substrate and enables polymer morphology and the doping level of the polymer attained to be controlled. The polymer can act as an electrode by intercalation / de-intercalation of dopants. Sweeping to positive (anodic) potentials, the polymer is in its conductive state and becomes oxidised. In contrast, sweeping to negative (cathodic) potentials, the polymer is in its non-conductive state and becomes reduced. The potential that redox switching occurs depends on the polymer ^[31].

A range of electrochemical methodologies in combination with acoustic impedance electrochemical quartz crystal microbalance experiments (EQCM) ^{[32] [33] [34] [35] [36] [37]}

[38] [39] will be used to examine DC capacitance behaviour, ion / solvent transport properties (polymer dynamics) and for electrochemical characterisation of the polymer films prepared [40] [41] [42] [43] [44]. X-Ray Spectroscopy (XPS) will be used to probe polymer composition (through element ratios) and investigate whether ions from the electrolyte are trapped in the oxidised or reduced polymer [45] [46] [47] [48] [49] [50] [51] [52] [53]. These fundamental research advances will aid in the selection of potential candidate conducting polymer cathodes and electrolytes for novel Zn-Polymer secondary batteries.

The aim of the studies in this thesis is to understand the processes of coupled charge / mass transport so as to understand the influence of the DES on performance of the proposed cell. This work aims to utilise a DES to overcome the limiting processes in molecular solvents.

1.8 References

- [1] Article in the Telegraph motoring section, Mike Rutherford, 6th September 2012
- [2] Report from SMMT (Society of Motor Manufacturers and Traders) Motor Industry Facts 2013 www.smmt.co.uk
- [3] Velders GJM, Andersen SO, Daniel JS, Fahey DW and McFarland M, *PNAS*, 2007, 104, 12, 4814-4819
- [4] Gerssen-Gondelach SJ and Faaij APC, *J. Power Sources*, 2012, 212, 111-129
- [5] Winter M and Brodd RJ, *Chem. Rev.*, 2004, 104, 10, 4245-4269
- [6] Spotnitz R, *2005 IEEE Vehicle Power and Propulsion Conference*, 2005, 334-337
- [7] Larminie J and Lowry J, *Electric Vehicle Technology Explained*, 2003, Wiley, England
- [8] Kiehne HA, *Battery Technology Handbook*, 2003, Marcel Dekker Inc, New York, 2nd Edn
- [9] Conway BE, *Electrochemical Supercapacitors: Scientific Fundamentals and Technological Applications*, Kluwer Academic/Plenum Publishing, 1999, New York
- [10] Hamann CH, Hamnett A and Vielstich W, *Electrochemistry*, 1998, Wiley-VCH, Germany, 1st Edn
- [11] Bard AJ and Stratmann M, *Encyclopedia of Electrochemistry*, 2007, Wiley-VCH, Germany, Macdonald DD and Schmuki P, Vol 5 Electrochemical Engineering
- [12] Xia Y, Fujieda T, Tatsumi K, Prosini PP and Sakai T, *J. Power Sources*, 2001, 92, 1-2, 234-243
- [13] Li Y and Dai H, *Chem. Soc. Rev.*, 2014, 43, 15, 5257-5275
- [14] Zhang J, Shan D and Mu S, *J. Power Sources*, 2006, 161, 1, 685-691
- [15] Li S, Zhang G, Jing G and Kan J, *Synthetic Metals*, 2008, 6, 158, 242-245
- [16] Zhijiang C and Chengwei H, *J. Power Sources*, 2011, 196, 24, 10731-10736
- [17] Lu W, Fadeev AG, Qi B, Smela E, Mattes BR, Ding J, Spinks GM, Mazurkiewicz J, Zhou D, Wallace GG, MacFarlane DR, Forsyth SA and Forsyth M, *Science*, 2002, 297, 5583, 983-987
- [18] Abbott AP and McKenzie KJ, *Phys. Chem. Chem. Phys.*, 2006, 8, 37, 4265-4279
- [19] Abbott AP, Ryder KS and Koenig U, *Trans. Inst. Met. Fin.*, 2008, 86, 4, 196-204
- [20] Abbott AP, Barron JC, Ryder KS and Wilson D, *Chem. Eur. J.*, 2007, 13, 22, 6495-6501
- [21] Kan JQ, Xue HG and Mu SL, *J. Power Sources*, 1998, 74, 1, 113-116
- [22] Bass K, Mitchell PJ, Wilcox GD and Smith J, *J. Power Sources*, 1991, 35, 3, 333-351
- [23] Vatsalarani J, Kalaiselvi N and Karthikeyan R, *Ionics*, 2009, 15, 1, 97-105
- [24] Lee JS, Kim ST, Cao R, Choi NS, Lui M, Lee KT and Cho J, *Adv. Energy Mater.*, 2011, 1, 1, 34-50
- [25] Inzelt G, Pineri M, Schultze JW and Vorotyntsev MA, *Electrochimica Acta*, 2000, 45, 15-16, 2403-2421

-
- [26] Ponce de Leòn C, Campbell SA, Smith JR and Walsh FC, *Trans. Inst. Met. Finish.*, 2008, 86, 1, 34-40
- [27] Lee CW, Sathiyarayanan K, Eom SW and Yun MS, *J. Power Sources*, 2006, 160, 2, 1436-1441
- [28] Skotheim TA and Reynolds JR, *Handbook of Conducting Polymers – Theory, Synthesis, Properties and Characterization*, 2007, CRC Press, USA 3rd Edn
- [29] Blanchard F, Carré B, Bonhomme F, Biensan P, Pagès H and Lemordant D, *J. Electroanal. Chem.*, 2004, 569, 9, 203-210
- [30] Niu L, Kvarnström C and Ivaska A, *J. Electroanal. Chem.*, 2004, 569, 2, 151-160
- [31] Morvant MC and Reynolds JR, *Synthetic Metals*, 1998, 92, 1, 57-61
- [32] Bund A and Neudeck S, *J. Phys. Chem. B*, 2004, 108, 46, 17845-17850
- [33] Hillman AR, Daisley SJ and Bruckenstein S, *Electrochem. Commun.*, 2007, 9, 6, 1316-1322
- [34] Hillman AR, Daisley SJ and Bruckenstein S, *Electrochimica Acta*, 2008, 53, 11, 3763-3771
- [35] Hillman AR, Efimov I and Ryder KS, *J. Am. Chem. Soc.*, 2005, 127, 47, 16611-16620
- [36] Hillman AR, Daisley SJ and Bruckenstein S, *Phys. Chem. Chem. Phys.*, 2007, 9, 19, 2379-2388
- [37] Huang JH, Kekuda D, Chu CW and Ho KC, *J. Mater. Chem.*, 2009, 19, 22, 3704-3712
- [38] Huang JH, Hsu CY, Hu CW, Chu CW and Ho KC, *ACS Applied Materials & Interfaces*, 2010, 2, 2, 351-359
- [39] Ispas A, Peipmann R, Adolphi B, Efimov I and Bund A, *Electrochimica Acta*, 2011, 56, 10, 3500-3506
- [40] Skotheim TA and Reynolds JR, *Handbook of Conducting Polymer - Processing and Applications*, , 3rd Edition
- [41] Snook GA, Peng C, Fray DC and Chen GZ, *Electrochem. Commun.*, 2007, 9, 1, 83-88
- [42] Snook GA, Kao P and Best AS, *J. Power Sources*, 2011, 196, 1, 1-12
- [43] Snook GA and Chen GZ, *J. Electroanal. Chem.*, 2008, 612, 1, 140-146
- [44] Lota K, Khomenko V and Frackowiak E, *J. Physics and Chemistry of Solids*, 2004, 65, 2-3, 295-301
- [45] Ruffo R, Celik-Cochet A, Posset U, Mari CM and Schottner G, *Solar Energy Materials & Solar Cells*, 2008, 92, 2, 140-145
- [46] Bach CMG and Reynolds JR, *J. Phys. Chem.*, 1994, 98, 51, 13636-13642
- [47] Pandey GP, Rastogi AC and Westgate CR, *J. Power Sources*, 2014, 245, 857-865
- [48] Pandey GP and Rastogi AC, *Electrochimica Acta*, 2013, 87, 158-168
- [49] Chusuei CC and Goodman DW, *Encyclopedia of Physical Science and Technology – Analytical Chemistry, X-Ray Photo-electron Spectroscopy Chapter*, 2001, Elsevier Ltd, Oxford UK, 3rd Edn

-
- [50] Spanninga SA, Martin DC and Chen Z, *J. Phys. Chem. C*, 2009, 113, 14, 5585-5592
- [51] Spanninga SA, Martin DC and Chen Z, *J. Phys Chem C*, 2010, 114, 35, 14992-14997
- [52] Spanninga SA, Martin DC and Chen Z, *J. Phys Chem C*, 2010, 114, 35, 14998-15004
- [53] Taouil AE, Lallemand F, Hihn JY, Melot JM, Blondeau-Patissier V and Lakard B, *Ultrasonics Sonochemistry*, 2011, 18, 1, 140-148

Chapter 2

Experimental Methodology

2.1 Electrochemical Quartz Crystal Microbalance (EQCM)

2.2 X-Ray Photo-electron Spectroscopy (XPS)

2.3 References

Chapter 2

Experimental Methodology

2.1 Electrochemical Quartz Crystal Microbalance (EQCM)

Conducting polymers have attracted immense technological interest as materials for a wide range of practical applications and uses. The redox driven transfers of mobile species between an electrolyte and a conducting polymer are integral to the functioning of the polymer within an electrochemical device.

The identities of the mobile species for different conducting polymer / electrolyte systems have been explored by a number of authors in the published literature, utilising an instrument called an electrochemical quartz crystal microbalance (EQCM). This tool can be used to investigate the physical properties of a material in contact with a quartz crystal, via the exploitation of the piezo-electric effect of quartz. This technique can monitor gravimetric and / or viscoelastic changes in surface attached species, dependent on the properties of the material deposited on to it and the study conducted ^[1]. This technique has been used to investigate the behaviour of conducting polymers, such as poly 3,4-ethylenedioxythiophene (PEDOT) **1**, polypyrrole (PPy) **2** ^{[2] [3] [4] [5] [6] [7]} and polyaniline (PAni) **6** ^{[8] [9] [10] [11] [12]}, focussing on understanding polymer dynamics and coupled charge / mass transport processes.

Devices used for the EQCM technique comprised of quartz crystals with well-defined thicknesses, covered partially with metal on both faces to form two electrodes. The metal most commonly used is Au but other noble metals such as Pt can also be used ^[13]. When a radio frequency (rf) oscillating voltage is applied across the gold electrode,

mechanical deformation of the quartz occurs. This creates a shear wave which oscillates parallel to the electrode on the quartz crystal (**Fig. 2.1**)^[14].

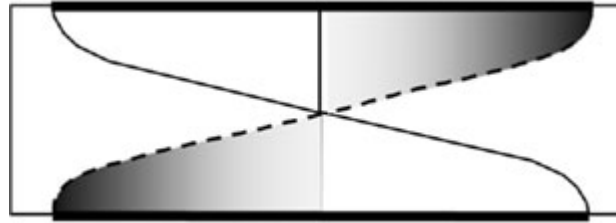


Fig. 2.1 - The motion of a shear wave oscillation for an unloaded quartz crystal^[14].

The frequency of this oscillation is known as the resonant frequency. The value of this fundamental frequency (f_0) is a function of the thickness (h) of the quartz crystal. A range of high frequency resonance devices can be prepared by cutting the quartz crystal at certain angles. AT cut crystals are cut at an angle of 35.25° from the z-axis. These are more commonly used than other crystal cuts, as they are cheaper to produce and their resultant response remains stable over a wider range of temperatures. For example, BT and SC cut crystals, prepared by cutting the crystal at different angles have slightly different temperature dependencies. The angles the crystals are cut for AT and BT cut crystals is shown in **Fig. 2.2**. As the shear mode oscillation is exploited in all these devices, they can also be termed thickness shear mode (TSM) resonators. Low frequency vibrational mode crystals (flexure mode and extensional mode) are used in consumer electronics such as watches and radios.

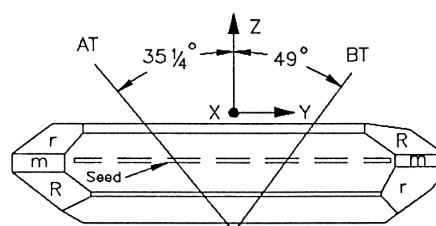


Fig. 2.2 - AT and BT cut TSM resonators from a single quartz crystal. Reproduced from the Fortiming Corporation website.

In this thesis, 10 MHz AT cut crystals ($h = 166 \mu\text{m}$) were used with the full admittance spectra (electrical conductance G vs frequency f) and peak frequencies recorded. The EQCM technique relied on either: both faces of the crystal exposed to air (referred to as a ‘dry’ crystal measurement), or one face exposed to air and the other exposed to a liquid medium (referred to as a liquid immersed ‘wet’ crystal measurement). In the latter case, the electrode exposed to a liquid medium, acted as a working electrode during electrochemical studies ^[14].

Changes in surface attached species to the working electrode will cause a corresponding shift in resonant frequency. As the mass on the crystal increased, the resonant frequency decreased. The opposite occurred as the mass on the crystal decreased, the resonant frequency increased. It was possible to relate decreases in resonant frequency of 1 Hz to increases in mass of *ca.* 1.1 ng, by the Sauerbrey equation (derived in 1959) **(2.1)** ^[15] ^[16].

$$\Delta f = \frac{-2(f_0)^2 \Delta m}{\sqrt{\mu_q \rho_q} A} \quad (2.1)$$

Where f_0 is the frequency of the unloaded (dry) crystal, μ_q is the shear modulus of the quartz ($2.947 \times 10^{11} \text{ g cm}^{-1} \text{ s}^{-2}$), ρ_q is the density of the quartz (2.648 g cm^{-3}), Δm is the change in mass and A is the piezo-active area ^[16]. The piezo-active area of the crystal, the area of one electrode defined by the overlap of the other electrode, was 0.21 cm^2 . The square root of the product of the shear modulus μ_q and the density of quartz ρ_q is known as the mechanical impedance of the quartz ^[3].

For the Sauerbrey equation **(2.1)** to be applied, the attached mass such as a polymer or metal has to be rigid to allow it to oscillate simultaneously with the quartz at the same

frequency. An acoustically thin film has a thickness that is of similar magnitude to the acoustic decay length of the shear wave in the media in-contact with the quartz crystal (air or liquid media). The acoustic decay length (δ) in a liquid, *i.e.* the penetration depth of the shear wave into the liquid can be determined by (2.2), where η_L and ρ_L are the viscosity and density of the liquid respectively.

$$\delta = \left(\frac{\eta_L}{\pi f_0 \rho_L} \right) \quad (2.2)$$

This determines the amount of viscously coupled fluid to the quartz crystal resonator (Fig. 2.3) [1]. Liquid further than the acoustic decay length can therefore be considered as bulk electrolyte. The acoustic decay length is *ca.* about 1% of the quartz crystal thickness. For a 10 MHz crystal the thickness of the quartz is 166 μm , therefore films *ca.* 2 μm are classified as acoustically thin [14].

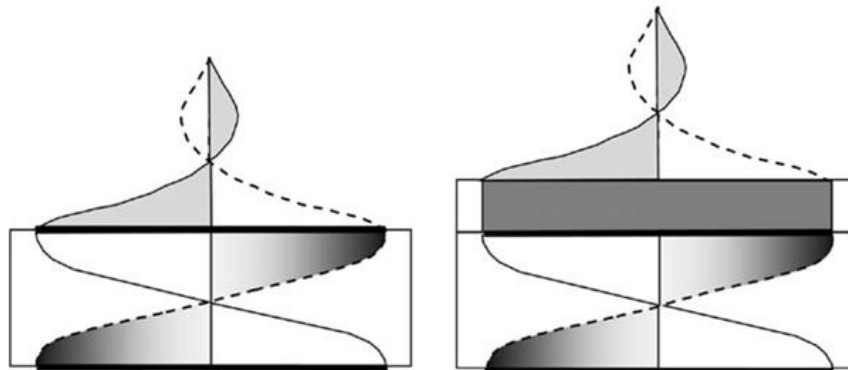


Fig. 2.3 - Left image - Motion of oscillation of EQCM crystal in a liquid, Right image - Motion of oscillation of EQCM crystal coated with an acoustically thin film in a liquid [1].

For a few decades it was thought that a liquid in contact with the crystal would severely dampen the frequency, so much so that the Sauerbrey equation (2.1) could not be applied. However, in the late 1980s, Kanazawa and Gordon showed that the Sauerbrey equation (2.1) could still be applied if the damping of the crystal by the liquid was considered [17][18].

The frequency of a crystal exposed to a liquid will decrease in frequency due to the presence of viscously coupled fluid. Depending on the viscosity of the liquid, the bandwidth of admittance spectra will vary, the greater the viscosity of the liquid, the greater the increase in bandwidth (*i.e.* the liquid dampens the signal). However, once immersed in the relevant electrolyte, the resonant frequency and the bandwidth stabilise (do not fluctuate). The bandwidth of the frequency response therefore related to the damping and loss of energy of the oscillation of the shear wave.

The damping of the frequency of the quartz crystal resonator by the liquid can provide an insight into the viscosity and density of this liquid media. **Fig. 2.4** shows the damping of the dry crystal by the 0.1 M LiClO₄ / MeCN solution, in which the bandwidth w (FWHH) increased by 2.342 kHz. **Fig. 2.5** shows the damping of the admittance spectra of the bare Au crystal in contact with Type III and Type IV DESs.

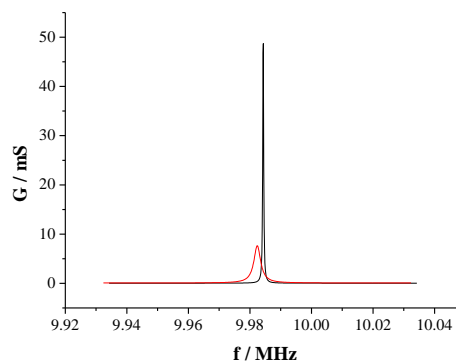


Fig. 2.4 - Admittance spectra for the bare Au crystal in air (**Black**) $w = 316$ Hz Q-factor = 31595 and the bare Au crystal in contact with 0.1 M LiClO₄ / MeCN (**Red**) $w = 2.66$ kHz Q-factor = 3755.

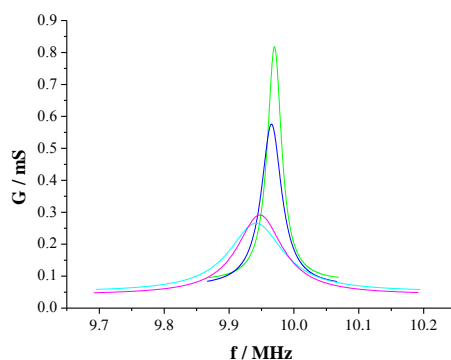


Fig. 2.5 - Admittance spectra for the bare Au crystal in contact with **Ethaline (Green)** $w = 26.43$ kHz Q-factor = 377.21, **Propaline (Blue)** $w = 37.82$ kHz Q-factor = 264, **ZnCl₂ / EG (Cyan)** $w = 102$ kHz Q-factor = 98, **ZnCl₂ / acetamide (Magenta)** $w = 85.272$ kHz Q-factor = 117.

The DESs dampen the signal significantly, in comparison to the bare Au crystal in air and the bare Au crystal exposed to a conventional molecular solvent, acetonitrile. Therefore, for clarity these admittance spectra are reported on a separate graph. Ethaline and Propaline give a similar magnitude perturbation on the admittance spectra, owed to their similar formulation of 1 ChCl: 2 HBD, with the hydrogen bond donor being ethylene glycol and propylene glycol respectively. The increase in bandwidth of Propaline with respect to Ethaline shows Propaline has a slightly higher viscosity due to the longer chain diol used. Propylene glycol has a viscosity of 48.6 cP (at 25 °C) compared to ethylene glycol which has a lower viscosity at 16.9 cP (at 25 °C) [19]. ZnCl₂ / EG and ZnCl₂ / acetamide have a similar bandwidth, due to similar viscosities. However, the bandwidth increase is larger than the Type III DESs, due to the slightly greater viscosities of the Type IV DESs [20] [21].

2.2 X-Ray Photo-electron Spectroscopy (XPS)

X-Ray Photo-electron Spectroscopy (XPS) is a surface analytical technique which probes the binding energy of electrons that have been photo-excited out of the surface

region of a solid (focusing on the top 10 nm of the surface). This technique can determine the elemental composition of a surface, as well as the chemical state of atoms present. For this reason XPS can also be termed Electron Spectroscopy for Chemical Analysis (ESCA). The technique involves an incident beam of x-rays, which photo-excites low energy core electrons (*e.g.* 1s and 2p orbital electrons) out of the solid to a detector, which records the kinetic energy of electrons; which in turn determines the binding energy of these emitted electrons. All elements except hydrogen can be detected, with the binding energy (eV) related to a specific element ^[22]. The binding energy E_B of a detected electron is found from the kinetic energy E_{kin} recorded, the energy of the incident photon beam $h\nu$, and the work function Φ of the spectrometer **(2.3)** ^[23].

$$E_B = h\nu - E_{kin} - \Phi \quad \text{(2.3)}$$

The core level binding energies for elements are documented in XPS handbooks and databases ^[24] ^[25]. The XPS instrumentation comprises of an x-ray gun, a transfer lens, a hemi-spherical analyser (HSA), a detector and two or more vacuum chambers ^[25]. The HSA acts as a kinetic energy filter to allow differently defined kinetic energy electrons to reach the detector. This is achieved by creating a potential difference between the two hemispheres to form an electrostatic field, which filters the electrons as they enter the analyser from the entrance slit, shown in the schematic in **Fig. 2.6** below. A retard plate (negative electrode) slows down the electrons to the required energy for detection of a particular element (to produce high resolution spectra) or the potential of the retard plate can be swept to produce survey spectra ^[23]. Slow electrons (*i.e.* with a low kinetic energy) are attracted to the inner hemisphere and are neutralised; whilst high kinetic energy electrons above the energy required to be detected, collide into the outer

hemisphere^[23]. This technique has been used by numerous researchers to determine the surface elemental composition of conducting polymers^{[26][27]}.

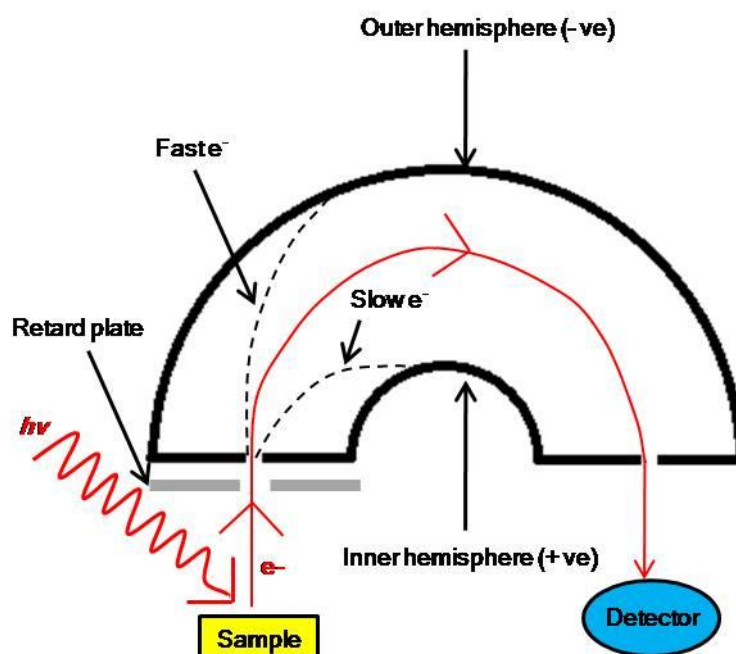


Fig. 2.6 - X-Ray Photo-electron Spectroscopy (XPS) instrumentation schematic highlighting the function of the hemi-spherical analyser^[23].

2.3 References

- [1] Hillman AR, *J. Solid State Electrochem.*, 2011, 15, 7-8, 1647-1660
- [2] Skopek MA, Mohamoud MA, Ryder KS and Hillman AR, *Chem. Commun.*, 2009, 8, 935-937
- [3] Plieth W, Bund A, Rammelt U, Neudeck S and Duc LM, *Electrochimica Acta*, 2006, 51, 11, 2366-2372
- [4] Briseno AL, Baca A, Zhou QZ, Lai R and Zhou FM, *Analytica Chimica Acta*, 2001, 441, 1, 123-134
- [5] Vorotyntsev MA, Vieil E and Heinze J, *J. Electroanal. Chem.*, 1998, 450, 1, 121-141
- [6] Efimov I, Koehler S and Bund A, *J. Electroanal. Chem.*, 2007, 605, 1, 61-67
- [7] Bruckenstein S, Chen J, Jureviciute I and Hillman AR, *Electrochimica Acta*, 2009, 54, 13, 3516-3525
- [8] Mohamoud MA and Hillman AR, *Electrochimica Acta*, 2006, 51, 27, 6018-6024
- [9] Bauermann LP and Bartlett PN, *Electrochimica Acta*, 2005, 50, 7-8, 1537-1546
- [10] Orata D and Buttry DA, *J. Am. Chem. Soc.*, 1987, 109, 12, 3574-3581
- [11] Inzelt G, *Electrochimica Acta*, 2000, 45, 22-23, 3865-3876
- [12] Hillman AR, Mohamoud MA and Efimov I, *Anal. Chem.*, 2011, 83, 14, 5696-5707
- [13] Gileadi E, *Physical Electrochemistry – Fundamentals, Techniques and Applications*, 2011, Wiley-VCH, Germany
- [14] Bard AJ, Stratman M and Unwin PR, *Encyclopedia of Electrochemistry*, 2003, Wiley-VCH, Germany, Hillman AR, Volume III
- [15] Sauerbrey G, *Z. Phys.*, 1959, 155, 206-222
- [16] Inzelt G, Bard AJ and Scholz F, *Electrochemical Dictionary*, 2008, Springer-Verlag, Berlin, Germany
- [17] Kanazawa KK and Gordon JG, *Analytica Chimica Acta*, 1985, 175, 99-105
- [18] Kanazawa KK and Gordon JG, *Anal. Chem.*, 1985, 57, 8, 1770-1771
- [19] Abbott AP, Barron JC, Frisch G, Gurman S, Ryder KS and Silva AF, *Phys. Chem. Chem. Phys.*, 2011, 13, 21, 10224-10231
- [20] Abbott AP and McKenzie KJ, *Phys. Chem. Chem. Phys.*, 2006, 8, 37, 4265-4279
- [21] Abbott AP, Barron JC, Ryder KS and Wilson D, *Chem. Eur. J.*, 2007, 13, 22, 6495-6501
- [22] Poole C, Townshend A and Worsfold P, *Encyclopedia of Analytical Science*, 2005, Elsevier Ltd, Oxford, UK, 2nd Edn, Tougaard S, X-Ray Photo-electron Spectroscopy, 446-456
- [23] Attard G and Barnes C, *Surfaces*, 1998, Oxford University Press, Oxford, UK
- [24] Wagner CD, Riggs WM, Davis LE, Moulder JF and Muilenberg GE, *Handbook of X-Ray Photo-electron Spectroscopy*, 1979, Perkin-Elmer Corporation, USA

-
- [25] Fairley N, CASA XPS Manual 2.3.15, 2009, Casa Software Ltd
- [26] Ruffo R, Celik-Cochet A, Posset U, Mari CM and Schottner G, *Solar Energy Materials & Solar Cells*, 2008, 92, 2, 140-145
- [27] Bach CMG and Reynolds JR, *J. Phys. Chem.*, 1994, 98, 51, 13636-13642

Chapter 3

Experimental and Data Analysis Procedures

3.1 Materials

3.1.1 Monomer Solution Preparation

3.1.2 Deep Eutectic Solvent (DES) Formulations

3.1.2.1 Type II

3.1.2.2 Type III

3.1.2.3 Type IV

3.2 Polymer DC Capacitance Studies

3.2.1 Experimental

3.2.1.1 General Experimental

3.2.1.2 Bracketed Electrolyte DC Capacitance Experiments

3.2.1.3 Long Term Cycling DC Capacitance Experiments

3.2.2 Data Analysis

3.2.2.1 Mass, Thickness and Polymerisation Efficiency Determination

3.2.2.2 DC Capacitance from Chronoamperometric Studies

3.2.2.3 DC Capacitance from Cyclic Voltammetric Studies

- 3.3 Electrochemical Quartz Crystal Microbalance (EQCM) Polymer Studies**
 - 3.3.1 Experimental**
 - 3.3.2 Data Fitting**
 - 3.3.3 Data Analysis**
 - 3.4 X-Ray Photo-electron Spectroscopy (XPS)**
 - 3.4.1 Experimental**
 - 3.4.2 Spectrometer Settings**
 - 3.5 Determination of the Electrochemically Active Area of an Electrode by Chronoamperometry**
 - 3.6 References**
-

Chapter 3

Experimental and Data Analysis Procedures

In this chapter, experimental and data analysis procedures used throughout this thesis are outlined. These include details on materials used, DES formulations, sample preparations, data acquisition, data analysis and instrumental technique protocols.

3.1 Materials

All chemicals were used as received (Aldrich and Fisher) with the novel monomers 2-(thiophene-2-yl)-1H pyrrole (referred to as TP) and 2-(2,3-dihydrothieno[3,4-b][1,4]dioxin-5-yl)-3-hexyl-1H-pyrrole (referred to as EDOT-hexylPy) used as received from a project collaborator, Prof. BA Trofimov (Irkutsk Institute of Chemistry) ^{[1][2]}.

3.1.1 Monomer Solution Preparation

Solutions of 0.1 M LiClO₄ / MeCN (0.266 g, 2.5 mmol in 25 cm³ MeCN), 0.1 M LiClO₄ / H₂O (0.266 g, 2.5 mmol in 25 cm³ H₂O) and 0.1 M LiBF₄ / MeCN (0.234 g, 2.5 mmol in 25 cm³ MeCN) were prepared for the addition of the relevant monomer.

0.1 M EDOT **1** (0.355 g, 2.5 mmol) solutions were prepared with either 0.1 M LiBF₄ or 0.1 M LiClO₄ in MeCN. 0.1 M Py **2** (0.168 g, 2.5 mmol) solutions were prepared with 0.1 M LiClO₄ in H₂O. For the novel monomers TP **3** and EDOT-hexylPy **4**, solutions were prepared using either 0.1 M LiBF₄ or 0.1 M LiClO₄ in MeCN, at concentrations of 0.05 M (0.1865 g, 2.5 mmol) or 0.1 M (0.373 g, 2.5 mmol) for TP **3** and

33 mM EDOT-hexylPy **4** (240 mg, 0.8 mmol). These concentrations were used throughout the project unless otherwise stated.

3,4-ethylenedioxythiophene (EDOT) **1**, a clear colourless liquid, produced a clear colourless solution on addition to either 0.1 M LiClO₄ or LiBF₄, both in MeCN. Pyrrole (Py) **2**, a clear yellow liquid produced a clear colourless solution on addition to 0.1 M LiClO₄ / H₂O. The novel monomer TP **3**, a light brown / red coloured powder, produced a brown / red solution in 0.1 M LiBF₄ / MeCN and an orange solution in 0.1 M LiClO₄ / MeCN. After three polymerisations from the same monomer solution, a dark green coloured solution formed. The novel monomer EDOT-hexylPy **4** a dark green oil, produced a dark green coloured solution on addition to 0.1 M LiBF₄ / MeCN and 0.1 M LiClO₄ / MeCN.

3.1.2 Deep Eutectic Solvent (DES) Formulations

Choline chloride ([HOC₂H₄N(CH₃)₃]⁺Cl⁻), ZnCl₂, Zn(NO₃)₂.6H₂O and the hydrogen bond donors (ethylene glycol, 1,2-propylene glycol, acetamide, 1,6-hexanediol and urea) were used as received (Aldrich and Fisher). The DESs were prepared by stirring the two components at *ca.* 60 °C until a colourless homogenous liquid was achieved ^[3] ^[4]. Care had to be taken on heating the liquids containing Zn species, as temperatures greater than 50 °C caused discolouration of the DES if not efficiently stirred. All DESs were stored in a thermostatted oven at 40 °C, which ensured that the choline chloride (ChCl) did not precipitate out of the DESs. If this occurred, homogenous liquids were easily restored by re-stirring and heating.

3.1.2.1 Type II

Zn(NO₃)₂·6H₂O : ChCl Type II DES was formed using a 1 : 2 molar ratio, Zn(NO₃)₂·6H₂O (26.632 g, 89.53 mmol, 297.46 g mol⁻¹) and ChCl (25 g, 0.1791 mol, 139.59 g mol⁻¹) which produced *ca.* 40 cm³ of liquid.

3.1.2.2 Type III

Ethaline, Propaline and Reline were prepared by using ChCl and a hydrogen bond donor; either ethylene glycol (HOC₂H₄OH) referred to as EG, 1,2-propylene glycol (H₃CCH(OH)CH₂OH) referred to as PG or urea (H₂NC(O)NH₂) respectively, in a 1 : 2 ChCl : HBD molar ratio.

ChCl (50 g, 0.3582 mol, 139.59 g mol⁻¹), a quaternary ammonium salt, heated with EG (44.453 g, 0.7162 mol, 62.07 g mol⁻¹) produced *ca.* 80 cm³ of Ethaline; with PG (54.499 g, 0.7162 mol, 76.09 g mol⁻¹) produced *ca.* 95 cm³ of Propaline; or with urea (43.011 g, 0.7162 mol, 60.05 g mol⁻¹) produced *ca.* 80 cm³ of Reline.

3.1.2.3 Type IV

All ZnCl₂ based eutectics consisted of ZnCl₂ (13.630 g, 0.1 mol, 136.3 g mol⁻¹) with a hydrogen bond donor in either a 1 : 3 molar ratio (1,6-hexanediol (HO(CH₂)₆OH) liquid) or 1 : 4 molar ratio (ethylene glycol and acetamide (CH₃C(O)NH₂) liquids).

The ethylene glycol based liquid was prepared by 1 ZnCl₂ : 4 EG (24.828 g, 0.4 mol, 62.07 g mol⁻¹) forming *ca.* 25 cm³ of liquid. The acetamide based liquid was prepared by 1 ZnCl₂ : 4 acetamide (23.628 g, 0.4 mol, 59.07 g mol⁻¹) forming *ca.* 25 cm³ of

liquid. The 1,6-hexanediol based liquid was prepared by 1 ZnCl₂ : 3 1,6-hexanediol (35.451 g, 0.3 mol, 118.17 g mol⁻¹) forming *ca.* 40 cm³ of liquid.

3.2 Polymer DC Capacitance Studies

3.2.1 Experimental

3.2.1.1 General Experimental

All DC capacitance studies were conducted using an electrochemical cell with a three electrode configuration: Pt working electrode (1.258 mm diameter), Pt foil counter electrode and Ag wire quasi-reference electrode. Data acquisitions were performed on an Autolab PGSTAT20 potentiostat / galvanostat controlled with General Purpose Electrochemical System (GPES version 9.0) software. Prior to each experiment or polymerisation, the working electrode was polished with 0.3 µm alumina on a polishing block and subsequently rinsed with water, acetone and acetonitrile. Counter and reference electrodes were polished gently with P100 abrasive paper and subsequently rinsed in the same manner as the working electrode. After polishing, the working electrode was cycled between vertex potentials $-1.2 \leq E / V \leq 1.2$ in 0.1 M LiClO₄ / MeCN or 0.1 M LiClO₄ / H₂O to ensure there were no contaminants present before polymerisation. Each electrolyte was N₂ purged prior to electrochemistry (to remove the majority of O₂) and all experiments were conducted under a N₂ atmosphere. Voltammograms were recorded with an equilibration period at 0 V for 30 s and a step potential of 2.44 mV (*i.e.* the potential resolution).

To establish the optimum oxidation potential for potentiostatic deposition, polymers (PEDOT, PPy, PTP and PEDOT-hexylPy) were potentiodynamically deposited on to

the polished Pt working electrode by cycling the potential in the range of $-1.3 \leq E / V \leq 1.3$ at a scan rate $\nu = 20 \text{ mV s}^{-1}$ for 5 or 10 scans.

Polymer films were subsequently deposited potentiostatically at the relevant oxidation potential for a specific time (PPy (0.8 V), PEDOT (1.1 V), PTP (0.8 V) for 30 s, 60 s or 120 s; for PEDOT-hexylPy (0.8 V and 1.1 V in one experiment) 180 s or 210 s at each potential) in an attempt to vary film thickness. Depositions were conducted at ambient temperature under a N_2 atmosphere with an interval time between data points of 0.05 s. The polymer modified Pt electrodes were rinsed with water, acetone and acetonitrile, dried and then transferred to monomer free electrolyte (the same electrolyte in which they were deposited, either 0.1 M LiClO_4 or 0.1 M LiBF_4 in MeCN or H_2O). The films were subjected to a double potential step involving an equilibration period of 0 V for 30 s; stepping to the oxidation potential of the polymer for 60 s and back to 0 V for 30 s. This charging (Q_{ox}) and discharging (Q_{red}) of a film produced a current response which initially spiked, followed by a time-dependent decay for each potential step. These time-dependent decays were due to the diffusion of charge balancing species between polymer and electrolyte. Integration of the resulting $i(t)$ traces enabled the quantification of the charge passed during a double potential step experiment (Q_{ox} and Q_{red}) and the total potentiostatic deposition charge (Q_{psd}). The ratio of $Q_{ox} : Q_{red}$ is 1 : 1 for a chemically reversible process. From experimental values for PEDOT the ratio was found to be 1 : 1, from this it can be deduced that the charging / discharging of PEDOT was a chemically reversible process. Therefore, assuming the same for the other polymers, averages of the absolute values of Q_{ox} and Q_{red} (\bar{Q}) were used for the calculation of the mass and the thickness of the polymer, polymerisation efficiency and the DC capacitance in monomer free electrolyte.

Further films were deposited potentiostatically under the same conditions to produce films for cyclic voltammetric studies in conventional electrolytes and DESs at 40 °C. For each electrolyte, the potentials of the polymer modified Pt electrodes were cycled between two vertex potentials (reported for each experiment in results section) for 3 scans at scan rates $v = 5, 10, 20, 50, 100, 150$ and 200 mV s^{-1} . The films were transferred to each electrolyte to investigate the DC capacitance of the polymers in each solvent system, enabling selection of an optimum electrolyte for a battery and for further electrochemical studies. The same polymer could not always be transferred to each electrolyte studied due to adhesion problems; therefore separate films had to be deposited to screen the conventional electrolytes and the DES systems. Methods for determining DC capacitance from two techniques, chronoamperometry **3.2.2.2** and cyclic voltammetry **3.2.2.3**, are discussed further in the data analysis section below and the results section (**Chapter 4**).

3.2.1.2 Bracketed Electrolyte DC Capacitance Experiments

Bracketed experiments tested whether the polymer films had changed in any physical way as a consequence of having been immersed in DESs, by observing whether the electrochemical behaviour varied when transferring a polymer from one electrolyte to another. Two PEDOT and two PTP films were potentiostatically deposited as described above, for 60 s at 1.1 V (PEDOT) and 0.8 V (PTP). One film was subjected to redox cycling at 40 °C between $-0.5 \leq E / \text{V} \leq 0.8$ at scan rates $v = 5, 10, 20, 50, 100, 150$ and 200 mV s^{-1} , firstly in 0.1 M $\text{LiClO}_4 / \text{MeCN}$, secondly in Ethaline, and the sequence repeated. The other film was studied in the same manner, immersed firstly in $\text{ZnCl}_2 / \text{EG}$, secondly in $\text{ZnCl}_2 / \text{acetamide}$ and repeated in the two electrolytes. DC capacitances were determined for each electrolyte as a function of scan rate.

3.2.1.3 Long Term Cycling DC Capacitance Experiments

The long term stabilities of PEDOT and PTP deposited potentiostatically from 0.1 M LiClO₄ / MeCN and 0.1 M LiBF₄ / MeCN respectively (1.1 V for PEDOT and 0.8 V for PTP, both for 120 s) were assessed by cyclic voltammetric studies. The freshly deposited films were subjected to double potential steps in the same manner as in section 3.2.1.1 and subsequently redox cycled in only one electrolyte at 20 mV s⁻¹ at 40 °C between $-0.8 \leq E / V \leq 0.8$ for 40 scans. Only the most promising electrolytes (found from the initial DC capacitance experiments) were subjected to long term cycling studies; Ethaline (Type III), Propaline (Type III), ZnCl₂ / EG (Type IV), ZnCl₂ / acetamide (Type IV) and 0.1 M LiClO₄ / MeCN as a conventional electrolyte for comparison. ‘Long term’ cycling studies in the context of this thesis were defined as subjecting polymer films to cyclic voltammetric studies for multiple scans (40 CVs) in a single electrolyte within a set potential window.

3.2.2 Data Analysis

3.2.2.1 Mass, Thickness and Polymerisation Efficiency Determination

The average charges (\bar{Q}) from the double potential step experiments, for each polymer film were used to determine the mass of polymer adhered to the electrode, by applying Faraday’s law ^{[5][6][7]}. Faraday’s law of electrolysis, equation (3.1), relates the total charge passed during an electrochemical reaction to the mass of material deposited m , *i.e.* oxidised or reduced at an inert electrode surface; where M is the molar mass of the material, n is the number of electrons transferred per ion in the reaction and F is Faraday’s constant (96485 C mol⁻¹).

$$Q = \frac{m.nF}{M} \quad (3.1)$$

Therefore, the number of moles of electrons n_e were calculated from equation (3.2) using the average double potential step charge (\bar{Q}) and Faraday's constant. The moles of the polymer film n_{poly} were found by division of n_e by the molar ratio of dopant anions to monomeric units in the oxidised film γ (electron stoichiometry) ^[8], equation (3.3). For PEDOT, $\gamma = 0.3$ and for PPy, $\gamma = 0.33$ ^[9], as charge neutrality upon oxidation requires one mole of electrons over a series of three monomer units in the polymer chain (Fig. 3.1) ^{[9][10]}. Therefore, for the novel polymers PTP and PEDOT-hexylPy electron stoichiometries were assumed to be $\gamma = 0.6$ as these contained two ring systems per monomer unit (Fig. 3.1).

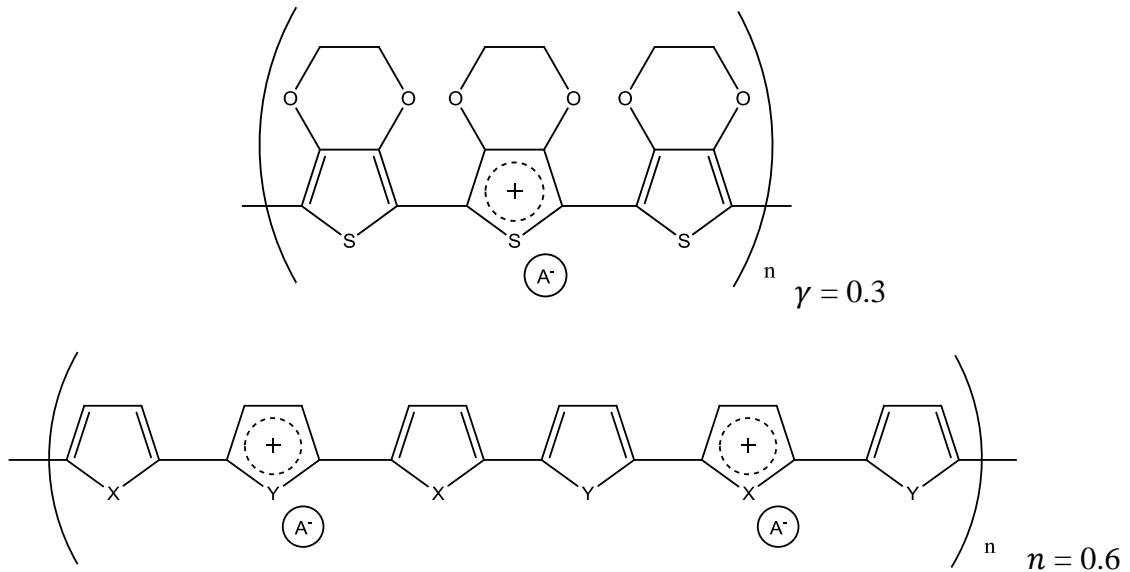


Fig. 3.1 - Molar ratios of dopant anions to monomeric units for PEDOT and for a polymer with a two ring monomer unit (PTP and PEDOT-hexylPy).

The product of n_{poly} with the molar mass of the monomer M gave the mass of polymer on the electrode m_{poly} , equation (3.4). These mass values were used to calculate mass specific capacitances (MSC) of the polymer films.

$$n_e = \frac{\bar{Q}}{nF} \quad (3.2)$$

$$n_{poly} = \left(\frac{n_e}{\gamma} \right) \quad (3.3)$$

$$m_{poly} = n_{poly} \times M \quad (3.4)$$

The masses were used to determine polymer volumes V using equation (3.5) by assuming the density of the polymers to be $\rho = 1.3 \text{ g cm}^{-3}$ (*i.e.* the monomer density). The volume V here refers to the dry polymer volume, *i.e.* no electrolyte present; the volume can vary depending on the extent of solvent uptake. If the polymer acts elastically, the polymer can swell / de-swell with solvent transfer. The thicknesses h of the films were subsequently calculated by dividing the volumes by the electrode area A , equation (3.6).

$$V = \frac{m}{\rho} \quad (3.5)$$

$$h = \frac{V}{A} \quad (3.6)$$

The efficiencies of polymerisations (P_{eff}) were calculated by taking into consideration the average charges of the double potential step (\bar{Q}), the total potentiostatic deposition charges (Q_{psd}) and electron stoichiometry γ , using equation (3.7). Multiplication of P_{eff} by 100 gave the percentage efficiency of electropolymerisation. The total charges passed during deposition (Q_{psd}) related to polymer adhered to the Pt working electrode and the formation of non-adherent oligomers in the monomer solution ^[11].

$$P_{eff} = \frac{\bar{Q}/\gamma}{Q_{psd}/2+\gamma} \quad (3.7)$$

3.2.2.2 DC Capacitance from Chronoamperometric Studies

The average charges (\bar{Q}) from double potential step experiments in conventional monomer free electrolytes were used to calculate DC capacitances of the films; either in

0.1 M LiClO₄ in MeCN (PEDOT, PEDOT-hexylPy and PTP) or H₂O (PPy). These were calculated through division of \bar{Q} by the applied potential, equation (3.8) (1.1 V for PEDOT and PEDOT-hexylPy, 0.8 V for PTP and PPy films). These were subsequently converted to mass specific capacitances (MSC) in F g⁻¹, for comparison with theoretical limits and literature data.

$$C = \frac{Q}{E_{app}} \quad (3.8)$$

3.2.2.3 DC Capacitance from Cyclic Voltammetric Studies

For polymer films prepared for initial cyclic voltammetric studies and bracketed experiments, the electrochemical behaviours were studied within a set potential window at different scan rates ν . The polymer films subjected to ‘long term’ cyclic voltammetric studies were only subjected to cyclic voltammetry at one scan rate (20 mV s⁻¹) for 40 scans, within a set potential window, in a single electrolyte, as discussed above in section 3.2.1.3. The DC capacitances were found from the voltammograms in the different electrolytes by the change in current Δi divided by scan rate ν . As changes in current related to the charging and discharging of the films, half values of Δi divided by scan rate ν were taken for DC capacitance values, using equation (3.9). Changes in current were measured from voltammograms as depicted in **Fig. 3.2**. This method of calculation has previously been reported by multiple authors ^{[12] [13] [14]}.

$$C = \frac{\Delta i/\nu}{2} \quad (3.9)$$

These capacitances were subsequently converted to mass specific capacitances (MSCs) with units of F g⁻¹.

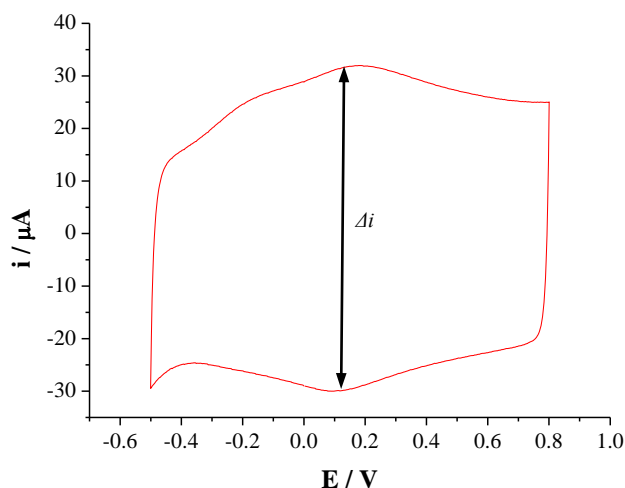


Fig. 3.2 - An example of the measurement of current change from a cyclic voltammogram, used to calculate DC capacitance (CV shown: PEDOT 30 s film in 0.1 M LiClO₄ / MeCN at 100 mV s⁻¹ at 40 °C).

For each scan rate, changes in current Δi were recorded five times across the potential window, avoiding Faradaic regions (peaks), consistent with previously established methods reported ^[15]. Averages of five capacitance values, at each scan rate, were reported for DC capacitances. For the initial cyclic voltammetric studies (polymer / electrolyte screening) capacitance values reported were acquired from an average of capacitance values at 7 scan rates; for films PEDOT, PTP and PPy (deposited at 30 s, 60 s and 120 s); for PEDOT-hexylPy film (deposited at 360 s and 420 s).

3.3 Electrochemical Quartz Crystal Microbalance (EQCM) Polymer Studies

3.3.1 Experimental

All EQCM experiments were performed in a jacketed electrochemical cell with a three electrode configuration; Au quartz crystal working electrode, Pt foil counter electrode and Ag wire quasi-reference electrode. Au coated quartz crystals purchased for use (International Crystal Manufacturing Co. Inc, Oklahoma City, USA) were 10 MHz

frosted quartz crystals with an evaporated 1000 Å Au layer (without a Cr or Ti binding under-layer). The electrochemical and piezoactive areas of the crystals were 0.23 cm² and 0.21 cm², respectively. The piezoactive area was used for all EQCM calculations, as this was the area under which the shear wave oscillation was constrained.

The EQCM circuitry, instrumentation and set-up were based on the method described by Bruckenstein and Shay ^[16] and applied in further publications elsewhere ^{[17][18][19][20]}.

The Au working electrode was controlled by an Autolab PGSTAT20 potentiostat / galvanostat running GPES (version 9.0) software and subsequently connected to two voltmeters (to enable the software to read the output from the potentiostat). **Fig. 3.3** shows the electrochemical cell set-up and instrumental configuration used. Crystal admittance spectra were recorded using a Hewlett Packard 87512A network analyser (transmission / reflectance unit) through a 50 Ω coaxial cable. Spectra and voltmeter readings were logged by a HP Agilent Virtual Engineering Environment program (VEE v.7.52) at an acquisition rate of one admittance spectra per 3 – 4 s. The voltmeter readings were scaled to the current scale selected on the potentiostat. The scale factors used were determined by Ohm's Law, by connecting a voltmeter to the potentiostat and conducting a potential step from 0 V to 1 V on a 1 kΩ resistor at each scale factor used (10 mA, 1 mA and 100 μA current scales gave scale factors of 0.101 V, 1.003 V and 10.03 V respectively). Division of the voltmeter readings (for current output) by the appropriate scale factor acquired the current *i* (in mA). The system was calibrated prior to any data acquisition with the working

electrode under dry and wet (*i.e.* in contact with electrolyte on one side of the crystal) conditions.



Fig. 3.3 - Jacketed electrochemical quartz crystal microbalance cell (left hand image) and instrument set-up (right hand image).

Each crystal was mounted at the bottom of a jacketed cell using a screw-in PTFE plate with rubber o-rings, isolating the piezoactive area on both crystal faces and also acting as seals.

The resonant frequency of the crystal was marginally increased due to the pressure applied by screwing into the PTFE cell. The peak frequency f_0 increased by 35 Hz due to mounting the crystal in the cell, which only represented a negligible increase of $3 \times 10^{-4}\%$. The Q-factor of the crystal (defined below in section 3.3.3) decreased by 11% due to being mounted in the cell. The bandwidth w increased by 12%. These changes in f_0 , Q-factor and w were small, such that the admittance spectra recorded of a dry crystal fixed into the cell or out of the cell were unable to be distinguished from each other in the spectra presented in **Fig. 3.4**. Mounting effects were avoided by recording the full admittance spectra after housing the crystal in the cell, with changes in f_0 measured from these spectra. **Fig. 3.4** and **Fig. 3.5** show examples of the full admittance spectra recorded by the network analyser.

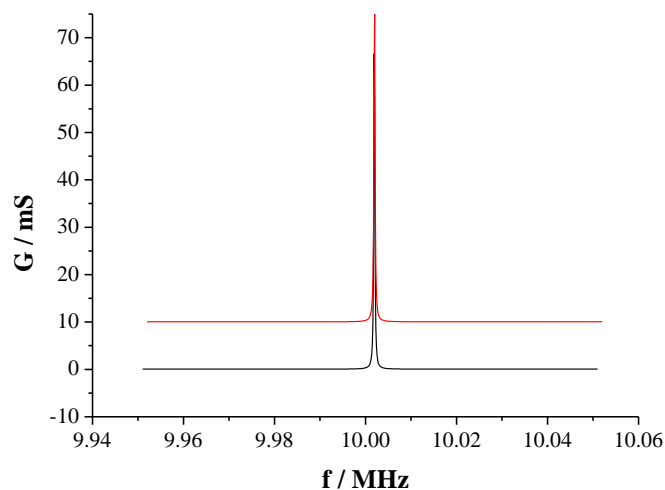


Fig. 3.4 - Admittance spectra for a dry crystal prior to mounting in the EQCM cell (**black**) and after mounting in the cell (**red** (offset by 10 mS for clarity)).

The top crystal face Au electrode (inside the jacketed cell) was exposed to the electrolyte and connected to the Autolab PGSTAT20. The bottom crystal face Au electrode was exposed to air and connected to the network analyser.

All voltammograms were recorded with an equilibration period at 0 V for 30 s with a step potential of 2.44 mV. Dry crystal and polymerisation experiment admittance spectra were recorded using a frequency span of 100 kHz and 200 kHz respectively and were conducted at ambient temperature; redox cycling spectra were recorded using a frequency span of 200 kHz, 500 kHz or 1 MHz dependent on the electrolyte used; and unless otherwise stated. The redox cycling of the resultant polymer films in the various electrolytes were conducted at 40 °C.

3.3.2 Data Fitting

Admittance spectra were automatically fitted from the raw data to a lorentzian distribution by a Visual Basics macro processed in Microsoft Excel, as previously

described elsewhere ^[21]. Representative frequency responses before and after fitting are shown in **Fig. 3.5**.

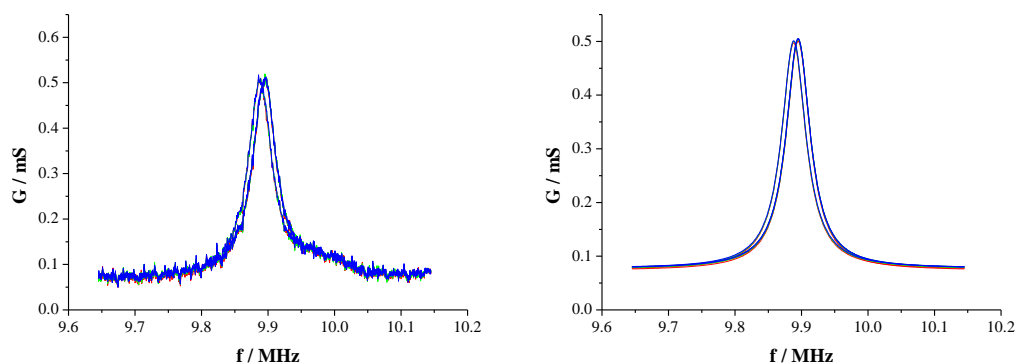


Fig. 3.5 - Raw data admittance spectra (right hand image) and Lorentzian fitted admittance spectra used for calculations (left hand image) (Spectra shown from a cyclic voltammetric study of a PEDOT modified Au coated quartz crystal in 0.1 M LiClO₄ / MeCN for 3 scans at 5 mV s⁻¹ between -0.3 ≤ E / V ≤ 1.1 at 40 °C).

As the admittance spectra did pick up some external noise, as shown by the left hand image in **Fig. 3.5**, the Lorentzian fitted frequency values were used for data analysis. Fitting of the spectra extracted the resonant frequency f_0 , the peak intensity (electrical conductance G) and the peak shape (which comprised of the inductance L , resistance R , and a baseline conductance value a). An admittance spectrum template file (**Fig. 3.6**) and the fitting programme interface (**Fig. 3.7**) were required to proceed with fitting. Firstly, the initial admittance spectrum recorded was manually fitted using the template file (**Fig. 3.6**) by inserting the full spectrum frequencies and conductance into columns A and B respectively, followed by the variation of values for L , R , a and f_0 (highlighted in yellow) to closely match the measured and calculated responses. This was a requirement before proceeding with the [Fit / Solve] command (grey button).

Once the first admittance spectrum had been fitted, the remainder were fitted using an Excel based macro programme (**Fig. 3.7**), as previously reported ^[21]. The [Copy / Fit 2] function was applied when investigating an unknown system, *i.e.* if the frequency or damping of the response could significantly change from the initial admittance spectrum. [Copy / Fit 2] fits every n^{th} spectra by using the calculated data from each preceding spectrum. Once the [Copy / Fit 2] function was complete, the [Results] function constructed a spreadsheet of data acquired from the fitted admittance spectra (**Fig. 3.8**).

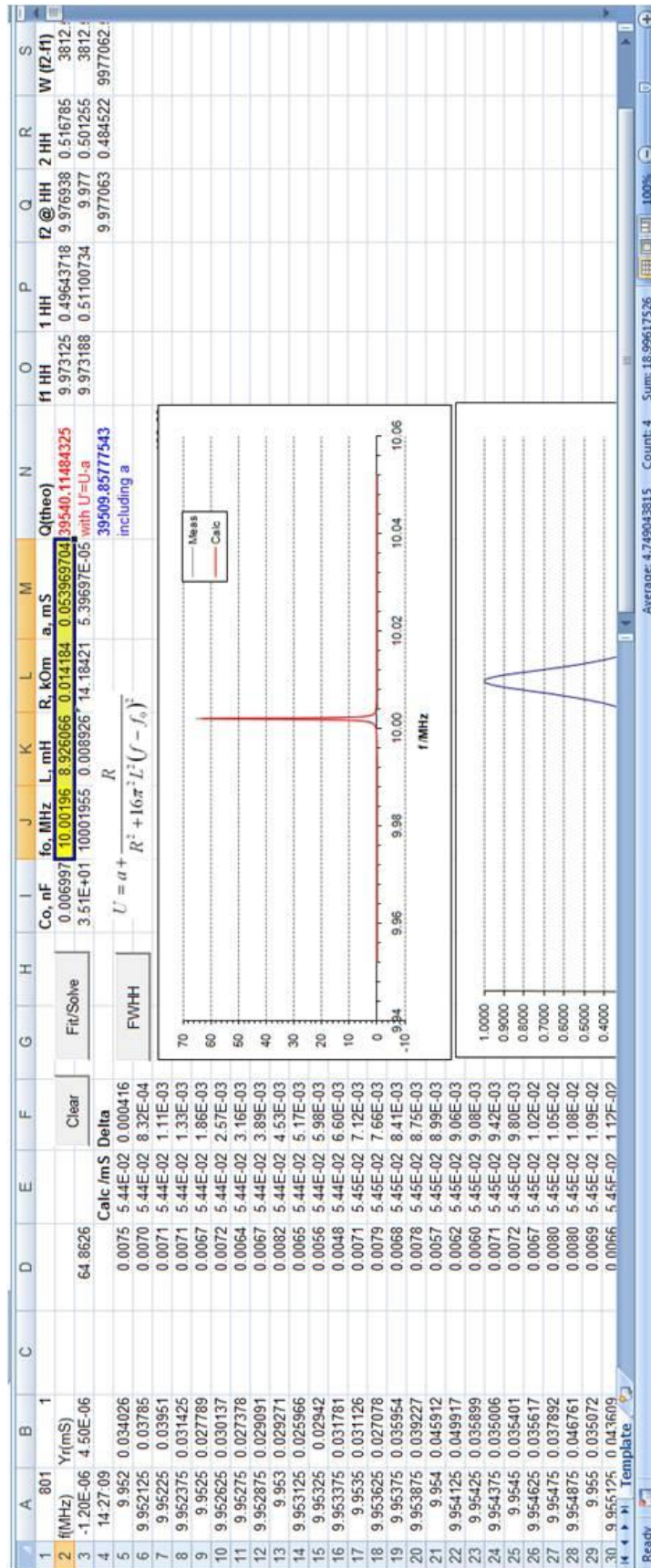


Fig. 3.6 - Admittance spectra fitting template.

QCM Data Fitter (HP and Agilent)

Full File Path:

Name of Template File: **% Error in HH (HHFW):** (0.5 +/-) 0.025

Root file name: **Status:**

Name for Results file: **Number of Files (from to):**

 Agilent Data format
 HP Data format
 Include HHFW calc.

These macros will copy data stored in either Agilent or HP ENA format, fit the data and then collect the resultant parameters in a single file. The template file (HP or Agilent) and the results file must already exist. When running these macros no other file should be open.

Copy / Fit 1: This uses the same template data parameters for every fit.
Copy / Fit 2: This uses the previous fit as a starting point for the current fit.

Fig. 3.7 - Admittance spectra fitting programme.

	A	B	C	D	E	F	G	H	I	J	K	L
	Co, nF	fo, MHz	L, mH	R, kOm	a, mS	Q (theory)	E1/ V	E2/V	time	HHFW /Hz	Q (data)	
1	0.006997	9.94654	7.093655	4.352092	0.060534	101.85	-0.02223	-0.30012	18:50:51	88125	112.8685	
2	0.006997	9.94657	7.093808	4.35319	0.060639	101.82	0.001938	-0.28546	18:50:55	86875	114.4929	
3	0.006997	9.946521	7.148646	4.346852	0.061295	102.76	0.01726	-0.26773	18:50:59	88125	112.8683	
4	0.006997	9.946609	7.121134	4.364145	0.061165	101.96	0.028148	-0.24762	18:51:03	88125	112.8693	
5	0.006997	9.946608	7.131124	4.345398	0.061864	102.54	0.032388	-0.22929	18:51:07	88125	112.8693	
6	0.006997	9.946552	7.084909	4.334124	0.061572	102.14	0.037074	-0.20974	18:51:10	83750	118.7648	
7	0.006997	9.946473	7.105249	4.346762	0.061393	102.14	0.041087	-0.19021	18:51:14	86875	114.4918	
8	0.006997	9.946602	7.119681	4.356257	0.063934	102.12	0.045097	-0.17068	18:51:18	88125	112.8692	
9	0.006997	9.946636	7.136615	4.350891	0.06604	102.49	0.047497	-0.15111	18:51:22	88125	112.8696	
10	0.006997	9.946867	7.069221	4.337601	0.06755	101.84	0.05122	-0.13157	18:51:26	88125	112.8723	
11	0.006997	9.947746	6.684964	4.293884	0.098618	97.29	0.05263	-0.11202	18:51:30	89375	111.3034	
12	0.006997	9.947545	6.362673	4.225	0.078237	94.11	0.052977	-0.09382	18:51:34	88125	112.8799	
13	0.006997	9.94647	7.16137	4.347728	0.076069	102.92	0.053429	-0.07539	18:51:37	88750	112.0729	
14	0.006997	9.946684	7.076774	4.329608	0.066962	102.13	0.054633	-0.05585	18:51:41	88125	112.8702	
15	0.006997	9.946641	7.120463	4.333995	0.065463	102.66	0.057323	-0.03631	18:51:45	83750	118.7659	
16	0.006997	9.946598	7.069388	4.330274	0.062864	102.01	0.05851	-0.01677	18:51:49	88125	112.8692	
17	0.006997	9.946526	7.091654	4.325563	0.065844	102.44	0.061258	0.002764	18:51:53	86875	114.4924	
18	0.006997	9.946555	7.115489	4.324083	0.061336	102.82	0.063463	0.022316	18:51:57	86875	114.4927	
19	0.006997	9.946542	7.070742	4.333366	0.060761	101.96	0.065381	0.041861	18:52:01	86875	114.4926	
20	0.006997	9.946586	7.084769	4.334598	0.06093	102.13	0.065013	0.059634	18:52:04	88125	112.8691	
21	0.006997	9.946531	7.090594	4.326541	0.06043	102.40	0.067557	0.079768	18:52:08	83750	118.7646	
22	0.006997	9.946559	7.077537	4.328704	0.060125	102.16	0.067725	0.098032	18:52:12	82500	120.5644	
23	0.006997	9.946495	7.033697	4.317095	0.059613	101.80	0.069173	0.117567	18:52:16	89375	111.2895	
24	0.006997	9.946525	7.105807	4.332295	0.06011	102.49	0.072027	0.137109	18:52:20	86875	114.4924	
25	0.006997	9.946494	7.126109	4.319091	0.060429	103.09	0.074941	0.156668	18:52:24	86875	114.492	
26	0.006997	9.946389	7.091665	4.325156	0.060196	102.45	0.075993	0.176213	18:52:27	86875	114.4908	
27	0.006997	9.946411	7.125059	4.337361	0.060101	102.64	0.078486	0.195517	18:52:31	86875	114.4911	
28	0.006997	9.946348	7.126947	4.314718	0.060866	103.21	0.080632	0.215293	18:52:35	83750	118.7624	
29	0.006997	9.946355	7.176941	4.314717	0.061577	103.21	0.080747	0.232998	18:52:39	82500	120.5619	
30	0.006997	9.946355	7.176941	4.314717	0.061577	103.21	0.080747	0.232998	18:52:39	82500	120.5619	

Fig. 3.8 - Results file example.

3.3.3 Data Analysis

For full EQCM data analyses see EQCM Chapter (**Chapter 5**). For analyses of admittance spectra, quality factors (Q-factors) were calculated using the Full Width at Half Height (FWHH), also termed the bandwidth (represented by w with units in Hz) ^[22] using equation (3.10); where f_0 is the peak frequency in Hz and w is the bandwidth in Hz. These Q-factors gave values for the damping of the crystal in contact with different media. The Q-factor referred to the ratio of peak energy stored to energy lost per admittance spectra acquired. For the quartz crystal in air, Q-factors can exceed 100,000 whilst in solution, Q-factors decrease to values in the thousands (≤ 3000) dependent on the electrolyte used. Damping of the crystal frequency response increased the amount of energy lost per spectra acquisition, thereby decreasing the Q-factor.

$$Q - factor = \frac{f_0}{w} \quad (3.10)$$

3.4 X-Ray Photo-electron Spectroscopy (XPS)

3.4.1 Experimental

PEDOT and PTP films were deposited on Au coated silanised glass from 0.1 M LiBF₄ / MeCN potentiodynamically at RT for 10 scans at 20 mV s⁻¹ between; $0 \leq E / V \leq 1.1$ (EDOT **1**); $0 \leq E / V \leq 0.8$ (TP **3**). Silanisation of the glass slides by using (3-mercaptopropyl)-trimethoxysilane (MPTS) ensured good adhesion of Au coated onto the glass substrates. Silanisation and Au coating of glass substrates were conducted using an established protocol reported elsewhere ^{[23][24]} (by Dr EL Smith, University of Leicester). Multiple films were prepared to examine the composition of freshly deposited films and those subjected to cyclic voltammetry in either 0.1 M LiClO₄ / MeCN or DES (Ethaline Type III and ZnCl₂ / EG Type IV), with the analysis of these results discussed in **Chapter 7**. Cyclic voltammetric studies were

conducted for 10 scans at 20 mV s^{-1} in a single electrolyte, with scans stopped either at the positive end (oxidised film) or negative end (reduced film) of the potential window used, during the 11th scan. XPS spectra were acquired from either the polymer-electrolyte interface side of the film or the polymer-Au interface side of the film. Polymer-Au interface samples, termed reverse side films, were achieved by removal of films off the Au electrodes using Sellotape[®], carefully avoiding any removal of the Au itself. Both types of sample were fixed to an Al stub (used for mounting the sample in the spectrometer) with carbon conductive tape.

As the samples were conducting, charging of the samples was not an issue *cf.* insulating materials which are charged in the incident x-ray beam (when electrons are ejected). To ensure the samples were not charged, carbon conductive tape was used to attach the sample to Al stubs and to the polymer film surface (bending over the edge of the glass substrate).

Table 3.1 contains the sample parameters for the PEDOT and PTP samples prepared for XPS. The procedures for analysis of XPS spectral data are discussed in **Chapter 7**.

Table 3.1 - XPS sample parameters (reverse side samples referred to as RS samples).

	Growth	Sample and Electrolyte	Potential window (vs. Ag wire)	Potential of sample / V
PEDOT-1	0.1 M PEDOT 0.1 M LiBF ₄ / MeCN 40 °C 10 scans 20 mV s ⁻¹ -0.3 ≤ E / V ≤ 1.1 (vs. Ag wire)	Pristine		
PEDOT-2		0.1 M LiClO ₄ / MeCN Oxidised + RS	-0.4 ≤ E / V ≤ 1.1	1.1
PEDOT-3		0.1 M LiClO ₄ / MeCN Reduced		-0.4
PEDOT-4		Ethaline Oxidised		1.1
PEDOT-5		Ethaline Oxidised repeat + RS		1.1
PEDOT-6		Ethaline Reduced		-0.4
PEDOT-7		Ethaline Reduced + RS		-0.4
PEDOT-8		ZnCl ₂ / EG Oxidised		1.1
PEDOT-9		ZnCl ₂ / EG Oxidised RS		1.1
PTP-1	0.1 M PTP 0.1 M LiBF ₄ / MeCN 40 °C 10 scans 20 mV s ⁻¹ -0.3 ≤ E / V ≤ 0.8 (vs. Ag wire)	Pristine		
PTP-2		LiClO ₄ / MeCN Reduced	-0.4 ≤ E / V ≤ 0.8	-0.4
PTP-3		LiClO ₄ / MeCN Reduced repeat + RS		-0.4
PTP-4		Ethaline Oxidised + RS		0.8
PTP-5		Ethaline Reduced + RS		-0.4

3.4.2 Spectrometer Settings

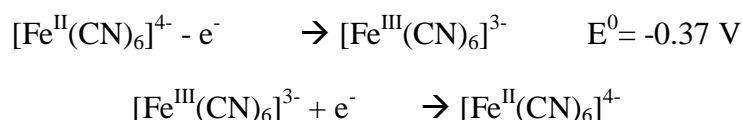
XPS measurements were made on the Scienta ESCA300 spectrometer at the National Centre for Electron Spectroscopy and Surface Analysis (NCESS) in Daresbury Laboratory, using monochromatic Al K α radiation (E = 1486.7 eV). All measurements were performed at room temperature. The following settings were used for data acquisition, as previously reported ^{[25] [26]}; with take off angle 90 °; slit 0.8 mm; energy

offset 0.563; and ep offset 5.39. Linear and Shirley backgrounds were used for peak fitting spectra using CASA XPS software.

3.5 Determination of the Electrochemically Active Area of an Electrode by Chronoamperometry

The electrochemical area of the Pt working electrode used for DC capacitance calculations (section 3.2 and Chapter 4) was quantified using chronoamperometry to give context to data analysis using the three electrode cell set-up shown above. This was determined using a reversible redox couple with a known diffusion coefficient ^[27].

The oxidation of Fe^{III} / Fe^{II} was investigated using the ferro / ferricyanide redox couple by stepping the potential from 0 V where no reaction took place, to 0.5 V which ensured full oxidation of the Fe^{II} species ^[28].



A 4 mM K₄[Fe(CN)₆].3H₂O (0.0422 g, 0.1 mmol) in 0.1 M KCl solution (0.186 g, 2.5 mmol in 25 cm³ H₂O) was prepared for chronoamperometry. Three *i*(*t*) transients were recorded at 25 °C at three different time intervals (int *t* = 0.5 s, 0.05 s, 0.02 s), *i.e.* progressively increasing the number of data points per trace. The potential was held at 0 V for 60 s and stepped to 0.5 V for 60 s for each transient recorded. Current *i* and time *t* values from the diffusion controlled region of the *i*(*t*) transient, highlighted by the green box in **Fig. 3.9A**, were used to produce a *i* vs. *t*^{-1/2} plot in **Fig. 3.9B**, to be able to use the Cottrell equation, equation (3.8). The diffusion coefficient

$D = 0.65 \times 10^{-5} \text{ cm}^2 \text{ s}^{-1}$ at $25 \text{ }^\circ\text{C}$ [27] was used for Cottrell equation calculations [29]. The gradient $di/dt^{-1/2}$, diffusion coefficient and known solution concentration C_0 allowed quantification of electrode area by equation (3.9); where A is the area of the electrode in cm^2 , i is the current in A, t is time in s, n is the number of electrons transferred per ion in the reaction, F is Faraday's constant (96485 C mol^{-1}), D is the diffusion coefficient in $\text{cm}^2 \text{ s}^{-1}$ and C_0 is the concentration in mol cm^{-3} . The average electrode area acquired was 0.0124 cm^2 with a diameter of 1.258 mm.

$$i(t) = nFAC_0 \cdot \sqrt{\frac{D}{\pi t}} \quad (3.8)$$

$$A = \frac{i(t)}{nFC_0} \cdot \sqrt{\frac{\pi t}{D}} \quad (3.9)$$

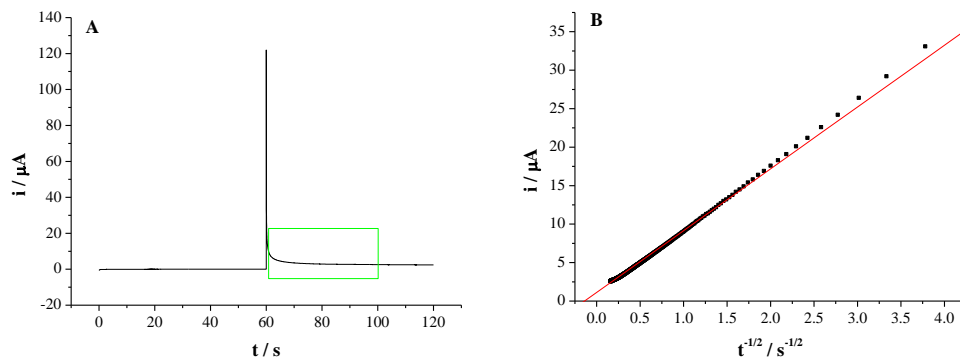


Fig. 3.9 - A) $i(t)$ transient for $\text{Fe}^{\text{III}} / \text{Fe}^{\text{II}}$ oxidation **B)** Resulting Cottrell plot (plotted using diffusion controlled region data highlighted by green box).

3.6 References

-
- [1] Trofimov BA, Mikhaleva AI, Nesterenko RN, Vasil'ev AN, Nakhmanovich AS and Voronkov MG, *Chem. Hetero. Comp.*, 1977, 13, 8, 920 (Translated from *Khim. Geterotsykl. Soedin.*, 1977, 8, 1136-1137)
- [2] Trofimov BA, Korostova SE, Mikhaleva AI, Sobenina LN, Vasil'ev AN and Nesterenko RN, *Chem. Hetero. Comp.*, 1983, 19, 2, 227 (Translated from *Khim. Geterotsykl. Soedin.*, 1983, 2, 273)
- [3] Abbott AP, Capper G, McKenzie KJ and Ryder KS, *J. Electroanal. Chem.*, 2007, 599, 2, 288-294
- [4] Abbott AP, Barron JC, Ryder KS and Wilson D, *Chem. Euro. J.*, 2007, 13, 22, 6495-6501
- [5] Faraday M, *Trans. Roy. Soc. London*, 1834, 124, 425-470
- [6] Ehl RG and Ihde AJ, *J. Chem. Educ.*, 1954, 31, 5, 226-232
- [7] Bard AJ, Stratmann M, Macdonald D and Schmuki P, *Encyclopedia of Electrochemistry*, 2007, Wiley-VCH, Germany, Volume V
- [8] Skoog DA, West DM, Holler FJ and Crouch SR, *Fundamentals of Analytical Chemistry*, 2004, Brooks / Cole Thomson Learning, USA, 8th Edn
- [9] Ahn YR, Song MY, Jo SM, Park CR and Kim DY, *Nanotechnology*, 2006, 17, 12, 2865-2869
- [10] Hillman AR, Daisley SJ and Bruckenstein S, *Electrochimica Acta*, 2008, 53, 11, 3763-3771
- [11] Ryder KS, *Iron-sulphur clusters in polymers on electrodes*, 1993, University of Sussex, PhD Thesis, uk.bl.ethos.336057
- [12] Ren X and Pickup PG, *J. Electroanal. Chem.*, 1994, 372, 1-2, 289-291
- [13] Snook GA, Kao P and Best AS, *J. Power Sources*, 2011, 196, 1, 1-12
- [14] Bobacka J, Lewenstam A and Ivaska A, *J. Electroanal. Chem.*, 2000, 489, 1-2, 17-27
- [15] Snook GA, Peng C, Fray DJ and Chen GZ, *Electrochem. Commun.*, 2007, 9, 1, 83-88
- [16] Bruckenstein S and Shay M, *Electrochimica Acta*, 1985, 30, 10, 1295-1300
- [17] Hillman AR, Loveday DC, Swann MJ, Bruckenstein S and Wilde CP, *J. Chem. Soc. Faraday Trans.*, 1991, 87, 13, 2047-2053
- [18] Hillman AR, Loveday DC and Bruckenstein S, *J. Electroanal. Chem.*, 1989, 274, 1-2, 157-166
- [19] Skompska M and Hillman AR, *J. Chem. Soc. Faraday Trans.*, 1996, 92, 20, 4101-4108
- [20] Hillman AR, Swann MJ and Bruckenstein S, *J. Electroanal. Chem.*, 1990, 291, 1-2, 147-162
- [21] Abbott AP, Nandhra S, Postlethwaite S, Smith EL and Ryder KS, *Phys. Chem. Chem. Phys.*, 2007, 9, 28, 3735-3743
- [22] Buck RP, Lindner E, Kutner W and Inzelt G, *Pure Appl. Chem.*, 2004, 76, 6, 1139-1160
- [23] Hillman AR, Saville PM, Glidle A, Richardson RM, Roser SJ, Swann MJ and Webster JRP, *J. Am. Chem. Soc.*, 1998, 120, 49, 12882-12890

-
- [24] Goss CA, Charych DH and Majda M, *Anal. Chem.*, 1991, 63, 1, 85-88
- [25] Glidle A, Pearson PE, Smith EL, Cooper JM, Cubitt R, Dalglish RM, Hillman AR and Ryder KS, *J. Phys. Chem. B*, 2007, 111, 16, 4043-4053
- [26] Smith EL, Glidle A, Mortimer RJ and Ryder KS, *Phys. Chem. Chem. Phys.*, 2007, 9, 46, 6098-6105
- [27] Sawyer DT, Sobkowiak A and Roberts Jr, *Electrochemistry for Chemists*, Wiley USA 1995, 2nd Edn
- [28] Rao SP, Singh SR and Bandakavi SR, *Indian J. Chem. Sec. A*, 1978, 44A, 6, 333-335
- [29] Nowinski SA and Anjo DM, *J. Chem. Eng. Data*, 1989, 34, 3, 265-268

Chapter 4

Polymer DC Capacitance Studies

4.1 Introduction

4.1.1 Determination of DC Capacitance

4.1.2 Current Research on

DC Capacitances of Conducting Polymers

4.2 Objectives

4.3 Results and Discussion

4.3.1 Potentiodynamic Polymer Deposition

4.3.2 Mass, Thickness, Polymerisation Efficiency Determination and DC Capacitance by Chronoamperometry

4.3.3 DC Capacitance by Cyclic Voltammetric Studies

4.3.3.1 Mass Specific Capacitances of PEDOT Films

4.3.3.2 Mass Specific Capacitances of PPy Films

4.3.3.3 Mass Specific Capacitances of PTP (LiClO₄ / MeCN) Films

4.3.3.4 Mass Specific Capacitance of PEDOT-hexylPy Films

4.4 Conclusions

4.5 References

Chapter 4

Polymer DC Capacitance Studies

4.1 Introduction

4.1.1 Determination of DC Capacitance

Quantification of the charge storage capabilities of conducting polymers in the form of DC capacitances provides a good comparative measure of performance for different polymer / electrolyte systems for battery applications ^[1]. The DC capacitance (charge storage per volt in units $C V^{-1} \equiv F$ (farads)) can be expressed in terms of the mass of the active material on the electrode (mass specific capacitance in $F g^{-1}$) or the electrode area (electrode specific capacitance in $F cm^{-2}$) ^[2]. Conducting polymers function over a wide range of potentials compared to a standard battery material *e.g.* a metal, which operates at a fixed potential. Normally a battery would simply be characterised by the total charge stored, since the energetics are fixed and defined by the potential difference, E_{cell} . In a conducting polymer battery the situation is different because the conducting polymer functions over a range of potentials defined by the conductivity window. Therefore, capacitances C (voltage dependent measurements) are generally more convenient for polymer systems, calculated from the charge passed (4.1).

$$Q = CV \quad (4.1)$$

Mass specific capacitances ($F g^{-1}$) can sometimes be misleading as capacitances may not simply increase with increasing mass. These mass specific capacitances are dependent on the redox behaviour of the polymer which involves dopant intercalation / expulsion, which can affect the capacitive performance, depending on which ions are in motion. The performance can also be affected by the morphology of the polymer deposit (a more porous structure being optimum) and the conductivity of

the electrolyte. It has been suggested for a complete evaluation of the charge storage of a polymer it is important to describe capacitance in terms of both mass (F g^{-1}) and area, the electrode specific capacitance (F cm^{-2}) *i.e.* the charge storage over a certain geometric area of substrate ^[2]. Electrode specific capacitances (F cm^{-2}), however, neglect to take into consideration the thicknesses of the polymer films. Therefore, electrode specific capacitances fail to give true representations of the charge storage of active materials. It would be more apt to represent capacitance as a volume specific capacitance (F cm^{-3}) an approach used by Suematsu *et al.* ^[3] to investigate capacitance of PPy films. However, it can be an arduous task to accurately measure a true thickness of the polymer which takes into account its porosity, especially if swelling / de-swelling occurs during redox switching.

Thicknesses measured from double potential step experiments (**Chapter 4.3.2**) assumed the polymer films were of the same porosity and had a density the same as the monomer density ($\rho = 1.3 \text{ g cm}^{-3}$). Therefore, for the purposes of this thesis, capacitances were calculated as mass specific (F g^{-1}) and electrode specific (F cm^{-2}) capacitances rather than trying to determine volume specific capacitances. Only the mass specific capacitances (F g^{-1}) are reported here as the electrode specific capacitances (F cm^{-2}) did not provide any further information other than that obtained by calculating mass specific capacitances.

In the literature, some papers have reported conflicting calculation methods for DC capacitances producing vastly different results for the same experiment. Lota *et al.* ^[11] calculated capacitance from the total current passed (*i.e.* Δi between oxidation and reduction half cycles at a fixed potential) divided by the scan rate v .

Park and Park ^[4] reported the same calculation. Ahn *et al.* ^[5] calculated the capacitance of electrodeposited ruthenium oxide, reporting $C = \Delta i / v$, however calculating capacitance from the data reported, only half the current passed was used for calculations *i.e.* $C = (\Delta i / v)/2$. Ren and Pickup ^[6] reported the conversion of cyclic voltammograms to capacitance by $C = \Delta i / v$ when investigating poly(1-methyl-3-(pyrrole-1-ylmethyl)pyridinium films in 0.1 M Et₄NClO₄ / MeCN. Capacitance values were reported over the entire oxidation and reduction process as a function of potential. The charge storage of the polymer therefore related to the oxidation half cycle capacitance values only. Snook *et al.* ^[7] reported that in the absence of Faradaic processes the cyclic voltammogram of a capacitor should be rectangular with the capacitance roughly equal to half the value of the difference in plateau currents divided by the scan rate $C = (\Delta i / v)/2$. Hughes *et al.* ^[8] reported capacitance as the output current (discharge current) divided by the scan rate $C = (\Delta i / v)/2$. Bobacka *et al.* ^[9] reported capacitance values by using an average of anodic and cathodic currents at 0.2 V divided by potential scan rate $C = (\Delta i / v)/2$.

As the majority of the literature reported capacitance as $C = (\Delta i / v)/2$ from cyclic voltammograms, capacitances were calculated in this manner throughout this thesis (see experimental chapter **3.2.2.3**).

$$C = \frac{\Delta i/v}{2} \quad (3.9)$$

Equation (3.9) shows that the charge storage of the conducting polymer would only relate to the oxidation of the polymer and not the reduction, the reduction would be classed as the discharge of the polymer.

4.1.2 Current Research on DC Capacitances of Conducting Polymers

For EV / HEV battery applications, it would be desirable to achieve a mass specific capacitance of greater than $\approx 200 \text{ F g}^{-1}$ to compete with other novel technologies.

Snook and Chen ^[10] investigated capacitances of PPy and PEDOT films using Electrochemical Quartz Crystal Microbalance (EQCM) experiments. Capacitances reported for PPy (electrodeposited from 0.1 M Py in 0.5 M LiCl / MeCN) and PEDOT (electrodeposited from 0.2 M EDOT in 0.5 M LiClO₄ / MeCN) films were 240 F g^{-1} and 92 F g^{-1} respectively. These were calculated during constant voltage deposition and not in monomer free electrolyte.

Lota *et al.* ^[11] prepared PEDOT films electrochemically (in LiClO₄ / MeCN) and measured the mass specific capacitance as 180 F g^{-1} in monomer free 1 M TEABF₄ / MeCN. They found this value 20 F g^{-1} greater than chemically prepared PEDOT films (using Fe(ClO₄)₃ as an oxidant). Theoretical capacitances were reported for different conducting polymers for a comparison against the experimental values. Capacitances were calculated using molar masses of the polymers, electron stoichiometry and oxidation potentials, equation (4.2), with values of 750 F g^{-1} for polyaniline, 620 F g^{-1} for polypyrrole, 485 F g^{-1} for polythiophene and 210 F g^{-1} for PEDOT.

$$C = \left(\frac{F}{E_{app} \cdot M} \right) \times \gamma \quad (4.2)$$

The group also reported the capacitance of a chemically prepared PEDOT carbon nanotube composite (15% PEDOT: 85% CNT) at 95 F g^{-1} (from a cyclic voltammetric study) and 69 F g^{-1} (from a galvanostatic study). A capacitor comprising a PEDOT

acetylene black (80% PEDOT: 20% AB) composite cathode and an activated carbon anode in 1 M TEABF₄ / MeCN electrolyte, reached a capacitance of 160 F g⁻¹.

Xu *et al.* [12] have studied mass specific capacitances of PEDOT and PPy (deposited from aqueous 0.1 M PTSNa solution) in LiClO₄ / MeCN. The mass specific capacitance had a weak dependency on scan rate for PEDOT films with 100 F g⁻¹ at 5 mV s⁻¹ and 90 F g⁻¹ at 10 mV s⁻¹. PPy films varied from ≈ 100 F g⁻¹ to 130 F g⁻¹ dependent on the morphology of the deposit.

Ingram *et al.* [13] deposited a ladder structured PPy using a surfactant to vary the morphology of the film. This improved charge transport within the film, with an electrode specific capacitance 400 mF cm⁻² and a mass specific capacitance of 160 F g⁻¹, much greater than the pure PPy deposited.

A textile style PEDOT material was produced by Laforgue [14] by electrospinning polyvinylpyrrolidone / p-toluenesulfonate based mats capable of oxidising EDOT during vapour-phase polymerisation. The PEDOT cathode exhibited a mass specific capacitance of 75 F g⁻¹ during galvanostatic testing in an all PEDOT based electric double layer capacitor. The electrolyte used was a solid polymer electrolyte made from 1-ethyl-3-methylimidazolium tetrafluoroborate (EMIBF₄) and polyvinylidene fluoride-co-hexafluoropropylene (PVDF-co-HFP).

Ryu *et al.* [15] produced a hybrid capacitor consisting of a PEDOT electrode and a PEDOT / activated carbon electrode. This was reported to give a capacitance of 50 F g⁻¹ after 1000 cycles in LiPF₆ in EC / DMC.

Randriamahazaka *et al.* ^[16] investigated PEDOT films (prepared from LiClO₄ in MeCN) in an ionic liquid, 1-ethyl-3-methylimidazolium bis(trifluoromethyl)sulphonyl)amide (EMITFSI) and reported a capacitance of 0.6 mF, however did not report a mass specific capacitance. It was possible to calculate a mass specific capacitance of 24 F g⁻¹, from the reported deposition charge (7 mC) knowing the polymerisation efficiency of PEDOT to be $\approx 75\%$.

4.2 Objectives

The focus of the work conducted in this chapter was to find a polymer / DES electrolyte combination in which the polymer has a high mass specific capacitance suitable for use in a Zn-Polymer secondary battery.

4.3 Results and Discussion

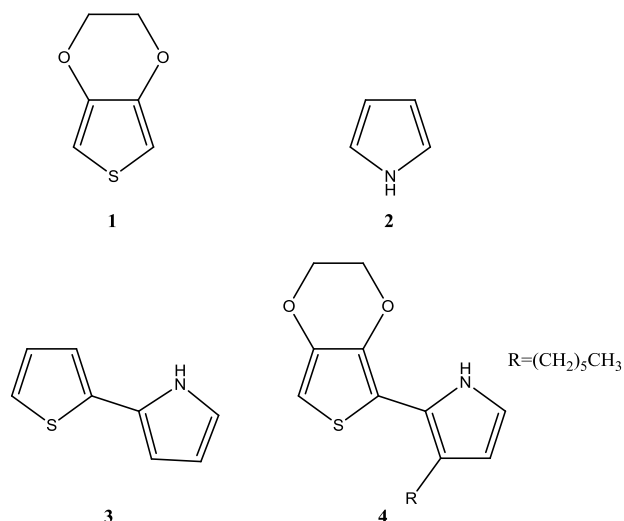
Research activities were focussed on studies of the electronic properties of electrodeposited conducting polymers from commercially available monomers 3,4-ethylenedioxythiophene (EDOT) **1** and pyrrole (Py) **2**; contrasting these with polymers from monomer precursors thiophene-pyrrole (TP) **3** and EDOT-hexylpyrrole (EDOT-hexylPy) **4**, shown in **Scheme 4.1**. PEDOT has been demonstrated as an attractive material in electrical storage applications because of its good thermal stability, good chemical stability and a fast reversible electrochemical response as a result of large potential changes ^{[21][17]}. However, PEDOT exhibits a low mass specific capacitance because of the high R.M.M of PEDOT (188 F g⁻¹) compared to other conducting polymers such as PPy (539 F g⁻¹) and PAni (389 F g⁻¹), as calculated by equation (4.2); where F is Faraday's constant (96485 C mol⁻¹), E_{app} the oxidation potential of the monomer, M is the molar mass of the monomeric unit and γ the electron

stoichiometry. PPy has the highest specific capacitance of the four systems (**1** – **4**) studied.

$$C = \left(\frac{F}{E_{app} \cdot M} \right) \times \gamma \quad (4.2)$$

The polymer from the monomer TP **3** possessed a high mass specific capacitance calculated as 485 F g⁻¹ using equation (4.2). Whereas, another polymer studied from the monomer EDOT-hexylPy **4** exhibited a low mass specific capacitance calculated as 181 F g⁻¹ using equation (4.2), approximately 4% lower than PEDOT.

The TP monomer **3** aims to produce a regioregular polymer rather a composite material with separate chains of thiophene and pyrrole which may be produced by copolymerisation of thiophene and pyrrole ^[18]. Production of a copolymer from a mixture of thiophene (1.7 V vs. SCE) and pyrrole (0.8 V vs. SCE) monomers can be difficult due to the large difference in oxidation potentials of the monomers ^[19]. Also the deposition of thiophene can be difficult as the potential for decomposition of the thiophene polymer *i.e.* irreversible oxidation, is lower than the oxidation potential to deposit a thiophene polymer. This has been termed in the literature as the ‘thiophene paradox’ ^[18]. The polymer PTP will hopefully combine the high chemical stability of polythiophene with the good electrical conductivity of polypyrrole in one regio-regular polymer ^[20]. Polymer films produced from TP **3** and EDOT-hexylPy **4** combine the properties of two different heterocycles in a regio-regular polymer, a benefit of using these complex monomers, rather than co-polymerisation of the individual heterocycles which has the potential of producing a film with regions of homopolymer.



Scheme 4.1 - Monomers used for DC capacitance studies, 3,4-ethylenedioxythiophene **1**, pyrrole **2**, 2-(thiophene-2-yl)-1H-pyrrole **3**, 2-(2,3-dihydrothieno[3,4-b][1,4]dioxin-5-yl)-1H-pyrrole **4**.

PPy has the highest specific capacitance of the four systems studied. However, these large capacitance values tend not to be practically achievable for PPy. This is because of a tendency for a high degree of cross-linkages and defects to occur during polymerisation, which produces dense ‘closed’ film morphologies. This occurs due to the lack of protecting groups at the 3,4 positions on the heterocyclic ring, therefore coupling can occur at these positions causing cross linkages of polymer chains. 3,4 coupling can reduce film conductivity due to poor electron transfer arising from a lack of a well-defined polymer backbone. The films lack of porosity means solvent and charge carriers cannot transfer a substantial thickness into the bulk film, so therefore PPy does not have a high charge storage capability. PEDOT films do not produce dense film morphologies, as the 3,4 positions are blocked by a ether linkage so only 2-2’ coupling can occur. The high porosity of PEDOT films allows faster ion transport into and out of the film ^[21]. However, even though PEDOT films are porous, it has been observed that the films can swell / de-swell due to solvent transfer ^{[22] [23]}.

The low theoretical values calculated for PEDOT and PEDOT-hexylPy by equation (4.2) are a result of the large molar masses of the monomeric units, highlighted in studies on PEDOT by Snook and Chen ^[10].

4.3.1 Potentiodynamic Polymer Deposition

The oxidation potentials of the monomers were measured during potentiodynamic deposition of PEDOT **1**, PPy **2**, PTP **3** and PEDOT-hexylPy **4** in supporting electrolyte (LiClO₄ or LiBF₄ in water or acetonitrile). The oxidation potentials were obtained from the voltammograms, **Fig. 4.1**, by identifying the crossover point in the $i(E)$ responses at anodic potentials and found to be 1.1 V for PEDOT and 0.8 V for PPy, PTP and PEDOT-hexylPy (vs. a Ag wire quasi-reference electrode). The crossover point indicated the nucleation and subsequent growth of the polymer.

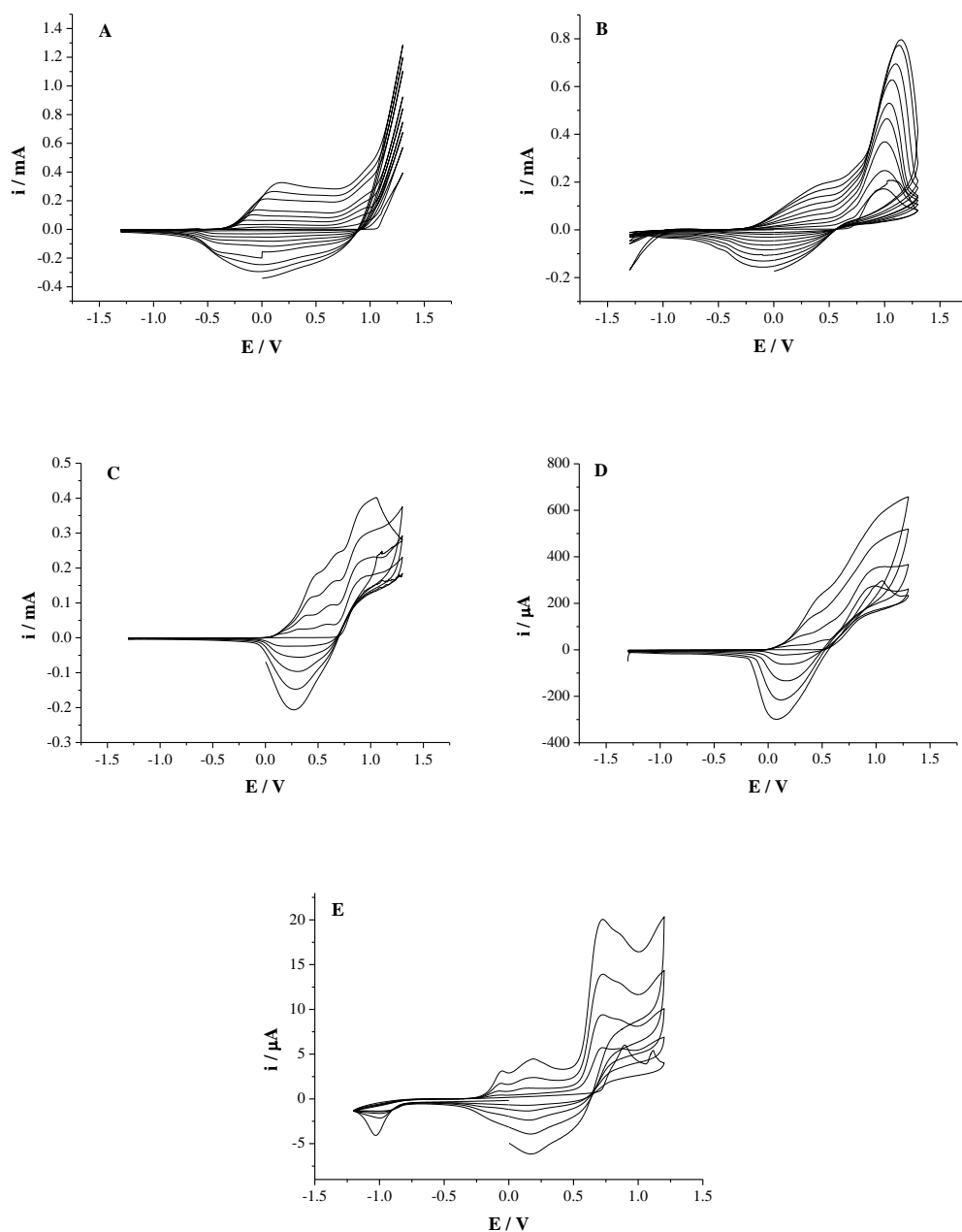


Fig. 4.1 - **A**) Potentiodynamic deposition of PEDOT from 0.1 M EDOT in 0.1 M LiClO₄ / MeCN under N₂ for 10 scans at RT at 20 mV s⁻¹ -1.3 ≤ E / V ≤ 1.3 **B**) PPy from 0.1 M Pyrrole in 0.1 M LiClO₄ / H₂O under N₂ for 10 scans at RT at 20 mV s⁻¹ -1.3 ≤ E / V ≤ 1.3 **C**) PTP film from 0.05 M 2-(thiophen-2-yl)-1H pyrrole in 0.1 M LiClO₄ / MeCN under N₂ for 5 scans at RT at 20 mV s⁻¹ -1.3 ≤ E / V ≤ 1.3 **D**) PTP film from 0.1 M 2-(thiophen-2-yl)-1H pyrrole in 0.1 M LiBF₄ / MeCN under N₂ for 5 scans at RT at 20 mV s⁻¹ -1.3 ≤ E / V ≤ 1.3 **E**) Potentiodynamic deposition of EDOT-hexylpyrrole film from 33 mM EDOT-hexylpyrrole in 0.1 M LiClO₄ / MeCN under N₂ for 5 scans at RT at 20 mV s⁻¹ -1.3 ≤ E / V ≤ 1.3 (vs. Ag wire reference electrode).

4.3.2 Mass, Thickness, Polymerisation Efficiency Determination and DC Capacitance by Chronoamperometry

Oxidation potentials were used for potentiostatic deposition of polymer films as described in **Chapter 3.2.1.1**. Growth data was subsequently used to calculate the mass of the polymer, thickness of the polymer and the polymerisation efficiency of the deposition process. These were established by the integration of the $i(t)$ traces in the monomer containing electrolyte (providing the potentiostatic deposition charge Q) and the $i(t)$ traces of the polymer in monomer free electrolyte (providing Q_{ox} and Q_{red}), along with the application of Faraday's Law. The DC capacitances were calculated using the double potential step data from the film in a monomer free electrolyte by dividing the average potential step charge \bar{Q} by the applied potential (4.3) and subsequently converting into mass and electrode specific capacitances as discussed in the experimental section 3.2.2.

$$C = \frac{\bar{Q}}{E_{app}} \quad (4.3)$$

The mass specific capacitance of PEDOT in 0.1 M LiClO₄ / MeCN measured using experimental charge data from double potential step experiments shown in **Table 4.1** was $\approx 188 \text{ F g}^{-1}$ as calculated by equation (4.3). This mass specific capacitance was the same as the value calculated from the molar mass of the monomeric unit by equation (4.2).

PPy mass specific capacitance in 0.1 M LiClO₄ / H₂O measured using experimental charge data from double potential step experiments (4.3) was 612 F g^{-1} ; this was 14% greater than calculated by equation (4.2).

The mass specific capacitance of PTP in 0.1 M LiClO₄ / MeCN measured using experimental charge data from double potential step experiments (4.3) was approximately 486 F g⁻¹; this was only 0.2% greater than calculated by equation (4.2).

PEDOT-hexylPy mass specific capacitance in 0.1 M LiClO₄ / MeCN measured using experimental charge data from double potential step experiments (4.3) was 181 F g⁻¹.

Table 4.1 shows the charge, mass, thickness and polymerisation efficiencies of the potentiostatically deposited polymer films used to calculate DC capacitance from equation (4.3).

Table 4.1 - Mass m , Thickness h and Polymerisation Efficiencies P_{eff} of PEDOT (1.1V), PPy (0.8V), PTP (0.8V) and PEDOT-hexylPy (0.8V and 1.1V) films deposited potentiostatically at the potentials given in brackets; from 0.1M LiClO₄ in MeCN (for PEDOT, PTP and PEDOT-hexylPy) or in H₂O (for PPy). These are reported with the associated double potential step charges (Q_{ox} , Q_{red} and \bar{Q}) and mass specific capacitance (in F g⁻¹) in monomer free electrolyte, 0.1M LiClO₄ in MeCN (for PEDOT, PTP and PEDOT-hexylPy) or in H₂O (for PPy), applying a potential step at the same potential as deposition.

Polymer	Deposition t / s	Deposition Q _{psd} / mC	Q _{ox} / mC	Q _{red} / mC	\bar{Q} / mC	m / μ g	P _{eff} / %	h / μ m	MSC / F g ⁻¹
PEDOT	30	5.43	0.54	-0.49	0.52	2.50	72.78	1.55	188
PEDOT	60	9.95	0.96	-0.93	0.95	4.58	72.83	2.84	188
PEDOT	120	20.62	1.93	-1.89	1.91	8.05	71.02	4.99	216
PPy	30	4.61	1.06	-0.10	0.58	1.19	96.52	0.74	612
PPy	60	12.27	2.14	-0.21	1.18	2.40	73.42	1.49	612
PPy	120	17.99	2	-0.50	1.25	2.56	53.31	1.59	612
PTP	30	2.84	0.19	-0.13	0.16	0.41	24.32	0.25	486
PTP	60	3.91	0.21	-0.16	0.19	0.49	20.95	0.30	486
PTP	120	8.79	0.51	-0.41	0.46	1.18	22.52	0.73	486
PEDOT-hexylPy	360	3.17	0.12	-0.10	0.11	0.56	15.14	0.35	181
PEDOT-hexylPy	420	5.02	0.20	-0.15	0.17	0.86	14.8	0.53	181

The $i(t)$ trace for the deposition of a PEDOT 30 s film (**Table 4.1**) is shown in **Fig. 4.2A**. The shape of the $i(t)$ traces for the deposition of PTP and PPy films looked similar to the PEDOT films due to the use of only one potential step for deposition, from 0 V to 0.8 V for both PTP and PPy deposition. The PEDOT hexylPy depicted two current spikes due to the double potential step used for deposition, from 0 V to 0.8 V followed by a step to 1.1 V (see experimental section **3.2.1.1**). **Fig. 4.2B** shows the corresponding PEDOT 30 s film in monomer free electrolyte subjected to a double potential step conducted as discussed in the experimental section **3.2.1.1**.

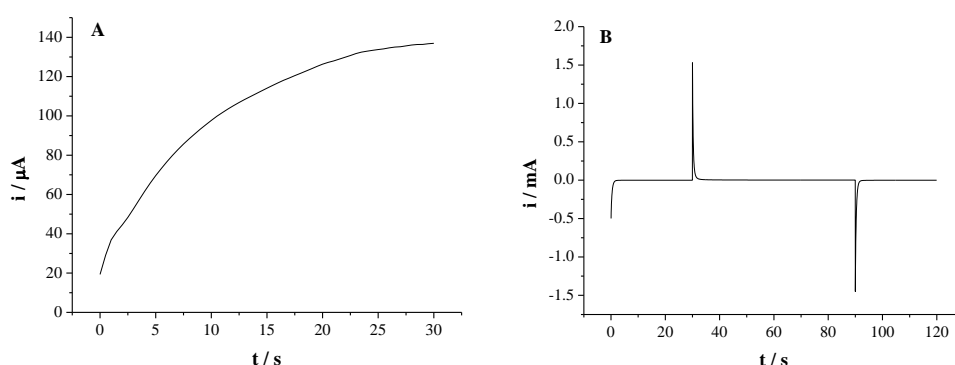


Fig. 4.2 - A) Potentiostatic deposition of an PEDOT film grown from 0.1 M LiClO₄ / MeCN at RT under N₂ at 1.1 V $Q_{psd} = 5.43$ mC **B)** Double Potential Step of PEDOT film (**Fig. 4.2A**) 0V for 30s, 1.1 V for 60s, 0V for 30s in 0.1 M LiClO₄ / MeCN at RT under N₂ $\bar{Q} = 0.52$ mC $P_{eff} = 72.78\%$, $m = 2.496$ μg.

The average of the measured values of Q_{ox} and Q_{red} *i.e.* (\bar{Q}) was used for the calculation of the mass and the thickness of the film, polymerisation efficiency and the DC capacitance of the film in the monomer free electrolyte used. An average was used as initially it was assumed that the charging and discharging of the film was a reversible process, so the ratio of $Q_{ox} : Q_{red}$ would be close to 1 : 1. However for the polymer films reported in **Table 4.1** Q_{red} values were slightly smaller than Q_{ox} values. This was attributed to incomplete discharge, potentially due to trapped ions within the film; or a slower discharge reaction than the charging reaction *i.e.* full discharge was not achieved

within the time frame selected for integration of the $i(t)$ traces. Q_{red} values were lower for PEDOT 30, 60 and 120 s film by 9%, 4% and 2% respectively; for PPy 30, 60, 120 s films lower by 90%, 90%, and 75% respectively; for PTP 30, 60, 120 s films lower by 34%, 23%, 20% respectively, and for EDOT-hexylPy 360 and 420 s films lower by 12% and 26% respectively. This suggested that the PPy, PTP and EDOT-hexylPy films took longer to discharge in comparison to the charging of the films. The significant difference in the Q_{red} for PPy suggests poor ion mobility (anion egress to maintain charge neutrality) possibly due to a dense ‘closed’ film morphology.

The capacitance values from the chronoamperometric experiments (double potential step experiments) using equation (4.3) were consistent with theoretical capacitances predicted from the monomer unit molar masses using equation (4.2).

4.3.3 DC Capacitance by Cyclic Voltammetric Studies

Further polymer films were deposited potentiostatically (deposition times and deposition potentials the same as reported for the films in **Table 4.1** above) to investigate DC capacitances of polymers in conventional solvent and DES electrolytes, by cyclic voltammetry. An example of the voltammograms recorded from which capacitance values were calculated using equation (3.9) (with the method described in the experimental section 3.2.2.3) is shown in **Fig. 4.3** for a PEDOT 30 s film in 0.1 M LiClO₄ / MeCN.

$$C = \frac{\Delta i/v}{2} \quad (3.9)$$

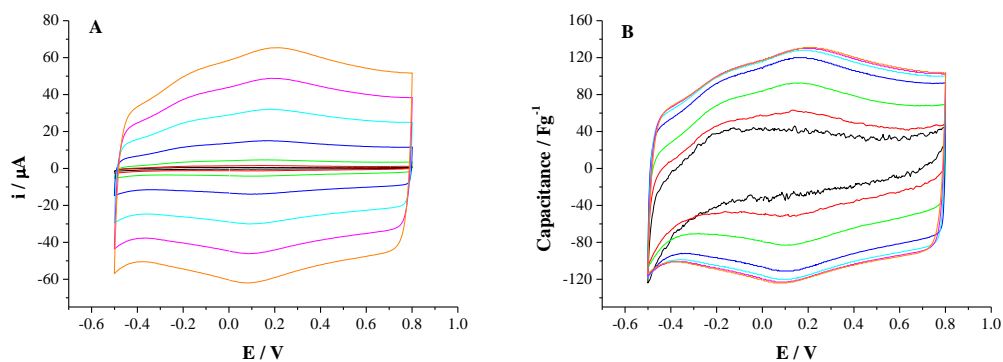


Fig. 4.3 - A) Cyclic voltammetric data for the redox cycling of a potentiostatically deposited PEDOT LiClO_4 film (1.1V for 30s) in 0.1M $\text{LiClO}_4 / \text{MeCN}$ at 40°C for 3 scans (figure shows 3rd scans only) $-0.5 \leq E / \text{V} \leq 0.8$ (vs. Ag wire) at 7 different scan rates 5 mV s^{-1} (black), 10 mV s^{-1} (red), 20 mV s^{-1} (green), 50 mV s^{-1} (blue), 100 mV s^{-1} (cyan), 150 mV s^{-1} (pink), 200 mV s^{-1} (orange) **B)** Current axis from cyclic voltammetric data converted to F g^{-1} using mass of film from double potential step data ($m = 2.496 \mu\text{g}$).

Sections 4.3.3.1 – 4.3.3.4 report the DC capacitances for PEDOT, PPy, PTP and PEDOT-hexylPy films in conventional electrolytes and DESs. The aim was to characterise the same polymer film in all the electrolytes, however this was not possible due to adhesion issues during rinsing and transferral of the polymer modified electrodes to different electrolytes. The values highlighted in the same colour in the separate tables below, for each thickness of film (reported by deposition time) indicate the same film being transferred to each electrolyte.

4.3.3.1 Mass Specific Capacitances of PEDOT Films

Table 4.2 shows that of the electrolytes investigated the highest mass specific capacitances for PEDOT films were observed in 0.1 M $\text{LiClO}_4 / \text{MeCN}$, Ethaline and Ethaline : H_2O (1 : 1). It would be advantageous for the battery electrolyte to have a high concentration of Zn, for the deposition / dissolution of Zn for the anode of the battery. Of the Zn based DESs investigated $\text{Zn}(\text{NO}_3)_2 \cdot 6\text{H}_2\text{O} / \text{ChCl}$ and the $\text{ZnCl}_2 / \text{EG}$ gave the highest mass specific capacitances. However, it would be best for a battery

device to avoid organic solvents and DESs containing water (for safety reasons). The use of 0.1 M LiClO₄ / H₂O as a battery electrolyte was ruled out as the aim was to avoid aqueous electrolytes due to zinc dendrite formation. Again, the same reason as not to use Ethaline : H₂O (1 : 1). Therefore for a battery with a PEDOT cathode it would be better to use either Ethaline or ZnCl₂ / EG as the electrolyte.

The mass specific capacitances of PEDOT in Reline and Reline : H₂O (1 : 1) were low at values between approximately 5 F g⁻¹ – 41 F g⁻¹. Therefore due to these low values Reline was not considered as a DES for use as a battery electrolyte with a PEDOT electrode.

The mass specific capacitance of PEDOT was low ($\leq 10 \text{ F g}^{-1}$) in ZnCl₂ / 1,6-hexanediol so this electrolyte was not considered further.

Table 4.2 - Mass specific capacitances for potentiostatically deposited PEDOT films (1.1 V for 30 s, 60 s and 120 s) measured from cyclic voltammograms, reported as an average of values from scan rates 5, 10, 20, 50, 100, 150 and 200 mV s⁻¹. Values highlighted in blue measured from a fresh polymer film.

Electrolyte	MSC / F g ⁻¹		
	30 s	60 s	120 s
0.1 M LiClO ₄ / MeCN	88	118	217
0.1 M LiClO ₄ / H ₂ O	68	81	175
Ethaline	71	89	206
Ethaline:H ₂ O 1:1	48	80	213
Reline	41	7	6
Reline:H ₂ O 1:1	33	9	5
Zn(NO ₃) ₂ .6H ₂ O / ChCl	25	164	283
ZnCl ₂ / EG	32	118	139
ZnCl ₂ / acetamide	25	85	88
ZnCl ₂ / 1,6-hexanediol	10	7	3

In experiments termed 'bracketed experiments' an as grown polymer was examined in one electrolyte, for example MeCN, transferred to another, for example a DES, and then returned to the initial electrolyte. This showed if there were any changes in the electro-activities of the films when transferred to multiple electrolytes. This procedure distinguishes between differences in the polymer behaviour that are due to the electrolyte (*e.g.* ion mobility) and chemical changes that could be the result of transferring the polymer from one solvent to another (*e.g.* MeCN to DES)

Fig. 4.4A shows the behaviour of PEDOT in 0.1 M LiClO₄ / MeCN and Ethaline. In both electrolytes the CVs remained the same even after exposure to a different electrolyte. Upon first exposure to 0.1 M LiClO₄ / MeCN the capacitance increased by 109% with increasing scan rate from 80 F g⁻¹ to 167 F g⁻¹ (5 mV s⁻¹ to 50 mV s⁻¹). The capacitance levelled off between 50 mV s⁻¹ to 200 mV s⁻¹ with a value of ≈ 170 F g⁻¹. After exposure to Ethaline and transferral back to 0.1 M LiClO₄ / MeCN there was minimal loss in electro-activity, with the same trend presented in **Fig. 4.4B**, an increase in capacitance with increasing scan rate (5 mV s⁻¹ to 50 mV s⁻¹) and levelling off between 50 mV s⁻¹ to 200 mV s⁻¹.

The first exposure of PEDOT to Ethaline (after exposure to 0.1 M LiClO₄ / MeCN) the capacitance increased by 90% with increasing scan rate from 81 F g⁻¹ to 153 F g⁻¹ between 5 mV s⁻¹ to 50 mV s⁻¹. The capacitance levelled off at 178 F g⁻¹ between 50 mV s⁻¹ to 200 mV s⁻¹. After exposure to 0.1 M LiClO₄ / MeCN for the second time and transferral back to Ethaline, the trend of capacitance behaviour remained the same in Ethaline increasing from 5 to 50 mV s⁻¹ and levelling off from 50 mV s⁻¹ to 200 mV s⁻¹.

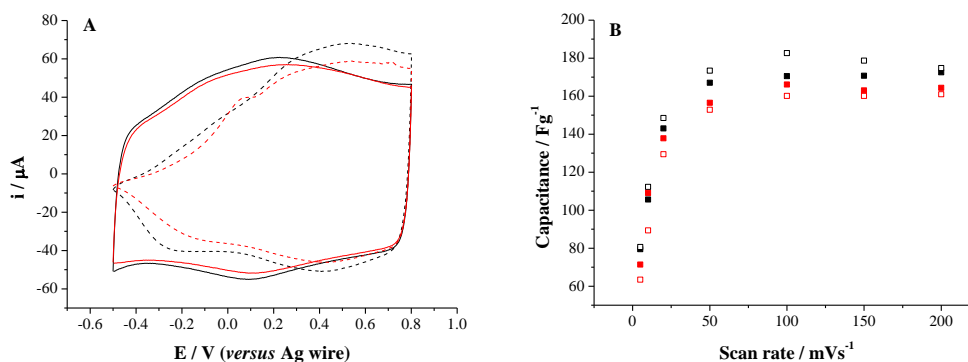


Fig. 4.4 - A) Bracketed cyclic voltammetric experiment of PEDOT film (polymerised potentiostatically from 0.1 M EDOT in 0.1 M LiClO₄ / MeCN at RT under N₂ (at 1.1 V *vs.* Ag wire for 60 s)) redox cycling firstly in 0.1 M LiClO₄ / MeCN (solid), secondly in ChCl / EG DES Ethaline (dashed) and repeated in that order (1st CV black, 2nd CV red) at 40 °C at 100 mV s⁻¹ -0.5 ≤ E / V ≤ 0.8 (mass of polymer film = 2.9966 μg, growth charge = 5.7 mC, P_{eff} = 83%). **B)** Mass specific capacitances from cyclic voltammetric data of EDOT (1.1 V, 60 s film used for redox cycling in **Fig. 4.4A**) during bracketed experiment at 7 different scan rates 5, 10, 20, 50, 100, 150 and 200 mV s⁻¹ redox cycling firstly in 0.1 M LiClO₄ / MeCN (solid squares), secondly in ChCl / EG DES Ethaline (outline squares) and repeated in that order (1st CV black, 2nd CV red) at 40 °C -0.5 ≤ E / V ≤ 0.8 (*vs.* Ag wire).

This ‘bracketing experiment’ showed that there was very little difference in capacitance between the MeCN and DES and importantly this experiment showed that there was no irreversible chemical changes in the polymer in going from MeCN to DES and back again. Some differences were observed in the appearance of the CVs in MeCN and DES. The differences are likely to be kinetic in nature, related to ion transport. The appearance of the CVs also suggests that polymer charging / discharging is faster in MeCN.

Fig. 4.5A shows the behaviour of PEDOT in ZnCl₂ / EG and ZnCl₂ / acetamide, from a bracketed experiment (method described above). In both electrolytes the CVs remained the same even after exposure to a different electrolyte. Upon first exposure to ZnCl₂ / EG the capacitance decreased by 39% with increasing scan rate from 165 F g⁻¹ to 101 F g⁻¹ (5 mV s⁻¹ to 200 mV s⁻¹) shown in **Fig. 4.5B**. After exposure to

ZnCl₂ / acetamide and transferral back to ZnCl₂ / EG there was minimal loss in electro-activity, an increase in capacitance with increasing scan rate 143 F g⁻¹ to 153 F g⁻¹ (5 mV s⁻¹ to 20 mV s⁻¹) and decreasing between 20 mV s⁻¹ to 200 mV s⁻¹ to 117 F g⁻¹.

For the first exposure to ZnCl₂ / acetamide the capacitance decreased by 62% with increasing scan rate 5 mV s⁻¹ – 200 mV s⁻¹ from 151 F g⁻¹ to 57 F g⁻¹. After exposure to ZnCl₂ / EG then transferral back to ZnCl₂ / acetamide there was minimal loss in electro-activity. The mass specific capacitance increased by 3% with increasing scan rate between 5 mV s⁻¹ – 20 mV s⁻¹ from 144 F g⁻¹ to 149 F g⁻¹. The capacitance then decreased by 58% to 63 F g⁻¹ between 20 mV s⁻¹ – 200 mV s⁻¹.

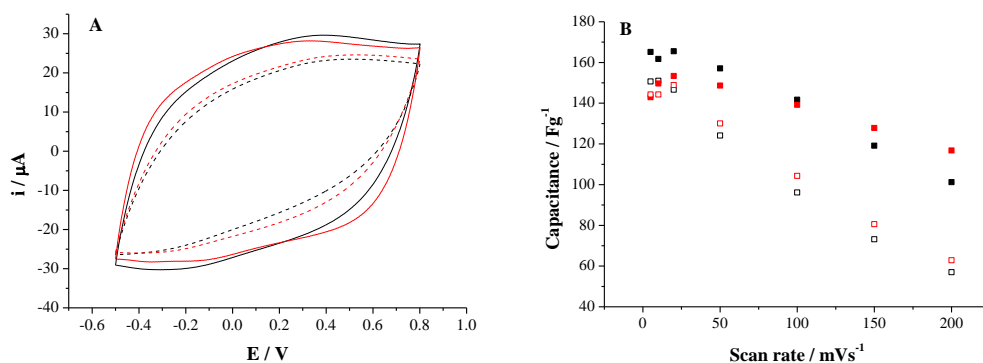


Fig. 4.5 - A) Bracketed cyclic voltammetric experiment of a PEDOT film (polymerised potentiostatically from 0.1 M EDOT in 0.1 M LiClO₄ / MeCN at RT under N₂ (at 1.1 V vs. Ag wire for 60 s)) redox cycling firstly in ZnCl₂ / ethylene glycol DES (solid), secondly in ZnCl₂ / acetamide DES (dashed) and repeated in that order (1st CV black, 2nd CV red) at 40 °C at 100 mV s⁻¹ -0.5 ≤ E / V ≤ 0.8 (mass of polymer film = 1.7026 μg, growth charge = 3.08 mC, P_{eff} = 88%) **B)** Mass specific capacitances from cyclic voltammetric data of PEDOT (1.1 V, 60 s film used for redox cycling in **Fig. 4.5A**) during bracketed experiment at 7 different scan rates 5, 10, 20, 50, 100, 150 and 200 mV s⁻¹ redox cycling firstly in ZnCl₂ / ethylene glycol DES (solid squares), secondly in ZnCl₂ / acetamide DES (outline squares) and repeated in that order (1st CV black, 2nd CV red) at 40 °C -0.5 ≤ E / V ≤ 0.8 (vs. Ag wire).

This ‘bracketing experiment’ showed that there was very little difference in capacitance between the two Type IV DESs. The appearances of the CVs for the two Type IV DESs

were very similar, suggesting similar kinetics. This could be because both electrolytes are viscous, as well as containing the salt ZnCl_2 . The bulk capacitance of the polymer was lowest in the most viscous electrolyte, $\text{ZnCl}_2 / \text{acetamide}$. This may be a result of poor ion access.

The behaviour of PEDOT over 40 cycles gives an appreciation of the change in mass specific capacitance over a longer usage period. The mass specific capacitance of PEDOT in $\text{LiClO}_4 / \text{MeCN}$ reduced by 11% over 40 CVs from 176 F g^{-1} to 156 F g^{-1} , shown in **Fig. 4.6**. The mass specific capacitance of PEDOT in Ethaline only decreased by 4% over 40 CVs from 208 F g^{-1} to 199 F g^{-1} , shown in **Fig. 4.7**. The mass specific capacitance of PEDOT in Propaline increased by 26% over 40 CVs from 172 F g^{-1} to 216 F g^{-1} , shown in **Fig. 4.8**. The mass specific capacitance of PEDOT in $\text{ZnCl}_2 / \text{EG}$ increased by 12% over 40 CVs from 189 F g^{-1} to 211 F g^{-1} , shown in **Fig. 4.9**. The mass specific capacitance of PEDOT in $\text{ZnCl}_2 / \text{acetamide}$ increased by 87% over 40 CVs from 43 F g^{-1} to 81 F g^{-1} , shown in **Fig. 4.10**.

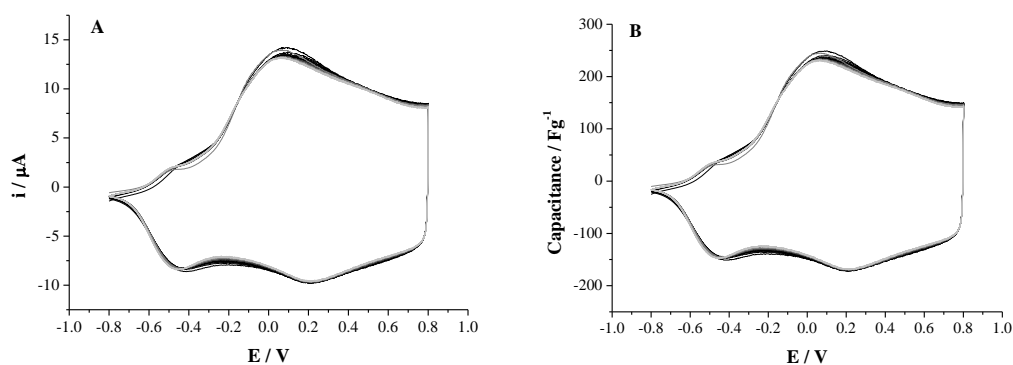


Fig. 4.6 - A) Cyclic voltammetric data for the redox cycling of a potentiostatically deposited PEDOT film (1.1 V for 120 s) in 0.1 M $\text{LiClO}_4 / \text{MeCN}$ at 40°C for 40 scans at 20 mV s^{-1} $-0.8 \leq E / \text{V} \leq 0.8$ (vs. Ag wire) (mass of polymer film = $2.85 \mu\text{g}$, growth charge = 5.06 mC , $P_{\text{eff}} = 89\%$). **B)** Current axis from cyclic voltammetric data converted to F g^{-1} using mass of film from double potential step data.

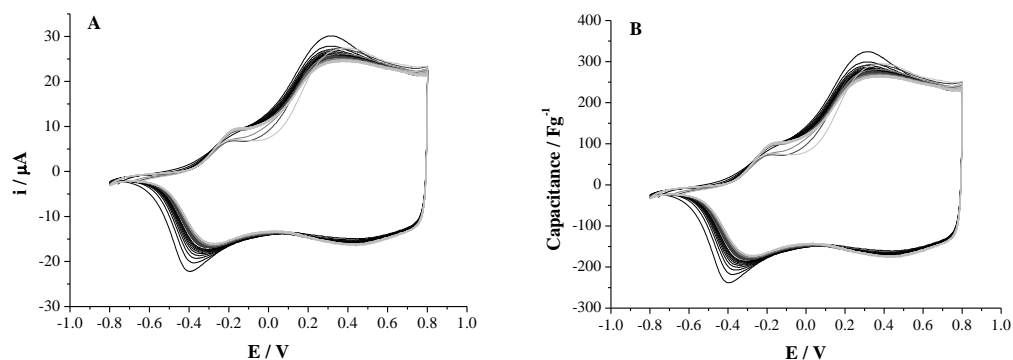


Fig. 4.7 - A) Cyclic voltammetric data for the redox cycling of a potentiostatically deposited PEDOT film (1.1 V for 120 s) in Ethaline at 40 °C for 40 scans at 20 mV s⁻¹ -0.8 ≤ E / V ≤ 0.8 (vs. Ag wire) (mass of polymer film = 4.65 μg, growth charge = 11.53 mC, $P_{\text{eff}} = 63.87\%$). **B)** Current axis from cyclic voltammetric data converted to F g⁻¹ using mass of film from double potential step data.

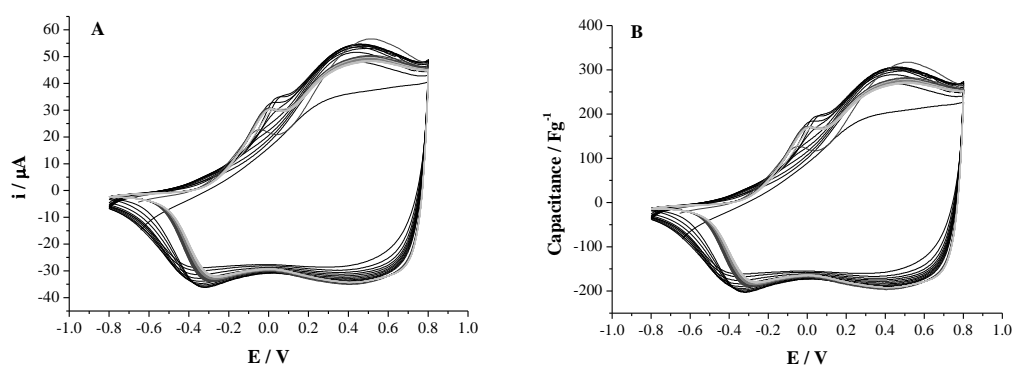


Fig. 4.8 - A) Cyclic voltammetric data for the redox cycling of a potentiostatically deposited PEDOT film (1.1 V for 120 s) in Propaline at 40 °C for 40 scans at 20 mV s⁻¹ -0.8 ≤ E / V ≤ 0.8 (vs. Ag wire) (mass of polymer film = 8.93 μg, growth charge = 22.59 mC, $P_{\text{eff}} = 62.58\%$). **B)** Current axis from cyclic voltammetric data converted to F g⁻¹ using mass of film from double potential step data.

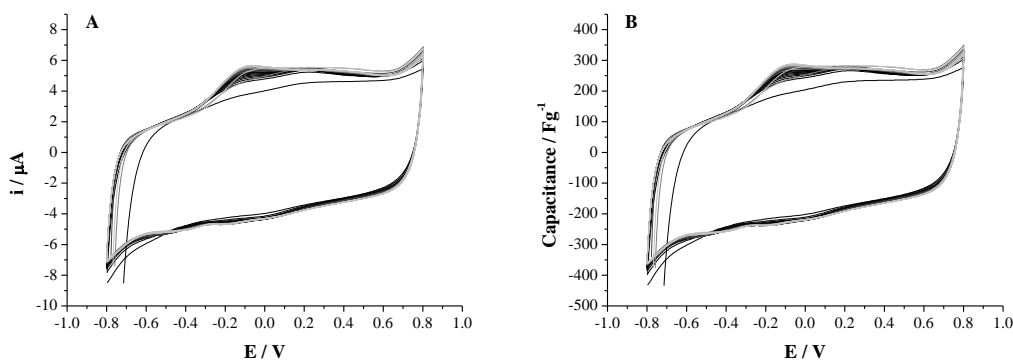


Fig. 4.9 - A) Cyclic voltammetric data for the redox cycling of a potentiostatically deposited PEDOT film (1.1 V for 120 s) in ZnCl₂ / ethylene glycol at 40 °C for 40 scans at 20 mV s⁻¹ -0.8 ≤ E / V ≤ 0.8 (vs. Ag wire) (mass of polymer film = 0.98 μg, growth charge = 2.59 mC, $P_{\text{eff}} = 60.12\%$). **B)** Current axis from cyclic voltammetric data converted to F g⁻¹ using mass of film from double potential step data.

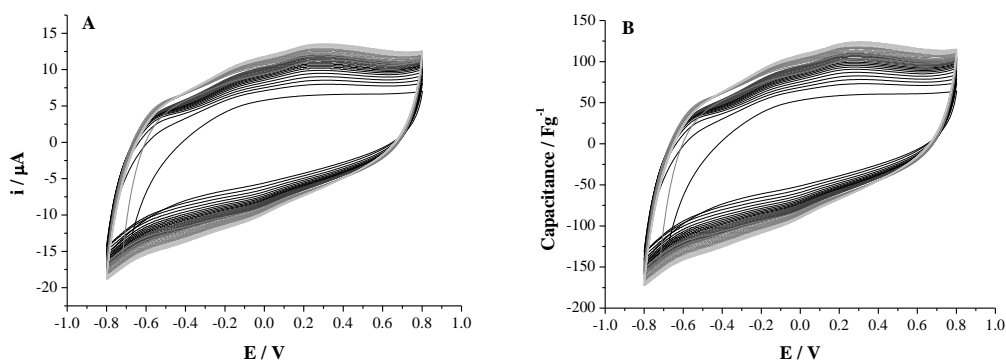


Fig. 4.10 - A) Cyclic voltammetric data for the redox cycling of a potentiostatically deposited PEDOT film (1.1 V for 120 s) in $\text{ZnCl}_2 / \text{acetamide}$ at 40°C for 40 scans at 20 mV s^{-1} $-0.8 \leq E / \text{V} \leq 0.8$ (vs. Ag wire) (mass of polymer film = $5.46 \mu\text{g}$, growth charge = 13.58 mC , $P_{\text{eff}} = 63.65\%$). **B)** Current axis from cyclic voltammetric data converted to Fg^{-1} using mass of film from double potential step data.

The mass specific capacitances recorded over a long period of redox cycling in MeCN and the DESs produced very interesting results. They showed that in the DES electrolytes (Ethaline, Propaline, $\text{ZnCl}_2 / \text{EG}$ and $\text{ZnCl}_2 / \text{acetamide}$), where initially the total charge stored is less than the theoretical maximum, the charge storage increased with cycling. In contrast, in MeCN the charge storage decreased with cycling. Both these phenomena are probably caused by changes in polymer dynamics, either opening up the matrix to allow counter ion diffusion (charge storage increasing) or else closing down the membrane and excluding counter ions. This is known for PEDOT in MeCN but observed for the first time here for DESs.

4.3.3.2 Mass Specific Capacitances of PPy Films

Table 4.3 reports the mass specific capacitances from potentiostatically deposited PPy. These capacitance values were much lower than observed for PEDOT in the electrolytes studied. Capacitances for PPy films ranged between $0.4 - 38 \text{ F g}^{-1}$, whereas PEDOT exhibited capacitances ranging from $5 - 283 \text{ F g}^{-1}$.

Table 4.3 - Mass specific capacitances for potentiostatically deposited PPy films (1.1 V for 30 s, 60 s and 120 s) measured from cyclic voltammograms, reported as an average of values from scan rates 5, 10, 20, 50, 100, 150 and 200 mV s⁻¹.

Electrolyte	MSC / F g ⁻¹		
	30s	60s	120s
0.1 M LiClO ₄ / MeCN	10	10	6
0.1 M LiClO ₄ / H ₂ O	38	33	28
Ethaline	6	5	4
Ethaline:H ₂ O 1:1	13	11	7
Zn(NO ₃) ₂ .6H ₂ O / ChCl	9	2	2
ZnCl ₂ / EG	7	3	2
ZnCl ₂ / acetamide	5	2	2
ZnCl ₂ / 1,6-hexanediol	3	0.4	1

The low bulk capacitances recorded for PPy in all electrolytes studied are most likely to be caused from a dense closed film morphology which significantly reduces ion transfers. It is unfortunate that PPy charge storage is not better as PPy is easy to polymerise. PEDOT, in the preceding sections, was shown to have a good bulk capacitance in various electrolytes. However, PEDOT is harder to deposit and relatively expensive in comparison to PPy. This shows that to produce a good electrochemical device what is needed is a polymer that deposits as easily as PPy but that has the capacitance properties as good as PEDOT. Therefore, two polymer systems deposited from mixed monomer precursors TP **3** and EDOT-hexylPy **4** hope to combine the properties of two different heterocycles in a regio-regular polymer.

4.3.3.3 Mass Specific Capacitances of PTP (LiClO₄ / MeCN) Films

Table 4.4 shows that out of the electrolytes investigated the highest mass specific capacitances for PTP films were observed in conventional molecular solvents and DESs in H₂O. Type III and Type IV DESs gave low values of mass specific capacitance, however further films were deposited to see if this was the case. PEDOT in Ethaline and

ZnCl₂ / EG gave high mass specific capacitances that were stable over a long period of redox cycling. The low mass specific capacitance recorded for the DES in **Table 4.4** may possibly be caused to exposure and redox cycling in a previous electrolyte. In this experiment a single PTP film was prepared and exposed to the electrolytes in the order reported in **Table 4.4**. It is possible that redox cycling in 0.1 M LiClO₄ / H₂O caused an irreversible chemical change to PTP which reduced the charge storage capability of the membrane. Further experiments, discussed in the proceeding sections, show that PTP has a high capacitance in DESs if not previously exposed to a water based electrolyte.

Table 4.4 - Mass specific capacitances for potentiostatically deposited PTP films (1.1 V for 30 s, 60 s and 120 s) measured from cyclic voltammograms, reported as an average of values from scan rates 5, 10, 20, 50, 100, 150 and 200 mV s⁻¹. Values highlighted in blue measured from a fresh polymer film.

Electrolyte	MSC / F g ⁻¹		
	30s	60s	120s
0.1 M LiClO ₄ / MeCN	166	294	149
0.1 M LiClO ₄ / H ₂ O	137	185	102
Ethaline	15	14	11
Ethaline:H ₂ O 1:1	53	114	46
Reline	18	6	5
Reline:H ₂ O 1:1	207	120	73
Zn(NO ₃) ₂ .6H ₂ O / ChCl	45	52	57
ZnCl ₂ / EG	12	24	5
ZnCl ₂ / acetamide	9	19	2
ZnCl ₂ / 1,6-hexanediol	0.7	9	0.4

In experiments termed ‘bracketed experiments’ an as prepared polymer film was exposed to one electrolyte, transferred to another and then the sequence repeated.

Fig. 4.11A shows the behaviour of PTP in 0.1 M LiClO₄ / MeCN and Ethaline. In both electrolytes the CVs remained the same shape even after exposure to a different

electrolyte, this showed that there was no irreversible chemical changes in the polymer in going from MeCN to DES and back again. Upon first exposure to 0.1 M LiClO₄ / MeCN the capacitance increased by 31% with increasing scan rate from 332 F g⁻¹ to 435 F g⁻¹ (5 mV s⁻¹ to 50 mV s⁻¹). The capacitance levelled off between 50 mV s⁻¹ to 200 mV s⁻¹ at a value of \approx 420 F g⁻¹. After exposure to Ethaline and transferral back to 0.1 M LiClO₄ / MeCN there was minimal loss in electro-activity, with the same trend presented in **Fig. 4.11B**, an increase in capacitance with increasing scan rate (5 mV s⁻¹ to 50 mV s⁻¹) and levelling off between 50 mV s⁻¹ to 200 mV s⁻¹.

The first exposure of PTP to Ethaline (after exposure to 0.1 M LiClO₄ / MeCN) the capacitance increased by 80% with increasing scan rate from 220 F g⁻¹ to 397 F g⁻¹ between 5 mV s⁻¹ to 50 mV s⁻¹. The capacitance decreased slightly from 397 F g⁻¹ to 329 F g⁻¹ between 50 mV s⁻¹ to 200 mV s⁻¹. After exposure to 0.1 M LiClO₄ / MeCN the trend of capacitance behaviour remained similar in Ethaline increasing from 5 to 50 mV s⁻¹ however decreasing slightly from 50 mV s⁻¹ to 200 mV s⁻¹.

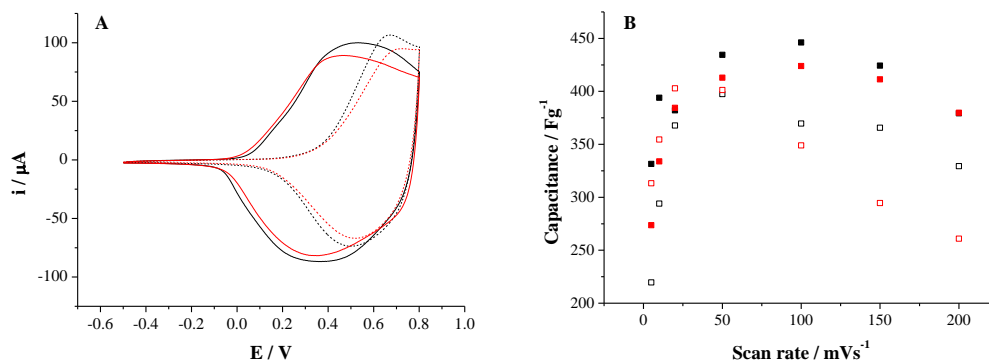


Fig. 4.11 - A) Bracketed cyclic voltammetric experiment of a PTP film (polymerised potentiostatically from 36 mM PTP in 0.1M LiBF₄ / MeCN at RT under N₂ (at 0.8V vs. Ag wire for 60s)) redox cycling firstly in 0.1 M LiClO₄ / MeCN (solid), secondly in ChCl / EG DES Ethaline (dashed) and repeated in that order (1st CV black, 2nd CV red) at 40 °C at 100 mV s⁻¹ -0.5 ≤ E / V ≤ 0.8 (mass of polymer film = 1.7582 μg, growth charge = 6.57 mC, P_{eff} = 45%) **B)** Mass specific capacitances from cyclic voltammetric data of PTP film (0.8V, 60s film used for redox cycling in **Fig. 4.11A**) during bracketed experiment at 7 different scan rates 5, 10, 20, 50, 100, 150 and 200 mV s⁻¹ redox cycling firstly in 0.1 M LiClO₄ / MeCN (solid squares), secondly in ChCl / EG DES Ethaline (outline squares) and repeated in that order (1st CV black, 2nd CV red) at 40 °C -0.5 ≤ E / V ≤ 0.8 (vs. Ag wire).

Fig. 4.12A shows the behaviour of PTP in ZnCl₂ / EG and ZnCl₂ / acetamide, from a bracketed experiment (method described above). In both electrolytes the CVs remained the same even after exposure to a different electrolyte. Upon first exposure to ZnCl₂ / EG the capacitance increased by 89% with increasing scan rate from 82 F g⁻¹ to 155 F g⁻¹ (5 mV s⁻¹ to 20 mV s⁻¹) then decreased to 72 F g⁻¹ shown in **Fig. 4.12B**. After exposure to ZnCl₂ / acetamide and transferral back to ZnCl₂ / EG there was minimal loss in electro-activity, an increase in capacitance with increasing scan rate 154 F g⁻¹ to a value of 222 F g⁻¹ (5 mV s⁻¹ to 20 mV s⁻¹) and decreasing between 20 mV s⁻¹ to 200 mV s⁻¹ to 54 F g⁻¹.

For the first exposure to ZnCl₂ / acetamide the capacitance decreased by 75% with increasing scan rate 5 mV s⁻¹ – 200 mV s⁻¹, from 44 F g⁻¹ to 11 F g⁻¹. After exposure to ZnCl₂ / EG then transferral back to ZnCl₂ / acetamide there was minimal loss in

electro-activity, however capacitances were lower than observed for $\text{ZnCl}_2 / \text{EG}$ Type IV DES. The mass specific capacitance decreased by 3% with increasing scan rate between $5 \text{ mV s}^{-1} - 200 \text{ mV s}^{-1}$ from 47 F g^{-1} to 8 F g^{-1} .

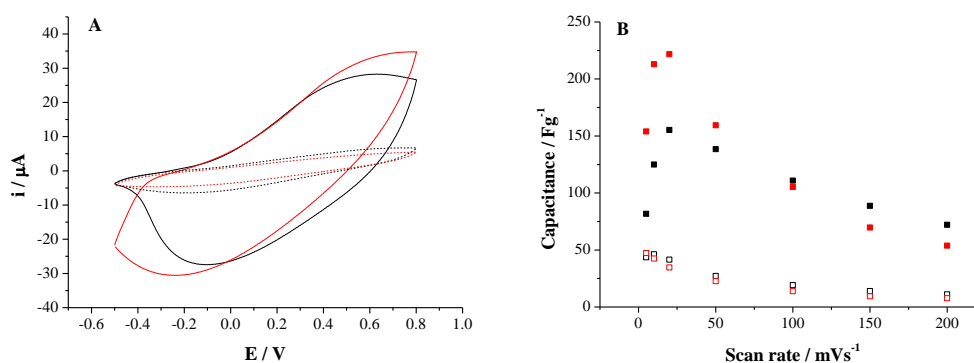


Fig. 4.12 - A) Bracketed cyclic voltammetric experiment of a PTP film (polymerised potentiostatically from 36 mM PTP in 0.1 M $\text{LiBF}_4 / \text{MeCN}$ at RT under N_2 (at 0.8 V vs. Ag wire for 60s)) redox cycling firstly in $\text{ZnCl}_2 / \text{ethylene glycol DES}$ (solid), secondly in $\text{ZnCl}_2 / \text{acetamide DES}$ (dashed) and repeated in that order (1st CV black, 2nd CV red) at 40°C at 100 mVs^{-1} $-0.5 \leq E / \text{V} \leq 0.8$ (mass of polymer film = $1.4562 \mu\text{g}$, growth charge = 5.87 mC , $P_{\text{eff}} = 42\%$) **B)** Mass specific capacitances from cyclic voltammetric data of PTP film (0.8 V, 60 s film used for redox cycling **Fig. 4.12A**) during bracketed experiment at 7 different scan rates 5, 10, 20, 50, 100, 150 and 200 mVs^{-1} redox cycling firstly in $\text{ZnCl}_2 / \text{ethylene glycol DES}$ (solid squares), secondly in $\text{ZnCl}_2 / \text{acetamide DES}$ (outline squares) and repeated in that order (1st CV black, 2nd CV red) at 40°C $-0.5 \leq E / \text{V} \leq 0.8$ (vs. Ag wire).

The bracketed experiment shows for a PTP film (prepared in 0.1 M $\text{LiBF}_4 / \text{MeCN}$) exposed to Ethaline the mass specific capacitance increases between 2 mVs^{-1} to 50 mVs^{-1} , at faster scan rates the capacitance values decrease slightly (**Fig. 4.11B**) in both electrolytes.

The same trend occurs with a PTP film (prepared in 0.1 M $\text{LiBF}_4 / \text{MeCN}$) exposed to $\text{ZnCl}_2 / \text{EG}$ (bracketed experiment), with an increasing capacitance at slow scan rates, but with a decrease in mass specific capacitance occurring at a 50 mVs^{-1} shown in **Fig. 4.12B**, compared to a decrease in capacitance observed at 100 mVs^{-1} in Ethaline.

However, the mass specific capacitance in ZnCl_2 / acetamide only decreased with increasing scan rate (from 2 mV s^{-1} to 200 mV s^{-1}).

Experiments were conducted to see if the trend between mass specific capacitance vs. scan rate is due to the properties of PTP or whether this trend changes dependent on the growth solution (different growth anion used). This can be seen by comparing data from films prepared using the same conditions in 0.1 M LiClO_4 / MeCN, in **Fig. 4.13**. The results suggest that in some electrolytes, growing the film in LiBF_4 / MeCN or LiClO_4 / MeCN has an effect on the capacitance values in monomer free electrolyte. Growth of PTP in LiBF_4 / MeCN gave higher capacitance values in Ethaline than PTP grown in LiClO_4 / MeCN. However, growth of PTP in LiClO_4 / MeCN gave higher capacitance values in ZnCl_2 / EG than PTP grown in LiBF_4 / MeCN. Further experiments would need to be conducted to see if this was consistent and repeatable, however investigating this further was not a focus.

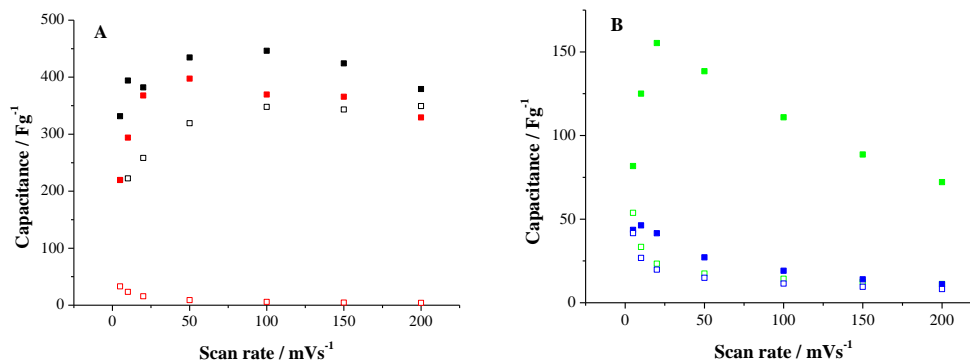


Fig. 4.13 - A) DC capacitance values for a PTP LiBF₄ film (polymerised potentiostatically from 36 mM PTP in 0.1 M LiBF₄ / MeCN at RT under N₂ (at 0.8 V vs. Ag wire for 60 s)) from **Fig. 4.8** (solid squares) compared with values for a PTP LiClO₄ / MeCN film (polymerised potentiostatically from 36 mM PTP in 0.1 M LiClO₄ / MeCN at RT under N₂ (at 0.8 V vs. Ag wire for 60 s)) (outline squares) redox cycling in 0.1 M LiClO₄ / MeCN (black) and in Ethaline (red) at 40 °C $-0.6 \leq E / V \leq 0.6$ at 7 different scan rates 5, 10, 20, 50, 100, 150 and 200 mVs⁻¹. **B)** DC capacitance values of a PTP LiBF₄ film (polymerised potentiostatically from 36 mM PTP in 0.1 M LiBF₄ / MeCN at RT under N₂ (at 0.8 V vs. Ag wire for 60 s)) (solid squares) compared with values for a PTP LiClO₄ / MeCN film (polymerised potentiostatically from 36 mM PTP in 0.1 M LiClO₄ / MeCN at RT under N₂ (at 0.8 V vs. Ag wire for 60 s)) (outline squares) redox cycling in ZnCl₂ / ethylene glycol DES (green) and in ZnCl₂ / acetamide DES (blue) at 40 °C $-0.6 \leq E / V \leq 0.6$ at 7 different scan rates 5, 10, 20, 50, 100, 150 and 200 mVs⁻¹.

PTP LiBF₄ film mass specific capacitances increased with increasing scan rate when redox cycling in 0.1 M LiClO₄ / MeCN and Ethaline. This trend also holds true with PTP LiClO₄ films when redox cycling in 0.1 M LiClO₄ / MeCN, however with the Ethaline the capacitance decreases with increasing scan rate (same trend as PTP LiBF₄ film in ZnCl₂ / acetamide).

The mass specific capacitance of a PTP LiBF₄ film during redox cycling in ZnCl₂ / EG, increases with increasing scan rate. This trend is not the same as the thiophene-pyrrole LiClO₄ film for ZnCl₂ / EG, the capacitance decreases with increasing scan rate. The same trend of decreasing capacitance occurs for PTP LiBF₄ and LiClO₄ films in ZnCl₂ / acetamide.

The behaviour of PTP over 40 CVs gave an appreciation of the change in mass specific capacitance over a long usage period. The mass specific capacitance of PTP in $\text{LiClO}_4 / \text{MeCN}$ remained constant over 40 CVs, with a small increase of 1% over 40 CVs from 514 F g^{-1} to 518 F g^{-1} , shown in **Fig. 4.14**. The mass specific capacitance of PTP in Ethaline decreased by 40% over 40 CVs from 278 F g^{-1} to 167 F g^{-1} , shown in **Fig. 4.15**. The mass specific capacitance of PTP in Propaline increased by 204% over 40 CVs from 25 F g^{-1} to 77 F g^{-1} , shown in **Fig. 4.16**. The mass specific capacitance of PTP in $\text{ZnCl}_2 / \text{EG}$ increased by 53% over 40 CVs from 135 F g^{-1} to 207 F g^{-1} (**Fig. 4.17**). The mass specific capacitance of PTP in $\text{ZnCl}_2 / \text{acetamide}$ increased by 189% over 40 CVs from 9 F g^{-1} to 26 F g^{-1} (**Fig. 4.18**).

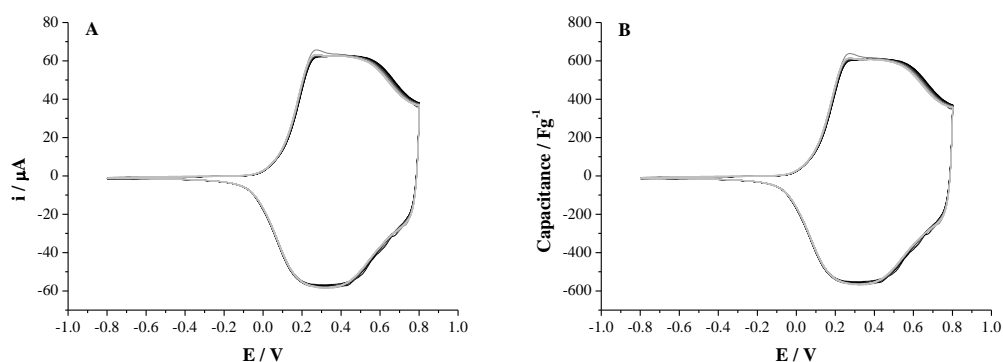


Fig. 4.14 - A) Cyclic voltammetric data for the redox cycling of a potentiostatically deposited PTP LiBF_4 film (0.8 V for 120 s) in $0.1 \text{ M LiClO}_4 / \text{MeCN}$ at 40°C for 40 scans at 20 mV s^{-1} $-0.8 \leq E / \text{V} \leq 0.8$ (vs. Ag wire) (mass of polymer film = $5.15 \mu\text{g}$, growth charge = 15.51 mC , $P_{\text{eff}} = 55.81\%$). **B)** Current axis from cyclic voltammetric data converted to F g^{-1} using mass of film from double potential step data.

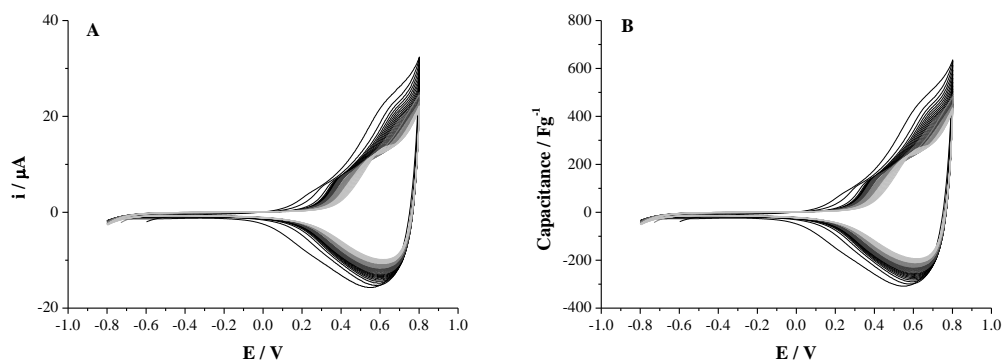


Fig. 4.15 - A) Cyclic voltammetric data for the redox cycling of a potentiostatically deposited PTP LiBF_4 film (0.8 V for 120 s) in Ethaline at 40 °C for 40 scans at 20 mV s^{-1} $-0.8 \leq E / \text{V} \leq 0.8$ (vs. Ag wire) (mass of polymer film = 2.5465 μg , growth charge = 17.28 mC, $P_{\text{eff}} = 24.78\%$). **B)** Current axis from cyclic voltammetric data converted to F g^{-1} using mass of film from double potential step data.

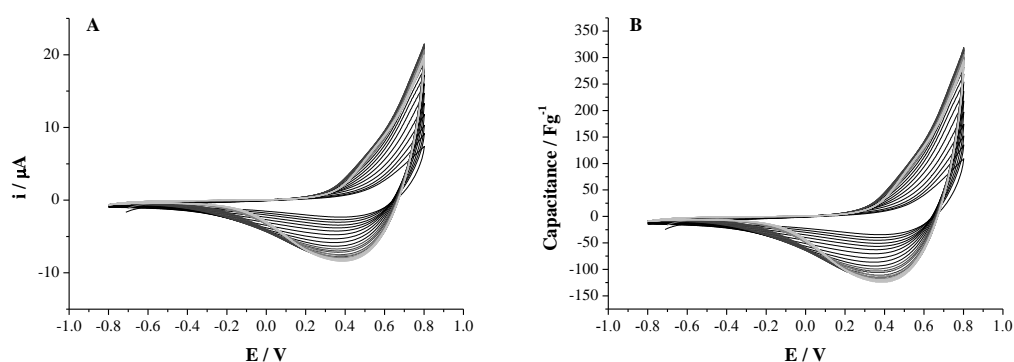


Fig. 4.16 - A) Cyclic voltammetric data for the redox cycling of a potentiostatically deposited PTP LiBF_4 film (0.8 V for 120 s) in Propaline at 40 °C for 40 scans at 20 mV s^{-1} $-0.8 \leq E / \text{V} \leq 0.8$ (vs. Ag wire) (mass of polymer film = 3.38 μg , growth charge = 18.05 mC, $P_{\text{eff}} = 31.47\%$). **B)** Current axis from cyclic voltammetric data converted to F g^{-1} using mass of film from double potential step data.

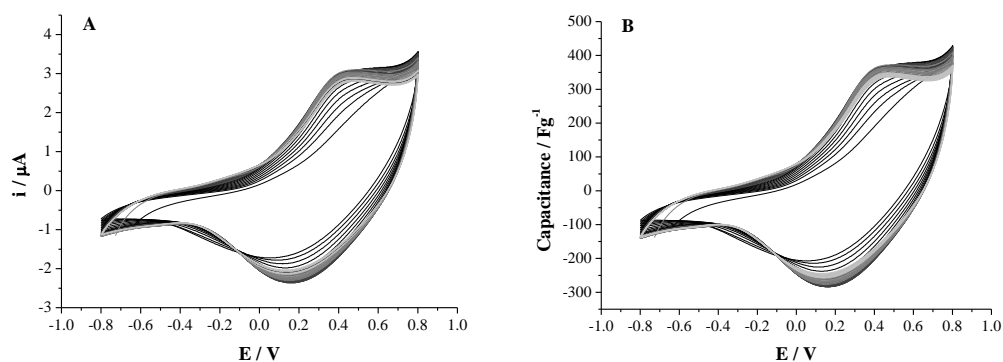


Fig. 4.17 - A) Cyclic voltammetric data for the redox cycling of a potentiostatically deposited PTP LiBF_4 film (0.8 V for 120 s) in ZnCl_2 / ethylene glycol at 40 °C for 40 scans at 20 mV s^{-1} $-0.8 \leq E / \text{V} \leq 0.8$ (vs. Ag wire) (mass of polymer film = 0.42 μg , growth charge = 19.03 mC, $P_{\text{eff}} = 3.679\%$). **B)** Current axis from cyclic voltammetric data converted to F g^{-1} using mass of film from double potential step data.

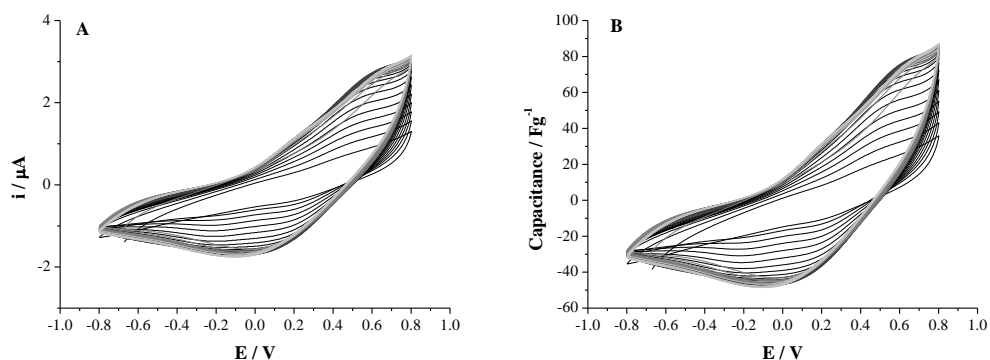


Fig. 4.18 - A) Cyclic voltammetric data for the redox cycling of a potentiostatically deposited PTP LiBF_4 film (0.8 V for 120 s) in ZnCl_2 / acetamide at 40°C for 40 scans at 20 mV s^{-1} $-0.8 \leq E / \text{V} \leq 0.8$ (vs. Ag wire) (mass of polymer film = $1.81\ \mu\text{g}$, growth charge = $16.64\ \text{mC}$, $P_{\text{eff}} = 18.29\%$). **B)** Current axis from cyclic voltammetric data converted to F g^{-1} using mass of film from double potential step data.

4.3.3.4 Mass Specific Capacitance of PEDOT-hexylPy films

Table 4.5 reports the mass specific capacitances from potentiostatically deposited PEDOT-hexylPy. The highest capacitances are observed with $0.1\ \text{M LiClO}_4 / \text{MeCN}$, Ethaline and $\text{ZnCl}_2 / \text{EG}$. These electrolytes were observed to produce high capacitances for the other polymers investigated, PEDOT, PPy and PTP. However, it should be noted that the PEDOT-hexylPy films were not stable as the appearance of the film deteriorated during redox switching and transferral to different electrolytes. This was attributed to the loss of non-adherent oligomers into the bathing solution due to the high solubility of PEDOT-hexylPy. The high solubility of PEDOT-hexylPy arises because of the hexyl chain on the pyrrole ring. Therefore because of the stability issue observed with PEDOT-hexylPy, this polymer was not considered further for use in a battery device.

Table 4.5 - Mass specific capacitances for potentiostatically deposited PEDOT-hexylPy films (0.8 V for 180 s and 1.1 V for 180 s to produce a 360 s film, 0.8 V for 210 s and 1.1 V for 210 s to produce a 420 s film) measured from cyclic voltammograms, reported as an average of values from scan rates 5, 10, 20, 50, 100, 150 and 200 mV s⁻¹.

Electrolyte	MSC / F g ⁻¹	
	360 s	420 s
0.1 M LiClO ₄ / MeCN	173	138
0.1 M LiClO ₄ / H ₂ O	76	71
Ethaline	157	73
Ethaline:H ₂ O 1:1	90	94
Reline	30	12
Reline:H ₂ O 1:1	55	95
Zn(NO ₃) ₂ .6H ₂ O / ChCl	76	52
ZnCl ₂ / EG	134	231
ZnCl ₂ / acetamide	32	34
ZnCl ₂ / 1,6-hexanediol	75	124

4.4 Conclusions

For the production of the Zn-Polymer battery device it is preferable not to use organic solvents and DESs containing water for safety reasons and to avoid zinc dendrite formation on the anode of the battery. Therefore for the battery device the more suitable electrolytes would be Type III or Type IV DESs rather than conventional systems.

Out of the two Type III DESs investigated Ethaline and Reline, the higher polymer capacitances were observed for Ethaline, therefore further electrochemical studies focussed on using Ethaline only in a device.

It would be advantageous for the electrolyte to contain a high concentration of zinc for the functioning of the anode of the device, therefore Zn based Type IV DESs were investigated. Four Type IV DESs were investigated Zn(NO₃)₂.6H₂O / ChCl, ZnCl₂ / EG, ZnCl₂ / acetamide and ZnCl₂ / 1,6-hexanediol. The use of Zn(NO₃)₂.6H₂O / ChCl in a device was ruled out due to containing water. Low

capacitances were observed for PEDOT, PPy and PTP in ZnCl_2 / 1,6-hexanediol so this electrolyte was also not considered further for using in a battery device. **Table 4.6** shows the variation in the mass specific capacitances of the different polymers in both conventional and DES electrolytes as well as highlighting the high mass specific capacitances observed for Ethaline.

Table 4.6 - Mass specific capacitances for potentiostatically deposited polymer films PEDOT, PPy and PTP (60 s films) and PEDOT-hexylPy (360 s film) measured from cyclic voltammograms, reported as an average of values from scan rates 5, 10, 20, 50, 100, 150 and 200 mV s^{-1} .

Electrolyte	MSC / F g^{-1}			
	PEDOT	PPy	PTP	PEDOT-hexylPy
0.1 M LiClO_4 / MeCN	118	10	217	173
0.1 M LiClO_4 / H_2O	81	33	175	76
Ethaline	89	5	206	157
Ethaline: H_2O 1:1	80	11	213	90
Reline	7	-	6	30
Reline: H_2O 1:1	9	-	5	55
$\text{Zn}(\text{NO}_3)_2 \cdot 6\text{H}_2\text{O}$ / ChCl	164	2	283	76
ZnCl_2 / EG	118	3	139	134
ZnCl_2 / acetamide	85	2	88	32
ZnCl_2 / 1,6-hexanediol	7	0.4	3	75

Experiments termed ‘bracketed experiments’ where the behaviour of a single film was investigated in two different electrolytes, showed there was no loss in electro-activities of the films when films were transferred to different electrolytes. Growing the polymer in MeCN and then transferring to DES seems to cause no irreversible chemical change in the polymer, evidenced by the ‘bracketed experiments’, but that substantial changes occur in the MSC of a film upon transfer to DES, depending on the nature of the electrolyte, physical properties, conductivity and viscosity. These MSC changes are likely to be due to changes in polymer configuration and electrolyte mobility (the focus

of Electrochemical Quartz Crystal Microbalance studies in **Chapter 5** and **Chapter 6**). PEDOT and PTP films are stable when cycled in DES and PTP provides a good polymer backbone in comparison to either PEDOT or PPy.

From cyclic voltammetric studies PEDOT and PTP gave the highest mass specific capacitances of the four systems studied. PEDOT-hexylPy provided relatively good mass specific capacitances however during redox switching in monomer free electrolytes and transferral into different electrolytes the appearance of the film deteriorated, attributed to PEDOT-hexylPy having a high solubility, due to the hexyl chain on the pyrrole ring. PPy exhibited the lowest capacitances therefore was not explored further for use in the Zn-Polymer battery.

4.5 References

- [1] Skotheim TA and Reynolds JR, *Handbook of Conducting Polymers - Processing and Applications*, 3rd Edition
- [2] Snook GA, Peng C, Fray DJ and Chen GZ, *Electrochem. Commun.*, 2007, 9, 1, 83-88
- [3] Suematsu S, Oura Y, Tsujimoto H, Kanno H and Naoi K, *Electrochimica Acta*, 2000, 45, 22-23, 3813-3821
- [4] Park JH and Park OO, *J Power Sources*, 2002, 111, 1, 185-190
- [5] Ahn YR, Song MY, Jo SM, Park CR and Kim DY, *Nanotechnology*, 2006, 17, 12, 2865-2869
- [6] Ren XM and Pickup PG, *J. Electroanalytical Chem.*, 1994, 372, 1-2, 289-291
- [7] Snook GA, Kao P and Best AS, *J. Power Sources*, 2011, 196, 1, 1-12
- [8] Hughes M, Chen GZ, Shaffer MSP, Fray DJ and Windle AH, *Chem. Mater.*, 2002, 14, 4, 1610-1613
- [9] Bobacka J, Lewenstam A and Ivaska A, *J. Electroanalytical Chem.*, 2000, 489, 1-2, 17-27
- [10] Snook GA and Chen GZ, *J. Electroanal. Chem.*, 2008, 612, 1, 140-146
- [11] Lota K, Khomenko V and Frackowiak E, *J. Physics and Chemistry of Solids*, 2004, 65, 2-3, 295-301
- [12] Xu Y, Wang J, Sun W and Wang S, *J. Power Sources*, 2006, 159, 1, 370-373
- [13] Ingram MD, Staesche H and Ryder KS, *J. Power Sources*, 2004, 129, 1, 107-112
- [14] Laforgue A, *J. Power Sources*, 2011, 196, 1, 559-564
- [15] Ryu KS, Lee YG, Hong YS, Park YJ, Wu XL, Kim KM, Kang MG, Park NG and Chang SH, *Electrochimica Acta*, 2004, 50, 2-3, 843-847
- [16] Randriamahazaka H, Plesse C, Teyssié D and Chevrot C, *Electrochem. Commun.*, 2004, 6, 3, 299-305
- [17] Carlberg C, Chen XW and Ingnäs O, *Solid State Ionics*, 1996, 85, 1-4, 73-78
- [18] Roncali J, *Chem. Rev.*, 1992, 92, 4, 711-738
- [19] Naitoh S, Sanui K and Ogata N, *J. Chem. Soc., Chem. Commun.*, 1986, 17, 1348-1350
- [20] Ping Z, Federspiel P, Grünberger A and Nauer GE, *Synthetic Metals*, 1997, 84, 1-3, 837-838
- [21] Hillman AR, Daisley SJ and Bruckenstein S, *Phys. Chem. Chem. Phys.*, 2007, 9, 19, 2379-2388
- [22] Baba A, Lübben J, Tamada K and Knoll W, *Langmuir*, 2003, 19, 21, 9058-9064
- [23] Hillman AR, Efimov I and Ryder KS, *J. Am. Chem. Soc.*, 2005, 127, 47, 16611-16620

Chapter 5

Comparison of the Charging Behaviour of PEDOT in DESs

5.1 Introduction

5.1.1 Objectives

5.1.2 Experimental

5.2 Results and Discussion - Redox Driven Exchange Processes of Potentiodynamically Deposited PEDOT

5.2.1 Behaviour in 0.1 M LiClO₄ / MeCN

5.2.2 Behaviour in ZnCl₂ / EG (Type IV) DES

5.2.3 Behaviour in Ethaline (Type III) DES

5.2.4 Behaviour in Ethaline containing 0.3 M ZnCl₂

5.3 Conclusions

5.4 References

Chapter 5

Comparison of the Charging Behaviour of PEDOT in DESs

5.1 Introduction

5.1.1 Objectives

In this chapter, the behaviours of PEDOT films electrochemically deposited on Au coated quartz crystals were investigated when exposed to a conventional molecular solvent (MeCN) which contained the salt LiClO₄, Type III DESs and Type IV DESs. The redox behaviour of PEDOT in the two different types of DES media were compared against the widely reported and established behaviour of PEDOT in molecular solvents ^{[1][2][3][4][5][6][7][8][9][10]}. However, it was unclear whether the wealth of knowledge on the behaviour in molecular solvents could be applied to that of highly ionic media, DESs, due to the absence of ‘solvent’ in the standard sense. The absence of a molecular solvent can influence the ion dynamics associated with the doping and undoping of a conducting polymer. Therefore, the motivation for this study was to gravimetrically explore whether the p-doping (undoping) in DESs involved mixed ion transport (anions and cations), single ion transport or whether neutral species were involved. The behaviour of PEDOT in DESs was compared to the published work on PEDOT ^{[1][2][11][12]}. Numerous researchers have investigated PEDOT for use in an electrochemical device due to its good charge storage capability; however EDOT can be hard to polymerise and is relatively expensive.

Within an electrochemical device, the conducting polymer can be in a partially converted redox state, which can result in changes in electrochemical behaviour and polymer dynamics. The EQCM studies attempt to examine these properties *in situ* with

the film in a continuously changing, partially converted redox state ^{[13] [14] [15] [16]}.

The experiments performed aimed to explore the electrochemical behaviour of PEDOT by varying:

- Electrolyte type
- Film thickness
- Timescale of the electrochemical study in one electrolyte (*i.e.* changing the potential scan rate)
- Exposure time to potential perturbations (*i.e.* long periods of redox cycling in one electrolyte)
- Electrodeposition conditions in terms of electrochemical control regimes (*i.e.* potentiodynamically and potentiostatically deposited films)

The overarching aim was to suggest identities of mobile species during p-doping and undoping of PEDOT in the different electrolyte media *i.e.* the ion dynamics, to fit the observed gravimetric data (coupled mass / charge data). In all these cases, the experiments monitored the electro-activity, behaviour and stability in different electrolytes and any resultant changes in the doping (undoping) regimes.

The first objective of the studies was to identify anion and cation transfers in DES media and how these respond to applied potential and variation of experimental timescale (varying scan rate in a voltammetric experiment). The second objective was to compare the behaviour of PEDOT in two different types of DES media; a Type III DES (composed of a quaternary ammonium salt (QAS) choline chloride and a hydrogen bond donor (HBD) ethylene glycol (EG) in a 1 : 2 mole ratio) and a Type IV DES (composed of a metal salt $ZnCl_2$ and the same hydrogen bond donor as Type III DES

ethylene glycol in a 1 : 4 mole ratio). The third objective was to investigate whether prolonged redox cycling led to deterioration of the film performance in terms of capacitance and response.

The methodologies for identification and quantification of the mobile species using the EQCM in this thesis were adopted from Bund and Neudeck ^[1]. The article reported the p-doping (undoping) behaviour of potentiostatically deposited PEDOT films on Au quartz crystals in acetonitrile and aqueous solutions of a range of salts ^[1]. The changes in the frequency of the crystal were related to changes in surface attached mass via the application of the Sauerbrey Equation ^[17] **(5.1)** (see Experimental Methodology **Chapter 2** for more details).

The frequency changes enabled quantification of the mass of the polymer deposited and the mass exchange of the polymer with monomer free electrolyte during redox cycling. The mass exchanges during doping (undoping) as a function of charge were used to quantify the apparent molar mass exchanges (M_{app}) for each regime, achieved by application of Faraday's Law of electrolysis **(5.1)** ^{[1][18][19]} where Δm is the mass change in surface bound species during redox cycling of a polymer film in monomer free electrolyte, Q is the charge passed, n is the valency number (electrons transferred per ion) and F is Faraday's constant (96485 C mol^{-1}). Apparent molar mass exchanges (M_{app}) for the doping and undoping regimes were calculated by the product of gradients from the doping and undoping regions of a Δm vs Q plot and Faraday's constant (using equation **(5.1)**).

$$\frac{\Delta m}{Q} = \frac{M_{app}}{nF} \quad \text{(5.1)}$$

These M_{app} values were expressed as a combination of the molar masses of mobile species transferred across the polymer / electrolyte interface. Contributions to M_{app} were possible from any mobile species present; anions (M_{anion}), cations (βM_{cation}) and / or solvent (αM_{solv}) (5.2) and were dependent on the polymer investigated, experimental conditions, the redox state and behaviour of the polymer, as well as the physical properties of the mobile species, in terms of the sizes of the ions and their mobilities^[20]. Therefore equation (5.2) has no unique solution and is underdetermined as there are more variables than measurements, so the simplest solution will be used to determine the origin of M_{app} as this will tend to be the most likely, feasible scenario.

$$M_{app} = M_{anion} + \alpha M_{solv} + \beta M_{cation} \quad (5.2)$$

The term α represented the number of solvent molecules exchanged per anion. The sign of α did not indicate the ingress or egress of solvent, but rather showed whether the solvent movement was opposed to anion movement ($\alpha =$ negative) or coupled in the same direction, *i.e.* complementary to anion movement ($\alpha =$ positive). The β term was similar to the α term, in that it represented the number of cations exchanged per anion; a negative sign related to cation movement opposed to anion movement and a positive sign related to cation movement coupled with anion movement *i.e.* in the same direction.

In general, it is understood that to maintain electro-neutrality during p-doping, anions ingress into the polymer matrix and / or cations egress, with the reverse occurring upon undoping^{[20][21]}. As well as coupled electron / ion transfers and solvent transfers, the redox process also can involve polymer reconfiguration processes, such as swelling or collapse^[22].

Bund and Neudeck ^[1] reported no significant contributions of [Li]⁺, [Na]⁺ or [TBA]⁺ cations during p-doping and undoping of PEDOT in acetonitrile and aqueous solutions of a range of salts. Only anion and solvent transfers were observed to fit the gravimetric data reported, *i.e.* M_{app} values were expressed as contributions from only anions and solvent species (5.3), with α reported as -1 for both p-doping and undoping ^[1].

$$M_{app} = M_{anion} + \alpha M_{solv} \quad (5.3)$$

Due to the absence of molecular solvent in the DES media cation transfers will have to be considered for the behaviour of PEDOT in the DESs as expressed in (5.4).

$$M_{app} = M_{anion} + \beta M_{cation} \quad (5.4)$$

Alternatively the involvement of a neutral species xM_{neut} , may have to be considered to replace the αM_{solv} as expressed in (5.5).

$$M_{app} = M_{anion} + xM_{neut} \quad (5.5)$$

In this thesis, M_{app} values during oxidation (p-doping) were reported as overall molar mass exchanges from the cathodic vertex potential to the anodic vertex potential of cyclic voltammograms. The M_{app} values for reduction (undoping) were reported from the anodic vertex potential to the cathodic vertex potential. In other words, the M_{app} were determined as overall molar mass exchanges from one end of the potential window to the other, therefore M_{app} values are also referred to throughout as end-to-end molar mass exchanges. Ion and solvent fluxes were also determined to probe the properties of the polymers in partially converted redox states ^{[2] [23] [24]}. These M_{app} values and fluxes helped to develop an understanding of the mass exchanges and properties of a PEDOT cathode with a selected battery electrolyte during device usage.

5.1.2 Experimental

PEDOT A, B, BB, BA, C1, C2 films were deposited potentiodynamically (see **Table 5.1** for conditions); from 0.1 M EDOT in 0.1 M LiClO₄ / MeCN solution, and the behaviour investigated in monomer free 0.1 M LiClO₄ / MeCN, Type III DESs and Type IV DESs. For details on the EQCM set-up see Experimental Chapter section **3.3.1**. PEDOT films labelled with the first letter **A** were exposed to 0.1 M LiClO₄ / MeCN, **B** exposed to ZnCl₂ / EG Type IV DES and **C** exposed to Ethaline Type III DES. PEDOT films labelled with a single letter and with a number were deposited potentiodynamically at 5 mV s⁻¹; labelled with the second letter **A** were deposited potentiodynamically at 20 mV s⁻¹; labelled with the second letter **B** were deposited at 5 mV s⁻¹.

Table 5.1 - PEDOT potentiodynamic deposition (using 0.1 M EDOT solution) and experimental conditions.

Redox Cycling at 40 °C									
PEDOT Films	Growth in 0.1 M LiClO ₄ / MeCN	Growth Q / mC (2 d.p)	wet mass / μg (4 s.f)	wet thickness / μm (2 d.p)	dry mass / μg (4 s.f)	dry thickness / μm (2 d.p)	Electrolyte	scan rate	number of scans and potential window
A	5 scans at 5 mV s ⁻¹ -0.3 ≤ E / V ≤ 1.1	13.54	65.57	2.4	43.11	1.58	0.1 M LiClO ₄ / MeCN	5, 10, 20 mV s ⁻¹ (x2)	3 CVs per scan rate -0.3 ≤ E / V ≤ 1.1
B	5 scans at 5 mV s ⁻¹ -0.3 ≤ E / V ≤ 1.1	4.38	21.19	0.78	16.13	0.59	1 ZnCl ₂ / 4 EG	5, 10, 20 mV s ⁻¹ (x2)	3 CVs per scan rate -0.3 ≤ E / V ≤ 1.1
BA	5 scans at 20 mV s ⁻¹ -0.3 ≤ E / V ≤ 1.2	4.37	21.14	0.77	30.95	1.13	1 ZnCl ₂ / 4 EG	5 mV s ⁻¹	40 CVs -0.3 ≤ E / V ≤ 1.1
BB	5 scans at 5 mV s ⁻¹ -0.3 ≤ E / V ≤ 1.1	3.18	15.38	0.56	21.77	0.8	0.1 M LiClO ₄ / MeCN	5 mV s ⁻¹	9 CVs -0.3 ≤ E / V ≤ 1.1
							1 ZnCl ₂ / 4 EG	5 mV s ⁻¹	9 CVs -0.3 ≤ E / V ≤ 1.1
							0.1 M LiClO ₄ / MeCN	5 mV s ⁻¹	9 CVs -0.3 ≤ E / V ≤ 1.1
C1	5 scans at 5 mV s ⁻¹ -0.3 ≤ E / V ≤ 1.2	5.03	24.34	0.89	32.47	1.19	Ethaline	5 mV s ⁻¹	40 CVs -0.3 ≤ E / V ≤ 0.8
C2	5 scans at 5 mV s ⁻¹ -0.3 ≤ E / V ≤ 1.2						0.3 M ZnCl ₂ in Ethaline	5 mV s ⁻¹	40 CVs -0.3 ≤ E / V ≤ 0.8

5.2 Results and Discussion - Redox Driven Exchange Processes of Potentiodynamically Deposited PEDOT

Fig. 5.1 shows a representative $i(E)$ response and mass increases (determined from the changes in frequency Δf of the quartz crystal) during the electrodeposition of PEDOT from acetonitrile solution as a function of potential. The deposition behaviours of the films were typical of those observed for PEDOT so these were not considered further. PEDOT A was the thickest film deposited at $2.4 \mu\text{m}$, compared to the other potentiodynamically deposited films with thicknesses which ranged between $40 \text{ nm} - 1.32 \mu\text{m}$.

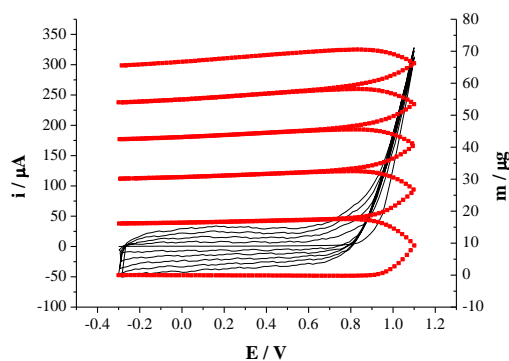


Fig. 5.1 - Cyclic voltammetric data and m vs. E for the potentiodynamic deposition of PEDOT A on an EQCM crystal Au electrode from 0.1 M EDOT in 0.1 M $\text{LiClO}_4 / \text{MeCN}$ at RT for 5 scans at 5 mV s^{-1} cycling the potential between $-0.3 \leq E / \text{V} \leq 1.1$ (vs. Ag wire) depositing a film with a mass of $65.57 \mu\text{g}$ and a thickness of $2.4 \mu\text{m}$ (assuming $\rho = 1.3 \text{ g cm}^{-3}$). Current trace shown by the black solid line and mass shown by the red square data points.

The main focus of this research was to understand the electrochemical behaviour of PEDOT films in DESs. Therefore, how the acoustic admittance spectra varied in this media compared to molecular solvents had to be considered when investigating the behaviour of PEDOT exposed to this type of electrolyte using the EQCM.

The overall redox switching of PEDOT exposed to DES media in terms of the $i(E)$ responses were considered and compared to the established behaviour in acetonitrile.

This was followed by consideration of gravimetrically determined mass changes during (dis)charging of PEDOT (in terms of the overall apparent molar exchanges (M_{app}) to identify ion transfers.

Initial studies compared the behaviour of acoustically thick films of PEDOT exposed to a Type IV DES and acetonitrile solution. Studies deliberately focussed on thicker films than previously studied, as an electrochemical device would require a relatively thick polymer film for durability purposes.

5.2.1 Behaviour in 0.1 M LiClO₄ / MeCN

The behaviour of **PEDOT A** during a voltammetric experiment in 0.1 M LiClO₄ / MeCN at 5 mV s⁻¹ with the associated mass changes per redox cycle as a function of potential presented in **Fig. 5.2A** showed no pronounced redox peaks. **PEDOT A** gave a capacitor type $i(E)$ response on the Au substrate, the same as observed for PEDOT on Pt in **Chapter 4**. The observed mass changes as a function of the total charge passed during the cyclic voltammogram reported in **Fig. 5.2B** showed no mass retention was observed over the three scans at 5 mV s⁻¹. The oxidation involved an increase in current coupled with an increase in mass ($\approx 6 \mu\text{g}$), which related to $\approx 9\%$ of the total mass of the polymer. During reduction the reverse situation occurred, with a decrease in current coupled with a decrease in mass ($\approx 6 \mu\text{g}$) returning the film back to the mass at the start of the experiment. The CV of **PEDOT A** was studied at long and short timescales, achieved by varying the potential scan rate (5, 10 and 20 mV s⁻¹). The end-to-end molar mass exchanges (M_{app}) calculated for the doping and undoping regimes at the three different scan rates investigated are reported in **Table 5.2**.

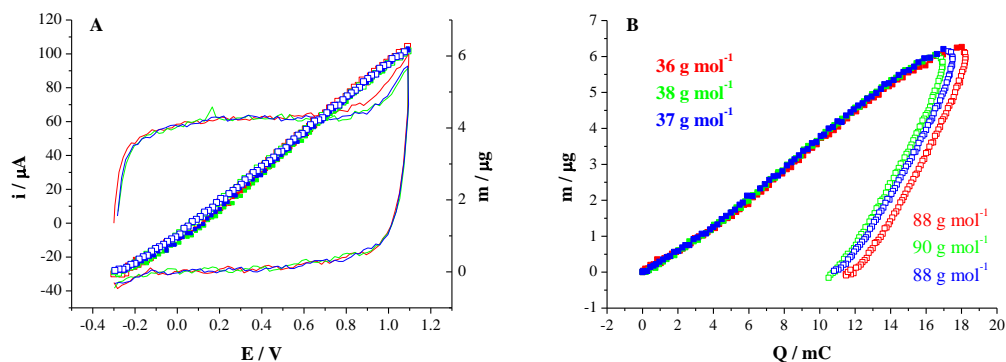


Fig. 5.2 - A) Cyclic voltammetric data and m vs. E **B)** m vs. Q for the redox cycling of PEDOT A in 0.1 M LiClO₄ / MeCN at 40 °C for 3 scans at 5 mV s⁻¹ -0.3 ≤ E / V ≤ 1.1 (vs. Ag wire) with associated M_{app} (g mol⁻¹). Doping = solid squares, undoping = outline squares (1st scan = red, 2nd scan = green, 3rd scan = blue).

Table 5.2 - M_{app} from m vs. Q graphs for PEDOT A during redox cycling in 0.1 M LiClO₄ / MeCN at 40 °C between -0.3 ≤ E / V ≤ 1.1 (vs. Ag wire) for 3 scans at 3 scan rates (5, 10, 20 mV s⁻¹) and the sequence repeated. Data highlighted in yellow from data in Fig. 5.2B. Mobile species molar masses for this electrolyte M_{anion} [ClO₄]⁻ = 99 g mol⁻¹ and $M_{solvent}$ MeCN = 41 g mol⁻¹. ↑ represents a mass increase, ↓ represents a mass decrease.

scan rate	M_{app} / g mol ⁻¹					
	Oxidation scan 1	Reduction scan 1	Oxidation scan 2	Reduction scan 2	Oxidation scan 3	Reduction scan 3
5 mV s ⁻¹	↑ 36	↓ 88	↑ 38	↓ 90	↑ 37	↓ 88
5 mV s ⁻¹	↑ 32	↓ 74	↑ 33	↓ 73	↑ 33	↓ 71
10 mV s ⁻¹	↑ 45	↓ 61	↑ 45	↓ 58	↑ 42	↓ 60
10 mV s ⁻¹	↑ 39	↓ 47	↑ 40	↓ 54	↑ 42	↓ 52
20 mV s ⁻¹	↑ 46	↓ 66	↑ 48	↓ 67	↑ 48	↓ 67
20 mV s ⁻¹	↑ 43	↓ 50	↑ 47	↓ 53	↑ 47	↓ 54

Bund and Neudeck ^[1] reported the doping process of potentiostatically deposited PEDOT in 0.1 M LiClO₄ / MeCN (0.2 V to 0.6 V at 10 mV s⁻¹) involved the entry of one [ClO₄]⁻ anion for electro-neutrality associated with the expulsion of one solvent molecule (MeCN). The paper reported that no cation exchange would occur in this electrolyte within the potential window probed ^[1]. The undoping M_{app} were reported as the same as the doping M_{app} , indicating a reverse of the mobile species transfers

observed for the doping process. Therefore, α values of -1 were reported for both regimes ^[1] (using equation (5.3)).

$$M_{app} = M_{anion} + \alpha M_{solv} \quad (5.3)$$

The M_{app} values reported in **Table 5.2** were therefore expressed as a combination of only anion and solvent transfers (5.3), with the polymer acting in a permselective manner, due to the low salt concentration of the supporting electrolyte. The values of α and the identities of mobile species suggested to fit the observed gravimetric data for the doping and undoping regimes are reported in **Table 5.3**.

Table 5.3 - Mobile species transfers and α values to fit the assumption of $M_{app} = M_{anion} + \alpha M_{solv}$ for **PEDOT A** during redox cycling in 0.1 M LiClO₄ / MeCN at 40 °C between $-0.3 \leq E / V \leq 1.1$ (vs. Ag wire) at 3 scan rates (5, 10, 20 mV s⁻¹) and the sequence repeated. The terms IN and OUT referred to the polymer film and the associated direction of transport of mobile species *i.e.* into or out of the polymer film. Mobile species molar masses for this electrolyte M_{anion} [ClO₄]⁻ = 99 g mol⁻¹ and M_{solv} MeCN = 41 g mol⁻¹.

scan rate	Doping			n [ClO ₄] ⁻ : n MeCN	Undoping			n [ClO ₄] ⁻ : n MeCN
	Anion	Solvent	α		Anion	Solvent	α	
5 mV s ⁻¹	[ClO ₄] ⁻ IN	MeCN OUT	-1.5	0.7	[ClO ₄] ⁻ OUT	MeCN IN	-0.3	3.3
5 mV s ⁻¹			-1.6	0.6			-0.6	1.7
10 mV s ⁻¹			-1.3	0.8			-1	1
10 mV s ⁻¹			-1.4	0.7			-1.2	0.8
20 mV s ⁻¹			-1.3	0.8			-1	1
20 mV s ⁻¹			-1.3	0.8			-1.1	0.9

The doping M_{app} values reported for **PEDOT A** (**Table 5.2**) in 0.1 M LiClO₄ / MeCN were interpreted as the entry of a [ClO₄]⁻ anion ($M_{anion} = 99$ g mol⁻¹) and the expulsion of a small amount of solvent ($M_{solv} = 41$ g mol⁻¹); ranging from 1.3 to 1.6 MeCN expelled per [ClO₄]⁻ anion entering the film. At scan rates 10 mV s⁻¹ and 20 mV s⁻¹ less solvent was expelled per [ClO₄]⁻ anion entering, with a value of α of -1.3. Therefore, at short timescales (10 and 20 mV s⁻¹) coupled electron / anion transfer must be the rate determining process and preferred over solvent transfers. Solvent transfers occur by

‘diffusional’ pathways which tend to be slower than charged species transfers which occur due to electric field gradients^[22]. This information from the literature supports the observed doping gravimetric data that at shorter timescales more $[\text{ClO}_4]^-$ transfer occurs.

The gravimetric data for the undoping of **PEDOT A**, suggested the expulsion of the $[\text{ClO}_4]^-$ anion and the entry of a smaller amount of solvent *cf.* the amount expelled during doping. The amount of solvent entry ranged between 0.3 to 1.2 MeCN per $[\text{ClO}_4]^-$ anion expelled, dependent on the scan rate. The drop in solvent transfer from doping to undoping was possibly due to the movement of the anion out of the polymer into the electrolyte impeding the movement of solvent in the opposite direction.

At faster scan rates during undoping (10 mV s^{-1} and 20 mV s^{-1}) more solvent entry into the film was observed, with values of α of between -1 and -1.2. This suggested the movement of anion out of the polymer film created space for solvent to re-enter. As the anion transfers out of the polymer this creates space for solvent entry into the film via diffusion. The solvent entries at short timescales (10 mV s^{-1} and 20 mV s^{-1}) were observed to be greater than at long timescales.

Molar percentage contributions of species were calculated using the α values from **Table 5.3**. During doping, solvent (MeCN) was observed as the dominant mobile species at $\approx 60\%$ (in molar terms), whilst the anion only contributed to $\approx 40\%$ of the M_{app} . During undoping at 5 mV s^{-1} , the dominant mobile species was anion egress at $\approx 60 - 80\%$, whilst the solvent only contributed to $\approx 20 - 40\%$ of the M_{app} . At faster

scan rates (10 mV s^{-1} and 20 mV s^{-1}) equal contributions of anion and solvent transfers were observed ($\approx 50\%$ for both $[\text{ClO}_4]^-$ egress and MeCN ingress).

MSCs are consistent with the values determined for PEDOT films deposited on a Pt disc electrode exposed to the same electrolyte (**Chapter 4** PEDOT in $0.1 \text{ M LiClO}_4 / \text{MeCN}$ $\text{MSC} = 88 - 217 \text{ F g}^{-1}$). The MSCs were observed to decrease at faster scan rates with a reduction of $\approx 30\%$.

In this electrolyte, anion and solvent fluxes were determined from the EQCM data using the mass time differentials ^{[2] [23] [24]}. However, these did not provide any further insight in polymer ion dynamics than already acquired by the EQCM data.

The admittance spectra obtained over the three scans are reported in **Fig. 5.3** for the cathodic and anodic vertex potential for each CV. The peak admittance only varied by 3% over the three scans at 5 mV s^{-1} . **PEDOT A** did not significantly swell during the redox switching in the $0.1 \text{ M LiClO}_4 / \text{MeCN}$ electrolyte, as this would dampen the frequency of the quartz crystal. This would mean the bandwidth and therefore the Q-factor would change over the redox process, if the film swells and becomes more flexible. This demonstrated that the polymer remained rigid *i.e.* the response did not include any viscoelastic effects.

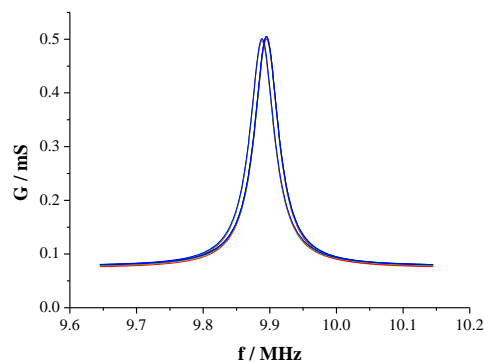


Fig. 5.3 - Admittance spectra of **PEDOT A** redox cycling only in 0.1 M LiClO₄ / MeCN (**Fig. 5.2A**) (1st CV = red, 2nd = green, 3rd = blue). Admittance spectra recorded with a frequency span = 500 kHz.

5.2.2 Behaviour in ZnCl₂ / EG (Type IV) DES

The behaviour of **PEDOT B** during a voltammetric experiment in ZnCl₂ / EG at 5 mV s⁻¹ with the associated mass changes per redox cycle as a function of potential, presented in **Fig. 5.4A**, showed no pronounced oxidation peaks. However, a reduction peak was observed at ≈ 0.45 V. Hysteresis was observed in the CV, *i.e.* the response was not reversible, as the cathodic peak current increased by 3.72 μ A over the three scans at 5 mV s⁻¹ (from 12.15 μ A to 15.87 μ A). The observed mass changes as a function of the total charge passed during the cyclic voltammetric study reported in **Fig. 5.4B**, showed a small mass retention per scan (≈ 0.33 μ g) at 5 mV s⁻¹.

The oxidation of **PEDOT B** in ZnCl₂ / EG exhibited an increase in current coupled with an increase in mass (≈ 3 μ g for 5 mV s⁻¹ experiment), which represented 14% of the total mass of the film. During reduction, the reverse situation occurred (the same as **PEDOT A** in the conventional solvent above), with a decrease in current coupled with a decrease in mass (≈ 2.7 μ g). The mass did not return to its initial value after each scan (and over 3 scans at 5 mV s⁻¹), the film retained some species after reduction, assumed to be neutral species. An increase of ≈ 1 μ g was found over the 3 scans, which

represented $\approx 5\%$ of the total mass of the film. This meant a mass increase of $\approx 0.33 \mu\text{g}$ was found per scan, which represented $\approx 2\%$ of the total mass of the film. This mass increase per scan ($0.33 \mu\text{g}$) as a percentage of the mass increase upon oxidation ($3 \mu\text{g}$) was found to be 11%.

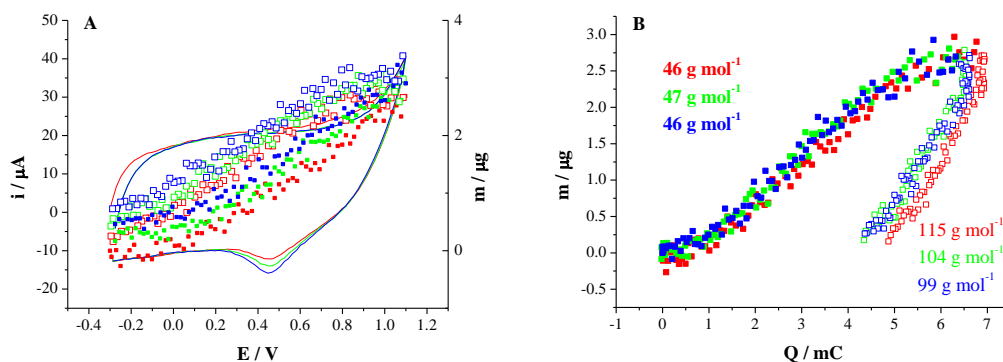


Fig. 5.4 - A) Cyclic voltammetric data and m vs. E **B)** m vs. Q for the redox cycling of **PEDOT B** in $\text{ZnCl}_2 / \text{EG}$ at 40°C for 3 scans at 5 mV s^{-1} $-0.3 \leq E / \text{V} \leq 1.1$ (vs. Ag wire) with associated M_{app} (g mol^{-1}).
Doping = solid squares, undoping = outline squares (1st CV = red, 2nd = green, 3rd = blue).

PEDOT B was subjected to voltammetric studies at long and short timescales, achieved by varying the potential scan rate. The end-to-end molar mass exchanges (M_{app}) calculated for the doping and undoping regimes at the three different scan rates investigated are reported in **Table 5.4**.

Table 5.4 - M_{app} from m vs. Q graphs for **PEDOT B** during redox cycling in $ZnCl_2 / EG$ at $40^\circ C$ between $-0.3 \leq E / V \leq 1.1$ (vs. Ag wire) for 3 scans at 3 scan rates (5, 10, 20 $mV s^{-1}$) and the sequence repeated. Data highlighted in yellow from data in **Fig. 5.4B**. Mobile species molar masses for this electrolyte $M_{anion} [ZnCl_4]^{2-} = 104 g mol^{-1}$, $M_{neut} EG = 62 g mol^{-1}$. \uparrow represents a mass increase, \downarrow represents a mass decrease.

scan rate	$M_{app} / g mol^{-1}$					
	Oxidation scan 1	Reduction scan 1	Oxidation scan 2	Reduction scan 2	Oxidation scan 3	Reduction scan 3
5 $mV s^{-1}$	$\uparrow 46$	$\downarrow 115$	$\uparrow 47$	$\downarrow 104$	$\uparrow 46$	$\downarrow 99$
5 $mV s^{-1}$	$\uparrow 43$	$\downarrow 55$	$\uparrow 42$	$\downarrow 58$	$\uparrow 41$	$\downarrow 57$
10 $mV s^{-1}$	$\uparrow 53$	$\downarrow 81$	$\uparrow 57$	$\downarrow 79$	$\uparrow 57$	$\downarrow 82$
10 $mV s^{-1}$	$\uparrow 47$	$\downarrow 68$	$\uparrow 51$	$\downarrow 67$	$\uparrow 53$	$\downarrow 70$
20 $mV s^{-1}$	$\uparrow 61$	$\downarrow 93$	$\uparrow 65$	$\downarrow 91$	$\uparrow 66$	$\downarrow 88$
20 $mV s^{-1}$	$\uparrow 51$	$\downarrow 80$	$\uparrow 57$	$\downarrow 71$	$\uparrow 63$	$\downarrow 82$

Before attempts could be made to suggest possible solutions to the observed gravimetric data (M_{app} for doping and undoping) for PEDOT in the Type IV DES $ZnCl_2 / EG$, an understanding of metal speciation (metal ions), non-metal ions and neutral species contained within the DES had to be established, as well as an idea of the physical state of the system at the start of the voltammetric experiment. Employing the knowledge of speciation from the literature ^{[25] [26]}, the contributions to the M_{app} during oxidation and reduction in the Type IV DES could be suggested.

Ionic speciation in solution was previously investigated using fast atom bombardment (FAB) mass spectrometry for the Type III ^[25] and Type IV systems ^[26]. The negative FAB spectra for all the Type IV eutectics ($ZnCl_2$ with either EG, acetamide, hexanediol and urea) exhibited peaks at m / z 171, 307 and 442, determined to be the anionic species $[ZnCl_3]^-$, $[Zn_2Cl_5]^-$ and $[Zn_3Cl_7]^-$ respectively ^[26], the same as reported present in Ethaline containing 0.3 M $ZnCl_2$ ^[25].

Metal containing cationic species were observed in all these systems too, exhibiting varying peak values dependent on the hydrogen bond donor used. For the EG Type IV DES the species were determined to be $[\text{ZnCl}(\text{HOC}_2\text{H}_4\text{OH})]^+$ and $[\text{ZnCl}(\text{HOC}_2\text{H}_4\text{OH})_2]^+$. This was similar to the acetamide Type IV DES with the cationic species being $[\text{ZnCl}(\text{H}_3\text{CC}(\text{O})\text{NH}_2)]^+$, $[\text{ZnCl}(\text{H}_3\text{CC}(\text{O})\text{NH}_2)_2]^+$ and an additional species $[\text{ZnCl}(\text{H}_3\text{CC}(\text{O})\text{NH}_2)_3]^+$. The 1,6-hexanediol system also exhibited monozinc cations containing one, two or three 1,6-hexanediol but also showed the presence of a dizinc species $[\text{Zn}_2\text{Cl}_3(\text{HOC}_6\text{H}_{12}\text{OH})]^+$ ^[26].

However, FAB spectroscopy was not an ideal technique for investigating liquid phase ion species. FAB spectroscopy is considered to be a destructive technique as fragmentation can occur during ionisation by the atom beam and within the sample chamber. Therefore, the zinc species observed by FAB spectroscopy may have already undergone fragmentation. Further investigation of speciation has been reported by Abbott *et al.* ^[27], applying a non-destructive technique, Extended X-Ray Absorption Fine Structure spectroscopy (EXAFS). The study involved elucidating the speciation of ZnCl_2 in the Type III DESs, Ethaline and Reline. The x-ray absorption data obtained showed the anionic zinc species $[\text{ZnCl}_4]^{2-}$, were present in both liquids ^[27]. In FAB spectroscopy, the Zn anion loses a Cl through fragmentation. Therefore, $[\text{ZnCl}_4]^{2-}$ anions were assumed to be the dominant anions in Type IV DESs.

The M_{app} in this electrolyte indicated a combination of the transfers of zincate anions $[\text{ZnCl}_4]^{2-}$ and the transfers of a neutral species, probably EG, expressed by equation (5.5).

The most likely possibility for the contributions to the doping M_{app} of **PEDOT B** in $ZnCl_2 / EG$ involved the ingress of a zinc based anion $[ZnCl_4]^{2-}$ ($M_{anion} = 207 \text{ g mol}^{-1}$, with 104 g mol^{-1} used in M_{app} expression as zincate anion has a 2- charge) and the egress of ethylene glycol ($M_{neut} = 62 \text{ g mol}^{-1}$), with varying amounts of EG expelled per $[ZnCl_4]^{2-}$ anion entering the film. The reverse situation was assumed for the undoping of PEDOT in the $ZnCl_2 / EG$ Type IV DES. Therefore, the M_{app} were expressed as the exchange of an anionic and a neutral species (5.5), with negative γ values.

$$M_{app} = M_{anion} + \gamma M_{neut} \quad (5.5)$$

A couple of other possibilities for doping mechanisms to fit the gravimetric data in this Type IV DES were considered, but were ruled out on feasibility grounds. The first possibility was that a chloride anion could enter the film as a dopant. However, this would not occur as the DES does not contain free chloride ions. The second possibility was a mixed ion exchange mechanism with the entry of $[ZnCl_4]^{2-}$ and Cl^- and the expulsion of EG. This too was unlikely to occur due to the lack of free chloride ions and also due to the complex nature of this mechanism.

The mobile species and γ values determined to fit the gravimetric data at each potential scan rate are reported in **Table 5.5**.

Table 5.5 - Mobile species transfers and α values to fit the assumption of $M_{app} = M_{anion} + \gamma M_{neut}$ for **PEDOT B** during redox cycling in $ZnCl_2 / EG$ at $40^\circ C$ between $-0.3 \leq E / V \leq 1.1$ (vs. Ag wire) for 3 scans at 3 scan rates (5, 10 20 $mV s^{-1}$) and the sequence repeated. The terms IN and OUT referred to the polymer film and the associated direction of transport of mobile species i.e. into or out of the polymer film. . Mobile species molar masses for this electrolyte $M_{anion} [ZnCl_4]^{2-} = 104 g mol^{-1}$, $M_{neut} EG = 62 g mol^{-1}$.

scan rate	Doping				Undoping		
	Anion	Neutral	γ		Anion	Neutral	γ
5 $mV s^{-1}$	$[ZnCl_4]^{2-}$ IN	EG OUT	-1		$[ZnCl_4]^{2-}$ OUT	-	0
5 $mV s^{-1}$			-1			EG IN	-0.8
10 $mV s^{-1}$			-0.8			EG IN	-0.4
10 $mV s^{-1}$			-0.8			EG IN	-0.6
20 $mV s^{-1}$			-0.6			EG IN	-0.2
20 $mV s^{-1}$			-0.8			EG IN	-0.4

For doping at a slow scan rate (5 $mV s^{-1}$) more EG was expelled per zincate anion entering, with a γ value of -1 *cf.* at faster scan rates (10 $mV s^{-1}$) slightly less EG was expelled per zincate anion entering the film, determining a γ value of between -0.6 to -0.8.

The gravimetric data for the undoping of **PEDOT B**, suggested the expulsion of the $[ZnCl_4]^{2-}$ anion and the entry of a smaller amount of EG *cf.* the amount expelled during doping.

Molar percentage contributions of species to satisfy electro-neutrality were able to be calculated using the γ values from **Table 5.5**. During doping, the dominant mobile species observed to contribute more to the M_{app} was the zincate anion, $[ZnCl_4]^{2-}$ at $\approx 60\%$ (in molar terms), whilst EG only contributed to $\approx 40\%$ at fast scan rates (10 $mV s^{-1}$ and 20 $mV s^{-1}$). At a slow scan rate of 5 $mV s^{-1}$ equal contributions of anion and neutral species transfers were observed ($\approx 50\%$ for both $[ZnCl_4]^{2-}$ ingress and EG egress). During undoping, the dominant mobile species was anion egress at 60 – 100%, whilst the solvent only contributed to $\approx 0 - 40\%$ of the M_{app} . Therefore, it took longer

for the undoping process to equilibrate compared to the doping process. This phenomenon did not occur with **PEDOT A** in 0.1 M LiClO₄ / MeCN. The reason the polymer took longer to equilibrate in the DES could be attributed to the higher viscosity of the DESs. Consequently, this resulted in slower mass transport in this electrolyte, *cf.* aqueous or organic solvents.

The admittance spectra obtained over the three scans for **PEDOT B** in ZnCl₂ / EG are reported in **Fig. 5.5**.

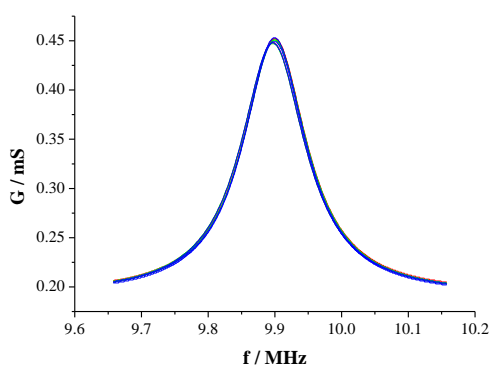


Fig. 5.5 - Admittance spectra for **PEDOT B** redox cycling only in ZnCl₂ / EG (**Fig. 5.4A**) (1st CV = red, 2nd = green, 3rd = blue). Admittance spectra recorded with a frequency span = 500 kHz.

The conductance only varied by 2% over the three scans, this inferred the film remained rigid during the cyclic voltammetric experiment.

The mass retention and the equilibration of PEDOT in this Type IV DES were further investigated by a long redox cycling experiment, **PEDOT BA** in ZnCl₂ / EG at 40 °C (40 CVs at 5 mV s⁻¹).

The total charge passed as a function of scan rate, are reported in **Fig. 5.6**. This showed a decrease in electro-activity at fast scan rates.

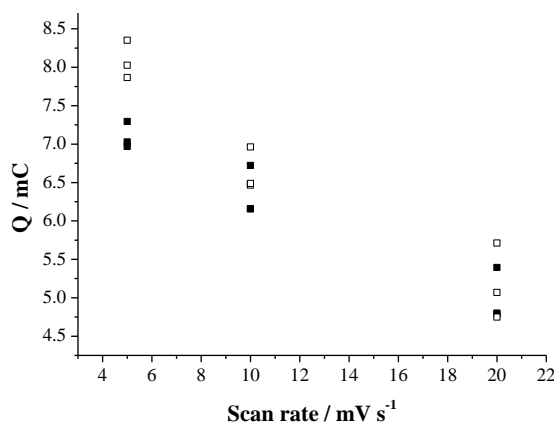


Fig. 5.6 - Total Charge vs. scan rate with the solid squares showing data for 1st set of CVs (5, 10, 20 mV s⁻¹) and outline squares showing data for 2nd set of CVs.

PEDOT BA was subjected to a long term redox switching experiment in ZnCl₂ / EG at 40 °C at 5 mV s⁻¹, with the resultant CV reported in **Fig. 5.7A**. The $i(E)$ response exhibited hysteresis, as observed by the increase in current at the anodic potential limit and the increase in current of the cathodic peak at ≈ 0.4 V. The reduction peak experienced a slight cathodic shift in potential from 0.44 V to 0.4 V. The CV shape and the appearance of the cathodic peak were consistent with the results above for the redox cycling of **PEDOT B** in ZnCl₂ / EG. The same $i(E)$ response for **PEDOT B** and **PEDOT BA** in ZnCl₂ / EG confirmed the reproducibility of the polymer from the deposition method used.

The mass as a function of the total charge passed during the course of the 40 CVs is reported in **Fig. 5.7B**. Over the first 5 scans, the mass of the film increased by ≈ 1.5 μg , which represented $\approx 5\%$ of the total mass of the film. After 5 scans the mass decreased by 5.5 μg , levelling off after 30 scans.

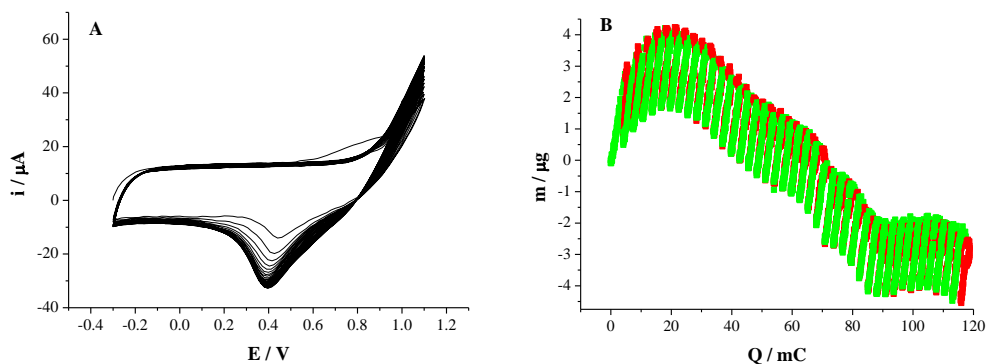


Fig. 5.7 - A) Cyclic Voltammetric data **B)** m vs. Q for the redox cycling of **PEDOT BA** in $\text{ZnCl}_2 / \text{EG}$ at 40°C for 40 scans at 5 mV s^{-1} $-0.3 \leq E / \text{V} \leq 1.1$ (vs. Ag wire). Doping = green squares and undoping = red squares.

The doping and undoping M_{app} calculated for each of the 40 CVs are reported in

Table 5.6.

Table 5.6 - M_{app} from m vs. Q graphs for **PEDOT BA** during redox cycling in $\text{ZnCl}_2 / \text{EG}$ at 40°C for 40 scans at 5 mV s^{-1} $-0.3 \leq E / \text{V} \leq 1.1$ (vs. Ag wire). Average doping = 57 g mol^{-1} (st dev $\sigma = 3$) average undoping = 65 g mol^{-1} (st dev $\sigma = 18$) ox = oxidation red = reduction. Mobile species molar masses for this electrolyte $M_{\text{anion}} [\text{ZnCl}_4]^{2-} = 104 \text{ g mol}^{-1}$, $M_{\text{neut}} \text{EG} = 62 \text{ g mol}^{-1}$. \uparrow represents a mass increase, \downarrow represents a mass decrease.

$M_{app} / \text{g mol}^{-1}$											
scan	Ox	Red	scan	Ox	Red	scan	Ox	Red	scan	Ox	Red
1	$\uparrow 58$	$\downarrow 145$	11	$\uparrow 55$	$\downarrow 69$	21	$\uparrow 54$	$\downarrow 56$	31	$\uparrow 59$	$\downarrow 50$
2	$\uparrow 64$	$\downarrow 112$	12	$\uparrow 51$	$\downarrow 67$	22	$\uparrow 54$	$\downarrow 58$	32	$\uparrow 58$	$\downarrow 50$
3	$\uparrow 65$	$\downarrow 94$	13	$\uparrow 55$	$\downarrow 66$	23	$\uparrow 53$	$\downarrow 62$	33	$\uparrow 59$	$\downarrow 59$
4	$\uparrow 63$	$\downarrow 91$	14	$\uparrow 55$	$\downarrow 62$	24	$\uparrow 48$	$\downarrow 58$	34	$\uparrow 57$	$\downarrow 50$
5	$\uparrow 62$	$\downarrow 84$	15	$\uparrow 54$	$\downarrow 63$	25	$\uparrow 57$	$\downarrow 52$	35	$\uparrow 59$	$\downarrow 51$
6	$\uparrow 60$	$\downarrow 79$	16	$\uparrow 53$	$\downarrow 60$	26	$\uparrow 57$	$\downarrow 55$	36	$\uparrow 59$	$\downarrow 51$
7	$\uparrow 59$	$\downarrow 77$	17	$\uparrow 57$	$\downarrow 57$	27	$\uparrow 54$	$\downarrow 56$	37	$\uparrow 59$	$\downarrow 55$
8	$\uparrow 57$	$\downarrow 75$	18	$\uparrow 52$	$\downarrow 58$	28	$\uparrow 52$	$\downarrow 55$	38	$\uparrow 57$	$\downarrow 54$
9	$\uparrow 56$	$\downarrow 71$	19	$\uparrow 56$	$\downarrow 57$	29	$\uparrow 53$	$\downarrow 58$	39	$\uparrow 58$	$\downarrow 55$
10	$\uparrow 56$	$\downarrow 71$	20	$\uparrow 57$	$\downarrow 55$	30	$\uparrow 56$	$\downarrow 53$	40	$\uparrow 57$	$\downarrow 55$

By concentrating on the individual m vs. Q plots for each voltammogram reported in **Fig. 5.7** (i.e. the initial mass of each scan starting at zero taken from the data in **Fig. 5.7B**), it was observed that the undoping regime involved a combination of two different mechanisms. As can be seen in **Fig. 5.8A**, the doping process remained constant over the 40 scans. For undoping, the mechanism switched from a single process (scan 1 – 10) to a multiple step process (after scan 11). A constant multiple step undoping process was observed after ≈ 20 scans, a clearer observation of this can be seen in **Fig. 5.8B** using m vs. Q plots for the 1st, 20th and 40th scans.

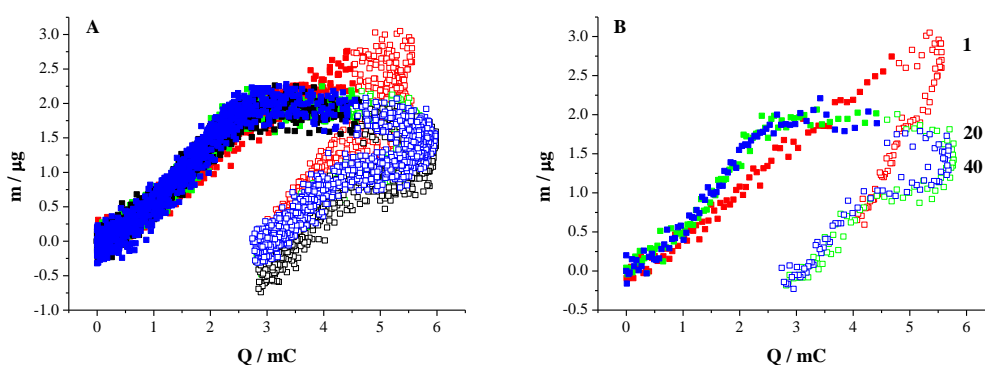


Fig. 5.8 - A) m vs. Q (initial mass of each scan starting at zero) for the redox cycling of **PEDOT BA** in $\text{ZnCl}_2 / \text{EG}$ at 40°C for 40 scans at 5 mV s^{-1} $-0.3 \leq E / \text{V} \leq 1.1$ (vs. Ag wire). Scans 1 - 10 (Red), scans 11 - 20 (Green), scans 21 - 30 (Black), scans 31 - 40 (Blue) with solid squares representing doping and outline squares representing undoping. **B)** m vs. Q 1st CV (red), 20th CV (green) and 40th CV (blue).

The doping and undoping M_{app} were expressed as a combination of anion (M_{anion}) and neutral species transfer (γM_{neut}) (5.5), the same as for **PEDOT B** in $\text{ZnCl}_2 / \text{EG}$.

The end-to-end doping M_{app} suggested the ingress of $[\text{ZnCl}_4]^{2-}$ and the expulsion of EG; ranging between 0.7 – 0.9 EG expelled per $[\text{ZnCl}_4]^{2-}$ entering the film.

The doping M_{app} for the 20th scan (-0.3 V to 0.7 V) and the 40th scan (-0.3 V to 0.9 V) were 63 g mol^{-1} and 65 g mol^{-1} respectively. This also suggested the ingress of $[\text{ZnCl}_4]^{2-}$

and the expulsion of EG, with the M_{app} values and related γ values reported in

Table 5.7.

Table 5.7 - Doping M_{app} , mobile species transfers and γ values to fit the assumption of $M_{app} = M_{anion} + \gamma M_{neut}$ for **PEDOT BA** during redox cycling in $ZnCl_2 / EG$ at $40^\circ C$ at $5 mVs^{-1}$ for selected scans and average doping between various potential ranges (shown in column 2). The terms IN and OUT referred to the polymer film and the associated direction of transport of mobile species *i.e.* into or out of the polymer film. Mobile species molar masses for this electrolyte $M_{anion} [ZnCl_4]^{2-} = 104 g mol^{-1}$, $M_{neut} EG = 62 g mol^{-1}$. \uparrow represents a mass increase, \downarrow represents a mass decrease.

scan	$M_{app} / g mol^{-1}$	Doping			
		Anion	Neutral	γ	n $[ZnCl_4]^{2-} : n EG$
1	$\uparrow 58$	$[ZnCl_4]^{2-}$ IN	EG OUT	-0.7	1.4
20	$\uparrow 57$			-0.8	1.3
40	$\uparrow 57$			-0.8	1.3
average over 40 scans	$\uparrow 57$ ($\sigma = 3$)			-0.8	1.3

The end-to-end undoping M_{app} for the 20th scan, 40th scan, the average doping M_{app} over 40 scans and the average over the final 20 were fitted to (5.5), like the doping regime. This initially indicated the egress of $[ZnCl_4]^{2-}$ and the ingress of EG, ranging between 1 – 1.4 EG expelled per $[ZnCl_4]^{2-}$ entering the film (Table 5.8).

Table 5.8 - Undoping M_{app} , mobile species transfers and γ values to fit the assumption of $M_{app} = M_{anion} + \gamma M_{neut}$ for **PEDOT BA** during redox cycling in $ZnCl_2 / EG$ at $40^\circ C$ at $5 mVs^{-1}$ for selected scans and average undoping between various potential ranges (shown in column 2). The terms IN and OUT referred to the polymer film and the associated direction of transport of mobile species *i.e.* into or out of the polymer film. Mobile species molar masses for this electrolyte $M_{anion} [ZnCl_4]^{2-} = 104 g mol^{-1}$, $M_{neut} EG = 62 g mol^{-1}$.

scan	$M_{app} / g mol^{-1}$	Undoping			
		Anion	Neutral	γ	$n [ZnCl_4]^{2-} : n EG$
20	↓ 55	$[ZnCl_4]^{2-}$ OUT	EG IN	-0.8	1.3
40	↓ 55			-0.8	1.3
average over 40 scans	↓ 65 ($\sigma = 18$)			-0.6	1.7

In a bracketed experiment, the behaviour of a single PEDOT film was studied when exposed to a molecular solvent (0.1 M $LiClO_4 / MeCN$), a Type IV DES $ZnCl_2 / EG$ and then transferred back to fresh molecular solvent (0.1 M $LiClO_4 / MeCN$). This methodology, referred to in this thesis as a bracketed cyclic voltammetric study, was employed when investigating polymer DC capacitance in **Chapter 4**.

The behaviour of **PEDOT BB** was firstly probed in 0.1 M $LiClO_4 / MeCN$ at $40^\circ C$ during a cyclic voltammetric study at $5 mV s^{-1}$. The resultant CV reported in **Fig. 5.9A**, showed a capacitor type $i(E)$ response. The observed mass changes as a function of the total charges passed over the cyclic voltammograms reported in **Fig. 5.9B**, showed a small mass retention per scan ($\approx 0.6 \mu g$). An increase in current coupled with an increase in mass ($\approx 2.3 \mu g$) was observed during doping, which related to 15% of the total mass of the polymer. The reverse situation occurred during undoping, with a decrease in current coupled with a decrease in mass ($\approx 1.7 \mu g$).

The doping and undoping M_{app} reported in **Table 5.9** and **Table 5.10** respectively, were found by the product of the gradient of a m vs. Q plot and Faraday's constant (using equation (5.1)).

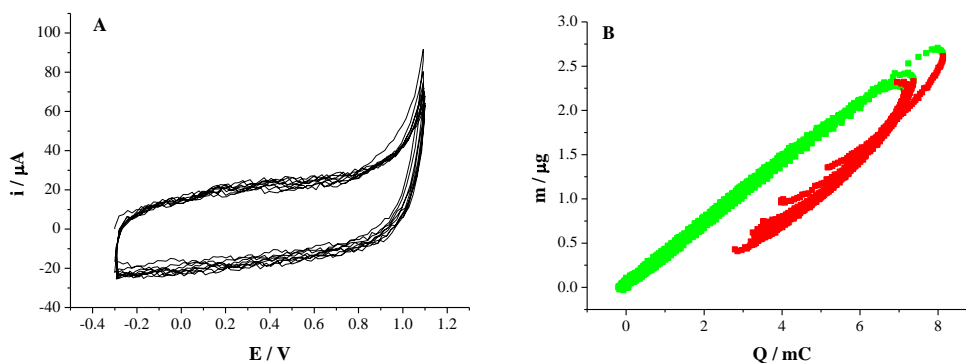


Fig. 5.9 - A) Cyclic Voltammetric data **B)** m vs. Q for the redox cycling of PEDOT BB in 0.1 M LiClO₄ / MeCN at 40 °C for 9 scans at 5 mV s⁻¹ -0.3 ≤ E / V ≤ 1.1 (vs. Ag wire).
Doping = green squares, undoping = red squares.

Table 5.9 - M_{app} from m vs. Q graphs for PEDOT BB during doping in 0.1 M LiClO₄ / MeCN at 40 °C for 9 scans at 5 mV s⁻¹ between -0.3 ≤ E / V ≤ 1.1 (vs. Ag wire) average doping = 33 g mol⁻¹ (st dev σ = 2). Mobile species molar masses for this electrolyte M_{anion} [ClO₄]⁻ = 99 g mol⁻¹, M_{solv} MeCN = 41 g mol⁻¹. ↑ represents a mass increase, ↓ represents a mass decrease.

scan	Doping				
	$M_{app} / \text{g mol}^{-1}$	Anion	Solvent	α	$n [\text{ClO}_4]^- : n \text{ MeCN}$
1	↑ 33	[ClO ₄] ⁻ IN	MeCN OUT	-1.6	0.6
2	↑ 32			-1.6	0.6
3	↑ 32			-1.6	0.6
4	↑ 32			-1.6	0.6
5	↑ 32			-1.6	0.6
6	↑ 32			-1.6	0.6
7	↑ 32			-1.6	0.6
8	↑ 38			-1.5	0.7
9	↑ 33			-1.6	0.6

Table 5.10 - M_{app} from m vs. Q graphs for **PEDOT BB** during undoping in 0.1 M LiClO₄ / MeCN at 40 °C for 9 scans at 5 mV s⁻¹ between -0.3 ≤ E / V ≤ 1.1 (vs. Ag wire) average undoping = 40 g mol⁻¹ (st dev σ = 1). Mobile species molar masses for this electrolyte M_{anion} [ClO₄]⁻ = 99 g mol⁻¹, M_{solv} MeCN = 41 g mol⁻¹. ↑ represents a mass increase, ↓ represents a mass decrease.

Undoping					
scan	$M_{app} / \text{g mol}^{-1}$	Anion	Solvent	α	n [ClO ₄] ⁻ : n MeCN
1	↓ 40	[ClO ₄] ⁻ OUT	MeCN IN	-1.4	0.7
2	↓ 38			-1.5	0.7
3	↓ 38			-1.5	0.7
4	↓ 39			-1.5	0.7
5	↓ 40			-1.4	0.7
6	↓ 41			-1.4	0.7
7	↓ 42			-1.4	0.7
8	↓ 41			-1.4	0.7
9	↓ 41			-1.4	0.7

The average doping M_{app} for **PEDOT BB** in 0.1 M LiClO₄ / MeCN at 5 mV s⁻¹ over the 9 scans was $33 \pm 2 \text{ g mol}^{-1}$. The M_{app} was again expressed as contributions from both anion and solvent transfer (5.3), the same as reported for **PEDOT A** in 0.1 M LiClO₄ / MeCN by Bund and Neudeck^[1].

$$M_{app} = M_{anion} + \alpha M_{solv} \quad (5.3)$$

Therefore, the average doping M_{app} indicated the entry of a [ClO₄]⁻ anion and the expulsion of solvent, ≈ 1.6 MeCN expelled per [ClO₄]⁻ anion entering the film. Therefore, α values for doping were determined as -1.6 in 0.1 M LiClO₄ / MeCN for **PEDOT BB**.

The average undoping M_{app} for **PEDOT BB** over the 9 scans was $40 \pm 1 \text{ g mol}^{-1}$. This gravimetric data indicated the expulsion of a [ClO₄]⁻ anion and the entry of solvent ≈ 1.4 MeCN enters per [ClO₄]⁻ anion expelled. Again, the M_{app} were expressed as in equation (5.3) with α determined as -1.4 or -1.5 for undoping.

After the cyclic voltammetric experiment in 0.1 M LiClO₄ / MeCN, **PEDOT BB** was transferred to the Type IV DES ZnCl₂ / EG for an electrochemical study (9 scans at 5 mV s⁻¹). The resultant CV for **PEDOT BB** in ZnCl₂ / EG is reported in **Fig. 5.10A**. The observed mass changes as a function of the total charge passed over the cyclic voltammograms are shown in **Fig. 5.10B**. During doping an increase in current was coupled with an increase in mass ($\approx 2 \mu\text{g}$), which related to 13% of the total mass of the polymer. During undoping, the reverse situation occurred with a decrease in current coupled with a decrease in mass ($\approx 2 \mu\text{g}$). Therefore, no mass retention was observed by the polymer in this electrolyte.

The M_{app} for the doping and undoping regimes reported in **Table 5.11** were found by the product of the gradient of a m vs. Q plot and Faraday's constant (5.1).

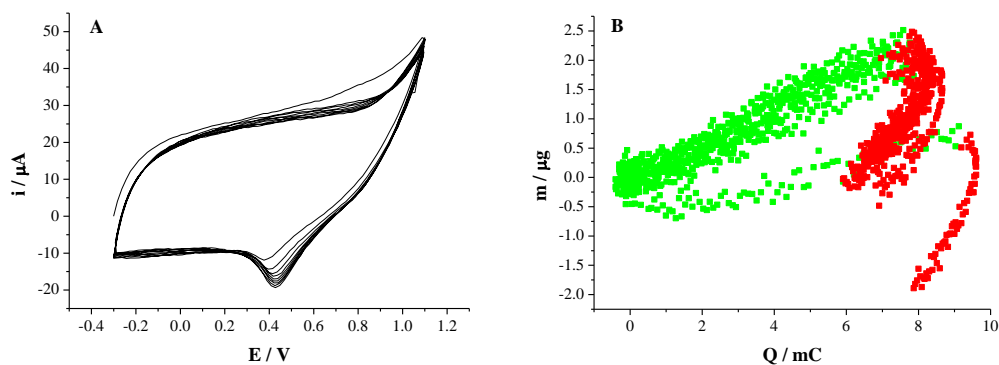


Fig. 5.10 - A) Cyclic Voltammetric data **B)** m vs. Q for the redox cycling of **PEDOT BB** in ZnCl₂ / EG at 40 °C for 9 scans at 5 mV s⁻¹ $-0.3 \leq E / V \leq 1.1$ (vs. Ag wire). Doping = green squares, undoping = red squares.

Table 5.11 - M_{app} from m vs. Q graphs for **PEDOT BB** during redox cycling in $ZnCl_2 / EG$ at $40\text{ }^\circ\text{C}$ for 9 scans at 5 mVs^{-1} between $-0.3 \leq E / V \leq 1.1$ (vs. Ag wire) (after redox switching in $0.1\text{ M LiClO}_4 / \text{MeCN}$) average doping = 27 g mol^{-1} (st dev $\sigma = 5$) average undoping = 99 g mol^{-1} (st dev $\sigma = 16$). Mobile species molar masses for this electrolyte $M_{anion} [ZnCl_4]^{2-} = 104\text{ g mol}^{-1}$, $M_{neut} EG = 62\text{ g mol}^{-1}$. \uparrow represents a mass increase, \downarrow represents a mass decrease.

scan	Doping				Undoping			
	$M_{app} / \text{g mol}^{-1}$	Anion	Neutral	β	$M_{app} / \text{g mol}^{-1}$	Anion	Neutral	β
1	$\uparrow 13$	$[ZnCl_4]^{2-}$ IN	EG OUT	-1.5	$\downarrow 130$	$[ZnCl_4]^{2-}$ OUT	EG IN	0
2	$\uparrow 25$			-1.3	$\downarrow 115$			0
3	$\uparrow 28$			-1.2	$\downarrow 112$			0
4	$\uparrow 30$			-1.2	$\downarrow 101$			0
5	$\uparrow 30$			-1.2	$\downarrow 89$			-0.2
6	$\uparrow 30$			-1.2	$\downarrow 88$			-0.3
7	$\uparrow 30$			-1.2	$\downarrow 86$			-0.3
8	$\uparrow 29$			-1.2	$\downarrow 86$			-0.3
9	$\uparrow 29$			-1.2	$\downarrow 82$			-0.4

The doping M_{app} for the initial scan was slightly different to the other 8 M_{app} values, therefore the initial scan was omitted from the discussion. An average doping M_{app} over the 8 scans was $29 \pm 2\text{ g mol}^{-1}$. The observed gravimetric data of PEDOT in $ZnCl_2 / EG$ (**PEDOT B**) suggested that M_{app} were expressed by contributions from an anionic zinc species $[ZnCl_4]^{2-}$ and neutral species γM_{neut} transfers, probably EG (as in equation (5.5)). The average doping M_{app} therefore indicated the entry of $[ZnCl_4]^{2-}$ and the expulsion of EG, ≈ 1.2 EG expelled per $[ZnCl_4]^{2-}$ entering the film. This produced a γ value of -1.2 for doping of **PEDOT BB** in $ZnCl_2 / EG$, after a cyclic voltammetric experiment in $0.1\text{ M LiClO}_4 / \text{MeCN}$.

The average undoping M_{app} (omitting the initial scan) was $95 \pm 12\text{ g mol}^{-1}$. This observed gravimetric data fitted the expulsion of $[ZnCl_4]^{2-}$ and the entry of EG, ≈ 0.1 EG enters per $[ZnCl_4]^{2-}$ expelled, which related to M_{app} being expressed as in (5.5) and a value -0.1 for γ during undoping in $ZnCl_2 / EG$.

After the cyclic voltammetric experiment in $\text{ZnCl}_2 / \text{EG}$, **PEDOT BB** was transferred to fresh 0.1 M $\text{LiClO}_4 / \text{MeCN}$ to observe whether the electrochemical behaviour was restored in the molecular solvent after conditioning with the Type IV DES, $\text{ZnCl}_2 / \text{EG}$. The resultant CV is reported in **Fig. 5.11A**, with the observed mass changes as a function of the total charge passed over the cyclic voltammograms shown in **Fig. 5.11B**. A capacitor type $i(E)$ response was observed for **PEDOT BB** in 0.1 M $\text{LiClO}_4 / \text{MeCN}$ after being exposed to $\text{ZnCl}_2 / \text{EG}$. The $i(E)$ responses were the same as observed for **PEDOT BB** in 0.1 M $\text{LiClO}_4 / \text{MeCN}$ before being exposed to $\text{ZnCl}_2 / \text{EG}$.

An increase in current coupled with an increase in mass ($\approx 1.5 \mu\text{g}$) was observed during doping, which related to 10% of the total mass of the polymer. The reverse situation occurred during undoping, with a decrease in current coupled with a decrease in mass ($\approx 1.5 \mu\text{g}$). Therefore, no mass retention was observed in 0.1 M $\text{LiClO}_4 / \text{MeCN}$ after exposure to $\text{ZnCl}_2 / \text{EG}$.

End-to-end molar mass exchanges (M_{app}) for the doping and undoping regimes reported in **Table 5.12** and **Table 5.13** were found by the product of the gradient of a m vs. Q plot and Faraday's constant (using equation (5.1)).

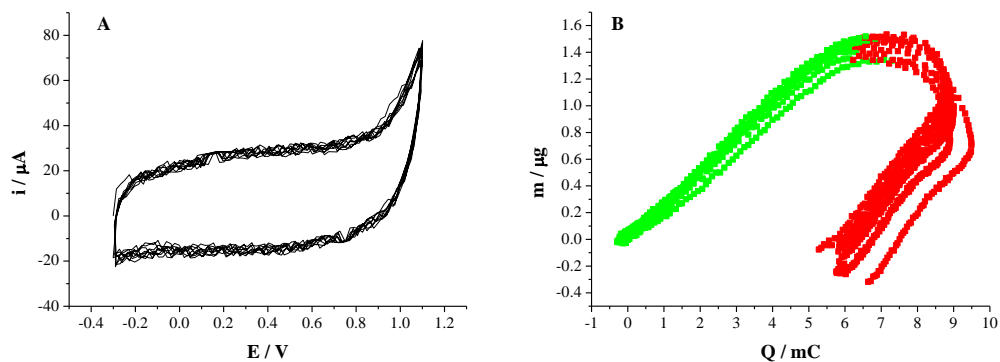


Fig. 5.11 - A) Cyclic Voltammetric data **B)** m vs. Q for the redox cycling of **PEDOT BB** in 0.1 M LiClO_4 / MeCN (after redox switching in ZnCl_2 / EG) at 40°C for 9 scans at 5 mV s^{-1} $-0.3 \leq E / \text{V} \leq 1.1$ (vs. Ag wire). Doping = green squares, undoping = red squares.

Table 5.12 - M_{app} from m vs. Q graphs for **PEDOT BB** during doping in 0.1 M LiClO_4 / MeCN at 40°C for 9 scans at 5 mV s^{-1} between $-0.3 \leq E / \text{V} \leq 1.1$ (vs. Ag wire) (after redox switching in ZnCl_2 / EG) average doping = 23 g mol^{-1} (st dev $\sigma = 1$). Mobile species molar masses for this electrolyte $M_{\text{anion}} [\text{ClO}_4]^- = 99\text{ g mol}^{-1}$, $M_{\text{solv}} \text{MeCN} = 41\text{ g mol}^{-1}$. \uparrow represents a mass increase, \downarrow represents a mass decrease.

scan	Doping				
	$M_{\text{app}} / \text{g mol}^{-1}$	Anion	Solvent	α	$n [\text{ClO}_4]^- : n \text{MeCN}$
1	$\uparrow 21$	[ClO ₄] ⁻ IN	MeCN OUT	-1.9	0.5
2	$\uparrow 23$			-1.9	0.5
3	$\uparrow 23$			-1.9	0.5
4	$\uparrow 24$			-1.8	0.6
5	$\uparrow 24$			-1.8	0.6
6	$\uparrow 23$			-1.9	0.5
7	$\uparrow 23$			-1.9	0.5
8	$\uparrow 24$			-1.8	0.6
9	$\uparrow 24$			-1.8	0.6

Table 5.13 - M_{app} from m vs. Q graphs for **PEDOT BB** during undoping in 0.1 M LiClO₄ / MeCN at 40 °C for 9 scans at 5 mVs⁻¹ between $-0.3 \leq E / V \leq 1.1$ (after redox switching in ZnCl₂ / EG) average undoping = 31 g mol⁻¹ (st dev $\sigma = 4$). Mobile species molar masses for this electrolyte $M_{anion} [ClO_4]^- = 99 \text{ g mol}^{-1}$, $M_{solv} \text{ MeCN} = 41 \text{ g mol}^{-1}$. \uparrow represents a mass increase, \downarrow represents a mass decrease.

Undoping					
scan	$M_{app} / \text{g mol}^{-1}$	Anion	Solvent	α	$n [ClO_4]^- : n \text{ MeCN}$
1	$\downarrow 33$	[ClO ₄] ⁻ OUT	MeCN IN	-1.6	0.6
2	$\downarrow 31$			-1.7	0.6
3	$\downarrow 24$			-1.8	0.6
4	$\downarrow 26$			-1.8	0.6
5	$\downarrow 28$			-1.7	0.6
6	$\downarrow 32$			-1.6	0.6
7	$\downarrow 35$			-1.6	0.6
8	$\downarrow 32$			-1.6	0.6
9	$\downarrow 35$			-1.6	0.6

The average doping M_{app} for **PEDOT BB** in 0.1 M LiClO₄ / MeCN over the 9 scans was $23 \pm 1 \text{ g mol}^{-1}$. The M_{app} was expressed as a combination of anion and solvent transfer (5.3), the same as reported above for PEDOT in this electrolyte [1]. The average doping M_{app} indicated the entry of a [ClO₄]⁻ anion and the expulsion of solvent ≈ 1.9 MeCN expelled per [ClO₄]⁻ anion entering the film. For the doping of **PEDOT BB** in 0.1 M LiClO₄ / MeCN after conditioning with the Type IV DESs ZnCl₂ / EG α was determined as -1.9. This indicated a greater amount of solvent expulsion in this electrolyte after exposure to the DES *cf.* **PEDOT BB** behaviour in the initial experiment in 0.1 M LiClO₄ / MeCN.

The average undoping M_{app} for **PEDOT BB** over the 9 scans was $31 \pm 4 \text{ g mol}^{-1}$. This indicated the expulsion of the [ClO₄]⁻ anion and the entry of solvent, ≈ 1.7 MeCN entering per [ClO₄]⁻ expelled. Therefore a value of -1.7 was determined for α for undoping.

5.2.3 Behaviour in Ethaline (Type III) DES

PEDOT C1 was exposed to Ethaline (Type III DES) at 40 °C for a long cyclic voltammetric study (40 CVs) at 5 mV s⁻¹, producing the $i(E)$ response presented in **Fig. 5.12A**. The mass changes as a function of charge passed over the course of the 40 CVs are reported in **Fig. 5.12B**.

During doping, an increase in current was associated with an increase in mass, ($\approx 0.7 \mu\text{g}$), which represented 3% of the total mass of the film. During undoping the reverse process occurred, with a decrease in current coupled with a decrease in mass ($\approx 0.7 \mu\text{g}$). Over the first 2 scans, the mass increased ($\approx 2 \mu\text{g}$), which represented 8% of the total mass of the film. After the first scans (3 – 30 scans) the mass remained relatively constant at $\approx 2 \mu\text{g}$, gradually decreasing between 31 – 40 scans to a value of ($\approx 1 \mu\text{g}$), shown in **Fig. 5.12B**.

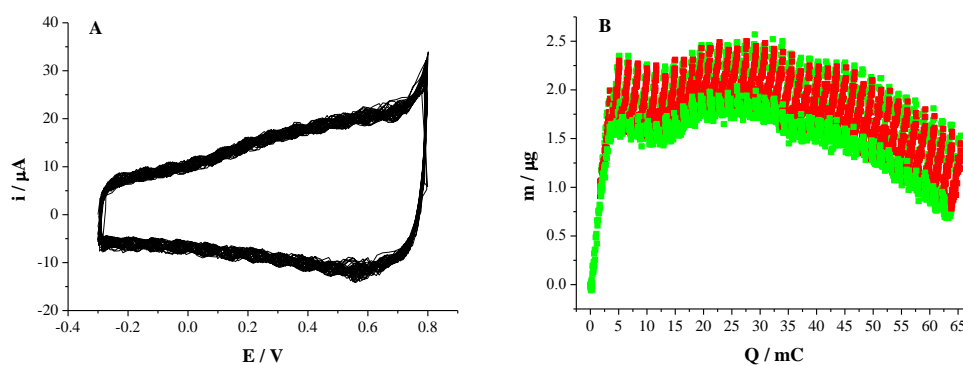


Fig. 5.12 - A) Cyclic voltammetric data **B)** m vs. Q for the redox cycling of PEDOT C1 in Ethaline at 40 °C for 40 scans at 5 mV s⁻¹ $-0.3 \leq E / V \leq 0.8$ (vs. Ag wire). Doping = green and undoping = red.

The doping and undoping M_{app} calculated for each of the 40 CVs are reported in **Table 5.14**.

Table 5.14 - M_{app} from m vs. Q graphs for **PEDOT C1** during redox cycling in Ethaline for 40 scans at 5 mV s^{-1} at 40°C $-0.3 \leq E / \text{V} \leq 0.8$ (vs. Ag wire). average doping = 19 g mol^{-1} (st dev $\sigma = 8$) average undoping = 28 g mol^{-1} (st dev $\sigma = 4$) ox = oxidation red = reduction. Mobile species molar masses for this electrolyte $M_{\text{anion}} [\text{2EG.Cl}]^- = 160 \text{ g mol}^{-1}$, $M_{\text{cation}} [\text{Ch}]^+ = 104 \text{ g mol}^{-1}$. \uparrow represents a mass increase, \downarrow represents a mass decrease.

scan	$M_{app} / \text{g mol}^{-1}$										
	Ox	Red	scan	Ox	Red	scan	Ox	Red	scan	Ox	Red
1	$\uparrow 60$	$\downarrow 50$	11	$\uparrow 19$	$\downarrow 23$	21	$\uparrow 15$	$\downarrow 27$	31	$\uparrow 18$	$\downarrow 27$
2	$\uparrow 41$	$\downarrow 35$	12	$\uparrow 17$	$\downarrow 27$	22	$\uparrow 16$	$\downarrow 25$	32	$\uparrow 18$	$\downarrow 25$
3	$\uparrow 19$	$\downarrow 33$	13	$\uparrow 16$	$\downarrow 29$	23	$\uparrow 19$	$\downarrow 24$	33	$\uparrow 19$	$\downarrow 27$
4	$\uparrow 16$	$\downarrow 32$	14	$\uparrow 15$	$\downarrow 26$	24	$\uparrow 17$	$\downarrow 28$	34	$\uparrow 17$	$\downarrow 27$
5	$\uparrow 16$	$\downarrow 30$	15	$\uparrow 16$	$\downarrow 27$	25	$\uparrow 17$	$\downarrow 24$	35	$\uparrow 17$	$\downarrow 27$
6	$\uparrow 16$	$\downarrow 31$	16	$\uparrow 17$	$\downarrow 25$	26	$\uparrow 16$	$\downarrow 27$	36	$\uparrow 18$	$\downarrow 26$
7	$\uparrow 16$	$\downarrow 27$	17	$\uparrow 17$	$\downarrow 24$	27	$\uparrow 17$	$\downarrow 28$	37	$\uparrow 20$	$\downarrow 30$
8	$\uparrow 18$	$\downarrow 30$	18	$\uparrow 16$	$\downarrow 26$	28	$\uparrow 17$	$\downarrow 26$	38	$\uparrow 18$	$\downarrow 28$
9	$\uparrow 16$	$\downarrow 27$	19	$\uparrow 16$	$\downarrow 26$	29	$\uparrow 18$	$\downarrow 27$	39	$\uparrow 20$	$\downarrow 28$
10	$\uparrow 19$	$\downarrow 25$	20	$\uparrow 16$	$\downarrow 26$	30	$\uparrow 19$	$\downarrow 26$	40	$\uparrow 18$	$\downarrow 28$

The doping M_{app} remained relatively constant over the 40 scans at an average of $19 \pm 8 \text{ g mol}^{-1}$. The undoping M_{app} also remained relatively constant over the 40 scans at an average of $28 \pm 4 \text{ g mol}^{-1}$.

The individual m vs. Q plots for each voltammogram are reported in **Fig. 5.12** (*i.e.* the initial mass of each scan starting at zero taken from the data in **Fig. 5.12B**) showed the m vs. Q plots were reversible (disregarding the first two scans in this electrolyte). The m vs. Q data for the 1st 20th and 40th scans are presented in **Fig. 5.13**.

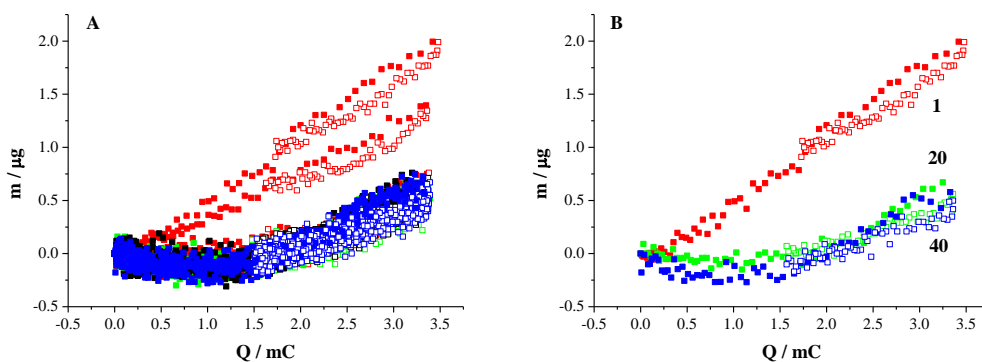


Fig. 5.13 - A) m vs. Q (initial mass of each scan starting at zero) for the redox cycling of **PEDOT C1** in Ethaline at 40 °C for 40 scans at 5 mV s⁻¹ -0.3 ≤ E/V ≤ 0.8. Scans 1 - 10 (red), scans 11 - 20 (green), scans 21 - 30 (black), scans 31 - 40 (blue) with solid squares representing doping and outline squares representing undoping. **B)** m vs. Q for the 1st CV (red), 20th CV (green) and 40th CV (blue).

The M_{app} were assumed to be expressed as a combination of anion and cation transfers (mixed ion transfers) only. From the expression of M_{app} (5.2), used by Bund and Neudeck^[1], the solvent term was removed due to the lack of solvent in the conventional sense. The gravimetric data on the electrochemical behaviour of PEDOT within this electrolyte were fitted to a mixed ion transfer process (5.4).

$$M_{app} = M_{anion} + \beta M_{cation} \quad (5.4)$$

The end-to-end doping M_{app} for the 1st, 20th, 40th and the average doping M_{app} over 40 scans indicated the ingress of [2EG.Cl]⁻ and the exit of choline cation [Ch]⁺, ≈ 1.4 [Ch]⁺ expelled per [2EG.Cl]⁻ entering into the film, which represented a β value of -1.4 in terms of (5.4). The doping M_{app} values and related β values are reported in **Table 5.15**.

Table 5.15 - Doping M_{app} , mobile species transfers and β values to fit the assumption of $M_{app} = M_{anion} + \beta M_{cation}$ for **PEDOT C1** during redox cycling in Ethaline at 40 °C at 5 mV s⁻¹. The terms IN and OUT referred to the polymer film and the associated direction of transport of mobile species *i.e.* into or out of the polymer film. Mobile species molar masses for this electrolyte M_{anion} [2EG.Cl]⁻ = 160 g mol⁻¹, M_{cation} [Ch]⁺ = 104 g mol⁻¹. ↑ represents a mass increase, ↓ represents a mass decrease.

scan	Doping				
	$M_{app} / \text{g mol}^{-1}$	Anion	Cation	β	$n \text{ [2EG.Cl]}^- : n \text{ [Ch]}^+$
1	↑ 60	[2EG.Cl] ⁻ IN	[Ch] ⁺ OUT	-1	1
20	↑ 16			-1.4	0.7
40	↑ 18			-1.4	0.7
average over 40 scans	↑ 19 ($\sigma = 8$)			-1.4	0.7

The end-to-end undoping M_{app} for the 1st, 20th, 40th and the average undoping M_{app} over 40 scans indicated a direct reverse of the doping process. The undoping M_{app} values and β values are reported in **Table 5.16**. The M_{app} fitted the egress of the [2EG.Cl]⁻ anion and the entry of choline cation, with ≈ 1.3 [Ch]⁺ entering per [2EG.Cl]⁻ expelled, which represented a β value of -1.3.

Table 5.16 - Undoping M_{app} , mobile species transfers and β values to fit the assumption of $M_{app} = M_{anion} + \beta M_{cation}$ for **PEDOT C1** during redox cycling in Ethaline at 40 °C at 5 mV s⁻¹. The terms IN and OUT referred to the polymer film and the associated direction of transport of mobile species *i.e.* into or out of the polymer film. Mobile species molar masses for this electrolyte M_{anion} [2EG.Cl]⁻ = 160 g mol⁻¹, M_{cation} [Ch]⁺ = 104 g mol⁻¹. ↑ represents a mass increase, ↓ represents a mass decrease.

Undoping					
scan	$M_{app} / \text{g mol}^{-1}$	Anion	Cation	β	$n [2EG.Cl]^- : n [Ch]^+$
1	↓ 50	[2EG.Cl] ⁻ OUT	[Ch] ⁺ IN	-1.1	0.9
20	↓ 26			-1.3	0.8
40	↓ 28			-1.3	0.8
average over 40 scans	↓ 28 ($\sigma = 4$)			-1.3	0.8

5.2.4 Behaviour in Ethaline containing 0.3 M ZnCl₂

PEDOT C2 was exposed to Ethaline (Type III DES) containing 0.3 M ZnCl₂ at 40 °C for a long cyclic voltammetric study (40 CVs) at 5 mV s⁻¹, producing the $i(E)$ response presented in **Fig. 5.14A**. The Type III DES Ethaline used in this experiment contained a zinc salt to liken this to the electrolyte environment the polymer would experience within a battery device. The mass changes as a function of total charge passed over the course of the 40 CVs are reported in **Fig. 5.14B**.

During doping, an increase in current was associated with an increase in mass, ($\approx 1 \mu\text{g}$), which represented 3% of the total mass of the film. During undoping the reverse process occurred, with a decrease in current coupled with a decrease in mass ($\approx 1 \mu\text{g}$). Over the first 10 scans, the mass of the film increased ($\approx 4 \mu\text{g}$), which represented 11% of the total mass of the film. After the first 10 scans (11 – 40 scans) the mass decreased gradually to a value of ($\approx 3 \mu\text{g}$), shown in **Fig. 5.14B**.

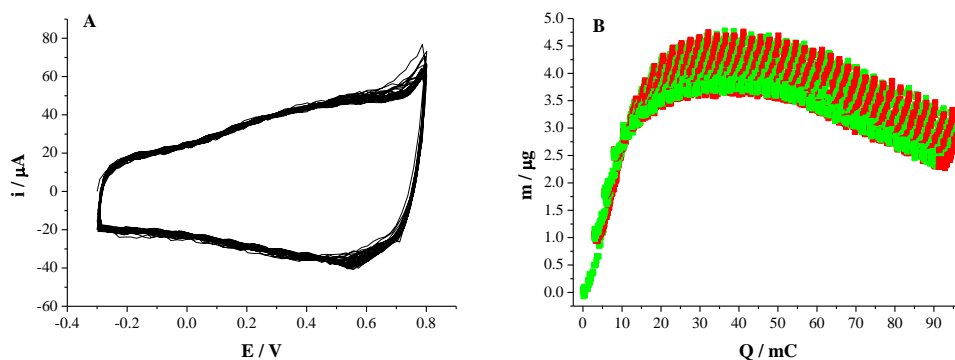


Fig. 5.14 - A) Cyclic voltammetric data **B)** m vs. Q for the redox cycling of **PEDOT C2** in 0.3 M ZnCl_2 in Ethaline at 40°C for 40 scans at 5 mV s^{-1} $-0.3 \leq E / \text{V} \leq 0.8$ (vs. Ag wire). Doping = green and undoping = red.

As discussed above, zinc speciation within Type III DESs, Ethaline and Reline containing ZnCl_2 , has previously been reported by Abbott *et al.* [27] as $[\text{ZnCl}_4]^{2-}$, indicated by EXAFS absorption data. Therefore, it was assumed the zincate anion $[\text{ZnCl}_4]^{2-}$ would be present in the electrolyte however it would not be assumed to take part in satisfying electro-neutrality due to the low concentration of ZnCl_2 present in the liquid in comparison to ChCl and EG.

Therefore the M_{app} were assumed to be expressed as a combination of anion $[\text{2EG.Cl}]^-$ and cation $[\text{Ch}]^+$ transfers (mixed ion transfers) only. From the expression of M_{app} (5.2) used by Bund and Neudeck [1] the solvent term is removed due to the lack of solvent in the conventional sense. The gravimetric data on the electrochemical behaviour of conducting polymer within this electrolyte were fitted to a mixed ion transfer process (5.4).

$$M_{app} = M_{anion} + \beta M_{cation} \quad (5.4)$$

The average end-to-end doping M_{app} over 40 scans of $11 \pm 0.5\text{ g mol}^{-1}$ indicated the ingress of $[\text{2EG.Cl}]^-$ and the exit of choline cation $[\text{Ch}]^+$, $\approx 1.4 [\text{Ch}]^+$ expelled per

$[2\text{EG.Cl}]^-$ entering into the film, which represented a β value approximately -1.4 in terms of (5.4). The average end-to-end undoping M_{app} over 40 scans of $16 \pm 2 \text{ g mol}^{-1}$ indicated a direct reverse of the doping process. The M_{app} fitted the egress of the $[2\text{EG.Cl}]^-$ anion and the entry of $[\text{Ch}]^+$ cations, with $\approx 1.4 [\text{Ch}]^+$ entering per $[2\text{EG.Cl}]^-$ expelled, which represented a β value of -1.4 the same as the doping M_{app} for **PEDOT C2**. The results of this experiment show that the addition of 0.3 M ZnCl_2 to Ethaline has no effect on the ion dynamics of PEDOT. Results in terms of the gravimetric data and the same appearance of the CVs in 0.3 M ZnCl_2 / Ethaline and in neat Ethaline suggest that the Zn ions do not play a part, negating any possibility that this will cause an irreversible chemical change to the polymer within a Zn-Polymer electrochemical device.

5.3 Conclusions

In these studies ion transfers during the p-doping (undoping) of PEDOT in DES media and a molecular solvent system were explored in terms of the individual anion and cation contributions to the gravimetric data. Experiments showed that PEDOT film ion dynamics varied with DES composition, experimental timescale and prolonged exposure to redox switching.

Gravimetric data for the behaviour of PEDOT in acetonitrile solution was consistent with widely reported behaviour in the literature ^{[1][2]}. The electro-neutrality condition was satisfied by equal contributions of anion $[\text{ClO}_4]^-$ and solvent (MeCN) transfers at 10 mV s^{-1} and 20 mV s^{-1} ; with anion ingress and solvent egress occurring during doping and transfers reversed during undoping (anion egress and solvent ingress). At a lower scan rate (5 mV s^{-1}) *i.e.* a longer experimental timescale it was observed that solvent

transfers were dominant (solvent transfers contributed to 60% of the molar mass exchanges).

Gravimetric data obtained for the Type IV DES, in terms of apparent molar mass exchanges, were fitted to anion $[\text{ZnCl}_4]^{2-}$ and neutral molecule (EG) transfers. The transfers here were similar to that observed in a molecular solvent in regards to ion dynamics. During p-doping anion ingress and neutral molecule egress occurred with anion ingress contributing to 60% of the molar mass exchange. Transfers were reversed during undoping with anion $[\text{ZnCl}_4]^{2-}$ egress and ethylene glycol ingress, with anion dominance as well during undoping (60% contribution).

In contrast, PEDOT behaviour in the Type III DES resulted from transfers of anions and cations. In Ethaline it was observed that cation transfers dominated in the maintenance of electro-neutrality of PEDOT. Gravimetric data showed that during doping cation $[\text{Ch}]^+$ egress and anion ingress $[\text{2EG.Cl}]^-$ occurred, whereas during undoping these transfers were reversed. Cation transfers dominated the electrochemical behaviour of PEDOT in Ethaline (contributing to 60% of the molar mass exchange) in contrast to the dominance of anion transfers in the Type IV DES. This arises due to mobility constraints, in that larger anions are less mobile and less readily accommodated for in the matrix of the polymer.

Viscosity effects associated with the DES were significant but, via acoustic admittance measurements, it was possible to record changes in ion populations. These were presented as a function of timescale (potential scan rate in a voltammetric experiment) for potentiodynamically grown PEDOT films subsequently exposed to ZnCl_2 / EG,

Ethaline and ZnCl_2 / Ethaline (where Ethaline is a 1 : 2 stoichiometric mixture of ChCl and EG). Significantly, exposure to cycling over prolonged periods showed a drift in the initial mass of the film, suggested to arise due an increase in the electro-activity of the film. This is consistent with increases in bulk capacitance observed for PEDOT in DES in **Chapter 4**.

5.4 References

- [1] Bund A and Neudeck S, *J. Phys. Chem. B*, 2004, 108, 46, 17845-17850
- [2] Hillman AR, Daisley SJ and Bruckenstein S, *Electrochem. Commun.*, 2007, 9, 6, 1316-1322
- [3] Huang JH, Hsu CY, Hu CW, Chu CW and Ho KC, *ACS Applied Materials and Interfaces*, 2010, 2, 2, 351-359
- [4] Ispas A, Peipmann R, Adolphi B, Efimov I and Bund A, *Electrochimica Acta*, 2011, 56, 10, 3500-3506
- [5] Ispas A, Peipmann R, Bund A and Efimov I, *Electrochimica Acta*, 2009, 54, 20, 4668-4675
- [6] Kvarnström C, Neugebauer H, Blomquist S, Ahonen HJ, Kankare J and Ivaska A, *Electrochimica Acta*, 1999, 44, 16, 2739-2750
- [7] Niu L, Kvarnström C and Ivaska A, *J. Electroanal. Chem.*, 2004, 569, 2, 151-160
- [8] Niu L, Kvarnström C, Dong S and Ivaska A, *Synthetic Metals*, 2001, 121, 1-3, 1389-1390
- [9] Pigani L, Heras A, Colina Á, Seeber R and López-Palacios J, *Electrochem. Commun.*, 2004, 6, 11, 1192-1198
- [10] Snook GA, Peng C, Fray DJ and Chen GZ, *Electrochem. Commun.*, 2007, 9, 1, 83-88
- [11] Huang JH, Kekuda D, Chu CW and Ho KC, *J. Mater. Chem.*, 2009, 19, 22, 3704-3712
- [12] Blanchard F, Carré B, Bonhomme F, Biensan P, Pagès H and Lemordant D, *J. Electroanal. Chem.*, 2004, 569, 2, 203-210
- [13] Gileadi E, *Physical Electrochemistry - Fundamentals, Techniques and Applications*, 2011, Wiley-VCH, Germany
- [14] Bard AJ, Stratman M and Unwin PR, *Encyclopedia of Electrochemistry*, 2003, Wiley-VCH, Germany, Hillman AR, Volume III
- [15] Inzelt G, Bard AJ and Scholz F, *Electrochemical Dictionary*, 2008, Springer-Verlag, Berlin, Germany
- [16] Da Silva E, *High Frequency and Microwave Engineering*, 2001, Butterworth-Heinemann Oxford
- [17] Sauerbrey G, *Z. Phys.*, 1959, 155, 206-222
- [18] Faraday M, *Trans. Roy. Soc. London*, 1834, 124, 425-470
- [19] Hamann CH, Hamnett A and Vielstich W, *Electrochemistry*, 1998, Wiley-VCH, Germany
- [20] Plieth W, Bund A, Rammelt U, Neudeck S and Duc LM, *Electrochimica Acta*, 2006, 51, 11, 2366-2372
- [21] Hillman AR, Swann MJ and Bruckenstein S, *J. Electroanal. Chem.*, 1990, 291, 1-2, 147-162
- [22] Hillman AR and Bruckenstein S, *J. Chem. Soc. Faraday Trans.*, 1993, 89, 2, 339-348
- [23] Hillman AR, Daisley SJ and Bruckenstein S, *Electrochimica Acta*, 2008, 53, 11, 3763-3771
- [24] Hillman AR, Daisley SJ and Bruckenstein S, *Phys. Chem. Chem. Phys.*, 2007, 9, 19, 2379-2388

-
- [25] Abbott AP, Capper G, McKenzie KJ and Ryder KS, *J. Electroanal. Chem.*, 2007, 599, 2, 288-294
- [26] Abbott AP, Barron JC, Ryder KS and Wilson D, *Chem. Eur. J.*, 2007, 13, 22, 6495-6501
- [27] Abbott AP, Barron JC, Frisch G, Gurman S, Ryder KS and Silva AF, *Phys. Chem. Chem. Phys.*, 2011, 13, 21, 10224-10231

Chapter 6

Comparison of the Charging Behaviour of PTP in DESs

6.1 Introduction

6.1.1 Objectives

6.1.2 Literature Review on Monomer TP

6.1.3 Experimental

6.2 Redox Driven Exchange Processes of PTP

6.2.1 Behaviour in LiClO₄ / MeCN

6.2.2 Behaviour in ZnCl₂ / EG (Type IV) DES

6.2.3 Behaviour in Ethaline (Type III) DES

6.2.4 Behaviour in Ethaline containing 0.3 M ZnCl₂

6.3 Conclusions

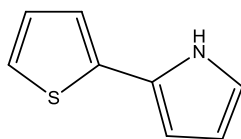
6.4 References

Chapter 6

Comparison of the Charging Behaviour of PTP in DESs

6.1 Introduction

In this chapter, the behaviour of polymer films deposited from the mixed monomer precursor thiophene-pyrrole, 2-(thiophene-2-yl)-1H pyrrole **3** (referred to as TP for the monomer and PTP for the polymer) were probed in a conventional molecular solvent (MeCN) containing the salt LiClO₄, Type III and Type IV DESs.



3

The aim of the work reported here was to try and understand charge and mass transfers that underpin the capacitance measurements presented in **Chapter 4**, in a similar way to the corresponding analysis of PEDOT charge and mass transfers in **Chapter 5**. An understanding of charge and mass transfers of a PTP cathode with a selected battery electrolyte was established by investigating apparent molar mass exchanges (M_{app}) of PTP films in contact with monomer free electrolytes during redox cycling ^[1]. The same methodology was used to investigate M_{app} during doping and undoping of PEDOT using Electrochemical Quartz Crystal Microbalance (EQCM) studies in **Chapter 5**. For a discussion of mobile species transfers expressed by M_{app} , the related equations as well as the theory behind the EQCM technique, see **Chapter 5**.

6.1.1 Objectives

The motivation of using the mixed monomer precursor TP **3** rather than a co-polymerisation of thiophene and pyrrole stems from the control of polymer structure

with the former. The latter method, co-polymerisation of mixed monomers provides no control over polymer structure due to differing monomer solubilities and varying deposition potentials. Therefore, it is hard to know what structure is produced using a co-polymerisation approach. It could be a random, block co-polymer or a phase segregated mixture of homo-polymers, each of which would have different properties. This could mean the polymers produced may not be reproducible, affecting the quality of a device produced with the polymer. Whereas, using the mixed monomer precursor TP would produce a much more structured polymer with reproducible behaviour as the thiophene and pyrrole rings are in one molecule.

Another motivation for using the precursor TP is to seek an alternative polymer structure for charge storage rather than using conventional conducting polymers such as PEDOT, PAni, PPy or polythiophene. Pyrrole is easy to polymerise but has chemical stability limitations whereas thiophene is chemically more stable and has a more anodic oxidation potential when polymerised which helps to optimise energy density ^[2]. However, thiophene can be difficult to polymerise electrochemically in molecular solvents ^[2]. Therefore, combining the two systems in a single regio-regular polymer (from a single monomer precursor) may provide a polymer with optimal properties in terms of chemical stability and ease of polymerisation.

In addition to these motivations, as the heterocyclic synthetic chemistry has been established this poses the opportunity to further substitute the pyrrole in order to give better cycle stability and perhaps a more open and porous morphology.

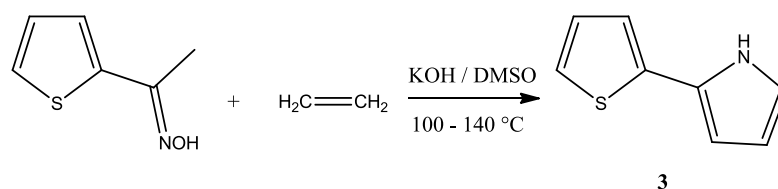
The overarching goal of the work in this Chapter was to investigate the electrochemical behaviour of PTP in a conventional molecular solvent (MeCN) and DESs, focussing on the redox driven mass charge transfers of PTP to see if the polymer was suitable for use in an electrochemical device. The initial objective of the EQCM studies was to identify individual contributions of anion, cation and solvent transfers in maintaining electro-neutrality. The second objective was to determine whether these transfers were affected by varying the timescale of the electrochemical study (scan rate in a voltammetric study), varying exposure time to potential perturbations (long periods of redox cycling), changing film thickness or varying the electrodeposition conditions in terms of the electrochemical control regimes. The third objective focussed on the DESs and the effect, if any, of changing the quaternary ammonium salt (QAS), choline chloride (Type III DES) to a metal salt ZnCl_2 (Type IV DES) and adding a small amount of ZnCl_2 to a Type III DES. Experiments performed aimed to understand the redox driven ion transfers of PTP and whether electro-neutrality of the film was dominated by anion or cation transfers in the DESs.

Research into the current state of the art for this polymer is discussed below and will help support with understanding the electrochemical behaviour of PTP and its suitability as a material for charge storage devices.

6.1.2 Literature Review on Monomer TP

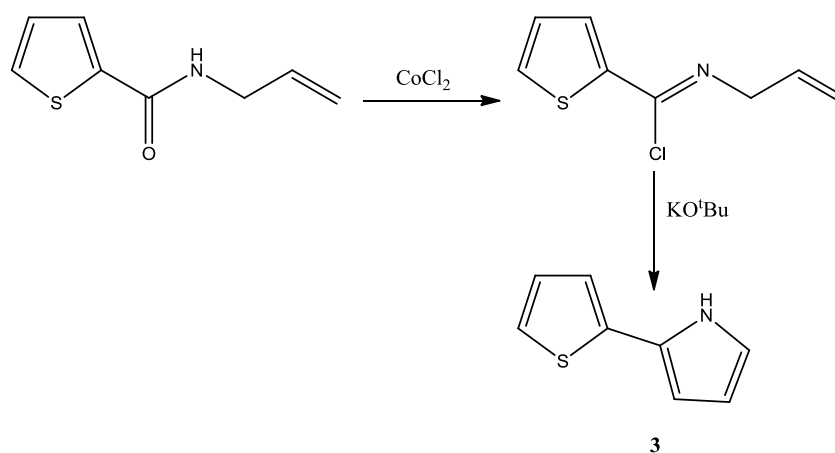
A literature search highlighted that studies had not yet been conducted into the behaviour of PTP in terms of redox driven ion transfers. In some published articles the monomer was also referred to 2-(2-thienyl)pyrrole rather than the full IUPAC name 2-(thiophene-2-yl)-1H-pyrrole.

In 1977, Trofimov *et al.* ^[3] published the synthesis of TP via the reaction of methyl 2-thienyl ketoxime with acetylene in the presence of KOH at 100 – 140 °C to give 2-(2-thienyl)pyrrole in a 60% yield (m.p. 62 °C from 50% aqueous methanol) shown in **Scheme 6.1**. Spectral analyses (IR, UV, ¹³C NMR) reported the presence of thiophene and pyrrole rings. However, no specific synthetic procedure was published. The same procedure was published again by Trofimov *et al.* ^[4] five years later for the formation of TP (50% yield) using the ketoxime in the presence of KOH in DMSO at 100 °C (**Scheme 6.1**), however no analytical data, spectral data or procedure were published in the article.



Scheme 6.1 - Synthesis of TP by Trofimov *et al.* KOH and acetylene reaction ^[3].

In 1978, Engel and Steglich ^[5] synthesised TP using the reaction of N-allylcarboxamide (2-thienoylallylamide) with phosgene reported in **Scheme 6.2**. The formation of the pyrrole ring occurred by a 1, 5 dipolar ring closure of the nitrile ylide via elimination of HCl using potassium tert-butoxide. Engel and Steglich registered TP for CAS (CAS 52101-46-7) and synthesised a range of 2-aryl and 2-heteroaryl pyrroles to use as precursors in chemotherapeutics. TP was produced in an 86% yield with m.p. 78 °C (sublimation in a vacuum).



Scheme 6.2 - Synthesis of TP by Engel and Steglich from 2-thienyl N-allylcarboxamide ^[5].

Neither Trofimov *et al.* ^{[3][4]} or Engel and Steglich ^[5] reported in these peer reviewed articles the polymerisation of TP. It was not until 1986 (eight years after the first reported synthesis of TP ^[3]) that the polymerisation of this novel heterocycle was published. Naitoh *et al.* ^[6] conducted the potentiodynamic polymerisation of TP (4 mM monomer used) from 0.1 M Bu_4NHSO_4 / MeCN at 20 mV s^{-1} ($-1.0 \leq E / \text{V} \leq 1.7$). The synthetic protocol used by these authors to produce the TP monomer was the same as outlined by Engel and Steglich ^[5]. A violet coloured polymer film was produced upon oxidation, which changed to orange in colour upon reduction with a conductivity of 0.082 S cm^{-1} . The $i(E)$ response produced during polymerisation exhibited two oxidation peaks at 0.8 V and 1.3 V attributed to the formation of cation radicals and dication radicals respectively, shown in **Fig. 6.1**. Naitoh *et al.* ^[6] also conducted the polymerisation in nitrobenzene achieving a higher conductivity film (3.3 S cm^{-1}) resulting in a violet / blue coloured film upon oxidation. The UV-Visible absorbance spectra were obtained for the PTP films ^[6].

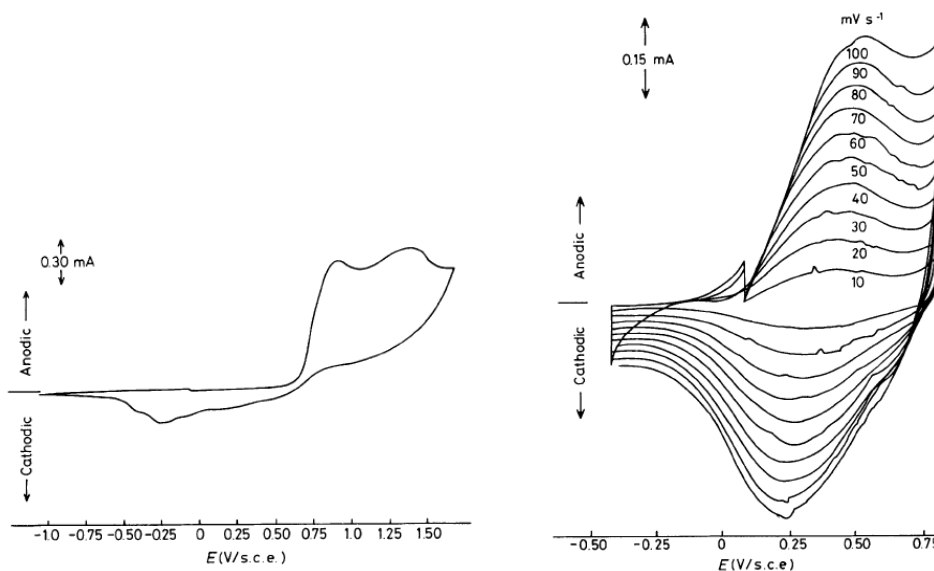


Fig. 6.1 - Naitoh *et al.* ^[6] potentiodynamic deposition of poly(2-(2-thienyl)pyrrole) from 4 mM 2-(2-thienyl)pyrrole in 0.1 M Bu₄NHSO₄ / MeCN at 20 mV s⁻¹ at RT -1.0 ≤ E / V ≤ 1.7 (vs. sce reference electrode) (left) and cyclic voltammetric experiment of poly(2-(2-thienyl)pyrrole) film in monomer free 0.1 M Bu₄NHSO₄ / MeCN electrolyte at a range of different scan rates at RT -0.4 ≤ E / V ≤ 0.8 (right).

In 2007, Pozo-Gonzalo *et al.* ^[7] investigated the electrochemical and electrochromic behaviour of potentiodynamically prepared PTP. The same procedure as Trofimov *et al.* ^[3] (**Scheme 6.1**) was used to synthesise the TP monomer as well as exchanging the KOH for LiOH. The monomer exhibited two irreversible oxidation potentials during polymerisation, 0.86 V and 1.3 V, attributed to pyrrole and thiophene respectively (**Fig. 6.2**). These are lower oxidation potentials than the individual heterocycles, pyrrole (1.0 – 1.5 V in MeCN) and thiophene (2.02 V). This is due to increased electron delocalisation in 2-(2-thienyl)pyrrole allowing easier electron removal. This shows that combining the two heterocycles provides improved deposition conditions.

Polymerisation was conducted using a 3 electrode system; either a Pt or ITO glass working electrode, Pt flag counter electrode and Ag / AgCl reference electrode using

10 mM 2-(2-thienyl)pyrrole in 0.1 M LiClO₄ / MeCN solution. The resulting potentiostatic deposition cyclic voltammograms are shown in **Fig. 6.2**.

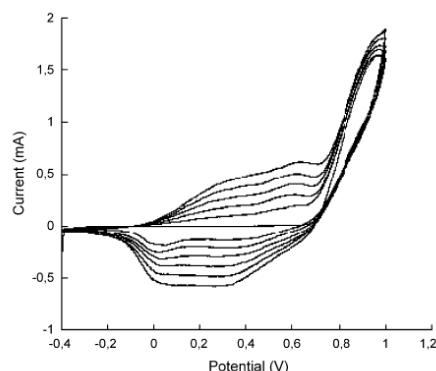


Fig. 6.2 - Pozo-Gonzalo *et al.* [7] potentiodynamic deposition of poly(2-(2-thienyl)pyrrole) from 10 mM 2-(2-thienyl)pyrrole in 0.1 M LiClO₄ / MeCN $-0.4 \leq E / V \leq 1.0$ at RT for 5 scans (new oxidation wave at *ca.* 0.6 V, due to increased conjugation length of polymer in comparison to the monomer).

The [ClO₄]⁻ doped film exhibited orange (reduced) to black (oxidised) electrochromic behaviour. This occurred during deposition and during cyclic voltammetric experiments in monomer free 0.1 M LiClO₄ / MeCN electrolyte, with the cyclic voltammogram shown in **Fig. 6.3**. This electrochromic behaviour combined the properties of both polypyrrole (yellow reduced, black oxidised) and polythiophene (red reduced, blue oxidised) [5]. The cyclic voltammogram showed two oxidation peaks at 0.66 V and 0.79 V, inferred to be the polaron and bipolaron states respectively. The graph of peak current *vs.* scan rate shows that a redox active material is confined to the electrode, stable to p-doping, charge transport is not diffusion limited and there are no significant kinetic barriers for charging / discharging of the polymer film.

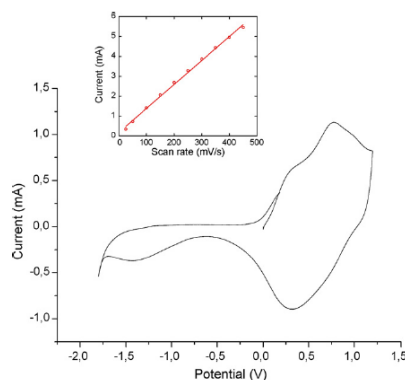


Fig. 6.3 - Pozo-Gonzalo *et al.* ^[1], cyclic voltammogram of poly(2-(2-thienyl)pyrrole) film in monomer free 0.1 M LiClO₄ / MeCN -0.8 ≤ E / V ≤ 1.2. Inset plot shows the peak current as a function of potential (linear fit R > 0.99).

The band gap of poly(2-(2-thienyl)pyrrole) was found to be 1.6 – 1.7 eV, lower than the homopolymers *cf.* polypyrrole (2.85 eV) and polythiophene (2.3 eV). This is attributed to an increased electron delocalisation within the polymer film. The morphology was investigated by AFM and was reported to have a granular morphology (60 nm granules / surface roughness 3.5 nm) when doped (oxidised) and becomes aggregated (65 – 90 nm granules / surface roughness 9.2 nm) when de-doped (reduced) ^[7].

Pozo-Gonzalo *et al.* ^[7] conducted model calculations of the dimer of 2-(2-thienyl) pyrrole to predict the stereochemistry of an un-doped polymer chain. It was assumed that the s-trans-s-trans-s-trans conformation would be preferred, however the calculations showed that the lower energy (preferred) conformation was the s-cis-s-trans-s-trans conformation (in an ABBA style) shown below in **Fig. 6.4**.

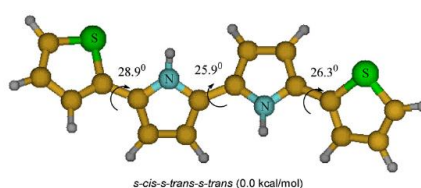


Fig. 6.4 - Pozo-Gonzalo *et al.* model calculations of preferred stereochemistry of 2-(2-thienyl)pyrrole dimer ^[7].

A year later, alkylated 2-(2-thienyl)pyrrole derivatives were synthesised to study the electrochromic behaviour of the resulting electropolymerised films by Pozo-Gonzalo *et al.* [8]. Polymerisation of heterocyclic monomers containing alkyl groups have shown to give a broader colour range *cf.* non-alkylated versions.

Ping *et al.* [9][10][11] polymerised 2-(2-thienyl)pyrrole prior to Pozo-Gonzalo *et al.* [7][8]. Ping and Nauer [9] firstly polymerised 2-(2-thienyl)pyrrole from 5 μM monomer in 0.5 mM LiClO_4 / MeCN for in-situ FTIR-ATR Spectroscopy, the potentiodynamic deposition cyclic voltammogram is shown in **Fig. 6.5**. The monomer was synthesised by the procedure outlined by Engel and Steglich [2].

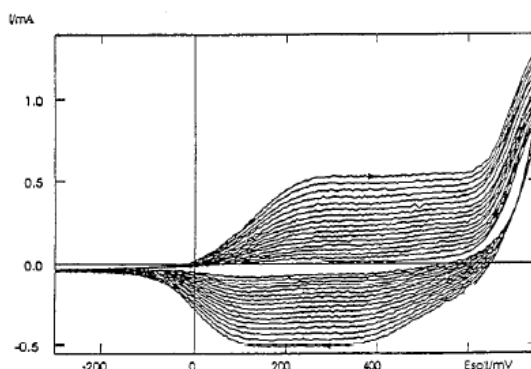


Fig. 6.5 - Ping and Nauer [9] potentiodynamic deposition of poly(2-(2-thienyl)pyrrole) from 5 μM monomer in 0.5 mM LiClO_4 / MeCN at 1 mV s^{-1} between $-0.3 \leq E / \text{V} \leq 0.8$ at RT (ZnSe / Au / Pt grid working electrode).

In another publication by Ping *et al.* [10] reported the polymerisation of 2-(2-thienyl)pyrrole from aqueous perchloric acid solution containing either NaClO_4 , LiClO_4 and NaBF_4 , for in-situ FTIR ATR spectroscopy. The acidic conditions produced polymers with larger chain lengths. From the potentiostatic deposition depicted in **Fig. 6.6**, it can be seen that with increasing cycles the charge consumed for oxidation increases more than the amount used for polymerisation. Ping *et al.* [10] attributed this to the existence of more conducting areas within the polymer film.

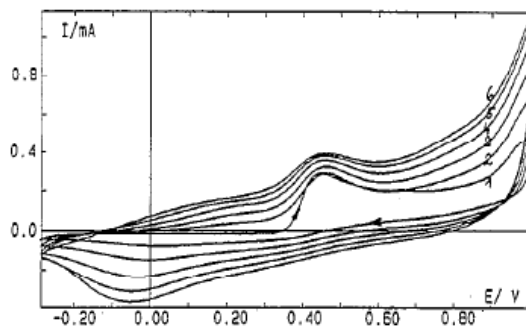


Fig. 6.6 - Ping *et al.* ^[10] potentiodynamic deposition poly(2-(2-thienyl)pyrrole from 5 mM 2-(2-thienyl)pyrrole in 0.5 M NaClO₄ in 1 M HClO₄ at 10 mV s⁻¹ between -0.3 ≤ E / V ≤ 0.8.

Ping and Nauer ^[11] also conducted in-situ FTIR ATR spectroscopy on poly(2-(2-thienyl)pyrrole redox behaviour with Bu₄NClO₄ and Bu₄NPF₆. However no cyclic voltammograms were shown, only the IR spectral data was published.

Nauer *et al.* ^[12] also conducted high frequency resistance measurements during the polymerisation of 2-(2-thienyl)pyrrole in 0.1 M LiClO₄ / MeCN and also during redox cycling in monomer free electrolyte with different anions and cations. The monomer was synthesised via an improved route of the reaction by Engel and Steglich ^[5], however the synthesis referenced had not been published. The potentiodynamic deposition and associated high frequency resistance data (**Fig. 6.7**) showed that the resistance increased at the cathodic end of the cyclic voltammogram upon each subsequent deposition cycle.

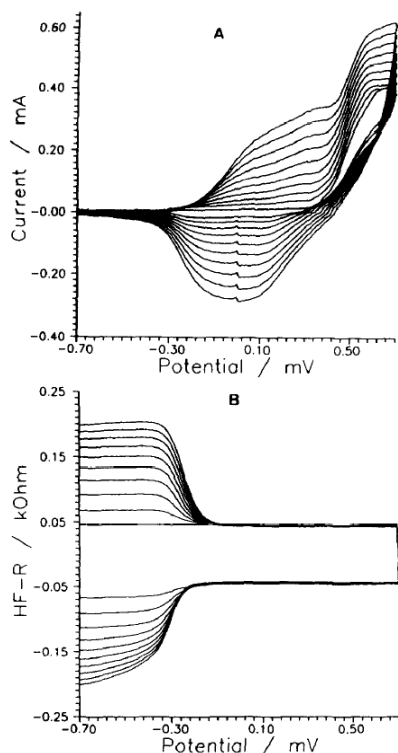


Fig. 6.7 - Cordruwisch *et al.*^[12] potentiodynamic deposition of poly(2-(2-thienyl)pyrrole) from 10 mM monomer in 0.1 M LiClO₄ / MeCN (Pt working electrode) at 50 mV s⁻¹ between -0.7 ≤ E / V ≤ 1.0 at RT.

The upper and lower parts of the resistograms are measured during the anodic and cathodic sweeps respectively.

The resistance behaviour was investigated in monomer free electrolyte. The cyclic voltammogram in 0.1 M LiClO₄ / MeCN is shown in **Fig. 6.8** with the associated resistance data. Similar experiments were conducted by changing the cation and anion of the supporting salt. The cyclic voltammograms were not reported for the different anion and cation systems, only the differences in resistance were compared. The cation and anion have an effect on the resistance in the cathodic region (reduction) but do not make a substantial difference in the anodic region (oxidation). [Bu₄N]⁺, [Na]⁺ and [Li]⁺ cations with a [PF₆]⁻ anion were used to see the cation effect on resistance. [Bu₄N]⁺ cations with [BF₄]⁻, [ClO₄]⁻ and [PF₆]⁻ anions were used to compare the effect of changing the anion. The resistograms are shown in **Fig. 6.9**. Cordruwisch *et al.*^[12] reported that changing to [Na]⁺ and [Li]⁺ cations enhanced the high frequency resistance due to the favoured mobility of the smaller cations (in a large pored structure created

with $[\text{Bu}_4\text{N}]^+$ on polymerisation). The $[\text{BF}_4]^-$ anion enhances the high frequency resistance as it occupies a smaller volume in the polymer film; therefore it is less hindered upon ion exchange.

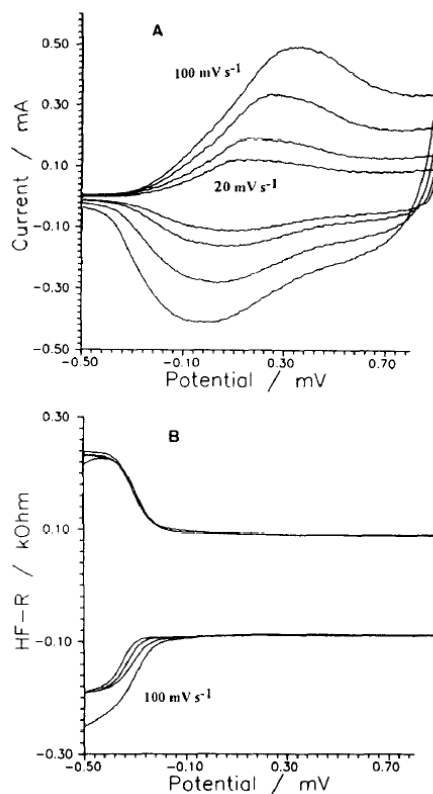


Fig. 6.8 - Cordruwisch *et al.* ^[12] cyclic voltammogram of poly(2-(2-thienyl)pyrrole) (grown in 0.1 M LiClO₄ / MeCN) (0.4 μm) in monomer free 0.1 M LiClO₄ / MeCN (Pt working electrode) at 20, 40, 60 and 100 mV s⁻¹ between -0.5 ≤ E / V ≤ 0.8 at RT. The upper and lower parts of the resistograms are measured during the anodic and cathodic sweeps respectively.

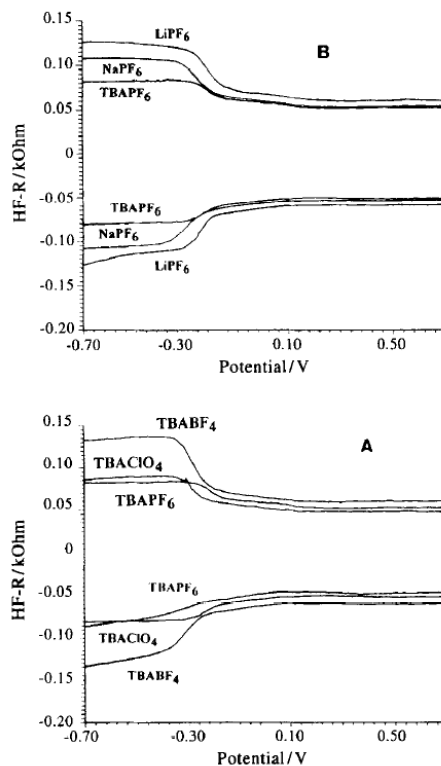


Fig. 6.9 - Cordruwisch *et al.* ^[12] high frequency resistance data of poly(2-(2-thienyl)pyrrole) (grown in 0.1 M Bu₄NPF₆ / MeCN) (0.5 μm) in acetonitrile with different supporting salts at 5 mV s⁻¹ between -0.5 ≤ E / V ≤ 0.8 at RT. The upper and lower parts of the resistograms are measured during the anodic and cathodic sweeps respectively.

6.1.3 Experimental

The PTP deposition and the associated redox cycling experimental conditions are reported below for potentiodynamically prepared films **PTP A, AA, B, BA, C, C1, C2** and **CA** in **Table 6.1**. All polymerisations were carried out in 0.1 M LiBF₄ / MeCN containing 0.1 M TP at ambient temperature. PTP films labelled with the first letter **A** were exposed to 0.1 M LiClO₄ / MeCN, **B** exposed to ZnCl₂ / EG Type IV DES and **C** exposed to Ethaline Type III DES. PEDOT films labelled with a single letter and with a number were deposited potentiodynamically at 5 mV s⁻¹; labelled with the second letter **A** were deposited potentiodynamically at 20 mV s⁻¹.

The behaviour of a PTP film was probed in either a conventional molecular solvent containing LiClO₄ (0.1 M LiClO₄ / MeCN), a Type III DES (Ethaline) or a Type IV DES (ZnCl₂ / EG). The specific electrolytes exposed to each PTP film are highlighted in **Table 6.1**.

End-to-end molar apparent molar mass exchanges (M_{app}) for the doping and undoping regimes of PTP in different electrolytes presented in the proceeding sections were calculated using Faraday's law of electrolysis, the same calculation as used for determining PEDOT M_{app} in **Chapter 5**. Apparent molar mass exchanges (M_{app}) for the doping and undoping regimes were calculated by the product of gradients from the doping and undoping regions of a Δm vs Q plot and Faraday's constant (using equation **(5.1)**). End-to-end refers to the mass charge data from one half cycle *i.e.* from the cathodic to the anodic vertex potential.

$$\frac{\Delta m}{Q} = \frac{M_{app}}{nF} \quad (5.1)$$

An example PTP deposition CV is reported for **PTP A** in **Fig. 6.10** below, along with the mass as a function of potential (found from the change in frequency Δf of the quartz crystal). The $i(E)$ responses were reproducible for all PTP depositions (**PTP A – C**). During polymerisation in 0.1 M LiBF₄ / MeCN a crossover of the current traces occurred at ≈ 0.75 V indicative of the nucleation and growth of the polymer. **PTP A** was found to be the thickest film deposited at 0.49 μm . The thicknesses for **PTP A – C** ranged between 0.11 – 0.49 μm (see **Table 6.1**). Dry mass and thickness measurements, reported in **Table 6.1**, were observed to be greater than the wet mass and thickness measurements. This could be attributed to insufficient drying of the films (solvent trapped within the pores of the polymer) and / or acoustically thick films.

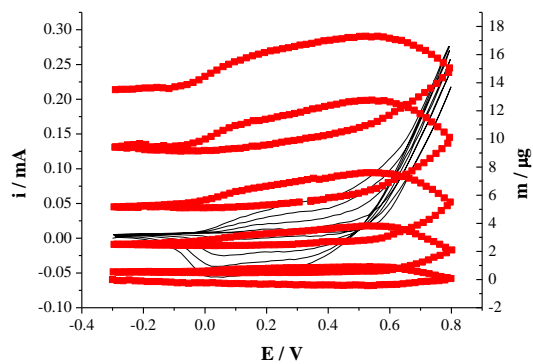


Fig. 6.10 - Cyclic voltammetric data and m vs. E for the potentiodynamic deposition of **PTP A** on an EQCM Crystal Au electrode from 0.1 M TP in 0.1 M LiBF₄ / MeCN at RT for 5 scans at 5 mV s⁻¹ $-0.3 \leq E / V \leq 0.8$ (vs. Ag wire) depositing a film with a mass of 13.50 μg and a thickness of 0.49 μm (assuming $\rho = 1.3 \text{ g cm}^{-3}$). Current trace shown by black solid line and mass shown by the red square data points.

Table 6.1 - PTP potentiodynamic deposition and experimental conditions.

Redox Cycling at 40 °C									
PTP Films	Growth in 0.1 M LiBF ₄ / MeCN	Growth Q / mC (2 d.p)	wet mass / µg (4 s.f)	wet thickness / µm (2 d.p)	dry mass / µg (4 s.f)	dry thickness / µm (2 d.p)	Electrolyte	scan rate	number of scans and potential window
A	5 scans at 5 mV s ⁻¹ -0.3 ≤ E / V ≤ 0.8	78.28	13.5	0.49	15.31	0.56	0.1 M LiClO ₄ / MeCN	2, 5, 10, 20 mV s ⁻¹ (x2)	3 CVs per scan rate -0.3 ≤ E / V ≤ 0.8
AA	5 scans at 20 mV s ⁻¹ -0.3 ≤ E / V ≤ 0.8	0.34	0.8703	0.03	3.518	0.13	0.1 M LiClO ₄ / MeCN	5 mV s ⁻¹	40 CVs -0.3 ≤ E / V ≤ 0.8
B	5 scans at 5 mV s ⁻¹ -0.3 ≤ E / V ≤ 0.8	198.23	4.519	0.17	14.91	0.55	1 ZnCl ₂ / 4 EG	2, 5, 10, 20 mV s ⁻¹ (x2)	3 CVs per scan rate -0.3 ≤ E / V ≤ 0.8
BA	5 scans at 20 mV s ⁻¹ -0.3 ≤ E / V ≤ 0.8	0.33	0.8594	0.03	5.993	0.22	1 ZnCl ₂ / 4 EG	5 mV s ⁻¹	40 CVs -0.3 ≤ E / V ≤ 0.8

Table 6.1 (continued) - PTP potentiodynamic deposition and experimental conditions.

Redox Cycling at 40 °C									
PTP Films	Growth in 0.1 M LiBF ₄ / MeCN	Growth Q / mC (2 d.p)	wet mass / μg (4 s.f)	wet thickness / μm (2 d.p)	dry mass / μg (4 s.f)	dry thickness / μm (2 d.p)	Electrolyte	scan rate	number of scans and potential window
C	5 scans at 5 mV s ⁻¹ -0.3 ≤ E / V ≤ 0.8	106.29	7.012	0.26	10.88	0.4	Ethaline	2, 5, 10, 20 mV s ⁻¹ (x2)	3 CVs per scan rate -0.3 ≤ E / V ≤ 0.8
C1	5 scans at 5 mV s ⁻¹ -0.3 ≤ E / V ≤ 0.8	88.4	9.396	0.34	8.308	0.3	Ethaline	5 mV s ⁻¹	40 CVs -0.3 ≤ E / V ≤ 0.8
C2	5 scans at 5 mV s ⁻¹ -0.3 ≤ E / V ≤ 0.8	97.63	4.9	0.18	21.63	0.79	0.3 M ZnCl ₂ in Ethaline	5 mV s ⁻¹	40 CVs -0.3 ≤ E / V ≤ 0.8
CA	5 scans at 20 mV s ⁻¹ -0.3 ≤ E / V ≤ 0.8	0.57	1.482	0.05	7.966	0.29	Ethaline	5 mV s ⁻¹	40 CVs -0.3 ≤ E / V ≤ 0.8

6.2 Redox Driven Exchange Processes of PTP

6.2.1 Behaviour in LiClO₄ / MeCN

The behaviour of **PTP A** (prepared in 0.1 M LiBF₄ / MeCN for 5 scans at 5 mV s⁻¹ at ambient temperature $-0.3 \leq E / V \leq 0.8$) during a voltammetric experiment in 0.1 M LiClO₄ / MeCN at 5 mV s⁻¹ at 40 °C, with the associated mass per redox cycle as a function of potential presented in **Fig. 6.11A**, which showed broad oxidation and reduction peaks at ≈ 0.4 V and ≈ 0.1 V respectively, with no current hysteresis observed over the three scans. The observed mass changes as a function of the total charges passed during the cyclic voltammetric study reported in **Fig. 6.11B** showed an increase in charge associated with an increase in mass during oxidation, with the trend reversed during reduction. Simplistically, this trend can be qualitatively interpreted as anion exchanges maintaining film electro-neutrality.

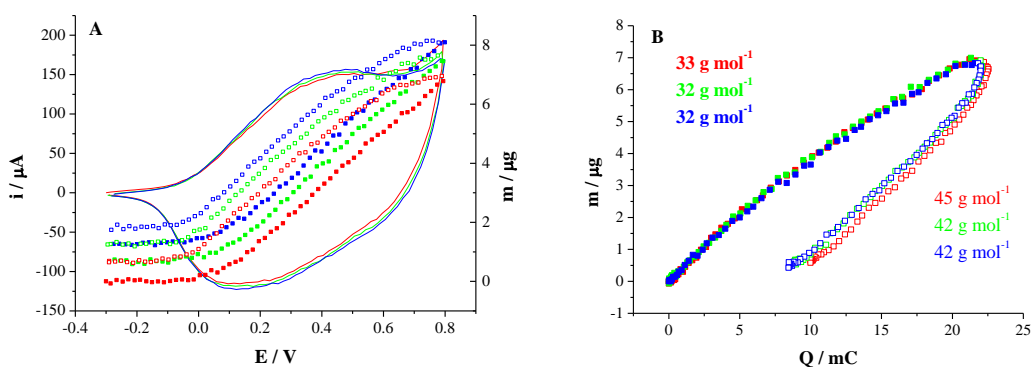


Fig. 6.11 - A) Cyclic voltammetric data and m vs. E **B)** m vs. Q for the redox cycling of **PTP A** in 0.1 M LiClO₄ / MeCN at 40 °C for 3 scans at 5 mV s⁻¹ $-0.3 \leq E / V \leq 0.8$ (vs. Ag wire) with associated M_{app} (g mol⁻¹). Doping = solid squares, undoping = outline squares (1st CV = red, 2nd = green, 3rd = blue).

The CV of **PTP A** was recorded at long and short timescales achieved by varying the potential scan rate. The end-to-end molar mass exchanges (M_{app}) calculated for the doping and undoping regimes at three different scan rates 5, 10 and 20 mV s⁻¹ respectively were \uparrow 32, 33, 35 (\pm 1) g mol⁻¹ (doping) and \downarrow 40, 38, 38 (\pm 3, 2, 1) g mol⁻¹

(undoping). The arrows indicate whether the mass of the film increased or decreased during redox switching.

For the behaviour of PTP in LiClO₄ / MeCN electrolyte, it was assumed that no cation exchange would occur, the same as observed for PEDOT in **Chapter 5**. Therefore, the M_{app} for both doping and undoping were assumed to be expressed as a combination of only anion [ClO₄]⁻ and solvent (MeCN) transfers **(5.3)**.

$$M_{app} = M_{anion} + \alpha M_{solv} \quad (5.3)$$

The doping M_{app} of **PTP A** in 0.1 M LiClO₄ / MeCN indicated the entry of a perchlorate anion ($M_{anion} = 99 \text{ g mol}^{-1}$) and the expulsion of acetonitrile ($M_{solv} = 41 \text{ g mol}^{-1}$). The calculation of α for doping was -1.6, interpreted as the molar ratio of MeCN to [ClO₄]⁻ transfers (nMeCN : [ClO₄]⁻ = 1.6). The undoping M_{app} were assumed to be expressed as the reverse of the ion and solvent transfers observed during doping *i.e.* [ClO₄]⁻ out and MeCN in. The calculation of α for undoping was -1.5, interpreted as the molar ratio of MeCN to [ClO₄]⁻ transfers (nMeCN : [ClO₄]⁻ = 1.5) The doping and undoping behaviours were relatively independent of scan rate, as demonstrated by similar M_{app} and α values. The solvent transfers during undoping ($\alpha = -1.5$) for **PTP A** were not significantly different to the doping ($\alpha = -1.6$) regime. The same anion and solvent exchanges were observed for **PEDOT A** albeit different molar ratios of anion to solvent transfer.

The admittance spectra obtained over the three scans are reported in **Fig. 6.12**, with admittance spectra presented from the beginning (-0.3 V), middle (0.8 V) and end (-0.3 V) of each cycle. The deposition of **PTP A** exhibited a decrease in Q-factor of 78%, therefore the polymer film would be classified as an acoustically thick

film. The Q-factor changed very little over the redox switching, 174 to 166, which meant the Sauerbrey equation could be applied to find out mass changes. Further films were therefore deposited to acquire acoustically thin films to compare and contrast the M_{app} (i.e. compare dm / dQ) from thinner films with that of thicker ones.

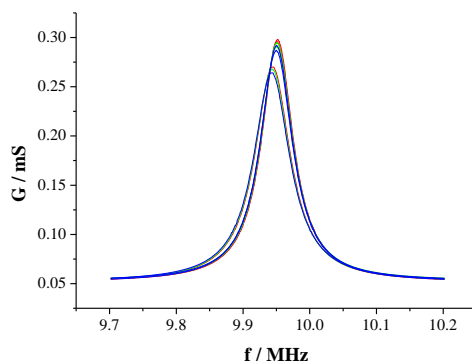


Fig. 6.12 - Admittance spectra for **PTP A** redox cycling only in 0.1 M LiClO₄ / MeCN (shown in **Fig. 6.11**), 1st CV = red, 2nd = green, 3rd = blue. Admittance spectra recorded at a frequency span = 500 kHz.

Further experiments were conducted to investigate whether the deposition electrochemical control regimes affected the behaviour of PTP. **PTP AA** was deposited at a faster potential scan rate (prepared in 0.1 M LiBF₄ / MeCN for 5 scans at 20 mV s⁻¹ at ambient temperature $-0.3 \leq E / V \leq 0.8$) exposed to 0.1 M LiClO₄ / MeCN at 5 mV s⁻¹ at 40 °C with the resultant CV and m vs. Q in **Fig. 6.13**. The average doping M_{app} was recorded at 15 ± 3 g mol⁻¹ and the average undoping M_{app} at 23 ± 22 g mol⁻¹. The M_{app} for doping and undoping were able to be expressed as a combination of anion transfer and solvent transfer (5.3).

$$M_{app} = M_{anion} + \alpha M_{solv} \quad (5.3)$$

The M_{app} values related to α values for **PTP AA** in LiClO₄ / MeCN for doping and undoping were -2 and -1.9 respectively. For doping this related to the ingress of [ClO₄]⁻ and the egress of MeCN with a molar ratio of solvent to anion of 2. Upon undoping these transfers reversed.

The admittance spectra obtained over the forty scans for **PTP AA** in 0.1 M LiClO₄ / MeCN are reported in **Fig. 6.14**. The deposition of **PTP AA** exhibited a decrease in Q-factor of only 2%, characteristic of an acoustically thin film. However during redox cycling of **PTP AA** in 0.1 M LiClO₄ / MeCN the Q-factor significantly decreased by 93% over the 40 CVs, indicative of significant swelling of the film.

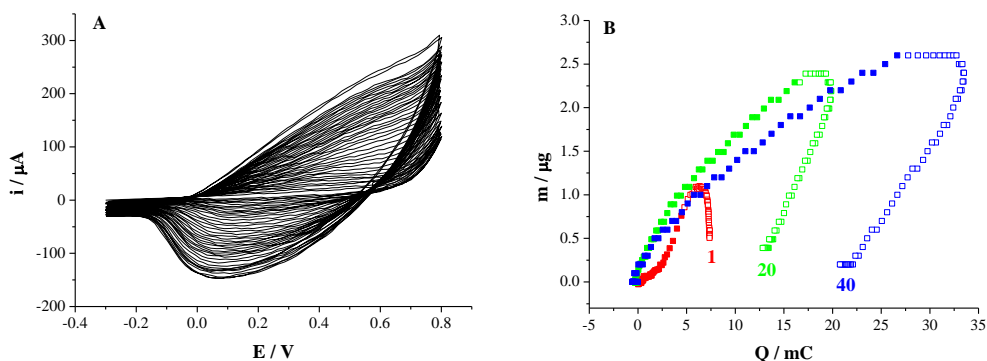


Fig. 6.13 - A) Cyclic voltammetric data **B)** m vs. Q for the redox cycling of **PTP AA** in 0.1 M LiClO₄ / MeCN at 40 °C for 40 scans at 5 mV s⁻¹ -0.3 ≤ E / V ≤ 0.8 (vs. Ag wire). Doping = solid squares, undoping = outline squares 1st CV (red), 20th (green) and 40th CV (blue).

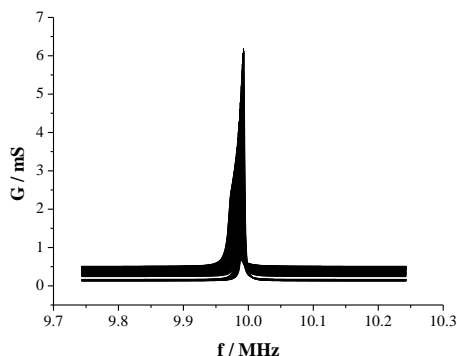


Fig. 6.14 - Admittance spectra for **PTP AA** redox cycling only in 0.1 M LiClO₄ / MeCN (shown in **Fig. 6.13**). Admittance spectra recorded with a frequency span = 500 kHz.

For all PTP films exposed to 0.1 M LiClO₄ / MeCN solvent transfer dominated the redox driven transfer of mobile species at 60% compared to only a 40% contribution of [ClO₄]⁻ to the apparent molar mass exchange of the film with the electrolyte.

6.2.2 Behaviour in ZnCl₂ / EG (Type IV) DES

The behaviour of **PTP B** (prepared in 0.1 M LiBF₄ / MeCN for 5 scans at 5 mV s⁻¹ at ambient temperature $-0.3 \leq E / V \leq 0.8$) during a voltammetric experiment in the Type IV DES ZnCl₂ / EG at 5 mV s⁻¹ with the associated mass changes per redox cycle (found from Δf) as a function of potential is presented in **Fig. 6.15A**. This showed a slight oxidation peak at ≈ 0.5 V and a broad reduction peak at ≈ -0.05 V. The oxidation involved an increase in current coupled with an increase in mass (≈ 1 μ g), which represented 22% of the mass of the film. During reduction the reverse situation occurred, with a decrease in current coupled with a decrease in mass (≈ 0.8 μ g).

A mass retention of 0.2 μ g per scan was observed, which represented $\approx 4\%$ of the total mass of the film. This increase over three scans (*i.e.* an increase of 0.6 μ g) represented $\approx 13\%$ of the total mass of the film. The mass retention per scan (0.2 μ g) as a percentage of the mass increase upon oxidation (1 μ g) was 20%. The data in **Fig. 6.15B** appears rather noisy which is attributed to the increase in viscosity of the DES compared to a molecular solvent such as acetonitrile.

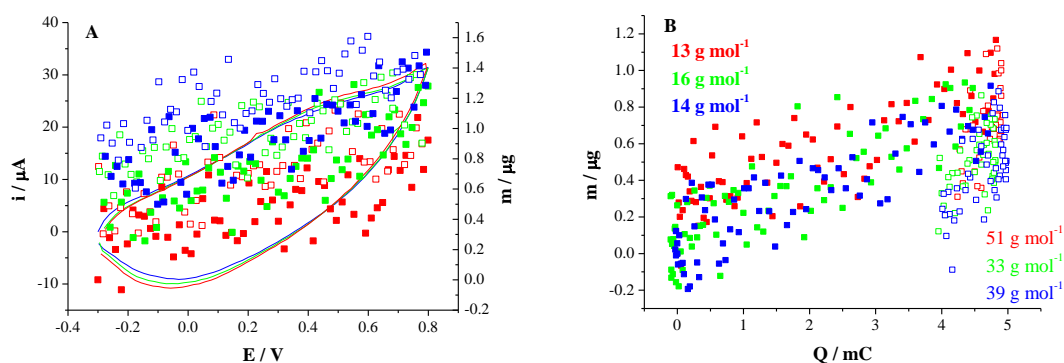


Fig. 6.15 - A) Cyclic voltammetric data and m vs. E **B)** m vs. Q for redox cycling of **PTP B** in ZnCl₂ / EG at 40 °C for 3 scans at 5 mV s⁻¹ $-0.3 \leq E / V \leq 0.8$ (vs. Ag wire) (with associated M_{app} (g mol⁻¹) doping = solid squares, undoping = outline squares (1st CV = red, 2nd = green, 3rd = blue).

PTP B was subjected to voltammetric studies at long and short timescales, achieved by varying the potential scan rate. The M_{app} varied at slightly at each scan rate in the DES; doping 11 (± 3), 10 (± 6), 13 (± 1) g mol⁻¹; undoping 31 (± 12), 14 (± 11), 17 (± 8) g mol⁻¹ for scan rates 5, 10 and 20 mV s⁻¹.

Using the knowledge of speciation within this DES (discussed in **Chapter 5**), M_{app} values were assumed to be expressed as a combination of anion transfers $[\text{ZnCl}_4]^{2-}$ with associated neutral species transfers (**5.5**), probably EG as observed with PEDOT in ZnCl₂ / EG (**Chapter 5**).

$$M_{app} = M_{anion} + \gamma M_{neut} \quad (5.5)$$

Doping M_{app} of **PTP B** in ZnCl₂ / EG indicated the entry of the zincate anion $[\text{ZnCl}_4]^{2-}$ ($M_{anion} = 104$ g mol⁻¹) and the expulsion of some neutral species, probably EG ($M_{neut} = 62$ g mol⁻¹); with ($\approx 1.4 - 1.6$ EG expelled per $[\text{ZnCl}_4]^{2-}$ entry), *i.e.* a value of γ of -1.4 to -1.6. The undoping M_{app} indicated a reverse of the anion and neutral species transfer observed during doping, with the expulsion of $[\text{ZnCl}_4]^{2-}$ from the film to maintain electro-neutrality and the entry of a small amount of EG ($\approx 1.1 - 1.8$ EG entering per $[\text{ZnCl}_4]^{2-}$ expelled), *i.e.* a value of γ of -1.1 to -1.8.

The drop in solvent transfer during undoping could be due to either faster kinetics of anion exchange than EG transfer or that the movement of EG into the polymer was impeded by the transfer of $[\text{ZnCl}_4]^{2-}$ in the opposite direction. The latter being more feasible as the $[\text{ZnCl}_4]^{2-}$ anion is bulky, so its transfer out of the polymer pores would slow the flow of EG into the polymer. At faster scan rates the M_{app} indicated the expulsion of the $[\text{ZnCl}_4]^{2-}$ anion but more neutral species entry compared to **PTP B** at 5 mV s⁻¹.

The admittance spectra obtained over the three scans are reported in **Fig. 6.16**. The deposition of **PTP B** exhibited a decrease in Q-factor of 91%, characteristic of an acoustically thick film. However during redox cycling in $\text{ZnCl}_2 / \text{EG}$ the admittance spectra obtained over the three scans, reported in **Fig. 6.16**, showed no change in Q-factor which showed that no swelling occurred with **PTP B** in this electrolyte. This satisfied the conditions to allow the Sauerbrey Equation to be applied, to find out mass changes during redox switching ^[13].

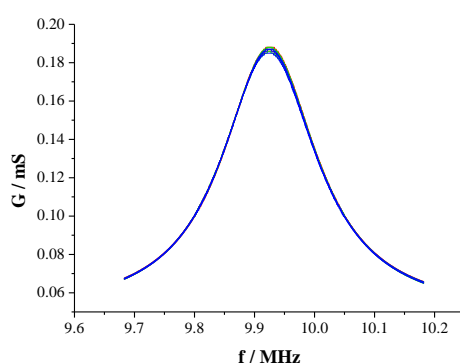


Fig. 6.16 - Admittance spectra for **PTP B** redox cycling only in $\text{ZnCl}_2 / \text{EG}$ (shown in **Fig. 6.15**) (1st CV = red, 2nd = green, 3rd = blue). Admittance spectra recorded with a frequency span = 500 kHz.

PTP BA (a film deposited at 20 mV s^{-1}) was subjected to a long term redox switching experiment in $\text{ZnCl}_2 / \text{EG}$ at $40 \text{ }^\circ\text{C}$ at 5 mV s^{-1} , with the resultant CV reported in **Fig. 6.17A**.

The doping of **PTP BA** involved an increase in current coupled with an increase in mass ($\approx 0.4 \text{ } \mu\text{g}$). The undoping involved a decrease in current coupled with a decrease in mass ($\approx 0.3 \text{ } \mu\text{g}$). This can be viewed clearly in the presentation of the individual m vs. Q plots in **Fig. 6.17B**. The overall mass increased by $\approx 0.2 \text{ } \mu\text{g}$, possibly due to an increase in electro-activity of the PTP over a long period of cycling.

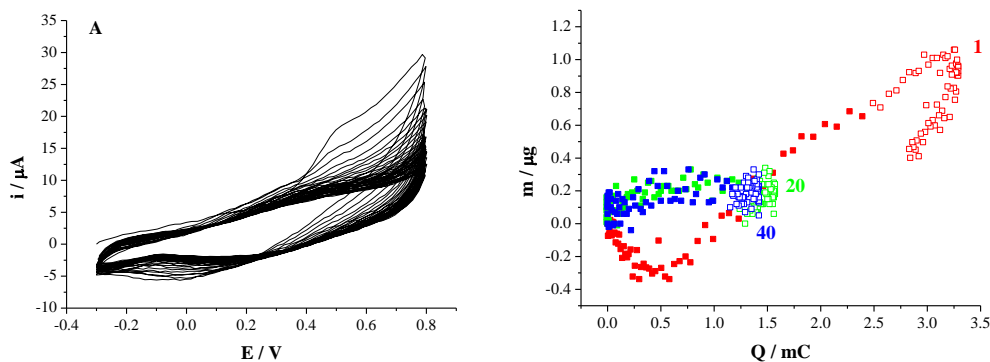


Fig. 6.17 - A) Cyclic voltammetric data **B)** m vs. Q for the redox cycling of **PTP BA** in $\text{ZnCl}_2 / \text{EG}$ at 40°C for 40 scans at 5 mV s^{-1} $-0.3 \leq E / \text{V} \leq 0.8$ (vs. Ag wire). Doping = solid squares, undoping = outline squares
1st CV (red), 20th CV (green) and 40th CV (blue).

The average doping M_{app} was recorded at $16 \pm 9\text{ g mol}^{-1}$ and the average undoping M_{app} at $26 \pm 9\text{ g mol}^{-1}$. Therefore, the M_{app} for doping and undoping were able to be expressed as a combination of anion and neutral species transfer (5.5).

$$M_{app} = M_{anion} + \gamma M_{neut} \quad (5.5)$$

The determined M_{app} values related to γ values for doping and undoping of -1.4 and -1.3 respectively. Doping M_{app} of **PTP BA** in $\text{ZnCl}_2 / \text{EG}$ indicated the entry of the zincate anion $[\text{ZnCl}_4]^{2-}$ and the expulsion of some neutral species, probably EG with (≈ 1.4 EG expelled per $[\text{ZnCl}_4]^{2-}$ entry), *i.e.* a value of γ of -1.4. The undoping M_{app} indicated a reverse of the anion and neutral species transfer observed during doping, with the expulsion of $[\text{ZnCl}_4]^{2-}$ from the film to maintain electro-neutrality and the entry of a small amount of EG (≈ 1.3 EG entering per $[\text{ZnCl}_4]^{2-}$ expelled). This was the same redox driven transfers of mobile species at the PTP film deposited at 5 mV s^{-1} .

The admittance spectra obtained over the forty scans for **PTP BA** in $\text{ZnCl}_2 / \text{EG}$ are reported in **Fig. 6.18**. The deposition of **PTP B** exhibited a decrease in Q-factor of 25%, characteristic of an acoustically thin film. The Q-factor did not vary significantly during

redox switching from 117 to 110, therefore within the prerequisite for the Sauerbrey equation to apply.

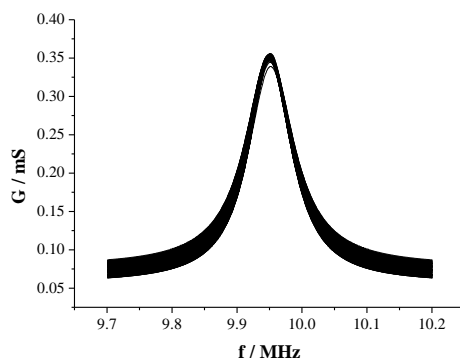


Fig. 6.18 - Admittance spectra for **PTP BA** redox cycling only in $\text{ZnCl}_2 / \text{EG}$ (shown in **Fig. 6.17**).
Admittance spectra recorded with a frequency span = 500 kHz.

6.2.3 Behaviour in Ethaline (Type III) DES

The behaviour of **PTP C** during a voltammetric study in the Type III DESs Ethaline, without the presence of any zinc species at 5 mV s^{-1} , along with the associated mass changes as a function of potential is presented in **Fig. 6.19A**. An oxidation peak was observed at $\approx 0.55 \text{ V}$, along with a reduction peak at $\approx 0.4 \text{ V}$. The observed mass changes as a function of the total charges passed during the cyclic voltammetric study reported in **Fig. 6.19B**, showed some mass retention per scan ($0.4 \mu\text{g}$). The oxidation involved an increase in current coupled with a small increase in mass ($\approx 0.1 \mu\text{g}$). During reduction, a decrease in current was coupled with an increase in mass ($\approx 0.3 \mu\text{g}$).

A mass retention of $0.4 \mu\text{g}$ per scan was observed, which represented $\approx 6\%$ of the total mass of the film. This increase over 3 scans (*i.e.* an increase of $1.2 \mu\text{g}$) represented $\approx 17\%$ of the total mass of the film.

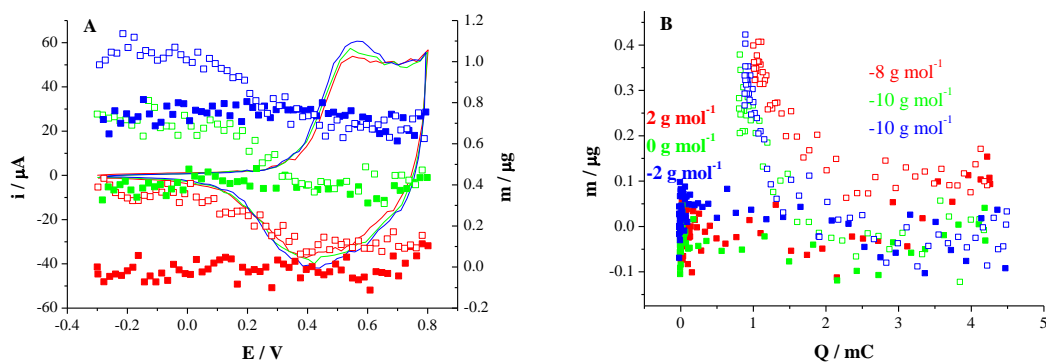


Fig. 6.19 - A) Cyclic voltammetric data and m vs. E **B)** m vs. Q for the redox cycling of PTP C in Ethaline at $40\text{ }^\circ\text{C}$ for 3 scans at 5 mV s^{-1} $-0.3 \leq E / \text{V} \leq 0.8$ (vs. Ag wire) with associated M_{app} (g mol^{-1}) doping = solid squares, undoping = outline squares (1st CV = red, 2nd = green, 3rd = blue).

PTP C was subjected to voltammetric studies at long and short timescales, achieved by varying the potential scan rate. The end-to-end molar mass exchanges (M_{app}) calculated for the doping and undoping regimes at the three different scan rates investigated were $-1, -2, -4 (\pm 2, 3, 2)\text{ g mol}^{-1}$ for doping and $-5, -8, -9 (\pm 6, 1, 1)\text{ g mol}^{-1}$. These M_{app} values were expressed as a combination of anion and cation transfers (5.4).

$$M_{app} = M_{anion} + \beta M_{cation} \quad (5.4)$$

The doping M_{app} fitted the ingress of $[2\text{EG.Cl}]^-$ and egress of $[\text{Ch}]^+$ with a value of β approximately -1.6 , in other words a molar ratio of $n[\text{Ch}]^+$ to $[2\text{EG.Cl}]^-$ of 1.6 . Upon undoping the ion transfers were reversed with the egress of $[2\text{EG.Cl}]^-$ and the ingress of $[\text{Ch}]^+$ with a value of β approximately -1.6 , in other words a molar ratio of $n[\text{Ch}]^+$ to $[2\text{EG.Cl}]^-$ of 1.6 .

The admittance spectra obtained over the three scans are reported in Fig. 6.20. This showed negligible variation in the admittance spectra over the three scans.

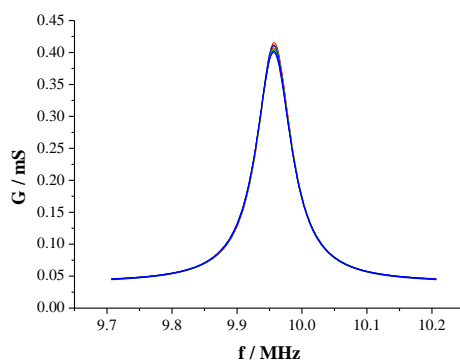


Fig. 6.20 - Admittance spectra for **PTP C** redox cycling only in Ethaline (shown in **Fig. 6.19**) (1st CV = red, 2nd = green, 3rd = blue). Admittance spectra recorded with a frequency span = 500 kHz.

PTP C1 (a PTP film deposited at 5 mV s^{-1}) was subjected to a long term switching experiment in neat Ethaline at $40 \text{ }^\circ\text{C}$ at 5 mV s^{-1} (no ZnCl_2 present), with the resultant CV reported in **Fig. 6.21A**. The $i(E)$ response shape and current passed was consistent with that observed for **PTP C** in Ethaline recorded at different scan rates above. An oxidation peak was observed at $\approx 0.55 \text{ V}$, along with a reduction peak at $\approx 0.45 \text{ V}$.

During oxidation an increase in current was coupled with a decrease in mass ($\approx 1 \text{ } \mu\text{g}$), which represented 14% of the total mass of the film. Whereas with undoping the reverse situation occurred, a decrease in current was coupled with an increase in mass ($\approx 0.8 \text{ } \mu\text{g}$). These processes were observed clearly with the individual m vs. Q plots presented in **Fig. 6.21B**.

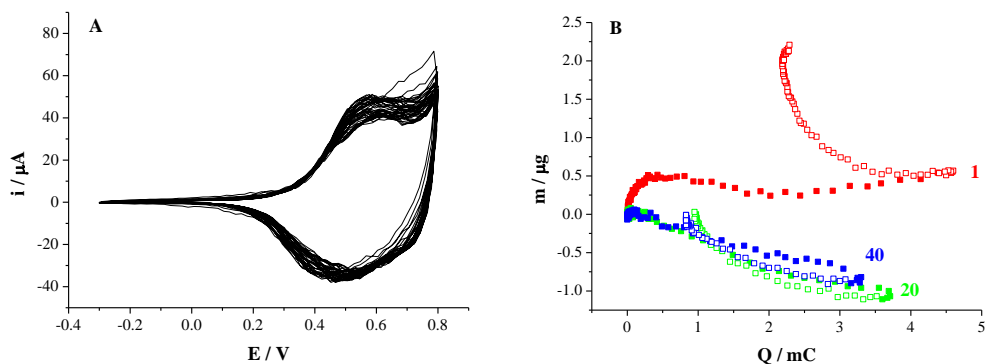


Fig. 6.21 - A) Cyclic voltammetric data **B)** m vs. Q for the redox cycling of **PTP C1** in Ethaline at 40 °C for 40 scans at 5 mV s^{-1} $-0.3 \leq E / \text{V} \leq 0.8$ (vs. Ag wire). Doping = solid squares, undoping = outline squares
1st CV (red), 20th CV (green) and 40th CV (blue).

The doping M_{app} remained fairly constant, except for the first 3 CVs. The average M_{app} over the remaining 37 scans, were determined for doping as $-29 \pm 3 \text{ g mol}^{-1}$ and $-44 \pm 4 \text{ g mol}^{-1}$ for undoping. These M_{app} values were expressed as a combination of anion and cation transfers (5.4).

$$M_{app} = M_{anion} + \beta M_{cation} \quad (5.4)$$

The determined M_{app} values related to β values for doping and undoping of approximately -1.8 and -2 respectively. Doping M_{app} of PTP in Ethaline indicated the entry of the anion $[2\text{EG.Cl}]^-$ and the expulsion of the cation $[\text{Ch}]^+$ ($\approx 1.8 [\text{Ch}]^+$ expelled per $[2\text{EG.Cl}]^-$ entry), *i.e.* a value of β of -1.8. The undoping M_{app} indicated a reverse of the anion and cation transfers observed during doping, with the expulsion of the anion $[2\text{EG.Cl}]^-$ from the film to maintain electro-neutrality and the entry of the cation $[\text{Ch}]^+$ ($\approx 2 [\text{Ch}]^+$ entering per $[2\text{EG.Cl}]^-$ expelled).

The admittance spectra obtained over the forty scans for **PTP C1** in this electrolyte are reported in **Fig. 6.22**. The Q-factor only varied a small amount during redox cycling

(199 to 179) therefore the Sauerbrey equation could be applied to determine mass charge transfers.

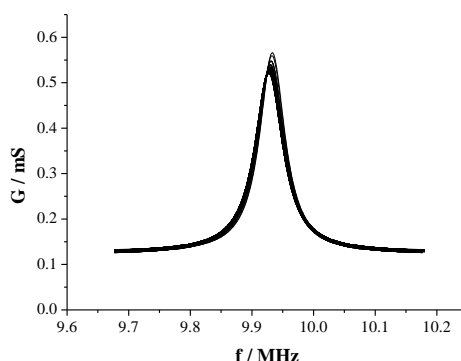


Fig. 6.22 - Admittance spectra for **PTP C1** redox cycling only in Ethaline (shown in **Fig. 6.21**). Admittance spectra recorded with a frequency span = 500 kHz.

PTP CA (a film deposited at a faster scan rate of 20 mV s^{-1}) was subjected to a long term redox switching experiment in Ethaline at $40 \text{ }^\circ\text{C}$ at 5 mV s^{-1} , with the resultant CV reported in **Fig. 6.23A**.

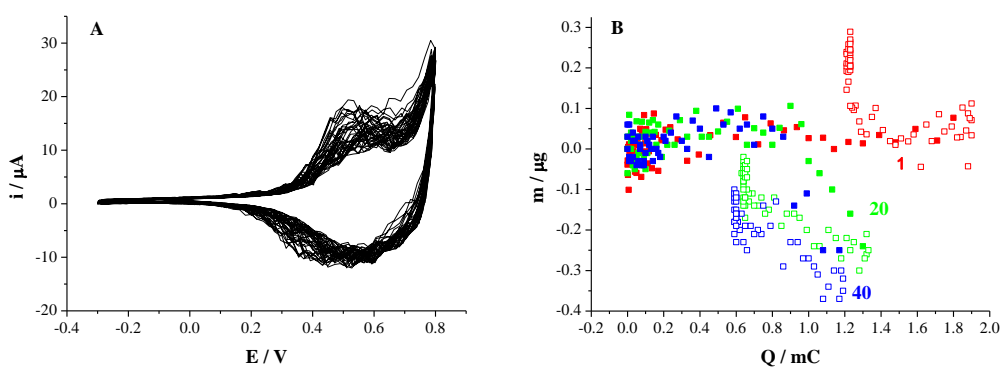


Fig. 6.23 - **A**) Cyclic voltammetric data **B**) m vs. Q for the redox cycling of **PTP CA** in Ethaline at $40 \text{ }^\circ\text{C}$ for 40 scans at 5 mV s^{-1} $-0.3 \leq E / \text{V} \leq 0.8$ (vs. Ag wire). Doping = solid squares, undoping = outline squares 1st CV (red), 20th CV (green) and 40th CV (blue).

For both the doping and undoping regimes, single sloped processes were observed for each scan. The single doping and undoping regimes can be seen clearly by focusing on the 1st, 20th and 40th CV m vs. Q plots, depicted in **Fig. 6.23B**. The first two scans differed slightly therefore the average M_{app} over the remaining 38 scans, were

determined for doping as $-4 \pm 2 \text{ g mol}^{-1}$ and $-23 \pm 6 \text{ g mol}^{-1}$ for undoping. These M_{app} values were expressed as a combination of anion and cation transfers (5.4).

$$M_{app} = M_{anion} + \beta M_{cation} \quad (5.4)$$

The determined M_{app} values related to β values for doping and undoping of approximately -1.6 and -1.8 respectively. Doping M_{app} of PTP in Ethaline indicated the entry of the anion $[2\text{EG.Cl}]^-$ and the expulsion of the cation $[\text{Ch}]^+$ ($\approx 1.6 [\text{Ch}]^+$ expelled per $[2\text{EG.Cl}]^-$ entry), *i.e.* a value of β of -1.6. The undoping M_{app} indicated a reverse of the anion and cation transfers observed during doping, with the expulsion of the anion $[2\text{EG.Cl}]^-$ from the film to maintain electro-neutrality and the entry of the cation $[\text{Ch}]^+$ ($\approx 1.8 [\text{Ch}]^+$ entering per $[2\text{EG.Cl}]^-$ expelled).

The admittance spectra obtained over the forty scans for **PTP CA** in Ethaline are reported in **Fig. 6.24**. The Q-factor did not change during the cyclic voltammetric study; therefore the Sauerbrey Equation could be applied to determine mass charge transfers of the polymer.

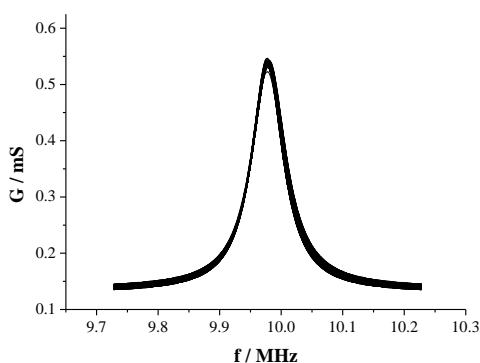


Fig. 6.24 - Admittance spectra for **PTP CA** redox cycling only in Ethaline (shown in **Fig. 6.23**). Admittance spectra recorded with a frequency span = 500 kHz.

6.2.4 Behaviour in Ethaline containing 0.3 M ZnCl₂

PTP C2 was subjected to a long term redox switching experiment in the Type III DES Ethaline containing 0.3 M ZnCl₂ at 40 °C at 5 mV s⁻¹, with the resultant CV reported in **Fig. 6.25A**. This electrolyte system was investigated as this would mimic the use of a Type III based DES in a battery device, which would require the presence of zinc in the DES. Some hysteresis was observed in the $i(E)$ response, with a decrease in current at the anodic potential limit over the first ≈ 20 scans, and then an increase. An oxidation peak was observed at ≈ 0.5 V along with a reduction peak at ≈ 0.45 V. The CV shape and current passed during redox switching in neat Ethaline (**PTP C**) was similar to the response in Ethaline containing ZnCl₂ (**PTP C2**). The CV shape remained consistent over the forty CVs.

The oxidation involved an increase in current coupled with a decrease in mass (≈ 0.8 μg), which represented 16% of the total mass of the film. During reduction the reverse situation occurred, with a decrease in current coupled with an increase in mass (≈ 0.7 μg), observed in the individual m vs. Q plots presented in **Fig. 6.25B**.

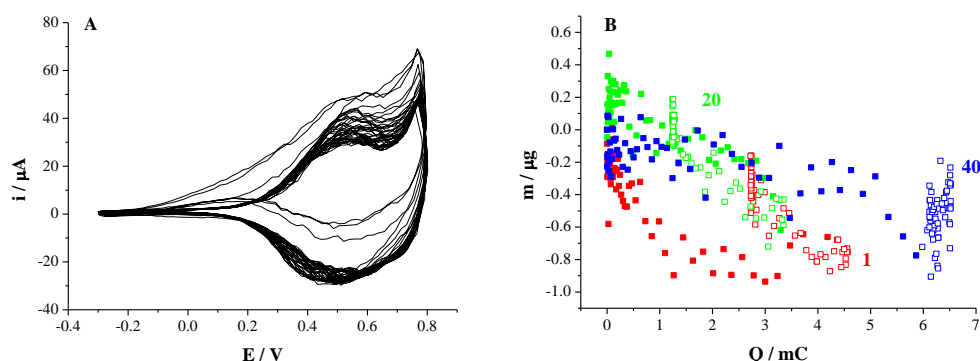


Fig. 6.25 - A) Cyclic voltammetric data **B)** m vs. Q for the redox cycling of **PTP C2** in 0.3 M ZnCl₂ in Ethaline at 40 °C for 40 scans at 5 mV s⁻¹ -0.3 $\leq E / V \leq 0.8$ (vs. Ag wire). Doping = solid squares, undoping = outline squares 1st CV (red), 20th CV (green) and 40th CV (blue).

The doping M_{app} remained constant over the 40 scans, producing an average over the forty scans of $-16 \pm 3 \text{ g mol}^{-1}$. The undoping M_{app} remained constant between scans 1 – 37, with the final three scans being significantly different. This could be attributed to loss of contact between the crystal and the external circuitry. The average undoping M_{app} over only the first 37 scans, gave an average M_{app} of $-25 \pm 3 \text{ g mol}^{-1}$. These M_{app} values were expressed as a combination of anion and cation transfers (5.4).

$$M_{app} = M_{anion} + \beta M_{cation} \quad (5.4)$$

The determined M_{app} values related to β values for doping and undoping of approximately -1.7 and -1.8 respectively. Doping M_{app} of PTP in Ethaline indicated the entry of the anion $[2\text{EG.Cl}]^-$ and the expulsion of the cation $[\text{Ch}]^+$ ($\approx 1.7 [\text{Ch}]^+$ expelled per $[2\text{EG.Cl}]^-$ entry), *i.e.* a value of β of -1.7. The undoping M_{app} indicated a reverse of the anion and cation transfers observed during doping, with the expulsion of the anion $[2\text{EG.Cl}]^-$ from the film to maintain electro-neutrality and the entry of the cation $[\text{Ch}]^+$ ($\approx 1.8 [\text{Ch}]^+$ entering per $[2\text{EG.Cl}]^-$ expelled).

As the shape of the $i(E)$ response of PTP in Ethaline containing 0.3 M ZnCl_2 was the same as the response in neat Ethaline, this inferred the identities of the mobile species were the same in this electrolyte. Also, as the concentration of ZnCl_2 was so small in comparison to the anion $[2\text{EG.Cl}]^-$ and cation $[\text{Ch}]^+$ it was not possible for the anion $[\text{ZnCl}_4]^{2-}$ to be involved in satisfying electro-neutrality.

The doping and undoping remained constant and were reversible, except for the change in response for undoping in the final 3 CVs. Consequently, the current for the final 3 CVs exhibited hysteresis, with a gradual increase in anodic current (perhaps due to partial detachment from the Au substrate).

The admittance spectra obtained over the forty scans for **PTP C2** in this electrolyte are reported in **Fig. 6.26**. The Q-factor only increased by 1 during the cyclic voltammetric study, allowing charge driven mass transfers to be calculated using the Sauerbrey equation.

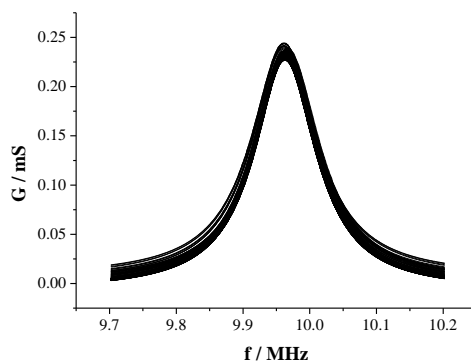


Fig. 6.26 - Admittance spectra of **PTP C2** redox cycling only in 0.3 M ZnCl_2 in Ethaline (shown in **Fig. 6.25**). Admittance spectra recorded with a frequency span = 500 kHz.

6.3 Conclusions

In these studies ion transfers during the p-doping (undoping) of PTP in DES media and a molecular solvent system were explored in terms of the individual anion and cation contributions to the gravimetric data. Experiments showed a clear difference in the maintenance of the electro-neutrality conditions in DES media compared to a molecular solvent. PTP film ion dynamics varied with DES composition, however did not significantly vary with experimental timescale (changing the scan rate) and prolonged exposure to redox switching. This is in contrast to PEDOT which did vary with timescale and exposure time.

The electro-neutrality condition of PTP in 0.1 M LiClO_4 / MeCN was satisfied by contributions of anion $[\text{ClO}_4]^-$ transfers (40% contribution to molar mass exchange) and solvent (MeCN) transfers (60% contribution to molar mass exchange) for all scan rates

5 mV s⁻¹, 10 mV s⁻¹ and 20 mV s⁻¹; with anion ingress and solvent egress occurring during doping and transfers reversed during undoping (anion egress and solvent ingress).

Gravimetric data obtained for the Type IV DES (apparent molar mass exchanges M_{app}) were fitted to anion $[\text{ZnCl}_4]^{2-}$ and neutral molecule (EG) transfers. The transfers here were similar to that observed in a molecular solvent in regards to the dominance of solvent transfer (in this case, ethylene glycol). During p-doping anion ingress and neutral molecule egress occurred with neutral molecule ingress contributing to 60% of the molar mass exchange. Transfers were reversed during undoping with anion $[\text{ZnCl}_4]^{2-}$ egress and ethylene glycol ingress, with neutral molecule dominance as well during undoping (60% contribution).

In contrast, PTP behaviour in the Type III DES resulted from transfers of anions and cations. In Ethaline it was observed that cation transfers dominated in the maintenance of electro-neutrality of PTP. Gravimetric data showed that during doping cations $[\text{Ch}]^+$ egress and anion ingress $[\text{2EG.Cl}]^-$ occurred, whereas during undoping these transfers were reversed. Cation $[\text{Ch}]^+$ transfers dominated the maintenance of electro-neutrality of PTP in Ethaline contributing to 60% of the molar mass exchange, with $[\text{2EG.Cl}]^-$ contributing to 40% for both doping and undoping. This is in contrast to the dominance of solvent transfers in acetonitrile solution and the Type IV DES. This arises due to mobility constraints, in that larger anions are less mobile and less readily accommodated for in the matrix of the polymer.

These studies described nanogravimetric acoustic wave (EQCM) studies of redox driven ion transfers for PTP films exposed to two DES formulations involving choline chloride (ChCl) as the QAS, ethylene glycol (EG) as the HBD and ZnCl_2 as the metal salt. Viscosity effects associated with the DES were significant but, via acoustic admittance measurements, one can obtain film ion population change data. These are presented as a function of timescale (potential scan rate in a voltammetric experiment) for potentiodynamically grown PTP films subsequently exposed to ZnCl_2 / EG, Ethaline and 0.3 M ZnCl_2 in Ethaline (where Ethaline is a 1:2 stoichiometric mixture of ChCl and EG). Significantly, for thicker films (consistent with practical applications), there was incomplete charge recovery at faster scan rates, with accompanying failure to restore the initial film ion composition. The failure to restore the initial film ion composition and drifts in gravimetrically determined masses were suggested to arise due to increasing electro-activities of the polymers. In terms of the suitability of the PTP system in a battery device, the mass charge transfers of PTP did not significantly vary with experimental timescale (changing the scan rate) and prolonged exposure to redox switching. This along with the high mass specific capacitance and stability is advantageous for a membrane in an electrochemical device.

6.4 References

- [1] Bund A and Neudeck S, *J. Phys. Chem. B*, 2004, 108, 46, 17845-17850
- [2] Skotheim TA and Reynolds JR, *Handbook of Conducting Polymers*, 2007, CRC Press, USA 3rd Edn
- [3] Trofimov BA, Mikhaleva AI, Nesterenko RN, Vasil'ev AN, Nakhmanovich AS and Voronkov MG, *Chem. Hetero. Comp.*, 1977, 13, 8, 920 (Translated from *Khim. Geterotsikl. Soedin.*, 1977, 8, 1136-1137)
- [4] Trofimov BA, Korostova SE, Mikhaleva AI, Sobenina LN, Vasil'ev AN and Nesterenko RN, *Chem. Hetero. Comp.*, 1983, 19, 2, 227 (Translated from *Khim. Geterotsikl. Soedin.*, 1983, 2, 273)
- [5] Engel N and Steglich W, *Angew. Chem.*, 1978, 17, 9, 676
- [6] Naitoh S, Sanui K and Ogata N, *J. Chem. Soc. Chem. Commun.*, 1986, 17, 1348-1350
- [7] Pozo-Gonzalo C, Pomposo JA, Alduncin JA, Salsamendi M, Mikhaleva AI, Krivdin LB and Trofimov BA, *Electrochimica Acta*, 2007, 52, 14, 4784-4791
- [8] Pozo-Gonzalo C, Salsamendi M, Pomposo JA, Grande HJ, Schmidt EY, Rusakov YY and Trofimov BA, *Macromolecules*, 2008, 41, 19, 6886-6894
- [9] Ping Z and Nauer GE, *Synthetic Metals*, 1997, 84, 1-3, 577-578
- [10] Ping Z, Federspiel P, Grünberger A and Nauer GE, *Synthetic Metals*, 1997, 84, 1-3, 837-838
- [11] Ping Z and Nauer GE, *Synthetic Metals*, 1997, 84, 1-3, 843-844
- [12] Cordruwisch E, Popkirov GS, Türk E, Theiner J and Nauer GE, *Electrochimica Acta*, 1996, 41, 7-8, 1369-1374
- [13] Hillman AR, *J. Solid State Electrochem.*, 2011, 15, 7-8, 1647-1660

Chapter 7

XPS of Conducting Polymer Films

7.1 Introduction

7.1.1 Objectives

7.1.2 Experimental

7.2 Elemental Composition of PEDOT Films

7.2.1 Pristine PEDOT Film

7.2.2 PEDOT Redox Behaviour in LiClO₄ / MeCN

7.2.3 PEDOT Redox Behaviour in Ethaline (Type III) DES

7.2.4 PEDOT Redox Behaviour in ZnCl₂ / EG (Type IV) DES

7.3 Elemental composition of PTP Films

7.3.1 Pristine PTP Film

7.3.2 PTP Redox Behaviour in LiClO₄ / MeCN

7.3.3 PTP Redox Behaviour in Ethaline (Type III) DES

7.3.4 PTP Film XPS Sulphur: Nitrogen Ratios

7.4 Summary of XPS Data

7.4.1 PEDOT Films

7.4.2 PTP Films

7.5 Conclusions

7.6 References

Chapter 7

XPS of Conducting Polymer Films

7.1 Introduction

7.1.1 Objectives

Charge driven mass transport processes are essential for the functioning of a conducting polymer as a battery electrode. Therefore, it is of interest to explore the anion / cation movements between a polymer in differently charged states and an electrolyte. This can help with understanding the performance of a polymer in an electrochemical device.

Research activities were focussed on understanding the chemical nature of conducting polymers exposed to DESs (high ionic strength media). The elemental composition of conducting polymer films was investigated using X-Ray Photo-electron Spectroscopy. This surface technique was used to detect the presence of dopant ions in polymer films oxidised (p-doped) and reduced (undoped) in a conventional molecular solvent, acetonitrile and DESs. The chemistries of the ‘as prepared’ polymers were also investigated *i.e.* films prior to exposure to monomer free electrolyte, termed hereafter as pristine samples. Conducting polymer films were produced from heterocyclic monomers EDOT **1** and TP **3**. Films were exposed to either a conventional molecular solvent, acetonitrile containing LiClO₄, a Type III DES Ethaline or a Type IV DES ZnCl₂ / EG.

Experiments examined the elemental composition (atomic percentages) of the surface of the polymer electrode *i.e.* the polymer-electrolyte interface, as well as examining the polymer-Au interface. The latter was achieved by removal of the polymers from Au

coated glass substrates. Investigating this interface explored whether dopant ions were able to diffuse through the matrix of the polymer. If no dopant ions were present this may suggest that bulky ions were unable to enter the polymer; ions do not diffuse that far into the polymer, or the polymer is thick. This would reduce the degree of oxidation or reduction of the polymer which would affect the charge storage capability of the polymer. Therefore, it needs to be considered whether a thinner polymer may be required in order to function effectively as a charge storage membrane.

Ruffo *et al.* ^[1] investigated the elemental analysis of chemically prepared PEDOT films (using iron (III) tosylate) and the identity of ion species present after redox switching in a monomer free electrolyte, LiClO₄ in propylene carbonate. From high resolution experiments, atomic percentages were determined at photo-electron binding energies for specific element orbital electrons, Cl (2p), S (2p) and Fe (2p_{3/2}). The ratio of the atomic percentages of Cl (2p) and S (2p) peaks indicated the doping level of the polymer. The results confirmed the ingress and egress of [ClO₄]⁻ anions upon oxidation and reduction respectively. In the oxidised PEDOT film the ratio of the atomic percentages of Cl (2p) *vs.* S (2p) indicated 1 [ClO₄]⁻ anion per 5 EDOT units. In the reduced film not all the [ClO₄]⁻ was expelled but significantly reduced to 1 [ClO₄]⁻ per 41 EDOT units.

Bach and Reynolds ^[2] studied the surface chemistry of poly-3-methylthiophene (P3MeT) films and compared dopant exchange behaviour of P3MeT redox cycled in TBAClO₄ and TBAREO₄, both in MeCN. In both cases, as well as during polymerisation of P3MeT (TBABF₄ / MeCN), anion exchanges occurred but no cation exchanges [TBA]⁺ did. The authors attempted depth profiling to determine the dopant anion exchanges throughout the thickness of the film. Unfortunately, Cl and F peaks

were removed when sputtered with an Ar ion beam (at 4 kV) which made depth profiling unsuitable for investigating the TBAClO₄ system. The authors allude that the lack of Cl and F peaks occurred due to the formation of gaseous molecules BF₃ and ClO₂ as a consequence of Ar ion bombardment. They highlighted that depth profiling should not be used if the researchers' aim is to collect chemical bond data, as sputtering can alter the structure of the polymeric material. Therefore, depth profiling using the Ar ion beam was unsuitable for the samples prepared.

Pandey ^[3] ^[4] investigated the elemental composition of PEDOT by XPS. The survey spectrum showed strong C (1s), O (1s) and S (2p) signals corresponding to the molecular structure of PEDOT. Evidence of dopant ion [ClO₄]⁻ presence was given by the Cl (2p) peak. The range of binding energies observed suggested that the positive charges were not localised on each monomer unit but spread over several units. A binding energy of 209 eV was characteristic of [ClO₄]⁻ anions, lower energies were attributed to [ClO₃]⁻. S (2p) peaks were attributed to S atoms of the thiophene ring systems in the PEDOT structure. Higher energy tails on the S (2p) peaks indicated a different charge state of PEDOT. The shift in binding energies of the S (2p) peaks to higher energies were attributed to the p-doping of the polymer and the [ClO₄]⁻ anions associated with the positively charged sulphur.

Energy Dispersive Analysis by X-Rays (EDAX), a technique generally used in situ with a Scanning Electron Microscope (SEM) was not applicable for investigating the surface composition of polymer films. This was due to the depth of analysis being much greater for the EDAX technique, on the order of approximately several microns, compared to XPS, which probes to depths of 10 nm into the film; approximately 5 – 20 atomic layers

of the surface. If the polymer samples prepared were subjected to EDAX analysis, the depth probed would be much greater than the thickness of the film. This was confirmed with the EDAX analysis of a pristine PTP film (**Chapter 7.3.1**), which produced spectra dominated by signals from the Au substrate.

7.1.2 Experimental

Survey scans of polymer samples were initially conducted to enable the rapid identification of possible chemical components. These scans were wide ranging, low resolution scans of binding energy which incorporated all visible photo-electric events. After survey scans were complete successive high resolution scans were conducted over narrower binding energy ranges for specific elemental orbital regions. The quantitative data (atomic percentages from peak areas) allowed the determination of the sulphur to nitrogen ratio (S : N ratio) of the polymer films produced from the monomer precursor, TP 3.

Atomic percentages were calculated from the peak areas (for oxygen, carbon, fluorine, boron, nitrogen, sulphur, chlorine and zinc) and relative sensitivity factors (r.s.f.) using equation (7.1), with the element of focus as the numerator, over the total sum of the area of each elemental peak present divided by the relevant r.s.f. for the element.

$$\text{at}\% = \frac{(\text{area}/\text{r.s.f.})}{\Sigma(\text{area}/\text{r.s.f.})} \times 100 \quad (7.1)$$

PEDOT 1 and PTP 3 were electrodeposited potentiodynamically in acetonitrile containing 0.1 M monomer and 0.1 M LiBF₄. Films were then exposed to either 0.1 M LiClO₄ / MeCN, Ethaline or ZnCl₂ / EG to produce oxidised and reduced samples

by conducting cyclic voltammetry. Different lithium salts were used (LiBF_4 for deposition and LiClO_4 for redox switching) to be able to distinguish between growth anions and redox switching anions in the acquired spectra.

Both linear and Shirley backgrounds were used on the XPS data to enable comparison of the atomic concentrations determined from the application of different backgrounds. Generally, the baseline does not change over the binding energy range for materials with large band gaps, for example conducting polymers ^{[5] [6] [7] [8]}. Therefore, a linear background can normally be applied to these materials. As a check, Shirley backgrounds were also applied to the data in this thesis. A Shirley background is utilised to account for changes in the baseline for the data over the energy peak range and changes in peak shape from a standard Gaussian peak. However, dependent on the peak shape, the Shirley background may unintentionally omit part of the area of a peak; therefore quantitative analyses were focussed on the atomic percentages found by linear background application. Larger carbon atomic percentages, *i.e.* percentages which deviate from theoretical values are commonly observed in XPS and can be related to trace amounts of hydrocarbon impurities on the surface of the polymer ^[2].

For details on sample preparation and experimental parameters see Experimental Section (**Chapter 3**).

7.2 Elemental Composition of PEDOT Films

7.2.1 Pristine PEDOT Film

A survey scan of the ‘as prepared’ PEDOT film referred to as a pristine sample (grown in 0.1 M LiBF₄ / MeCN) presented in **Fig. 7.1**, confirmed the deposition of PEDOT from the appearance of O (1s), C (1s) and S (2p_{3/2}) peaks at binding energies 533.1 eV, 286.3 eV and 163.65 eV respectively. Not all [BF₄]⁻ growth counter ions were removed from the film as evidenced by B (1s) (193.4 eV) and F (1s) (685.25 eV) peaks. It was possible to determine elemental ratios from atomic percentages acquired by high resolution experiments (see **Table 7.1**). Based on the structure of PEDOT, the ratio of atomic percentages for C (1s), O (1s) and S (2p) was 6 : 2 : 1 respectively. The experimental ratio of atomic percentages (52% : 17% : 11%) for the pristine PEDOT was close to expected at 5 : 2 : 1, confirming the deposition of PEDOT.

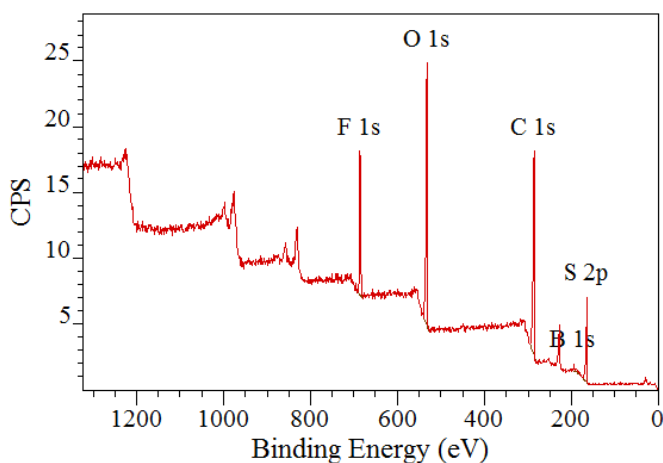


Fig. 7.1 - XPS survey spectrum for the pristine PEDOT film (grown potentiodynamically in 0.1 M LiBF₄ / MeCN at RT for 10 scans at 20 mV s⁻¹ between -0.3 ≤ E / V ≤ 1.1 (vs. Ag wire)).

The high resolution C (1s) peak was deconvoluted into four main peaks and a shake up peak. C (1s) contains four peaks 284.633 eV, 285.445 eV, 286.266 eV, 286.813 eV, 289.374 eV (5.371%, 3.4%, 14.82%, 19.79%, 6.652%) attributed to C-C/C-H, C-S, C=C-O and C-O-C ^{[41][9]}.

The S peak was split into S ($2p_{3/2}$) (163.611 eV, 14.5%) and S ($2p_{1/2}$) (164.732 eV, 17.59%) doublet with a split in binding energy of ≈ 1.1 eV consistent with the split observed in the literature for C-S-C in PEDOT ^[4]. The high binding energy tail at 165.909 eV (17.82%) suggested that the pristine film was in a partially oxidised state, as this peak has been reported to be due to positively charged sulphur. This is consistent with the presence of B (1s) and F (1s) peaks for the counter ion $[\text{BF}_4]^-$ which is required to maintain electro-neutrality of the film during p-doping ^{[4][9]}.

Further PEDOT films were prepared using 0.1 M LiBF_4 / MeCN and exposed to either 0.1 M LiClO_4 / MeCN, Ethaline or ZnCl_2 / EG for cyclic voltammetric experiments. Experiments were stopped at either the anodic or cathodic potential limit to produce PEDOT in an oxidised or reduced state respectively. This was conducted during the 11th cycle to ensure the counter ions migrated into the polymer matrix. Attempts were made to remove the polymer from the Au substrate to expose the polymer-Au interface, termed as reverse side polymer films in this thesis. The reverse side PEDOT film XPS analyses are reported in **Table 7.1**. The binding energies for the elements present for each PEDOT sample and the film masses (determined using the deposition charges (coulometric assays) are reported in **Table 7.2**. **Table 7.3** shows the ratio of C (1s) : O (1s) : S (2p) of the PEDOT samples, confirming whether PEDOT films deposited, the ratios of atomic percentages for C (1s), O (1s) and S (2p) for PEDOT deposition should be 6 : 2 : 1 respectively. Data in **Table 7.3** highlights whether there was an increase in carbon and / or oxygen in the film, arising from ion diffusion into the polymer.

Table 7.1 - PEDOT XPS atomic percentages.

PEDOT	O 1s		C 1s		F 1s		B 1s		N 1s		S 2p		Cl 1s		Zn 2p	
	L	S	L	S	L	S	L	S	L	S	L	S	L	S	L	S
Pristine (Grown in LiBF ₄)	17.15	17.52	52.41	51.49	17.84	18.08	1.917	2.345	x	x	10.68	10.57	x	x	x	x
LiBF ₄ Oxidised	13.84	13.84	59.42	58.46	x	x	4.306	5.016	1.112	1.14	1.302	1.308	20.02	20.24	x	x
LiBF ₄ Oxidised Reverse	x	x	61.64	62.37	38.36	37.63	x	x	x	x	x	x	x	x	x	x
LiBF ₄ Reduced	15.04	15.55	42.58	42.08	24.66	25.12	9.414	9.028	x	x	8.302	8.219	x	x	x	x
Ethaline Oxidised	15.27	15.26	63.32	62.97	x	x	x	x	5.619	5.701	5.542	5.606	10.25	10.46	x	x
Ethaline Oxidised (repeat)	13.17	13.32	63.62	63.35	x	x	x	x	7.933	7.979	1.559	1.568	13.71	13.78	x	x
Ethaline Oxidised Reverse	15.87	15.71	51.79	49.76	x	x	19.93	22.42	1.823	1.828	7.022	6.756	3.56	3.529	x	x
Ethaline Reduced	20.35	20.72	64.9	64.46	x	x	x	x	x	x	11.57	11.58	3.174	3.234	x	x
Ethaline Reduced Reverse	58.83	58.27	41.17	41.73	x	x	x	x	x	x	x	x	x	x	x	x
ZnCl ₂ / EG Oxidised	11.4	11.4	24.6	24.09	4.339	4.353	53.73	54.6	0.373	0.3491	0.3574	0.3367	0.8053	0.7933	4.395	4.079
ZnCl ₂ / EG Oxidised Reverse	x	x	41.07	39.43	44.83	43.66	3.22	3.176	7.02	9.923	3.854	3.814	x	x	x	x

Table 7.2 - PEDOT XPS binding energies and PEDOT film masses. Reverse refers to the polymer-Au interface side of the polymer film.

PEDOT	Binding Energy / eV								mass / mg	mass / mg (Peff = 75%)
	O (1s)	C (1s)	F (1s)	B (1s)	N (1s)	S (2p)	Cl	Zn (2p)		
Pristine (Grown in LiBF ₄ / MeCN)	533.1	286.3	685.25	193.4	x	163.65	x	x	6.482	4.862
LiClO₄ / MeCN Oxidised	533.8	285.5	x	198.05	400	164.1	285.55 Cl (2s)	x	2.121	1.591
LiClO₄ / MeCN Oxidised Reverse	x	282.1	682.85	x	x	x	x	x	2.121	1.591
LiClO₄ / MeCN Reduced	533.05	286.2	685.4	193.5	x	163.6	x	x	0.669	0.5018
Ethaline Oxidised	532.85	286.35	x	x	402.65	163.6	197.55 Cl (2p _{3/2})	x	3.562	2.672
Ethaline Oxidised (repeat)	532.6	286.25	x	x	402.6	163.7	197.5 Cl (2p _{3/2})	x	3.673	2.755
Ethaline Oxidised Reverse	533.2	286.35	x	197.2	402.5	163.8	197.25 Cl (2p _{3/2})	x	3.673	2.755
Ethaline Reduced	533.25	286.4	x	x	x	163.75	196.8 Cl (2p _{3/2})	x	0.6799	0.5099
Ethaline Reduced Reverse	529.4	285.7	x	x	x	x	x	x	2.777	2.083
ZnCl₂ / EG Oxidised	533.15	284.35	686.4	198.9	399.95	169.5	284.4 Cl (2s)	1022.8	6.405	4.809
ZnCl₂ / EG Oxidised Reverse	x	284.9	682	192.65	409	166.75	x	x	3.925	2.944

Table 7.3 - PEDOT XPS C (1s) : O (1s) : S (2p) ratios (calculated from the data in **Table 7.2**) Reverse refers to the polymer-Au interface side of the polymer film.

	C (1s) : O (1s) : S (2p)
PEDOT	ratio
Pristine (Grown in LiBF ₄ / MeCN)	5 : 2 : 1
LiClO ₄ Oxidised	46 : 11 : 1
LiClO ₄ Oxidised Reverse	-
LiClO ₄ Reduced	5 : 2 : 1
Ethaline Oxidised	11 : 3 : 1
Ethaline Oxidised (repeat)	41 : 8 : 1
Ethaline Oxidised Reverse	7 : 2 : 1
Ethaline Reduced	6 : 2 : 1
Ethaline Reduced Reverse	-
ZnCl ₂ / EG Oxidised	69 : 32 : 1
ZnCl ₂ / EG Oxidised Reverse	-

7.2.2 PEDOT Redox Behaviour in LiClO₄ / MeCN

The PEDOT films exposed to 0.1 M LiClO₄ / MeCN in an oxidised state exhibited O (1s) 533.8 eV (532.9 eV, 533.9 eV, 537.2 eV), C (1s) 285.5 eV (285.344 eV, 285.551 eV, 286.925 eV, 289.637 eV (12.52%, 16.42%, 11.03%, 9.746%) and S (2p_{3/2}) 164.1 eV (165.0 eV, 164.0 eV, a difference of 1.0 eV) peaks, the same as for the pristine PEDOT, which confirmed the polymer deposition. The S (2p) peak tails, at the higher binding energy end of the peak, indicated the positively charge sulphur in oxidised PEDOT. S (2p) peaks exhibited 2 peaks and a shake up peak (**Fig. 7.2**) at binding energies of 164.065 eV, 165.215 eV, 166.088 eV (16.75%, 15.86%, 17.24%). These correspond to S (2p_{3/2}), S (2p_{1/2}) for neutral S and a shake up peak (presumed to be due to S⁺), shown in **Fig. 7.2** with a high binding energy tail attributed to positively charge sulphur^{[9][10][11]}. It was also possible to deconvolute the S (2p) peak into 4 peaks 163.873 eV, 164.252 eV; 165.216 eV, 165.96 eV (7.552%, 8.784%, 15.38%, 18.18%) corresponding to S (2p_{3/2}), S (2p_{1/2}) for neutral S and S (2p_{3/2}), S (2p_{1/2}) for S⁺^[12].

This suggested that the doping level was 67% ($33.56 / 49.896 \times 100$) using the method reported by Taouli *et al.* [12].

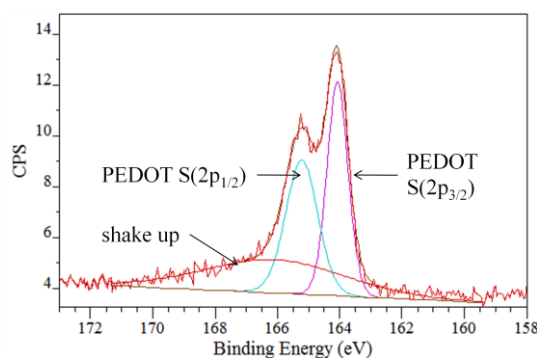


Fig. 7.2 - S (2p) peaks for PEDOT sample oxidised in 0.1 M LiClO₄ / MeCN.

The theoretical ratios of atomic percentages for C (1s), O (1s) and S (2p) for PEDOT deposition were 6 : 2 : 1 respectively. The ratio of atomic percentages for the reduced PEDOT in LiClO₄ / MeCN were closed to expected at 5 : 2 : 1 (43% : 15% : 8%) confirming the deposition of PEDOT (C (1s) 286.2 eV, O (1s) 533.05 eV, S (2p) 163.6 eV. However, considerably higher ratios of these peaks were determined at 46 : 11 : 1 for oxidised PEDOT (59.4% : 14% : 1.3%). The increase C (1s) atomic percentage for the oxidised film was initially assumed to be attributed to trapped MeCN in the oxidised film. However, this is unlikely in XPS due to the ultra high vacuum environment (10^{-9} mbar) and also the oxidised film should be the least solvated state and was sufficiently dried before experiments. The reason for an increase C (1s) atomic percentage is much more likely to be due to adsorbed material from the atmosphere. There is also a possibility that the ether linkages of the EDOT units are facing outwards (rather than the thiophene ring).

Gravimetric experiments (**Chapter 5**) suggested the ingress of [ClO₄]⁻ anions upon oxidation associated with the egress of solvent. The elevated O (1s) atomic percentage supports the hypothesis of [ClO₄]⁻ anion ingress into the polymer matrix.

The presence of Cl (1s) (285.5 eV) in the oxidised PEDOT also supported the findings from EQCM experiments that $[\text{ClO}_4]^-$ anions were the mobile species, which maintained electro-neutrality upon PEDOT oxidation in this electrolyte, acting as the dopant anions. The reduced PEDOT film did not exhibit any Cl peaks at 285 eV and had an O (1s) (533.05 eV) ratio the same as observed for the pristine film, which inferred that $[\text{ClO}_4]^-$ anions were expelled from the film upon reduction, consistent again with the findings from EQCM.

The reverse side oxidised PEDOT however did not show the presence of O (1s) expected at ≈ 534 eV or S ($2p_{3/2}$) ≈ 164 eV peaks in the HR experiments (possibly due to instrumental error). The reverse side spectra was noisy so was not analysed further.

7.2.3 PEDOT Redox Behaviour in Ethaline (Type III) DES

The PEDOT films exposed to Ethaline exhibited O (1s), C (1s) and S ($2p_{3/2}$) peaks, the same as for the pristine PEDOT, which confirmed the polymer deposition. The reverse side reduced PEDOT however did not show the presence of an S ($2p_{3/2}$) peak in the HR experiment (possibly due to instrumental error), however this was present in the survey spectrum.

The theoretical ratio of atomic percentages for C (1s), O (1s) and S ($2p_{3/2}$) for PEDOT deposition was 6 : 2 : 1 respectively. The experimental values for the reduced PEDOT in Ethaline were as expected at 6 : 2 : 1, confirming the deposition of PEDOT. However, for both the oxidised PEDOT films in this electrolyte, considerably higher ratios of these peaks were determined at 11 : 3 : 1 and 41 : 8 : 1 (for the repeat experiment) (see **Table 7.3**). The increase in the C (1s) and O (1s) peaks provides

evidence for the ingress of the $[2EG.Cl]^-$ upon oxidation, supporting the hypothesis which fitted the gravimetric data in **Chapter 5**. The experimental ratios for the oxidised PEDOT reverse side were 7 : 2 : 1, close to expected for a pristine film. This suggested that only a small amount of dopant anions, $[2EG.Cl]^-$, were able to penetrate to the polymer-Au interface.

All the PEDOT films oxidised in Ethaline showed the presence of Cl (1s) which also confirmed the presence of a Cl based anion upon p-doping. The oxidised reverse side showed the presence of Cl but with a lower atomic percentage than the oxidised film, which meant that lower amounts of $[2EG.Cl]^-$ penetrated to the polymer-Au interface.

The Ethaline reduced film did exhibit a Cl (1s) peak, which suggested that not all the dopant $[2EG.Cl]^-$ anions were expelled during undoping, with a small proportion remaining on the surface of the polymer even after successive rinses. However, the amount of Cl was much lower than observed for the oxidised PEDOT at the polymer-electrolyte interface, therefore, most of the dopant $[2EG.Cl]^-$ anions were expelled from the film during undoping. These results were consistent with the EQCM studies in the previous Chapter (**Chapter 5**).

The interpretation of gravimetric data from EQCM studies suggested a mixed ion exchange mechanism during p-doping and undoping in Ethaline. During oxidation (p-doping), as well as the ingress of $[2EG.Cl]^-$ anions, it was observed from M_{app} values that $[Ch]^+$ cations were also involved in satisfying the electro-neutrality condition, the egress of $[Ch]^+$ upon oxidation and ingress upon reduction. Therefore, N (1s) should not be present in the oxidised film but should be in the reverse film;

however the XPS results show the opposite of this. N (1s) is present in the oxidised films but not in the reduced films (see **Table 7.1**).

7.2.4 PEDOT Redox Behaviour in ZnCl₂ / EG (Type IV) DES

The oxidised PEDOT film exposed to the Type IV DES, ZnCl₂ / EG, exhibited O (1s), C (1s) and S (2p_{3/2}) peaks, the same shape and binding energy as for the pristine PEDOT, which confirmed the deposition of PEDOT. The presence of Zn (2p) and Cl (2s) in the oxidised film (**Fig. 7.3** red trace) suggested the involvement of zincate anion transfers during the p-doping of PEDOT. This confirmed the ingress of [ZnCl₄]²⁻ upon doping of PEDOT and supported by evidence from gravimetric data collected by EQCM studies. However, it was shown by the reverse side of an oxidised PEDOT film that the anion [ZnCl₄]²⁻ did not penetrate to the polymer-Au interface, shown clearly by the lack of a Zn peak (1022.8 eV) and negligible Cl peak (284.4 eV) in the survey spectra for the polymer-Au interface trace (**Fig. 7.3** brown trace).

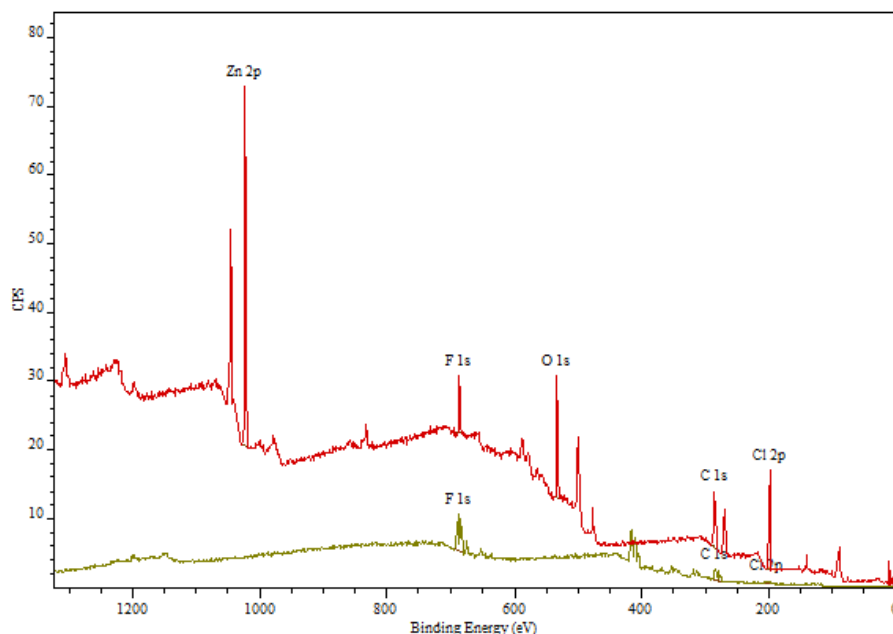


Fig. 7.3 - Survey spectra for PEDOT film after redox cycling in ZnCl₂ / EG in an oxidised state. Red trace = polymer-electrolyte interface, brown trace = polymer-Au electrode interface.

7.3 Elemental Composition of PTP Films

7.3.1 Pristine PTP Film

A survey scan of the as prepared pristine PTP film (grown in 0.1 M LiBF₄ / MeCN) presented in **Fig. 7.4** showed C (1s) 284.6 eV, N (1s) 399.85 eV and S (2p) 163.8 eV peaks. This suggested the deposition of PTP. A peak at 685.4 eV for F (1s) indicated that not all growth counter ions were removed from the film, even though the polymer was prepared in the reduced state and had been rinsed prior to XPS analysis. A B (1s) peak was observed for the pristine film, however gave a noisy high resolution spectrum which meant a binding energy could not be recorded.

The ratio of atomic percentages based on the structure of PTP for C (1s), S (2p) and N (1s) peaks for PTP deposition were 8 : 1 : 1 respectively. The experimental values for the pristine sample was above the expected value at 16 : 1 : 1 with peaks at binding energies 284.6 eV, 163.8 eV and 399.85 eV (75.88%, 6.337% and 4.701%) for C (1s), S (2p) and N (1s) peaks respectively. The deviation for the carbon atomic percentage could be related to hydrocarbon impurities on the surface of the polymer. It could be attributed to the orientation of polymer chains with alkene linkages orientated towards the x-ray beam. This was observed for P3MeT films in the literature ^[2]. The determined S : N ratio was as expected at a value of 1 : 1. **Table 7.4** shows atomic percentages determined by XPS of the PTP films studied. The binding energies for the elements present for each PTP sample and the film masses (determined using the deposition charges (coulometric assays) are reported in **Table 7.5**. **Table 7.6** shows the ratio of C (1s) : S (2p) : N (1s) of the PTP samples, confirming whether PTP films deposited, the ratios of atomic percentages for C (1s), S (2p) and N (1s) for PTP deposition should be 8 : 1 : 1 respectively.

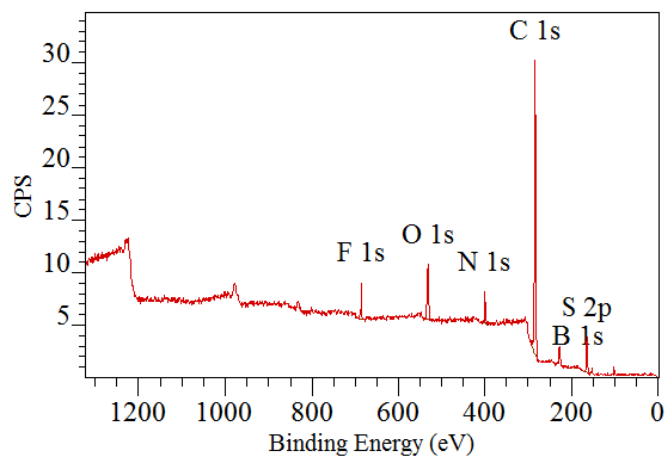


Fig. 7.4 - Survey spectra for the pristine PTP film, grown potentiodynamically in 0.1 M LiBF₄ / MeCN at RT for 10 scans at 20 mV s⁻¹ between -0.3 ≤ E / V ≤ 0.8 (vs. Ag wire).

Table 7.4 - PTP XPS atomic percentages.

PTP	O 1s		C 1s		F 1s		B 1s		N 1s		S 2p		Cl 1s	
	L	S	L	S	L	S	L	S	L	S	L	S	L	S
Pristine (Grown in LiBF ₄)	5.713	5.937	75.88	75.25	7.366	7.593	x	x	4.701	4.814	6.337	6.41	x	x
LiBF ₄ Reduced	3.83	3.978	50.68	48.46	29.69	31.3	3.306	3.517	5.544	5.647	6.952	7.098	x	x
LiBF ₄ Reduced (repeat)	6.188	6.383	51.2	49.85	26.9	28.03	3.703	3.688	5.284	5.225	6.728	6.827	x	x
LiBF ₄ Reduced Reverse	6.589	6.827	65.3	64.05	11.02	11.49	2.888	3.048	6.104	6.316	8.106	8.269	x	x
Ethaline Oxidised	8.57	8.757	62.93	62.25	6.403	6.518	x	x	8.731	8.88	4.477	4.488	8.893	9.105
Ethaline Oxidised Reverse	14.64	17.03	69.46	65.09	x	x	4.451	4.806	4.449	4.951	5.36	6.26	1.635	1.857
Ethaline Reduced	9.492	9.628	63.42	62.97	4.753	4.825	x	x	9.095	9.195	3.366	3.332	9.877	10.05
Ethaline Reduced Reverse	6.732	7.009	62.19	60.84	15.22	15.98	2.58	2.629	5.49	5.584	7.794	7.963	x	x

Table 7.5 - PTP XPS binding energies and PTP film masses. Reverse refers to the polymer-Au interface side of the polymer film.

PTP	Binding Energy / eV							mass / mg	mass / mg (Peff = 45%)
	O (1s)	C (1s)	F (1s)	B (1s)	N (1s)	S (2p)	Cl (2p)		
Pristine (Grown in LiBF₄ / MeCN)	532	284.6	685.4	x	399.85	163.8	x	0.814	0.3663
LiClO₄ / MeCN Reduced	531.8	284.5	685.45	193.7	399.75	163.7	x	1.693	0.7619
LiClO₄ / MeCN Reduced (repeat)	531.75	284.7	685.35	193.55	399.8	163.75	x	1.407	0.6332
LiClO₄ / MeCN Reduced Reverse	533	285.5	686.15	198.25	400.6	164.5	x	1.407	0.6332
Ethaline Oxidised	532.4	286.35	685.95	x	402.6	163.9	197.45	0.6466	0.2910
Ethaline Oxidised Reverse	538.4	290.45	x	202.95	404.65	168.9	203.3	0.6466	0.2910
Ethaline Reduced	532.7	286.55	686.1	x	402.65	164.1	197.6	1.064	0.4788
Ethaline Reduced Reverse	533.4	285.7	686.2	190.3	400.7	165.8	x	1.064	0.4788

Table 7.6 - PTP XPS C (1s) : S (2p) : N (1s) ratio. Reverse refers to the polymer-Au interface side of the polymer film.

PTP	C (1s) : S (2p) : N (1s)
	ratio
Pristine (Grown in LiBF₄ / MeCN)	16 : 1 : 1
LiClO₄ / MeCN Reduced	9 : 1 : 1
LiClO₄ / MeCN Reduced (repeat)	10 : 1 : 1
LiClO₄ / MeCN Reduced Reverse	11 : 1 : 1
Ethaline Oxidised	14 : 1 : 2
Ethaline Oxidised Reverse	16 : 1 : 1
Ethaline Reduced	19 : 1 : 3
Ethaline Reduced Reverse	11 : 1 : 1

7.3.2 PTP Redox Behaviour in LiClO₄ / MeCN

The PTP films which were reduced in LiClO₄ / MeCN exhibited C (1s), N (1s) and S (2p_{3/2}) peaks. Also in the HR experiments, B (1s) and F (1s) peaks were also observed which indicated that not all growth counter ions were removed from the film after redox cycling in a different supporting electrolyte, LiClO₄ / MeCN. This may be because the film has small pores which trapped some of the growth anions, so therefore the polymer may have been in a partially converted redox state (not fully reduced).

The theoretical ratio of atomic percentages for C (1s), S (2p_{3/2}) and N (1s) peaks for PTP deposition was 8 : 1 : 1. The experimental values for the reduced PTP film, repeat reduced PTP film and reverse side reduced PTP film were close to the expected values at values of 9 : 1 : 1, 10 : 1 : 1 and 11 : 1 : 1 respectively (see **Table 7.6**). The S : N ratio of 1 : 1 meant that no dissociation of the thiophene and pyrrole rings occurred during redox switching in monomer free electrolyte (after polymer deposition).

The lack of Cl peaks in the HR experiments for all three reduced films reinforced the findings from EQCM studies that [ClO₄]⁻ anions were expelled upon reduction of the film in 0.1 M LiClO₄ / MeCN.

7.3.3 PTP Redox Behaviour in Ethaline (Type III) DES

The PTP films exposed to Ethaline all exhibited C (1s), N (1s) and S (2p_{3/2}) peaks which confirmed the deposition of PTP films. As mentioned above, the ratio of atomic percentages for C (1s), S (2p_{3/2}) and N (1s) peaks based on the structure of PTP was 8 : 1 : 1. The experimental value for the reverse side reduced film was close to expected, at 11 : 1 : 1 (see **Table 7.6**). This supported the hypothesis made from EQCM studies

that $[2\text{EG.Cl}]^-$ anion were expelled upon reduction otherwise a higher C (1s) ratio would be observed. It could also suggest that the $[2\text{EG.Cl}]^-$ were unable to penetrate the polymer matrix (*i.e.* they were never there). The experimental values for the oxidised film, reverse side oxidised film and reduced film deviated from the theoretical ratio for C (1s), S ($2p_{3/2}$) and N (1s) peaks of 8 : 1 : 1 for a pristine film, as reported in **Table 7.6**.

Elevated amounts of C (1s) and N (1s) were observed for the oxidised PTP film, which supported the mobile species hypotheses made to fit the gravimetric data from EQCM studies (**Chapter 6**); the ingress of $[2\text{EG.Cl}]^-$ and the expulsion of $[\text{Ch}]^+$. However, the slightly elevated amount of N (1s) showed that not all the $[\text{Ch}]^+$ cations were expelled upon oxidation. The presence of Cl (1s) also agreed with the hypothesis of the ingress of $[2\text{EG.Cl}]^-$ to satisfy electro-neutrality upon oxidation (p-doping).

The reverse side oxidised and reduced films exposed to Ethaline only show a minimal amount of Cl (1s), which meant that the $[2\text{EG.Cl}]^-$ did not penetrate to the polymer-Au interface.

The reduced PTP exposed to Ethaline exhibited elevated amounts of C (1s) and N (1s), which suggested the involvement of $[\text{Ch}]^+$ cations; entering the film upon reduction (undoping). However, the presence of Cl inferred that all not the $[2\text{EG.Cl}]^-$ anions were expelled during undoping.

7.3.4 PTP Film XPS Sulphur : Nitrogen Ratios

The ratio of atomic percentages for S (2p) to N (1s) peaks for the PTP films showed confirmation of the deposition of the mixed monomer precursor TP **3** and that no

dissociation of the thiophene and pyrrole rings occurred, as the peaks were observed in a 1 : 1 ratio. This was true for the as prepared pristine PTP film, PTP films exposed to 0.1 M LiClO₄ / MeCN and the reverse side PTP films exposed to Ethaline. The S (2p) spectra and N (1s) spectra are shown for films that depicted a 1 : 1 S : N ratio in **Fig. 7.5** and **Fig. 7.6** respectively. The shifts in binding energy of the S and N peaks are probably attributed to association with a counterion for electro-neutrality, similar to that observed for S (2p) peaks in PEDOT reported in this thesis (section **7.2**) and in the literature ^{[4] [9]}.

The Ethaline oxidised and reduced films showed an increased atomic percentage for N (1s), approximately 5% compared to the ‘as prepared’ PTP, which highlighted the involvement of a [Ch]⁺ cation. The [Ch]⁺ cation was shown to be expelled from the film upon oxidation (p-doping), whereas the ingress of [Ch]⁺ occurred upon reduction (observed from the gravimetric data fit in **Chapter 6**). This meant that a higher nitrogen ratio should be observed in the reduced film, for which it was for the reduced PTP sample in Ethaline (see **Table 7.7**). As the S : N ratios were found to be approximately 1 : 1 for the reverse side PTP films exposed to Ethaline, this inferred that the [Ch]⁺ cation did not penetrate to the polymer-Au interface.

Table 7.7 - PTP XPS S (2p) : N (1s) ratio.

PTP	S : N % ratio			
	S (2p)		N (1s)	
	L	S	L	S
Pristine (Grown in LiBF ₄ / MeCN)	57.41	57.11	42.59	42.89
LiClO ₄ / MeCN Reduced	55.63	55.69	44.37	44.31
LiClO ₄ / MeCN Reduced (repeat)	56.01	56.65	43.99	43.35
LiClO ₄ Reduced Reverse	57.04	56.69	42.96	43.31
Ethaline Oxidised	33.9	33.57	66.1	66.43
Ethaline Oxidised Reverse	54.64	55.84	45.36	44.16
Ethaline Reduced	27.01	26.6	72.99	73.4
Ethaline Reduced Reverse	58.67	58.78	41.33	41.22

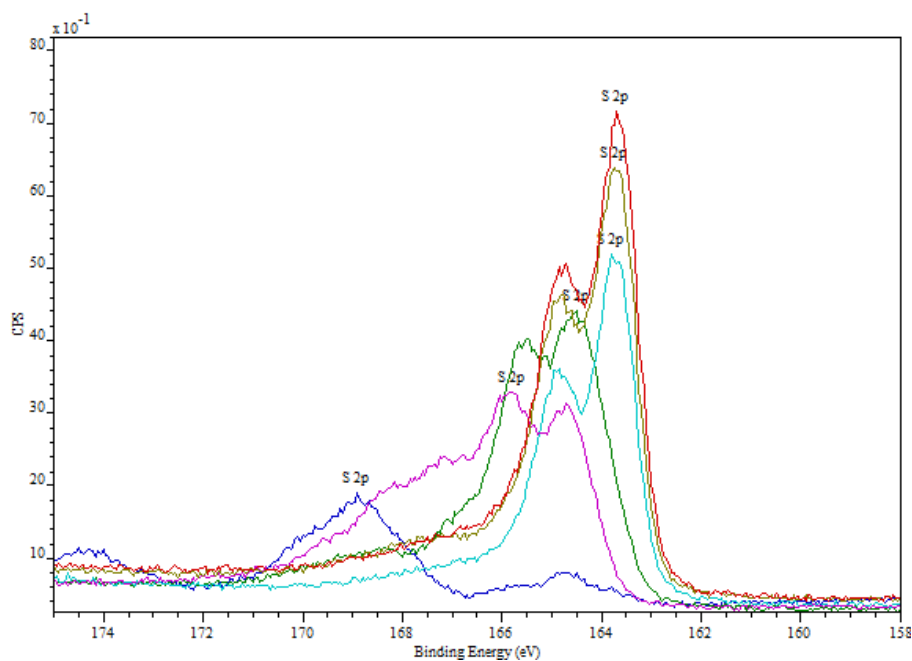


Fig. 7.5 - S (2p) peaks for PTP samples with a S (2p) : N (1s) ratio of 1 : 1, red = LiClO₄ Reduced brown = LiClO₄ Reduced (repeat), cyan = LiClO₄ Reduced reverse, green = Ethaline Reduced reverse, pink = Ethaline Reduced reverse and blue = pristine PTP.

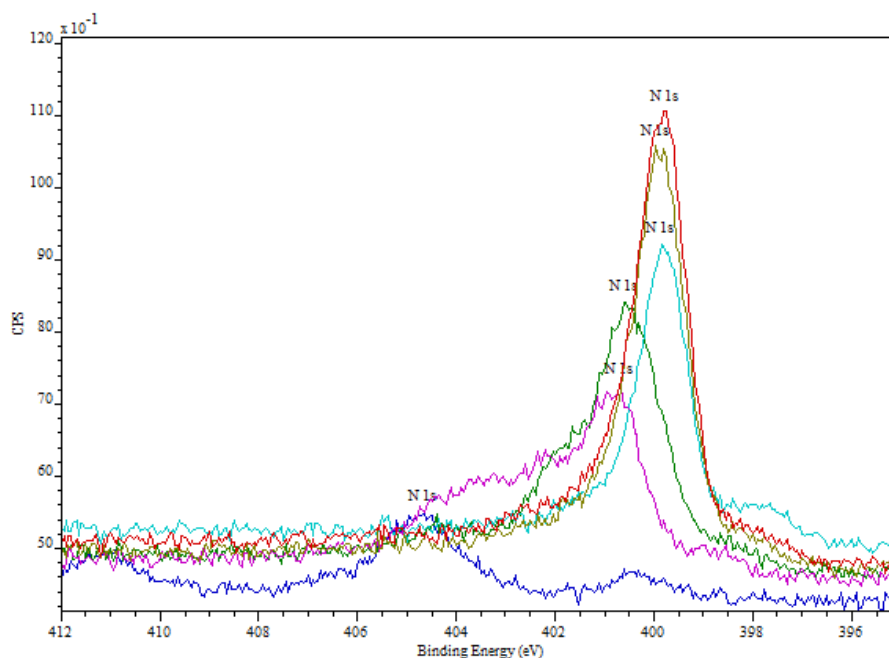


Fig. 7.6 - N (1s) peaks for PTP samples with a S (2p): N (1s) ratio of 1 : 1, red = LiClO₄ Reduced brown = LiClO₄ Reduced (repeat), cyan = LiClO₄ Reduced reverse, green = Ethaline Reduced reverse, pink = Ethaline Reduced reverse and blue = pristine PTP.

7.4 Summary of XPS Data

7.4.1 PEDOT Films

The elemental composition ratios of C (1s) : O (1s) : S (2p) peaks for pristine and reduced PEDOT were concordant with the theoretical ratio of PEDOT, at a value of 6 : 2 : 1, which confirmed the deposition of PEDOT using the conditions reported in the experimental section (**Chapter 3**).

The PEDOT film oxidised in 0.1 M LiClO₄ / MeCN exhibited an elevated O (1s) percentage ratio (*cf.* pristine film and theoretical ratio) and Cl peak which confirmed the presence of [ClO₄]⁻. This supported the suggestion from gravimetric experiments (**Chapter 5**) of anion ingress upon PEDOT p-doping.

For the PEDOT film reduced in 0.1 M LiClO₄ / MeCN, the lack of a Cl peak and an O (1s) percentage ratio the same as for the pristine PEDOT film, justified the

assumption made during gravimetric experiments that $[\text{ClO}_4]^-$ anions were expelled upon undoping.

The PEDOT film oxidised in Ethaline exhibited elevated C (1s) and O (1s) percentage ratios (*cf.* pristine film) and showed the presence of a Cl peak. This confirmed the suggestion of dopant anion ingress, $[\text{2EG.Cl}]^-$; assumed to fit the gravimetric data in

Chapter 5.

The reverse side Ethaline oxidised film showed a lower atomic percentage of Cl (*cf.* oxidised film) and similar C (1s) : O (1s) : S (2p) ratio to the pristine film. This suggested the bulky $[\text{2EG.Cl}]^-$ anion struggled to penetrate to the polymer-Au interface during doping.

A lower atomic percentage of Cl was observed for the PEDOT film reduced in Ethaline (*cf.* oxidised PEDOT in Ethaline), which suggested some but not all the dopant anions $[\text{2EG.Cl}]^-$ were expelled upon undoping.

EQCM studies of PEDOT exposed to Ethaline alluded a mixed ion exchange mechanism, which as well as $[\text{2EG.Cl}]^-$ anion transfers involved $[\text{Ch}]^+$ cation transfers in the opposing direction; egress during doping / ingress during undoping. However, observations from XPS conflicted this, with a N (1s) peak observed in the oxidised film and no N (1s) peak present in the reduced film; contrary to expected from gravimetric data.

For PEDOT oxidised in ZnCl_2 / EG, the presence of Zn and Cl peaks were consistent with the suggestion of $[\text{ZnCl}_4]^{2-}$ anion ingress during doping, made from interpretation of gravimetric data (**Chapter 5**).

The lack of Zn peaks and a negligible Cl atomic percentage for the reverse side PEDOT film oxidised in ZnCl_2 / EG suggested that the bulky $[\text{ZnCl}_4]^{2-}$ anions were unable to penetrate to the polymer-Au interface; likened to that observed for bulky $[\text{2EG.Cl}]^-$ anions for the reverse side oxidised PEDOT films in Ethaline.

7.4.2 PTP Films

The atomic percentage ratios of S : N peaks for pristine PTP, PTP reduced in LiClO_4 and the reverse side PTP in Ethaline films were consistent with the theoretical ratio of PTP, 1 : 1. This confirmed the polymerisation of PTP and also that no dissociation of the thiophene or pyrrole rings occurred.

The lack of Cl peaks observed in the spectra for the PTP film reduced in 0.1 M LiClO_4 / MeCN suggested $[\text{ClO}_4]^-$ anions were expelled upon reduction; consistent with gravimetric observations (**Chapter 6**). Unfortunately, due to time constraints and instrument availability, PTP films oxidised in 0.1 M LiClO_4 / MeCN could not be analysed.

Elevated C (1s) atomic percentages for the PTP oxidised in Ethaline (*cf.* pristine PTP) and the presence of Cl supported evidence from gravimetric data of $[\text{2EG.Cl}]^-$ anion ingress during p-doping; the same mobile species transfers as observed with PEDOT oxidised in Ethaline.

A lower percentage of N (1s) present in the PTP film oxidised in Ethaline compared to the reduced Ethaline film inferred the presence of a nitrogen containing mobile species. This supported the notion of $[\text{Ch}]^+$ cation egress during p-doping determined from EQCM studies (**Chapter 6**).

For the reverse side PTP films oxidised and reduced in Ethaline, only minimal amounts of Cl were recorded which suggested the bulky $[\text{2EG.Cl}]^-$ anion barely penetrated to the polymer-Au interface. Also the reverse side reduced PTP in Ethaline had a S : N ratio of 1 : 1, the same as the pristine PTP. If $[\text{Ch}]^+$ cations had reached the polymer-Au interface an elevated amount of N (1s) would have been recorded. Both the minimal amounts of Cl and N (1s), the same as a pristine film, suggested the electrolyte was unable to reach the polymer-Au interface.

The PTP film reduced in Ethaline exhibited elevated C (1s) and N (1s) atomic percentages (*cf.* pristine) which supported $[\text{Ch}]^+$ cation ingress during undoping. However, the presence of Cl suggested not all the $[\text{2EG.Cl}]^-$ anions were expelled during undoping.

The S : N ratio clearly showed a larger N (1s) ratio in the PTP film reduced in Ethaline compared to the oxidised sample, interpreted as $[\text{Ch}]^+$ cation ingress during doping and expulsion during undoping. These observations were consistent with gravimetric data interpretations (**Chapter 6**).

7.5 Conclusions

X-Ray Photo-electron Spectroscopy (XPS) studies were used to investigate the chemical compositions and ion exchange dynamics during redox cycling of conducting polymers from the heterocyclic monomers EDOT **1** and TP **3**; in either LiClO₄ / MeCN, a Type III DES or a Type IV DES. These studies aimed to characterise the behaviour of conducting polymers intended for the use in charge storage applications. XPS studies confirmed:

- Deposition of conducting polymers by atomic percentage ratios; PEDOT (C (1s) : O (1s) : S(2p)); PTP (C (1s) : S (2p) : N (1s) and S (2p) : N (1s))
- No dissociation of thiophene and pyrrole ring systems during electrochemical deposition of mixed monomer precursor TP **3**
- Mobile species in 0.1 M LiClO₄ / MeCN; both processes confirmed for PEDOT; only undoping process confirmed for PTP:
 - Ingress [ClO₄]⁻ during p-doping
 - Egress [ClO₄]⁻ during undoping (suggested by lack of Cl peaks)
- Mobile species in the Type III DES, Ethaline; p-doping mobile species confirmed for PEDOT and PTP; undoping confirmed for PTP:
 - Ingress [2EG.Cl]⁻ during p-doping and
 - Egress [Ch]⁺ during p-doping
 - Egress [2EG.Cl]⁻ during undoping and
 - Ingress [Ch]⁺ during undoping

- Mobile species in the Type IV DES, ZnCl_2 / EG; only confirmed for PEDOT:
 - Ingress $[\text{ZnCl}_4]^{2-}$ during p-doping
 - Egress EG during p-doping
 - Egress $[\text{ZnCl}_4]^{2-}$ during undoping
 - Ingress EG during undoping

Further work would investigate PEDOT reduced in ZnCl_2 / EG, PTP oxidised in 0.1 M LiClO_4 / MeCN and novel monomers PTP in the Type IV DES ZnCl_2 / EG. This would then be extended to the compositions of PEDOT and PTP redox switched in other DESs, other conducting polymers and conducting polymers deposited from DESs.

7.6 References

- [1] Ruffo R, Celik-Cochet A, Posset U, Mari CM, Schottner G, *Solar Energy Materials & Solar Cells*, 2008, 92, 2, 140-145
- [2] Bach CMG and Reynolds JR, *J. Phys. Chem.*, 1994, 98, 51, 13636-13642
- [3] Pandey GP, Rastogi AC and Westgate CR, *J. Power Sources*, 2014, 245, 857-865
- [4] Pandey GP and Rastogi AC, *Electrochimica Acta*, 2013, 87, 158-168
- [5] Attard G and Barnes C, *Surfaces*, 1998, Oxford University Press, Oxford, UK
- [6] Fairley N, *CASA XPS Manual 2.3.15*, 2009 Casa Software Ltd
- [7] Wagner CD, Riggs WM, Davis LE, Moulder JF and Muilenberg GE, *Handbook of X-Ray Photo-electron Spectroscopy*, 1979, Perkin-Elmer Corporation, USA
- [8] Chusuei CC and Goodman DW, *Encyclopedia of Physical Science and Technology – Analytical Chemistry, X-Ray Photo-electron Spectroscopy Chapter*, 2001, Elsevier Ltd, Oxford UK, 3rd Edn
- [9] Spanninga SA, Martin DC and Chen Z, *J. Phys. Chem. C*, 2009, 113, 14, 5585-5592
- [10] Spanninga SA, Martin DC and Chen Z, *J. Phys. Chem. C*, 2010, 114, 35, 14992-14997
- [11] Spanninga SA, Martin DC and Chen Z, *J. Phys. Chem. C*, 2010, 114, 35, 14998-15004
- [12] Taouil AE, Lallemand F, Hihn JY, Melot JM, Blondeau-Patissier V, Lakard B, *Ultrasonics Sonochemistry*, 2011, 18, 1, 140-148

Chapter 8

Conclusions and Further Work

8.1 Conclusions

8.2 Further Work

Chapter 8

Conclusions and Further Work

8.1 Conclusions

The main objective of this thesis was to investigate the feasibility of producing a Zn-Polymer battery using a DES as the battery electrolyte. Studies were focussed on the conducting polymer electrode as this electrode was deemed to be the limiting factor in terms of the charge storage capabilities of PolyZion batteries.

Overall, the best performing non-aqueous electrolytes were Ethaline and $\text{ZnCl}_2 / \text{EG}$ due to the high mass specific capacitances recorded in these two DESs. The best performing conducting polymers were PEDOT and PTP. PTP had a mass specific capacitance of 206 F g^{-1} and 139 F g^{-1} for Ethaline and $\text{ZnCl}_2 / \text{EG}$ respectively. In these electrolytes PEDOT had a mass specific capacitance of 89 F g^{-1} and 118 F g^{-1} respectively. A range of mass specific capacitances were recorded for the conducting polymers in DESs reported in this thesis, dependent on the thickness of the polymer film deposited.

Using the best performing electrolytes, investigations were conducted into the charge driven mass transfers of PEDOT and PTP in DESs. EQCM studies and XPS provided insight into these transfers and allowed individual ion and solvent contributions to be suggested. Gravimetric data obtained for both PEDOT and PTP in Ethaline showed during p-doping $[\text{Ch}]^+$ cation egress and $[\text{2EG.Cl}]^-$ anion ingress occurred, with the transfers reversed during undoping. Cation transfers dominated in satisfying electro-neutrality for PEDOT and PTP in Ethaline. In contrast, gravimetric data for

PEDOT and PTP in $\text{ZnCl}_2 / \text{EG}$ and in $\text{LiClO}_4 / \text{MeCN}$ fitted anionic mobile species involvement and solvent transfers. Gravimetric data obtained for both PEDOT and PTP in $\text{ZnCl}_2 / \text{EG}$ fitted $[\text{ZnCl}_4]^{2-}$ ingress and neutral molecule EG egress for p-doping, with the transfers reversed during undoping of the polymer. Anion transfers dominated the maintenance of electro-neutrality of PEDOT whereas neutral molecule transfers dominated the behaviour of PTP in $\text{ZnCl}_2 / \text{EG}$. Charge driven mass transfers of PEDOT and PTP in $\text{LiClO}_4 / \text{MeCN}$ fitted $[\text{ClO}_4]^-$ ingress and MeCN egress during doping, with the transfers reversed during undoping. These transfers were consistent with reports in the literature. The charging (discharging) behaviours of both PEDOT and PTP in $\text{LiClO}_4 / \text{MeCN}$ were dominated by solvent transfers.

The identities of mobile species which were suggested to fit the gravimetric data obtained from EQCM studies for the p-doping (undoping) of PEDOT and PTP were supported by spectral data from XPS. This spectral data also confirmed the deposition of these polymers.

8.2 Further Work

In regards to further work, the main focus would be trying to increase the surface area of the polymer electrode to improve the electrode charge storage capabilities. This could be achieved by depositing conducting polymer, either chemically or electrochemically, onto materials such as carbon foams or carbon nanotubes. The electrode material would need to have a high surface area to bring about a significant improvement in charge storage. The polymer layer deposited onto this high surface area material needs to be thin to encourage charge transfer without resistance. It may also be of interest to investigate whether the use of a Type III / Type IV DES hybrid electrolyte would

improve the DC capacitance. The hybrid liquid could be less viscous and therefore improve mass transport into and out of the polymer film, essential for the maintenance of the electro-neutrality condition.